THE RHEOLOGY OF CARAMEL

By

Giuseppina Barra

Thesis submitted to the University of Nottingham for the degree of

Doctor of Philosophy

February 2004

Division of Food Sciences
University of Nottingham
Sutton Bonington
LE12 5RD

DEDICATION

This thesis is dedicated to the memory of my beloved father

ABSTRACT

The rheology of caramel was determined as a function of processing temperature and hydrocolloid additions. As the processing temperature increased the water content decreased and the caramel viscosity increased. X-ray diffraction showed that although crystalline fat was present, for the most part the sugars were in the amorphous state. The exception was the lowest water content caramel (7.9% water w.w.b.) which had been processed to a temperature of 122ºC. This had a small amount of crystalline fructose. Caramel rheology was assessed by rotational and capillary rheometry. Rotational rheometry gave information on the steady shear viscosity, the dynamic parameters (storage and loss moduli and related functions) and the creep compliance and recovery response. Capillary rheometry gave shear viscosities at high shear rates and an extensional viscosity. It was found that caramel without added hydrocolloids had behavior which was close to a Newtonian liquid. The only exception to this was the values obtained for the Trouton ratio which ranged from 10 to 40. This was considerably higher than the value of 3 for a Newtonian fluid and may reflect the difficulties in making measurements on these relatively low viscosity systems in the capillary rheometer. The viscosities obtained from steady shear, oscillation and creep were combined and three approaches were used to model the data as a function of measurement temperature and water content. An empirical statistical model using a second order polynomial, an Arrhenius fit and a Williams Landel Ferry (WLF) model. The former and the latter gave a good fit to the data although the constants used in the WLF model varied with the water content of the caramel. Arrhenius plots showed curvature particularly at low water contents

Incorporation of the hydrocolloids carrageenan and gellan gum into the caramel made the material non-Newtonian and elastic. For carrageenan incorporation in

particular the Trouton ratio increased with carrageenan concentration reaching a value ~500 at a strain rate of $100s^{-1}$ for the caramel containing 0.2% carrageenan It was demonstrated that incorporation of carrageenan could be used to prevent cold flow in caramels processed at relatively high water contents.

Glass transition temperatures were measured by differential scanning calorimetry and calculated from the temperature dependence of the shift factors used to superimpose the oscillatory rheological data. Generally there was agreement between the two approaches although for some gellan gum containing samples the rheological T_g was about 10ºC higher than the DSC value. Fragility calculated from the WLF constants for caramel was high as has been reported for sugars. The Tg for both caramel and sugar water mixtures calculated using the Couchman-Karastz equation in the water content of interest (9-15% w.w.b.) was some 30-40°C higher than measured. It is suggested that this disagreement could be related to the high fragility of the sugar water systems.

Isoelectric point measurements using a streaming potential technique was shown to give information on the extent of the Maillard reaction and the presence of hydrocolloids.

Acknowledgements

My sincere thanks are given to my supervisor Professor John R. Mitchell who welcomed me into the Food Structure research group at Nottingham University. I am indebted to him for his support, supervision, valuable guidance and also for his friendship and humanity during the course of the PhD.

I am also grateful to my second supervisor Dr. Sandra Hill, for her encouraging attitude and guidance.

Special thanks go to Dr. Imad Farhat. He has been an inexhaustible source of support, valuable advice and friendship during all the time I have spent in Nottingham.

I would like also to express my gratitude to Nestlé, not only for their financial support during my PhD, but also for their human and technical support throughout the whole project. My special thanks go to Dr. Helen Chisholm for her supervision and for helping me in the sample preparation and deposit trials in the PTC plant of York, and to Dr. Steve Becket.

Kind thanks to Dr. Rukmel Aberseken from the University of York for performing light microscopy on caramels.

I would like to thank the staff of the Food Sciences division of Nottingham University: Val Street, Kath Brasnett, Lynne Moseley and Dr. William McNaughtan for their help, support and friendship throughout the project.

A special mention is reserved for Phil Glover, with his kindness, patience and humanity he has helped me in solving many of my daily problems, and Mike Chapman whose talent and creativity are immeasurable. He made everything possible!

Additionally I would like to thank all the PhD students from the Food Sciences Division who contributed to a pleasant atmosphere: Abde, Asgar and Mahsa, Celine, David, Javier, Irina, Lalitha, Marcin, Nameeta, Nuno and Anne-Laure and everyone else...

Particularly thanks to Dr. Carlos Carvalho, Dr. Agnes Namutebi, Dr. Taewee Tongdang (Krim), Dr. Marie-Astrid Ottenhof, Dr. Thierry Tran, and Dr. Linda Lopez for their support when I first arrived in the UK and after for their true friendship, and to Ayten Aylin Tas for always being very close to me.

Many thanks also to all my friends outside the Food Science environment in UK and all around the world: Andre, Stefano, Rutger, Samantha, Eric, Muhalb, Ahmed, Gery, Gabriele, Maria Rosaria, Marco, Tina, Odda, Edmondo and Aldo.

And last but not least thanks to my family: Mamma, Angelo, Giovanni and Barbara, zia Matilde and zia Emilia for their love, support and patience.

Grazie di cuore a tutti....

TABLE OF CONTENTS

LIST OF FIGURES

LIST OF TABLES

CHAPTER 1. INTRODUCTION

For the last two decades, the general trend followed by food scientists working on food structure was to apply a material science approach to food systems. This approach is based on a set of theories originally developed for inorganic systems and synthetic polymers to systematically understand the relationship between structure and properties and to develop engineered foods with specific characteristics.

The so-called food polymer science approach has been shown to be relevant to the understanding of the structure and the behaviour (processing and stability) of a wide variety of products from cereals to confectionery products.

Caramel is one of the most basic and versatile candy products, and an important component of many composite confectionery products. In the preparation of caramel, the ingredients (milk, fat, and sugar syrups) are mixed together and cooked at temperatures sufficiently high to allow the Maillard reaction to occur between reducing sugars and free amino acids (Jeffery, 2001; Kakuda, 1990).

The product is an emulsion consisting of a dispersed phase of fat droplets stabilised by milk proteins in an aqueous amorphous sugar matrix containing products of the Maillard reaction. The latter is responsible for the colour and the flavour of caramel. Partly because of the Maillard reaction, the physical characteristics of caramels and the structure and distribution of phases are strongly affected by the formulation and cooking conditions (O'Brian and Morrisey, 1989; Atapattu and Kakuda, 1998; Bondi et al. 1993).

There are caramel processing problems on an industrial scale related to rheology, in particular tailing. This is the name given to an undesirable phenomena observed during caramel deposition e.g. "Rolo" and caramel enrobing e.g. "Lion bar". Tailing has an adverse affect on the weight control and causes sweets to stick together, hence raising quality issues. Weight control during caramel enrobing (Lion bar) is also related to the rheological behaviour of the caramel. Another problem related to the rheology is so-called "cold flow" which affect the quality and principally the shape of the final product during storage.

AIM AND OBJECTIVES OF THE PROJECT

The objectives of this work are focused on the effect of the processing conditions on caramel rheology and the effect of the incorporation of hydrocolloids. Another objective of this project aims to establish a robust and reliable technique using a commercially available instrument to measure the extensional viscosity of caramel, and to relate the rheological properties, including extensional, shear and viscoelastic properties of caramels to the depositing and storage behaviour.

The project objectives can therefore be summarised:

1. To develop a reliable technique to measure the extensional viscosity of caramel at depositing temperature e.g. 70ºC, using commercially available instrument (JREI-Rosand capillary rheometer) and to establish a relationship between the rheological properties (e.g. Trouton ratio, viscoelasticity) of caramels with the performance/application properties of caramels.
2. To study the influence of the processing temperature and particularly to study caramel obtained with the same formulation but cooked at different final boiling temperature. It was suggested that both water content and Maillard polymeric products could contribute to the rheological behaviour.
3. To study the influence of the added hydrocolloids, κ-carrageenan and gellan gum on the rheological properties of caramels.

Chapter 2 presents a literature review on caramel considering the effects of ingredients on caramel preparation and the industrial scale process. The viscosity of sugar-water mixture is discussed. As the water content is reduced sugar solutions approach and eventually enter the glassy state, hence there is some theory on the glass transition and on the physical state of supercooled liquids. Finally the last section of chapter 2 contains some literature on hydrocollids and particularly on carrageenan and gellan gum that have been used for this project. Particularly importance has been given to the vitrification effect of biopolymers in systems containing high level of sugar.

Chapter 3 describes the materials used and principal methodologies employed. Particularly attention has been given to capillary rheological techniques as the

applicability of this techniques to caramel system was one of the objectives of the project. Chapter 4 focuses on the effect of final cooking temperature on the structure and rheological properties of caramels. The applicability of the WLF approach and Arrhenius kinetcs for modelling of viscosity rheological data to relate to the glass transition has been analysed and also the possibility of using empirical statistical models. Chapter 5 describes the effect of hydrocolloids in caramel systems. Arrhenius kinetics and a WLF approach have been used to model rheological data and hence to detect the vitrification event in these high sugar-hydrocolloids systems. Finally, an overall discussion of the results of this study in the context of the existing literature is reported in chapter 6.

CHAPTER 2. LITERATURE REVIEW

2.1 Caramel

The word "caramel", derives from the Spanish 17th century “caramelo”, which itself was derived from the Portuguese “caramelo”. It has also been suggested that it come from the medieval Latin “cannamellis”, for sugar cane, or from the Latin “caramellus”, which is the diminutive of calamus, "reed", this is because of the analogy between hardened sugar and a stem of a reed. No doubt, because of the simplicity of their composition, caramels were the first delicacies containing sugar, (Anonymous 2003).

Nowadays next to chocolate, caramel is the most important component in chocolate containing confectionery products. It is also an important product in its own right (e.g. toffees). Like chocolate it has worldwide appeal. It has a range of texture from brittle toffees to soft sauces in ice creams or filling in a moulded chocolate unit. It can also be used in nut or chocolate clusters.

Pyrz (1976) described caramel as a complex emulsion of a dispersed phase of fat globules and a highly concentrated sugar solution in which the non-fat milk solids

and other minor components are dispersed or dissolved (Guelfi 1988; McMaster, Smith et al. 1987; Morton et al. 2003)

Despite the wide range of caramels and fudge in the market place, caramels have common characteristics (Chung et al. 1999; Jeffery 2001) . These are:

- A continuous syrup structure holding the whole confection together
- Milk protein dispersed into the syrup
- A characteristic flavour produced by the Maillard reaction between the milk protein and reducing sugars in the recipe
- Fat emulsified into the syrup
- In grained caramel (fudge) sugar crystals are dispersed in the syrup.

A general composition for caramels is:

- Sugar solids (65-70 %)
- Water content (5-20 %)
- Fat (5-20 %)
- Total milk solids (5-10 %)
- Protein content (0.5-4 %)

Sugar solids

Sugars provide bulk and sweetness in caramel. Sugar solids in caramel generally consist of sugar and glucose syrup and the ratio of these, together with the type of glucose syrup, largely governs the texture of the final products. Sucrose (β-D-fructofuranosil-α-D-glucopyranoside) is a disaccharide consisting of α 1-4 linked glucose and fructose. Glucose syrups are hydrolysates of starch comprising of mixtures of low molecular weight glucose oligosaccharides. The mean number average molecular size can be related to the dextrose equivalent (DE). This is defined as the number of reducing groups similarly relate to the pure glucose monomer. For instance a glucose syrup containing only the glucose monomer would only have a DE of 100 and the disaccharide maltose consisting of two glucose units would have a DE of 50. The DE of the glucose syrup used can be varied to control moisture holding capability (water activity), tenderness and sugar graining in confectionery products. Typically the glucose syrup DE varies from 30 to 70 in caramel type products.

Caramels prepared from low DE glucose syrup generally are more chewy, caramels containing high DE glucose syrup have a soft texture at the same moisture content (Steiner, Foegeding et al. 2003). The type of glucose syrup is also important for the flavour of the caramel because it is the lower molecular compound dextrose or maltose which reacts more extensively with the milk protein to give a characteristic caramel flavour. It is possible to have a fructose containing glucose syrup by using a glucose isomerase in the manufacturing processes.

Water content

The water content is a critical parameter in the technology of these products as the rheological properties of caramels are strongly dependant of it. For equal recipes the higher the moisture content, the softer the texture of the caramel.

Controlling the final moisture content of the product is then critical to reproduce consistency. Moreover, the water activity of the product, which is governed by moisture content and composition, is critical to the shelf life.

Types of fat

The importance of the type of fat is related to its melting characteristics and how well it can be emulsified into the syrups. Fat is added to the confections to impart a richness of mouth feel. Milk fats are sometimes added to provide a dairy butter flavour.

Milk

Milk is a critical caramel ingredient (Bondi, Marcone et al. 1993). Sweetened condensed milk, sweetened skim milk and spray dried milk powder are the preferred milk ingredients. The source of protein has an influence on the Maillard reaction and hence on caramel flavour. No fat milk solids contribute body to the texture. Typically caramel contains 0.5-4 % milk protein depending on its application.

The Maillard reaction in caramels

The caramel flavour comes from a complex reaction between milk protein and reducing sugars. This reaction is called Maillard reaction and was first described by LC Maillard in 1912. The flavour and colour development depend on the amount of milk protein, the amount and type reducing sugars, the temperature, the time the caramel is held at the cooking temperature and the pH.

The concentration of milk protein is in the range 0.5-4 %, and the more present in the recipe, the greater the flavour and the colour development which takes place.

The main reducing sugars in caramels and fudges are lactose (in the milk), glucose, maltose and fructose present in glucose syrups and invert sugar. The

more reducing sugars the stronger the flavour and colour development. Fructose is particularly reactive as it is a 5 ring sugar, so that adding fructose to the recipe enhances colour and flavour development, as well as increasing the sweetness of the product.

The Maillard reaction rate become high when the cooking temperature reaches 110-115°C and then accelerates even further as the temperature rises. Time is an important factor because the longer the mixture of milk protein and reducing sugars are held at temperature, the more colour and flavour development take place.

Generally the higher the pH, the stronger the colour and flavour development. Above pH 7, very rapid browning occurs together with more complex reactions. Normally the pH of caramel should be in the region of 6.5-6.7 for controllable manufacture of caramel and fudge.

Manufacture of caramels (Weckel and Steinke 1973; Bainbridge 1997)

For many years caramels and fudge has been made in high pressure steam heated pan fitted with agitators. The agitator constantly scraps a thin film from the heated surface allowing rapid boiling.

The batch cooker fulfils many functions including:

- dissolving the sugar in water completely

- mixing together the rest of the ingredients, sometimes including reconstituting milk power in water

- emulsifying the fat into the syrup

- boiling off water to a controlled moisture content

- developing the flavour and colour of the Maillard reaction

- at the end if the process water can replace the steam in the jacket, cooling the cooked caramel to stop further Maillard reaction development.

On an industrial scale it is common to use a continues high temperature, short time, high shear process (HT-ST-HS) for caramel making.

Figure. 2.1 shows a simple continuous HT-ST-HS system. The premix, consisting of milk mix and sugar syrup is metered into the caramel cooker. White opaque, pudding like caramel is discharged to a temperature controlled, jacketed browning kettle that is slowly agitated.

The temperature is held constant and the level is controlled in the browning tank to produce the desired colour and flavour in the discharged material. Discharged caramel will be cooled and sent to an extrusion step to form ropes or slabs of finished caramel or sent to the depositing line for the preparation of nut /chocolate clusters for more complex finished products.

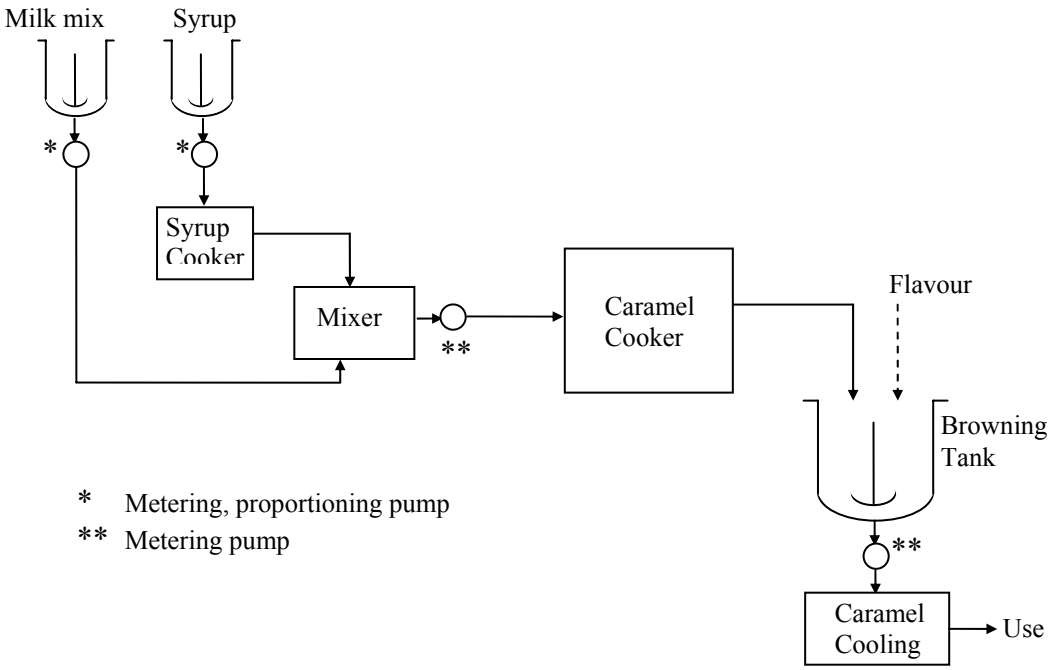

Figure 2.1 Flow diagram of a continuous high temperature – Short time – high shear caramel cooking system. Adapted from Bainbridge (1997).

2.2 Glass transition and physical state of supercooled liquids

The glass transition of low moisture food product is now widely recognized as a key-concept regarding their stability and processability (Blanshard and Lillford 1993, Slade and Levine 1995).

Glass transition or glass-liquid transition is the name given to phenomena observed when a glass is heated until it behaves like a supercooled melt. This phenomenon is observed for those materials that can be cooled sufficiently below their melting temperature without crystallizing.

A material in the glassy state behaves as a brittle solid-with rigidity or storage modulus typically about 10^9 Pa·s. Its structure is non-crystalline (amorphous) exhibiting a short range order only, as in a liquid. The supercooled melt is the

non-crystalline state observed between the glass transition temperature and the melting point. The mechanical behaviour can be that of a viscoelastic rubber (high molecular weight materials) or mainly viscous as a liquid (low molecular weight material).

As the temperature of the glassy material is raised through the temperature range of the glass transition, rather abrupt changes in many thermodynamic and physical properties are observed: increase in entropy and heat capacity and decrease in rigidity and viscosity.

The abrupt change in the heat capacity and volume thermal expansion coefficient that are the first derivative with the temperature of the fundamental thermodynamic properties enthalpy and volume, has resulted in the glass transition being considered as a second-order thermodynamic transition. There have been attempts to analyse the glass transition from a thermodynamic point and to define it as a transition from a liquid state to a solid state. However this approach has been criticized for various reasons. One of these is the dependence of the glass transition temperature on the cooling or heating rate. It is found that the lower is the cooling rate the lower the value of the T_g detected.

Another useful approach to analyse the glass transition is the use of the concept of free volume. The free volume is the space which is not occupied by the molecules.

The total volume V consists of the volume occupied by molecules V_0 and the free volume V_f such that $V=V_0+V_f$

Figure 2.2 shows the variation of the specific volume V (volume per unit mass) of a polymer with the temperature. The free volume is represented by the shaded area.

At temperatures above the glass transition the variation of the volume with the temperature will follow the laws of thermodynamic equilibrium until the free

volume reaches a value V_f* above the molecular volume V_0. V_f* is approximately 2.5% of the total volume. At this value there will not be enough space for the rotational and translational motions of the molecules to take place and the equilibrium is no longer reached because of limitation of molecular motions. The temperature at which this happen corresponds to the T_g and below this temperature the glass material is "frozen". The free volume is assumed to be constant at a value V_f* at temperatures below the glass transition and to increase as the temperature is raised above the T_g.

The fractional free volume, *f*, which is the ratio between the free volume and the total volume, $f = V_f / V$, will vary with the temperature according to the following relationship: $f = f_g + (T - T_g)\alpha_f$ where f_g is the fractional free volume in the glassy state $f_g = V_f^* / V$ and α_f is the thermal expansion coefficient of the free volume which will be given at a temperature close to the T_g by the difference between the thermal expansion coefficients of the rubbery and the glassy state.

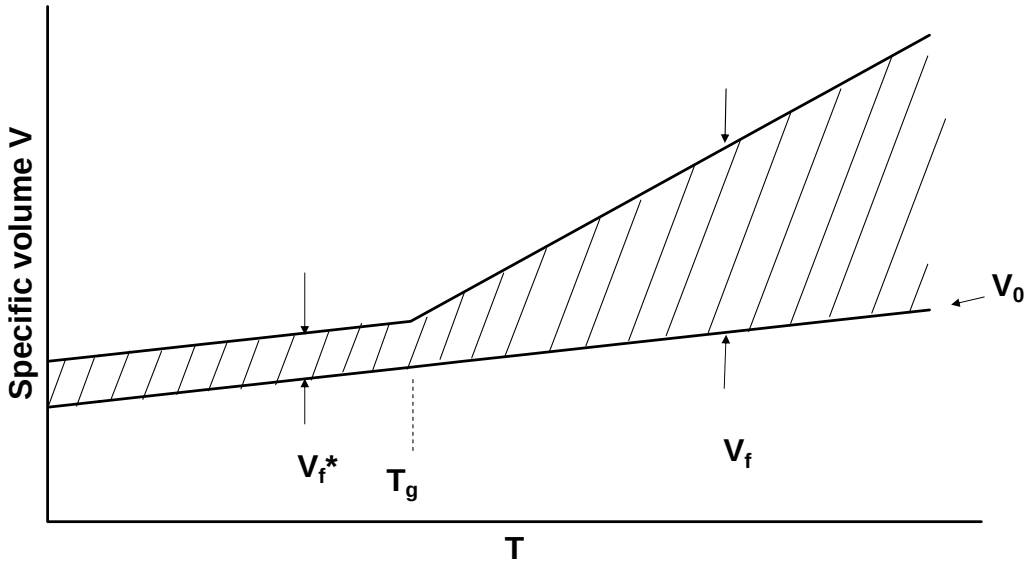

Figure 2.2 *Variation of the specific volume, V, of a polymer with temperature, T. The free volume is represented by the shaded area.*

It has been found for a whole range of different glassy polymers that f_g is remarkably constant and this concept of free volume has found important use in the analysis of the rate and temperature dependence of the viscoelastic behaviour of polymers between T_g and T_g+100K.

The glass transition temperature is a kinetic and relaxation process associated with primary relaxation of the material. The relaxation time is the time necessary for a material to recover the equilibrium condition after it has been perturbed from outside. The glass transition temperature region is the temperature range where the relaxation time of the material is similar to the experimental time scale.

Nowadays the glass transition temperature is often considered as the temperature where the viscosity reaches the value of 10^{12} Pa·s, or where the segmental relaxation time is 100 sec.

The sensitivity of the relaxation processes to temperature depends on the cooperative motion concerned and can be associated with an apparent activation energy (E_a). At very high temperature, such as in the melt, because the high free volume between the entities, the molecules or the structural units such as the repetitive elements of a polymer, can move independently from each other. Arrhenius behaviour of the dynamic properties is then observed. The activation energy E_a, corresponds to the minimum of the interaction energy between units and is independent of the temperature,

In the supercooled melt, however, the reduction of free volume induces a co-operative motions of the entities. The apparent activation energy then depends on both the changes with the temperature of the inter and intramolecular interactions and the variation of free volume. It increases with decreasing temperature, reaching the higher value at temperature close the T_g. Typical value of E_a at the glass transition are 200-400 kJ/mol.

At temperatures below the glass transition molecules stay in an isoconfigurational state and the co-operativity effect on the activation energy will be restricted. In the glassy state the change in the dynamic properties obeys the Arrhenius law again, with an apparent energy of activation lower than in the supercooled liquid, although the values are still high. However molecular relaxation processes also take place in the glassy state but with lower amplitude and co-operativity than those associate with the glass transition.

Sub-T_g relaxations are named according to their relative position to the main relaxation α . Even if several relaxations can be observed for biopolymers, only the secondary β relaxation has been extensively studied and its origin is still under investigation. According to Johary (Johary and Shastri, 1976) it corresponds to more localized molecular motion that persists in the glassy state. The E_a values for β relaxation in sugars are between 40 and 70 kJ/mol.

When a glassy material is stored at a temperature between the Tg and the β relaxation, a microstructural change, corresponding to the approaching of the system to a metastable equilibrium, may take place with some extra loss in enthalpy and in volume. This phenomena called "physical aging" is considered as a continuation of the α relaxation.

A wide number of model and theories has been developed in an attempt to describe the molecular dynamic around the glass transition: they range from the free volume theory, (Cohen & Turnbull, 1959), the entropy controlled co-operative motions (Adam and Gibbs, 1965), to more modern theoretical approach such as the mode-coupling theory, MCT, (Sjogren, 1989) and hierarchical correlated molecular motions (Perez, 1994).

The free volume theory, as we have seen before, assumes that the fractional free volume becomes constant at a value of about 0.025 at the glass transition. Another relation, relating the free volume to the glass transition has been suggested by

Boyer and Simha in 1973. They derived an equation of the form: $f_g = 10^{-4} T_g + 0.07$.

The Adam and Gibbs theory (Matsuoka & Hale, 1997) treats the glass transition as a cooperative process, the degree of co-operativity increases when the temperature decreases. MCT considers density-density correlation function analysed in a framework of a generalized oscillation equation. Finally the theory of Perez consider a hierarchy of degree of freedom, from fast (corresponding to the secondary β relaxation) to slow (the main α relaxation). The slowest motions are possible only when the fastest have occurred with such amplitude that they leave enough free space. The relaxations α and β are linked and change in the latter have consequences on the former.

For more developments of these issues the reader is invited to refer to the bibliography.

2.3 Rheology

Rheology is defined as the study of the flow and deformation of materials, with special emphasis being usually placed on the former (Barnes, 2000).

This science has been developed particularly for synthetic polymers as rheology will determine the process variables required during extrusion and pressing processes and is also used to test the of the quality final products.

Rheology is not only of technical importance, in fact it constitutes a powerful tool to investigate the structure of materials, particularly regarding the study of amorphous phases.

The texture of many foods is controlled mainly by natural polymers, particularly polysaccharides and proteins, and for this reason the interests of researchers in application of synthetic polymer theories to food sciences have increased.

Studies on the rheological behaviour of food can contribute to the development of new techniques for the assembling and processing of food materials resulting in new products available to the consumer.

Rheology is also a powerful tool for the development of products with optimised texture quality, as well as for design optimisation and control of those processing units, where food structure, and hence rheology, plays a significant role (Windhab, 1995).

2.3.1 Rheology of sugar systems

The rheology of sugar systems is central to the understanding of confectionery products such as caramel.

The sugar most extensively studied has been sucrose. The viscosity of sucrose solutions has been reviewed by Mathlouti and Génotelle 1995.

Sugar solutions in water show Newtonian behaviour and the viscosity is independent of the shear rate. Figure 2.3 shows the viscosity of sucrose solutions as a function of concentration at 20ºC. Figure 2.4 shows a three dimensional plot indicating the effect of both concentration and temperature.

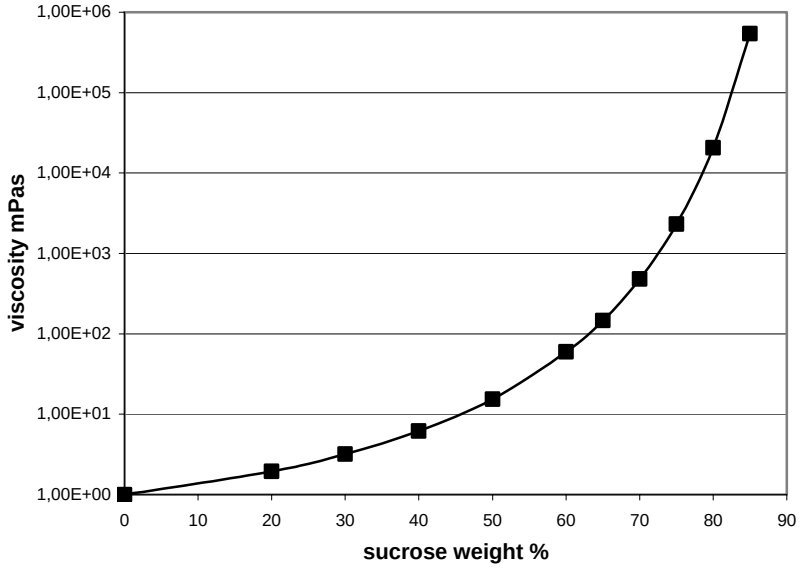

Figure. 2.3 Viscosity of sucrose solution as function of the concentration, adapted from Table 6.3 in Mathlouthi and Génotelle 1995.

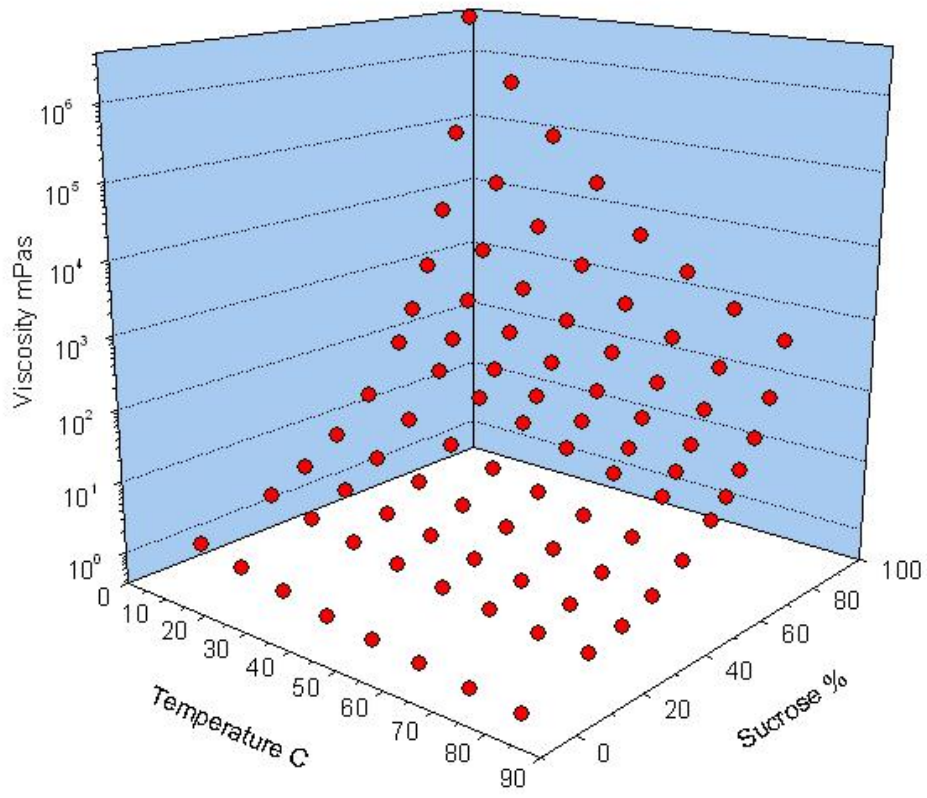

Figure. 2.4 *Temperature dependence of the viscosity of sucrose solution at different concentration, adapted from Table 6.3 in Mathlouthi and Génotelle 1995.*

In the high water content region the temperature dependence of viscosity can be expressed by an Arrhenius equation of the form:

$$\eta = \eta_0 \exp\left(-\frac{E_a}{RT}\right) \qquad \text{Eq.2.1}$$

with an activation energy, E_a, ranging from 17 K Joules/mole for the more dilute solutions to 105 K Joules/mole for the 85% sucrose solution.

At 20ºC amorphous sucrose enters the glassy state at a water content of 3%. This is illustrated in the state diagram (Figure 2.5)

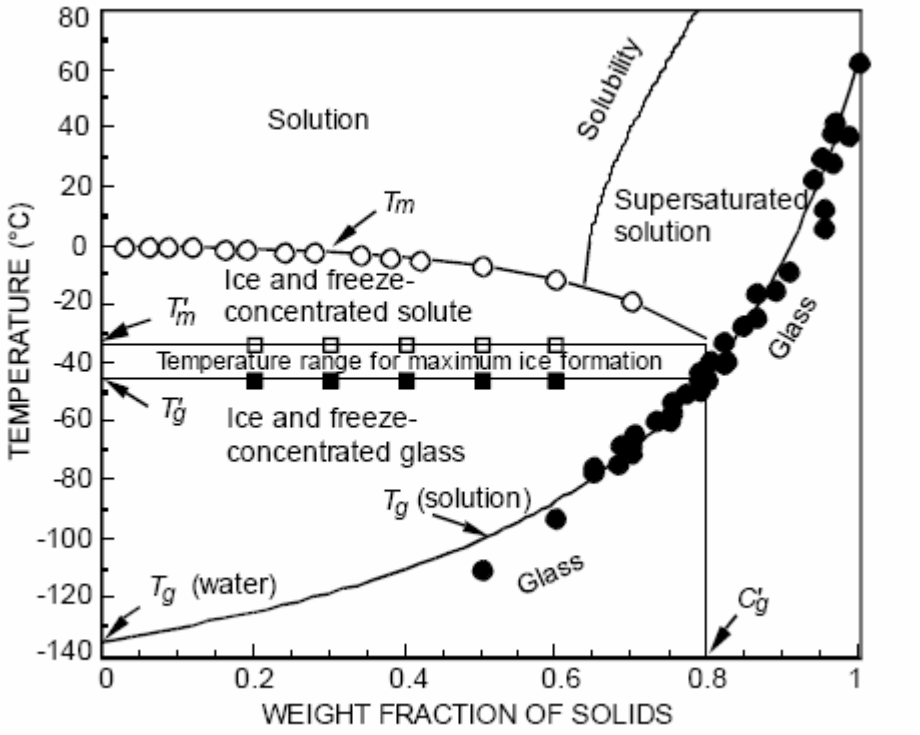

Figure. 2.5 State diagram of sucrose, adapted from (Roos 1995).
(We talk about state rather than phase diagram because as stated in section 2.2 the T_g is not a thermodynamic equilibrium event, in contrast to the melting transition)

Sucrose alone will crystallize between T_m and T_g but at concentration above the T_g this will be inhibited by kinetic effects. In many confectionery products the crystallization can be further inhibited by the presence of a second sugar.

The viscosity in the region above T_g is relevant to caramel rheology. This viscosity has been related to the glass transition by a Williams, Landel Ferry (WLF) equation based on the free volume theory.

For sugar solutions, the validity of WLF model (eq. 2.2) with the universal values of C_1 and C_2 has been also demonstrated (Maltini and Anese 1995; Cruz et al. 2001; Soesanto and Williams 1981). In this equation a_T is the shift factor required to superimpose rheological data obtained at temperature T to a reference temperature T_0.

$$\log a_T = -\frac{C_1^0 (T - T_0)}{C_2^0 + T - T_0} \qquad \text{Eq. 2.2}$$

The literature contains attempts to understand the physical meaning of these 2 constants. Angell *et al* (1994) on the basis of the equivalence of the WLF and Vogel-Tammann-Fulcher (VTF) models (eq. 4.8), attributed to C_1 the value of 16 or 17 and to C_2 a system-dependent value related to the fragility of liquids around the glass transition. Another approach involves the application of the free volume theory to the WLF equation. The constants $C°_1$ and $C°_2$ are equal to $B/2.303f_o$ and f_0 / α_f where f_0 is the dimensionless ratio of free volume to total volume, and α_f is the thermal expansion coefficient with the value of B being approximately unity. This approach has been used successfully in interpreting the viscoelasticity of high sugar biopolymer model systems (Kasapis et al, 2002, 2003).

Although these ideas have been not extensively applied to sucrose, the viscosity of many sugars at low water content has been interpreted using a similar approach.

2.3.2 Rheology of entangled polymers.

The first models (Lodge, 1964) to describe the rheological behaviour of polymeric melts or concentrated macromolecular solutions used a theory very similar to the theory of rubber elasticity. This is due to the fact that macromolecular liquids were similar to covalent crosslinked materials in the formation of a three-dimensional network that occupies all the volume. In the crosslinked materials chemical bonds between the chains were permanent, in the polymer melt or highly concentrated polymer solutions the links between the chains were temporary and they formed or destroyed under the effect of Brownian motion. The presence of these temporary links (entanglements) gave some elastic properties to the macromolecular liquid (Marrucci, 1986).

The theory of Lodge (Lodge, 1956) assumes that the formation and the destruction of the entanglements happens through states of equilibrium. The frequency with which the entanglements form or destroy is characteristic of the material at a certain temperature and its reciprocal is the relaxation time τ.

The stress-strain behaviour of an ideal rubber is given by:

$$\sigma = \nu kT\left(\frac{\lambda - 1}{\lambda^2}\right)$$

where ν is the so-called rubber factor (number of chains in the network per unit volume), k is the Boltzmann constant, and T the absolute temperature.

In the theory of Lodge a term was added to account for the impermanence of the links, and so the equation of the stress became:

$$\sigma = \nu kT \int_{-\infty}^{t}\left(\frac{\lambda(t',t) - 1}{\lambda(t',t)^2}\right)e^{-\frac{t-t'}{\tau}}dt'$$

where $\lambda(t',t)$ was the draw ratio reached in a range of time between t and t'.

The big difference between these two expressions is in the fact that in a rubber the stress is determined by only one deformation, λ, while in the case of polymeric liquids the stress depends on a weighted average of the deformations over time. The weight function for the deformation is called "*memory*" and in this case it is a simple exponential.

This theory was not able to explain some of the experimental evidence:

1. This theory was predicting constant viscosity ($\nu kT\tau$) but experimentally a strong decrease in the viscosity was observed when the strain rate was increased.

2. According to this theory the second normal stress difference, should have been zero and this was found not to be the case experimentally.

In the last 20 years the dynamics of entangled polymeric fluids has been one of the most rapidly advancing fields of soft condensed matter science (Marrucci, 2003). Until the 80s, polymer flow was only described phenomenologically by fitting the observed behaviour thought suitable and arbitrary extension of the Boltzmann equation. Early molecular approaches such as the Rouse and Zimm (Rouse, 1953; Zimm, 1956) theories were successful only for dilute solution but were inadequate for concentrated solutions and polymeric melts. The Rouse model replaces the polymer chain by a sequence of friction beads connected by springs. Predictions from this model matches the observed behaviour of polymeric melts of low molecular mass but fail completely at higher masses.

In Figure 2.6 relaxation spectra predicted by the Rouse theory are shown.

At low frequencies a proportionality was predicted between the loss modulus and the frequency and between the storage modulus and the frequency squared. At higher frequency for both loss and storage modulus the Rouse theory predicted

proportionality between both the loss and storage moduli and the square root of the frequency. Furthermore the Rouse theory presumed the viscosity to be proportional to the molecular weight or the concentration, but for macromolecular liquids over a critical value of concentration or molecular weight (Figure 2.7), the experimental viscosity was found to be strongly dependent on the concentration or molecular weight ($\eta \propto M^{3.4}$).

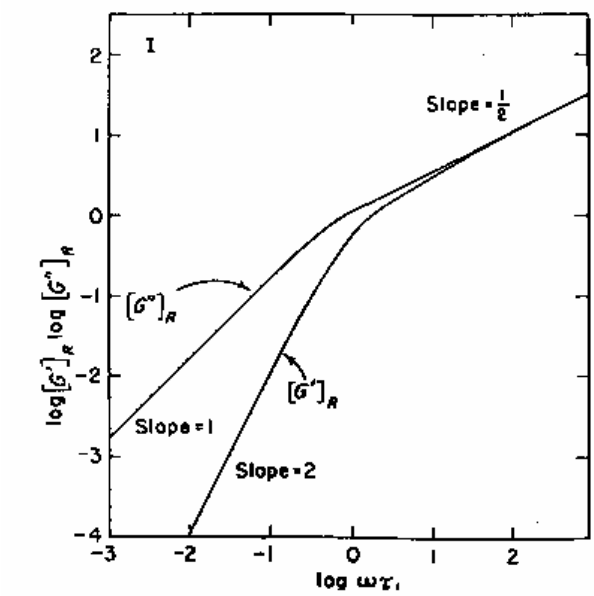

Figure 2.6. Prediction of the Rouse theory (De Mallie et al. 1962)

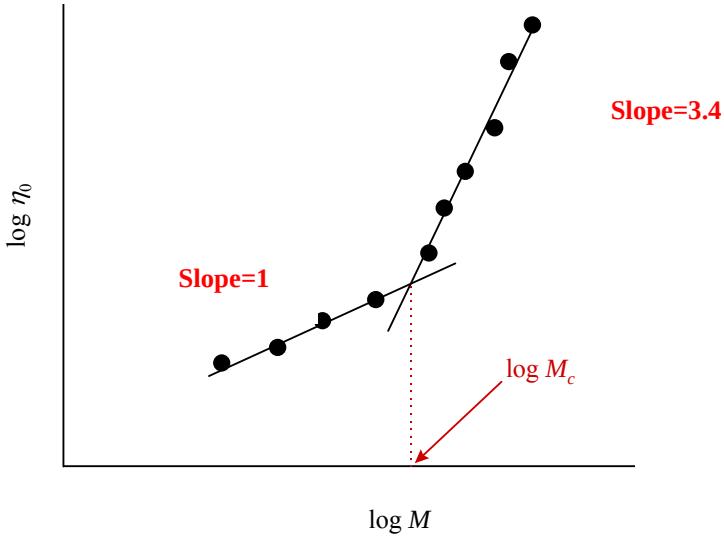

Figure. 2.7. Dependence of the viscosity on the molecular weight.

The failure of this theory was completely ascribed to the presence of "entanglements": High molecular weight, concentrated polymers in the liquid state interact with one polymer and hence their dynamics were strongly influenced by the constraint that the chains cannot cut across one another in their motion (Graessley, 1971).

Relaxation spectra with two distinct regions obtained for high molecular weight polymer melts was one of the pieces of the evidence of the presence of entanglements (Figure 2.8.).

The transition region at high frequencies was independent of chain length and therefore associated to local chain motions. The regions at low frequencies were associated with large scale rearrangements of chain conformation, and for a high molar mass sample with sufficiently narrow molar-mass distribution, was separate from the glass transition region. The resulting rubber like plateau region at intermediate frequencies was associated with a plateau modulus G_N^0. The experimental-observed viscoelastic response behaviour of entangled polymers could be summarised as follows (Watanabe, 1999):

- G_N^0 was independent of chain length, not sensitive to the temperature but it was decreasing upon dilution. The dilution dependence was essentially insensitive to both the solvent and polymer species (universal behaviour). The plateau modulus for the bulk polymer, $(G_N^0)_0$ related to that of the diluted species according to $G_N^0 = (G_N^0)_0 \phi^a$, where ϕ is the volume fraction of polymer in the solution and the exponent, a, lies in the range 2.0-3.0.

- The limiting value of the steady-state recoverable creep compliance J_∞, varied with the polymer concentration as: $J_\infty \propto \phi^{-a}$ and the product $J_\infty G_N^0$ was constant.

- The critical molar-mass from the bulk, viscous flow, Mc was insensitive to temperature, and was related to the volume-fraction of the polymer. $M_c=(M_c)_0\phi^b$ where b=a-1 and the product J_∞ M_c G_N^0 was an universal constant.

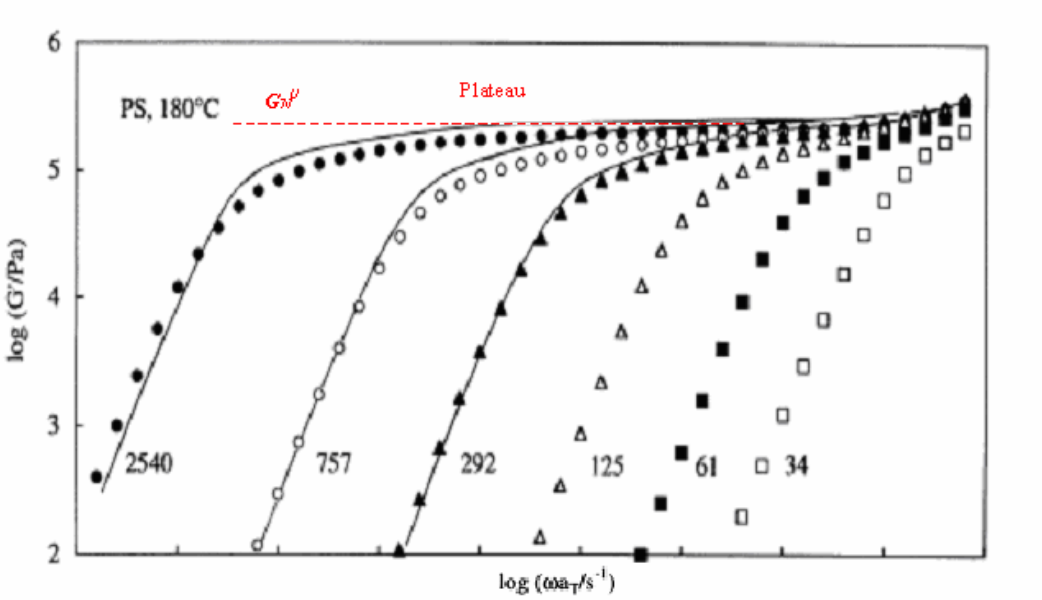

Figure 2.8. Storage modulus G' of bulk monodisperse linear polystyrene at 180ºC. The numbers indicate 10^3M. Adapted by Schausberger et al. (1985).

The first important step toward solving the entanglement problem was taken by Edwards (1967), who introduced the "tube" as a mean-field description of the topological confinement exerted on a given chain by the surrounding chains (Figure. 2.9A). Next de Gennes (1971) solved a fundamental aspect of the entangled dynamics by describing the diffusion of a chain along its own length, a process that was called "reptation" (Figure. 2.9B.). His theory was able to explain the dependence of the viscosity on M^3 (Marrucci, 1986). In this model, the long relaxation times are identified with the times necessary for a macromolecule to diffuse along to its own length. In this hypothesis the friction factor depends on the monomeric segments of the macromolecule and therefore is proportional to the molecular weight. The longitudinal diffusion of the macromolecule, D, is proportional to the reciprocal of the molecular weight. The time necessary for the chain to move in the distance L is:

$$t = \frac{L^2}{D}$$

In this case L is the distance of the tube that guest the polymeric chain and thence L is also proportional to the molecular weight M. Therefore the relaxation time t (the time for the chain to diffuse in the tube) will be proportional to M^3.

$$t \propto M^3$$

Finally, Doi and Edwards (1978, 1979) developed a full theory of the entangled state of liquid polymers by combining the idea of the tube with reptation. The tube and the macromolecular chain contained in it deform together. The different parts of the tube are orientated in different directions and hence they undergo different deformations. This implies that along the macromolecular chain, different stresses are applied on different parts of the macromolecule. The macromolecules can therefore relax through two main relaxation mechanisms. The first relaxation phenomenon, at short times, is to recover the equilibrium longitudinal stress. This happens through a mechanism where segments move from the least to the most stressed parts. The second relaxation process, at long times, is the diffusion of the macromolecule out of the deformed tube and the progressive creation of new tubes at equilibrium. This theory could explain the decrease in viscosity with the shear rate and also the existence of a second normal stress difference.

Although Doi and Edwards theory was successful in many aspects it was predicting an excessive shear thinning that would have caused highly unstable flow; subsequent developments were made successfully by Bent et al. (2003).

In today's theoretical picture, the tube experiences a Rouse-like motion due to aconstraint release, both thermal and convective in nature, while the chain within the tube undergoes reptation, fluctuation and possibly stretching (Marrucci, 2003) (Figure. 2.9C and D).

A summary of the effect of the dynamics of the polymer and particularly of the presence of entanglements on the viscoelastic response of the material is shown in Figure 2.10

Figure 2.10A. is a typical spectrum of a high molecular weight polymer. Clearly the viscoelasticity spectrum is divided into three frequency areas. In the area at very low experimental frequencies (very long timescale of the measurements), *viscous terminal region*, the loss modulus predominates over the storage modulus. At low enough frequencies G" is linear and G' is quadratic. At middle frequencies there is the *rubbery plateau region*, where the elastic behaviour dominates. A plateau for G' is observed and G" goes through a minimum. Finally, at high frequencies there is the *glass transition region.* In this region a crossover in G'G" at about 10^9Pa is observed. As the molecular weight is decreased (Figure 2.10B and C), the length of the rubber plateau, which is the distance between the two picks in G", diminished by a power of 3.4 of the molecular weight. The plateau reaches zero length at M_c, the critical molecular weight where the molecular weight of the viscosity decreases from $M^{3.4}$ to M.

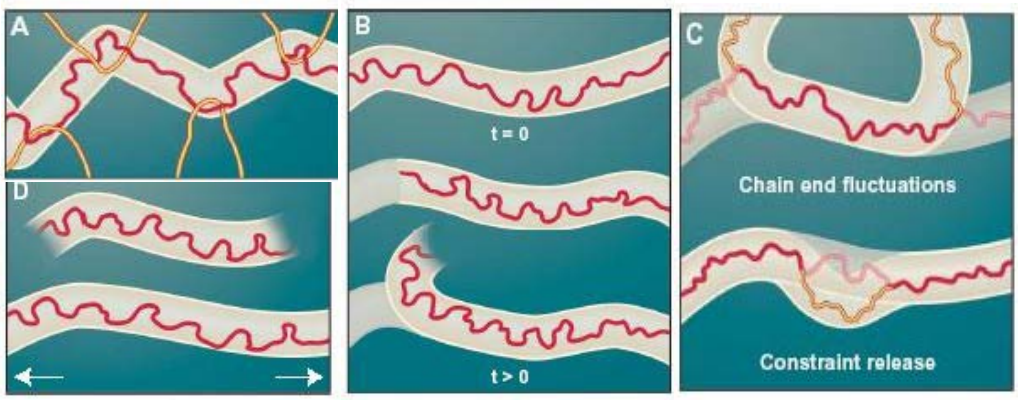

Figure.2.9. Polymer in motion, adapted from Marrucci, (2003).
(A) The motion of the red polymer chain is constrained by the surrounding orange chain, which cannot be crossed, as if the red chain were confined to a tube.
(B) The chain in the tube diffuses back and forth (reptation). Because the advancing chain end chooses its direction randomly, the tube continuously changes conformation.
(C) The tube may also relax through fluctuation of the chain ends (top) or when the motion of surrounding chains results in constrained release (bottom).
(D) In very fast flows, tube stretching may occur.

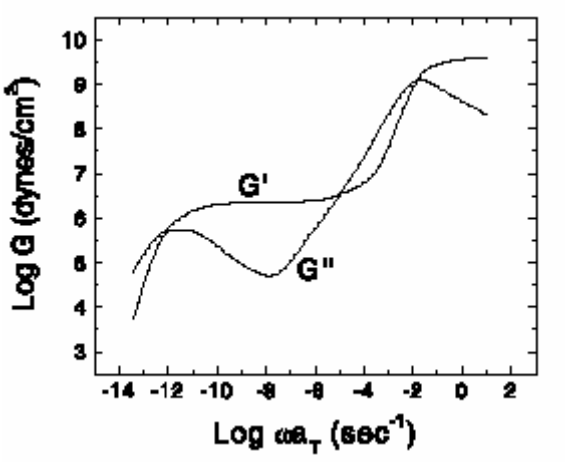

A

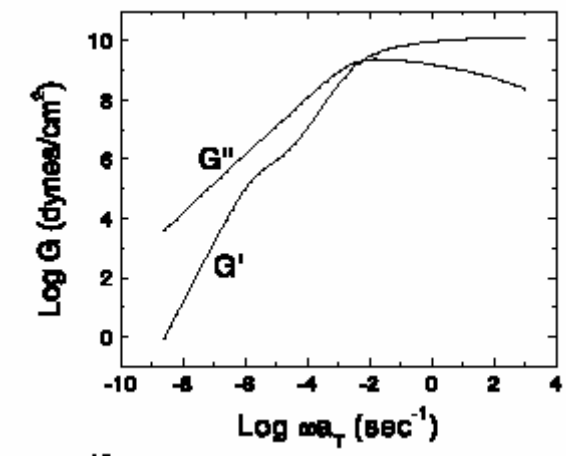

B

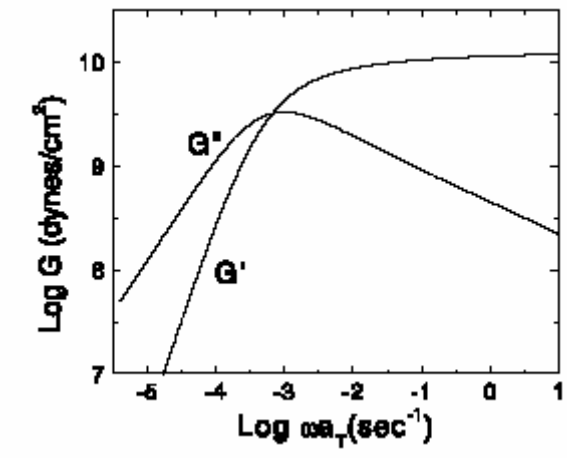

C

Figure 2.10. Mechanical spectra for (A) high-molecular weight entangled polymer (polystyrene $M=3.8\cdot10^6$), (B) low-molecular weight polymer (polystyrene $M=1.64\cdot10^4$), (C) non polymeric glass forming. Adapted from Plazek and Bero, (2002).

2.4 Structure and properties of some polymeric hydrocolloids: Carrageenan and Gellan gum

2.4.1 Carrageenan

Carrageenans are sulfated galactans found in numerous red seaweeds (Moirano 1977; Thomas 1999).

Traditionally Greek letters have been assigned comprised of certain idealised carrageenan disaccharides repeating units. (Figure 2.11)

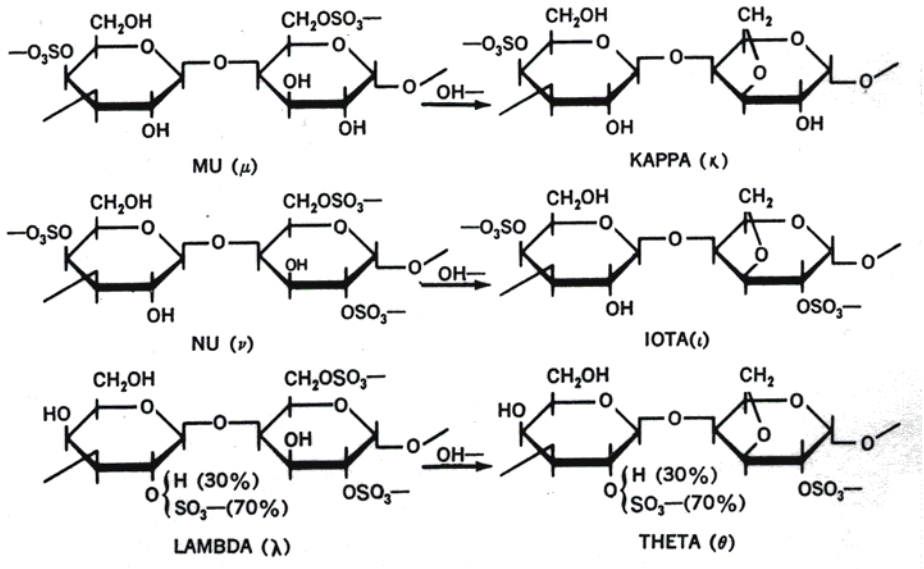

Figure 2.11 Repeating units of carrageenan (Moirano, 1977)

Native carrageenans often contain combinations of these idealised units, with variations in structure occurring not only between different species of seaweed but also within the different stages of a single species. Mu and nu carrageenan are the biochemical precursors of kappa and iota carrageenans. They both contain a sulphate ester group at position -6 on a 4- linked α-D-galactosyl unit. This affects the overall properties of the carrageenan by creating kinks in the polymer chain. As will be shown later, these kinks reduce the ability of the carrageenan to gel.

Another variety of carrageenan is lambda carrageenan that is the biological precursor of theta carrageenan but theta does not occur extensively in the seaweeds.

Kappa and iota carrageenans have the ability to form gels upon cooling hot solution. These gels are thermally reversible. According to Rees (Morris et al., 1980; Rees and Welsh, 1977), carrageenan forms a double helix responsible for the gelation.

Figure 2.12 shows the gel mechanism on heating or cooling: at temperature above the melting point of the gel, thermal agitation overcomes the tendency to form helices and the polymer exist in solution as random coil. On cooling, a three dimensional polymer network forms and the double helices form the junction points of the polymer chains (Morris et al., 1980; Robinson et al. 1980). Further cooling leads to aggregation of these junction zones through cations. κ-Carrageenan interacts specifically with K^+, Rb^+ and Cs^+. Iota carrageenan gels strongly with some divalent ions Ca^{2+} normally being used. Neither form gels with Na^+ ions .

The effect of sulfation on gelling properties can be explained sterically on the basis of the double helix secondary structure.

Sulfate at the carbon in position 2 of the 1-3 linked units occurs in lambda carrageenan and acts as wedging group to prevent the double helix formation. Sulfate on the carbon in position 4 on the 1-4 linked galactoside, as occurs in kappa and iota projects outward and does not interfere with double helix formation (Rees et al., 1969).

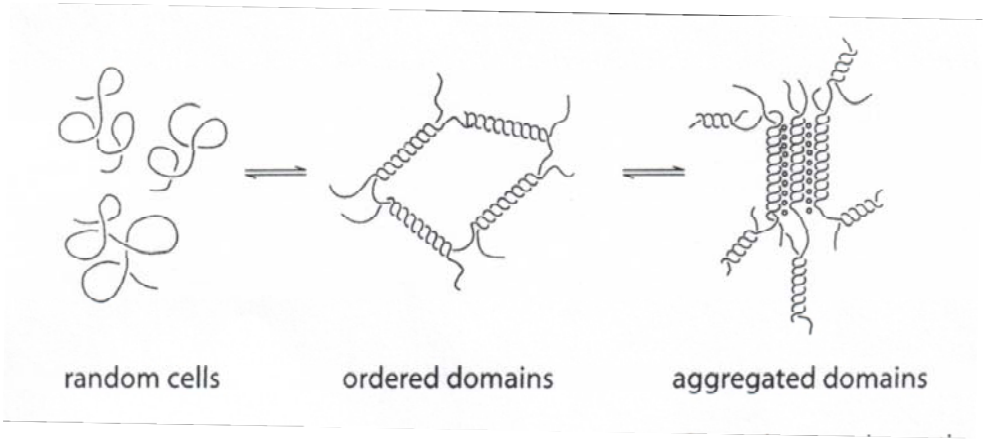

Figure 2.12. The domain model for carrageenan gelation ●-gel promoting cations. (Morris et al. 1980)

The inhibitory effect of kinks in the polymer can be seen in Figure 2.13.

Sulfation on the carbon in position 6 of the 1-4 linked galactoside forms kinks in the chain which tend to inhibit double helix formation (mu, nu and lambda).

Figure 2.13 shows that where a 1-6 linked unit is 6-sulfated, it tends to exist in the C1 chair conformation and this produce a kink in the chain. Closure of the ring to form the 3,6 anhidride, constrains the 1,4 pyranose unit to the 1C form with resultant removal of the kink.

The presence of the 3,6 anhydride leads to greater regularity in the polymer which results in enhanced gel potential due to the increased capability to form double helix. Thus the higher is the conversion in kappa and iota carrageenan with the conversion to the 3,6 anhydride, the higher is the gelling potential. For lambda the presence of the sulphate in position 2 of the 1,3 linked galactoside precludes the gelation and consequently the gelation will not be affected from the conversion in 3.6 anhydride.

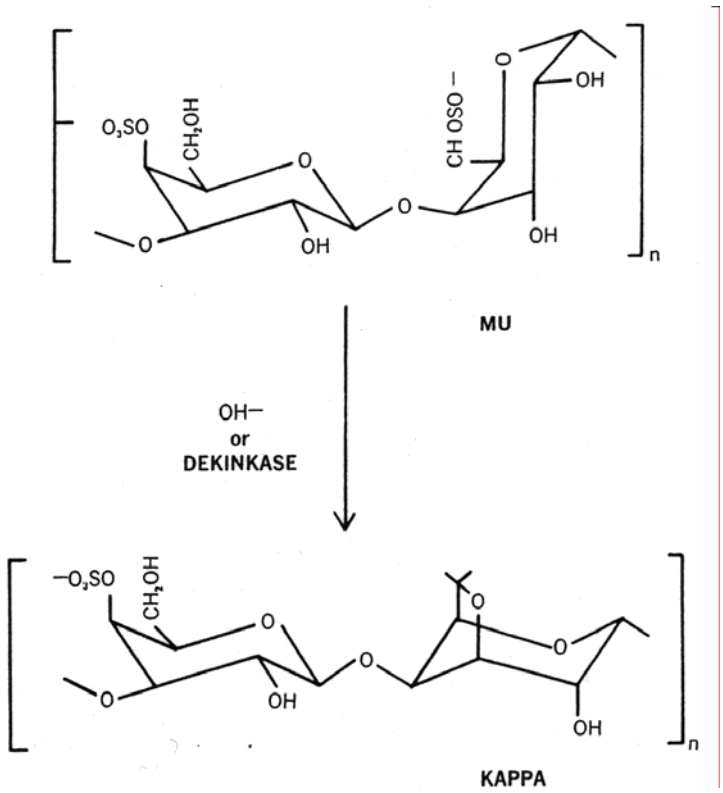

Figure 2.13 Change of conformation for the formation of the 3,6 anhydride (Adapted form Mueller and Rees, 1967)

Carrageenan gels are thermally reversible. The gelling temperature of a specific type of carrageenan is not sensitive to the carrageenan concentration and depends primally on the concentration of the gelling cation present.

All the carrageenans have the ability to form milk gel on cooling a solution of carrageenan in hot milk.

Since lambda that does not form gels with cations but forms milk gels the mechanism of gelling is not attributable to the presence of Ca^{2+} in the milk but may be attributable to formation of carrageenan-casein interactions (Figure 2.14).

Mangione et al (2003) reported gel-sol transitions temperature on cooling at about 22ºC and on heating in a range between 25 and 32ºC for solution of κ-carrageenan

concentration of 0.05, 0.1 and 0.2 % w.w.b. (wet weight basis) and salt concentration of 10 mM KCl.

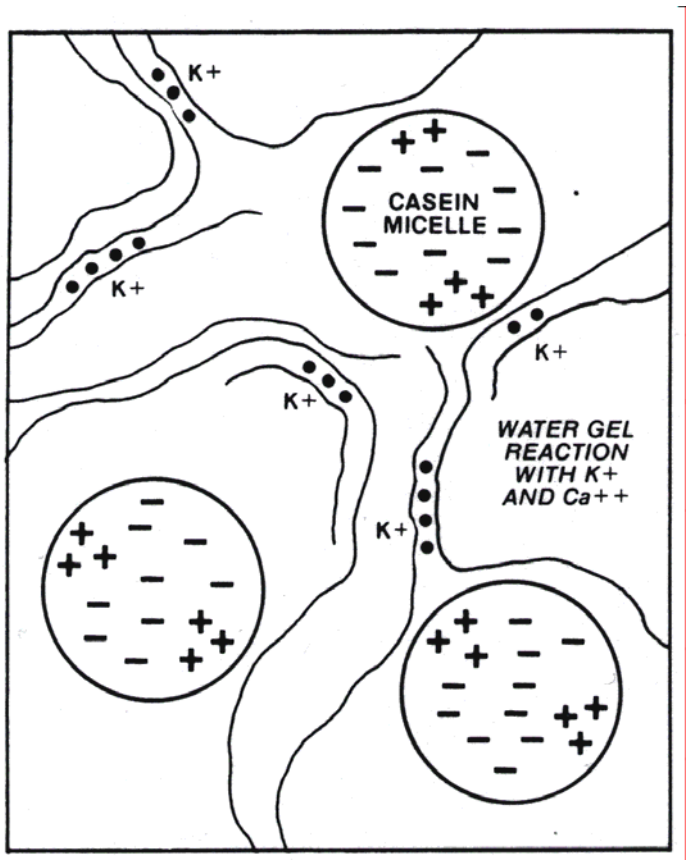

Figure 2.14 Carrageenan synergy with milk proteins. Adapted from Thomas, 1999.

2.4.2 Gellan gum

Gellan gum is a bacterial exopolysaccharide, discovered through the screening of thousands of bacteria and prepared commercially by aerobic submerged fermentation from *Sphingomonas elodea.* (Gibson and Sanderson 1999)

It has been used as a texture modifier to control viscoelasticity in the food industry and as a culture medium in biotechnology because it forms transparent gels which in the presence of calcium chloride are resistant to heat and acid. It consists of a tetrasaccharide unit, β-D-glucose, β-D-glucuronic acid, β-D-glucose and α-L-rhamnose.

The polymer as secreted by the microorganism, contains approximately 1.5 acyl substituents per tetrasaccharide repeating unit (Figure 2.15).

The commercial product is de-esterified by alkali and consists of an unsubstituted polymer with a well defined tetrasaccharide repeating unit (Figure 2.16)

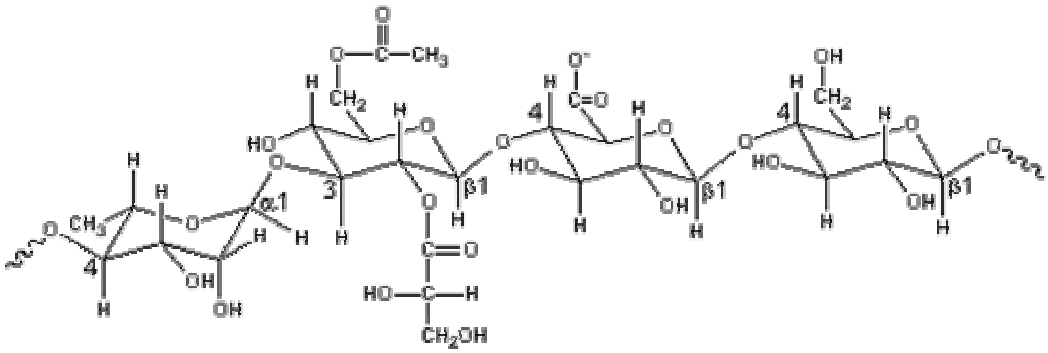

Figure 2.15 Substituted tetrasaccharide repeating unit of gellan gum; adapted from Gibson and Sanderson (1999)

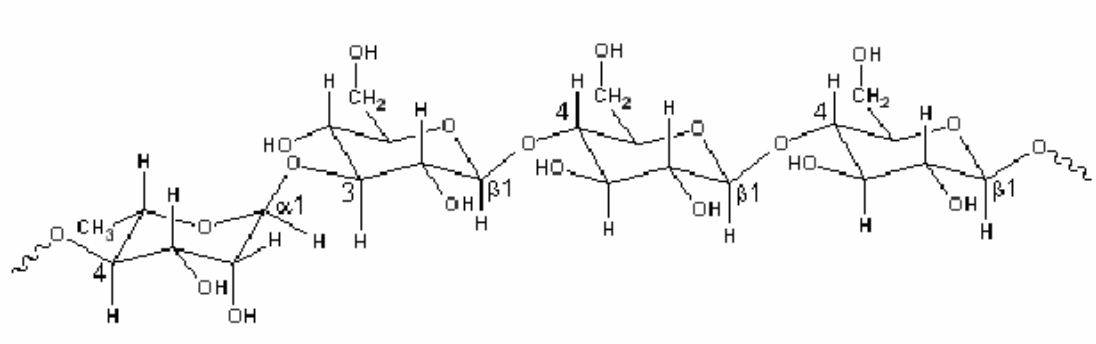

Figure 2.16 Unsubstituted tetrasaccharide repeating unit of gellan gum; adapted from Gibson and Sanderson (1999).

It is believed that gellan molecules form double helical conformations in solutions at lower temperatures, and above a certain critical concentration, they form aggregates which play the role of junction zones, resulting in a three-dimensional network.

In the solid state (Caroll et al., 1982, 1983; Upstill et al., 1986), gellan gum forms a coaxial triangular 3-fold double helix (pitch 56.4 Å) from two left-handed chains coiled around each other with the acetate residues on the periphery and glyceryl groups stabilizing the interchain associations.

The gel mechanism in water is not fully understood, but many authors believe that gelation initially occurs by the formation of the double helices followed by ion induced association of these double helices. Gunning and Morris in 1990 suggested that heating and cooling in the absence of gel-promoting cations favors the formation of fibrils by double helix formation between the ends of neighbouring molecules (Figure 2.17). When cations are present these fibrils associate, with the formation of the gel. Morris and colleagues in 1996 studied the effect of acyl substituents on the gel formation and they found double helix aggregation with formation of brittle gel when acyl substituents are absent and helix-helix aggregation resulting in elastic gel formation when acyl substituents are present (Morris et al., 1996).

Gelation depends on the ionic strength and the identity of the cation. Gellan gum will gel most strongly with divalent cations such as Ca^{2+} or Mg^{2+}.

A gel-sol transition occurs at about 50°C dependent on concentration.

The strength of gellan gum gels increases with the gum concentration. Compared with agar or κ-carrageenan gellan gum are stronger at equal gum concentration.

Thermoreversible gels form on cooling in the presence of cations even at low (0.1% w/w) concentrations.

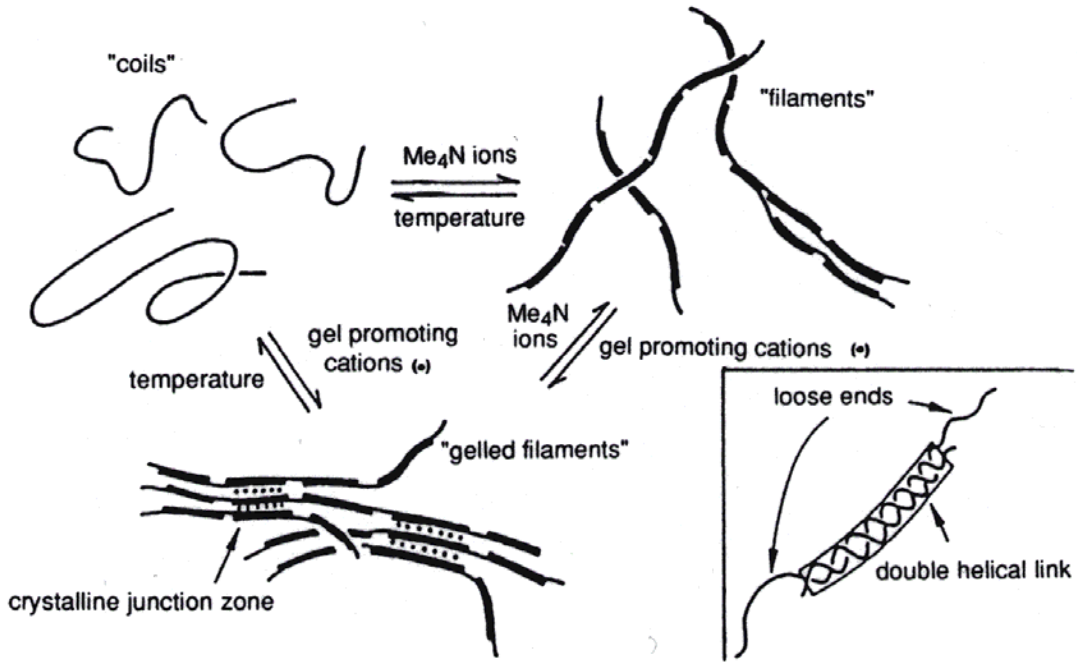

Figure 2.17 Model for gelation of gellan gum (Gunning and Morris 1990).

2.4.3 Effect of added co-solute in hydrocolloids

The effect of the addition of co-solute such as sugars and glucose syrups to carrageenan and gellan gum has been investigated by different authors. Addition of sugars at levels of up 40 or 50% creates gels which are stronger and more thermally stable then gels without sugars. At higher level of co-solute there is a dramatic drop in the network strength.

Kasapis and colleagues have investigated the effect on the glass transition temperature of the addition of co-solute in 0.5% κ-carrageenan gels (Evageliou, Kasapis et al. 1998; Kasapis 2001). By using small deformation dynamic oscillation, he found that addition of small amounts of κ-carrageenan (with potassium chloride) increase the glass transition temperature in systems containing 75% 80% and 85% mixtures of sucrose and glucose syrups. In contrast Kumagai et al. (2002) have found that the glass transition determined by using both NMR and calorimetric techniques of highly concentrated sugar systems was not affected by the presence of 0.9% κ-carrageenan. They attributed this discrepancy to the difference in sensitivity of the calorimetric and rheological techniques. The small deformation rheological test was sensitive mainly to the polysaccharide network while calorimetry monitored the most abundant component which was the sugar solution. In another report published by Kasapis and co-workers (Deszczynski, et al. 2002) they found that when the concentration of κ-carrageenans was 0.7% and sugars co-solute were 90% again the glass transition determined with rheological techniques was coincident with the glass transition determined calorimetrically. On the basis of these results it can be supposed that while the calorimetric response is sensitive to the high sugar matrix, the rheological response is sensitive to the polymer network until a very high concentration of the sugar co-solute is reached. Beyond this limit the amount of network is no longer able to affect the rheological response and the calorimetric and rheological glass transition temperatures will coincide.

Very similar studies have been also done on gellan gum systems. Sworn and Kasapis (1998) analysing systems where gellan gum concentration ranging from 0.72% to 0.82% with sugars co-solute ranging from 70 to 80%, concluded that the addition of gellan gum to high sugar solutions had marked effects on the flow properties of the system and also accelerated its vitrification.

CHAPTER 3. MATERIALS AND METHODS

This chapter describes the materials and the basic concepts of the methodologies used. A standard format was used: after a short introduction to the physical principles of the method, the details of the experimental procedure and parameters adopted are described.

3.1. MATERIALS

The materials used for the preparation of caramel systems (studied in chapters 4 and 5) are described in this section.

3.1.1. Caramel model systems (Chapter 4)

Commercial glucose 63DE and high fructose glucose syrups (HFCS) were supplied from Cerestar (Italy). Sweetened condensed milk (73% bulk skim) and

vegetable fat (100% palm kernel oil) were provided by Nestlé (York). Sodium carbonate and Sodium chloride have been purchased from the Sigma Chemical Co. (Poole, UK).

3.1.2. Modified recipes (Chapter 5)

κ-Carrageenan (Viscardin SD389) has been purchased from FMC Biopolymer Philadelphia USA. Gellan gum was supplied by Kelco Biopolymers. Sodium citrate was purchased from Sigma Chemical Co. (Poole, UK). The purity of both the hydrocolloids is unknown. All the other ingredients in the formulation (commercial grade) contain some impurities. However their contribution is negligible in relation to concentration (0.2% ash ref. Tables 4.1 and 5.1). Furthermore eventual enzyme residues would have been inactivated during the cooking process.

3.2. METHODS

3.2.1 Sample Preparation

3.2.1.1 Standard caramels

The samples were prepared using the common formulation shown in Table 3.1.

The ingredients were mixed and cooked in a BCH pan (20kg copper bottomed, steam heated, boiling pan with a scraped surface stirrer and extraction fan).

Different samples were obtained by cooking the caramel to 4 different final temperatures: 113.0, 117.0, 120.0 and 122.4 ºC. The temperatures are an average of the measured temperature in five different zones of the BCH pan.

Emulsification and premixing have been performed at a temperature of 80°C using a Silverson high shear mixer, then the caramel has been cooked under gentle agitation until the final temperature was reached. A rapid cooling stage followed the cooking was used in order to stop further Maillard reaction development.

Table 3.1 *Common formulation of caramels*

	% weigh (w.w.b.)
63 DE glucose syrup	60.0
HFCS	18.0
Vegetable fat	11.4
Sweet Skimmed Condensed milk	10.0
Salt	0.4
Sodium carbonate	0.2

3.2.1.2 Caramel containing hydrocolloids

Caramels containing κ−carrageenan or gellan gum were prepared following the method described for the standard recipe caramels (section 3.2.1.1). The final cooking temperature was 117°C. The new ingredients were incorporated during the emulsification stage. Table 3.2 shows the formulation of the caramels containing the hydrocolloids

Table 3.2 *Formulations for the caramels containing hydrocolloids*

Sample	Gelgum01	Gelgum02	Gelgum04	Carr005	Carr01	Carr02
63 DE glucose syrup	59.1	59	59	59.95	59.9	59.9
Invert sugar	20	20	19.8	18	18	17.9
Vegetable fat	10	10	10	11.4	11.4	11.4
Sweet Skimmed Condensed milk	10	10	10	10	10	10
salt	0.4	0.4	0.4	0.4	0.4	0.4
Sodium carbonate	0.2	0.2	0.2	0.2	0.2	0.2
Carrageenan		-	-	0.05	0.1	0.2
Gellan gum	0.1	0.2	0.4	-	-	-
Sodium citrate	0.2	0.2	0.2	-	-	-

3.2.2. Analytical methods

3.2.2.1. Moisture content determination.

The moisture content was determined gravimetrically using an oven drying method. The samples were dried using a vacuum oven at 70°C for 16 hours. These relatively mild conditions were selected to minimise further caramelisation and Maillard reaction developments which could lead to erroneous values of moisture content. Each measurement was done in triplicate. All moisture content values are reported on a percentage wet weight basis i.e. g of water per 100g of total sample weight (% w. w.b.).

3.2.2.2. Differential scanning calorimetry

Differential Scanning Calorimetry (DSC) is a thermal analysis technique used to measure changes in heat flows associated with material transitions. DSC measurements provide both qualitative and quantitative data on endothermic (heat absorbing) and exothermic (heat evolving) processes. DSC is commonly used to determine the glass transition temperature and crystalline melting point of polymeric materials, and recently has become one of the main tools used in food science in order to obtain valuable information on the thermally induced changes in food systems (John and Shastri, 1998).

3.2.2.2.1. Basic principles of the technique.

There are two different designs of DSC systems: power compensated DSC (Figure 3.1) and heat flux DSC.

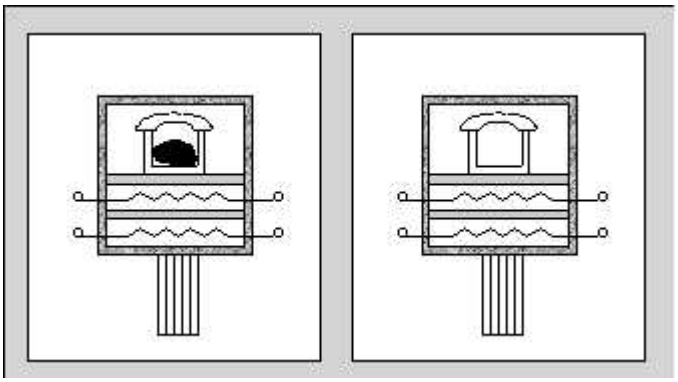

Figure 3.1. Schematic diagram of power compensated DSC.
Left: sample chamber. Right: reference chamber. In each chamber: microfurnace with (1) heater and (2) temperature sensor**.**

Both designs involve heating a sample pan and a reference pan through a programmable temperature profile. Heat flux DSC uses the same heater to heat both sample and reference, determining enthalpy changes through a measurement of the temperature difference between them. Power compensated DSC has separate heaters

for the sample and the reference and records the difference in electrical power required to heat up (or hold at constant temperature) the sample at the same rate as the reference.

The differential power $\frac{dQ}{dt}$ is measured ((MacNaughton and Mortimer, 1975):

$$\frac{dQ}{dt} = \frac{dQ_s}{dt} - \frac{dQ_r}{dt} \qquad \text{Eq. 3.1}$$

where, $\frac{dQ_s}{dt}$ is the heat input for the sample and $\frac{dQ_r}{dt}$ is the heat input in the reference.

The extra energy required to heat the sample when a first order thermal transition occurs is reflected by an endotherm, whereas an exotherm indicates release of energy by the sample and thus reduced energy input from the heater (MacNaughton and Mortimer, 1975).

Working in non-isothermal mode allows evaluation of the specific heat as well as enthalpy of crystallisation and fusion of a material. The recorded power is divided by the sample weight to produce the heat flow. The definition of specific heat is the quantity of energy required to raise the temperature of 1g of material by 1°K without a change of state. C_p ($J.g^{-1}.K^{-1}$) is obtained from:

$$C_p = \frac{\frac{dQ_s}{dt}}{\frac{\Delta T}{dt}} \frac{1}{m} \qquad \text{Eq. 3.2}$$

where $\frac{dQ}{dt}$ is the recorded differential power (J/s), $\frac{\Delta T}{\Delta t}$ the heating rate (K/s) and m the sample weight (g).

The results from DSC experiments are displayed as a thermal analysis curve in which the instrument signal (heat flow) is plotted against temperature or time. In fig 3.2 a simple and ideal thermogram for a generic material is shown.

At lower temperatures the system is in the glassy state, at the temperature T_g a change in slope indicating a second order transition (involving a change in heat capacity but no variation in latent heat) ascribed to a glass transition is observable. At this point the system is in the rubbery state, and the high mobility of the systems allows the molecules to rearrange to reach all the kinds of order (constitutional, configurational and conformational) necessary to allow crystallization to occur; this is represented by the exothermic event at T_c.

When enough temperature to break the crystalline structure is reached (T_m), a melting endothermic peak is observable.

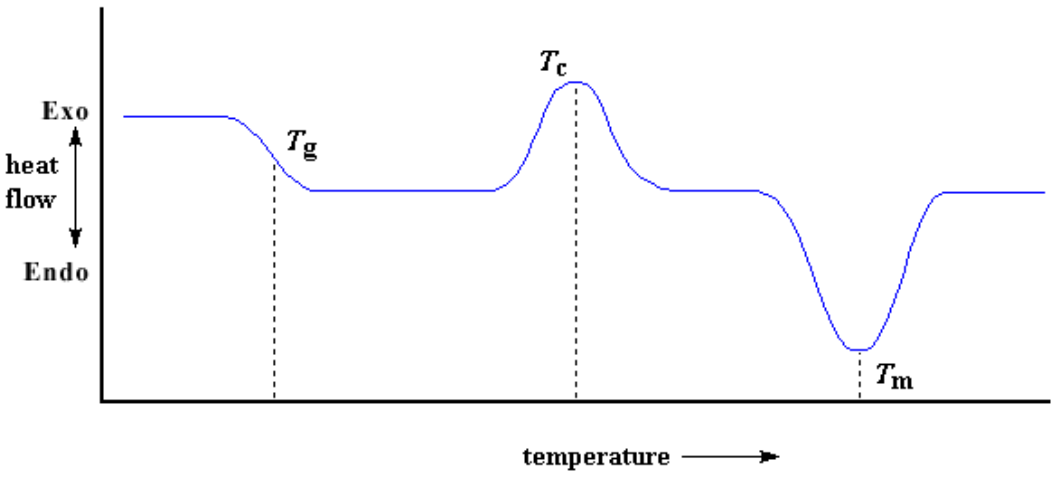

Figure 3.2 Schematic representation of a dynamic thermal analysis curve

3.2.2.2.2. Experimental conditions

DSC experiments were carried out using a Perkin Elmer DSC7. The instrument was calibrated for temperature and enthalpy with indium (To=156.6°C and H=28.45

J.g-1) and cyclohexane (To=6.7°C). Dry air was used as a purging agent over the head. Cooling was achieved with an intra-cooler allowing a temperature down to -60°C to be reached.

The samples of~5mg were sealed in aluminium DSC pans and scanned at 10ºC/min from -60ºC to 80ºC. After cooling at 50ºC/min an immediate rescan was run for each sample to eliminate relaxations and improve interpretation of the thermograms.

The glass transition temperature was taken as the onset temperature of the glass transition range. The Pyris analysis software calculates this automatically.

3.2.2.3. Wide angle X-ray diffraction.

X-ray diffraction probes the structure at a distance varying from a few Å (wide angle x-ray diffraction) to 10 nm (small angle x-ray diffraction). While amorphous systems give rise to diffuse x-rays patterns, in contrast, crystalline systems yielding well-defined sharp peaks, which are characteristic of the crystal geometry (Ewing, 1960). Therefore, it has the ability to distinguish between ordered and disordered states. It permits the analysis of crystalline substances with a high degree of accuracy and specificity.

3.2.2.3.1. Basic principles of the technique

A crystal lattice is a regular three dimension distribution (cubic, rhombic,...) of atoms in space. These are arranged so that they form a series of parallel planes separated from one another by a distance ***d*** which varies according to the nature of the material. According to the Bragg's law (eq.3.3), when a monochromatic beam of x-rays with wavelength λ is incident on a lattice plane of a crystal at an angle θ,

diffraction occurs when the distance by the rays reflected from successive planes differs by a complete number of wavelength. Varying and plotting the angular positions and intensities of the resultant diffraction peaks produces a pattern which is characteristic of the sample. When a mixture of different phase (amorphous and crystalline) is present, the diffractogram is formed by addition of the individual patterns. The sharper the peaks of the diffractogram, the finer the crystalline structure (Alexander, 1969).

$$n\lambda = 2d \sin \theta \qquad \text{Eq. 3.3}$$

Where n is a positive integer and defined as the reflection order.

The range of angles covered determines the technique of X-ray diffraction. Small angle X-ray diffraction scattering (SAXS) involves X-ray diffraction studies for scattering angles 2θ smaller than 3° whereas wide angle scattering (WAXS) deals with 2θ angles up to 180°. In this work, only WAXS measurements were performed.

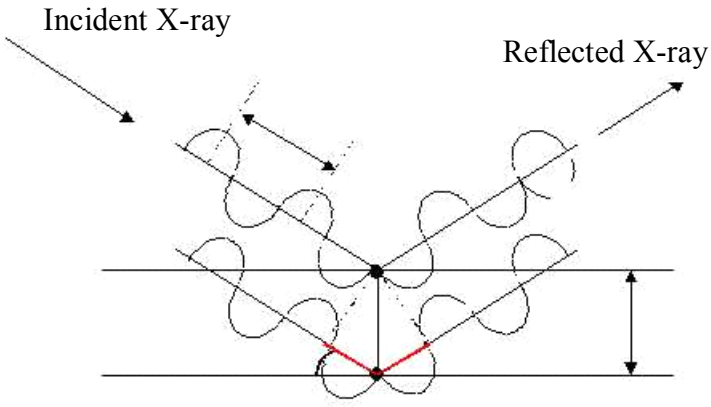

Figure 3.3 Path length difference between incident x-rays scattered by the electrons of two atoms.

3.2.2.3.2. Experimental conditions

X-ray diffraction has been performed in order to have a qualitative analysis of the crystallinity of materials relevant to this project.

The samples were placed on a holder and were analysed using a Bruker AXS D5005 X-ray diffractometer. The X-ray generator was equipped with a copper target, operating at 40kV and 50mA and produced CuK α radiation of approximately 1.54 Å wavelength. Data were recorded over an angular range between 4° to 38° (2) with an interval of 0.05°. The time spent to acquire the diffracted X-rays at each angle interval depended on the signal/noise ratio and was 3s.

3.2.2.4. Light microscopy

Polarised light microscopy was used to see the morphology of the caramels cooked at boiling temperature of 117C. The microscope used was a Leitz Diaplan scientific optical microscope with Lamphousing 103 Z, UKO universal condenser. The microscope was equipped with a heating stage from Planer Ltd. (UK). Photos were taken using a K1000 Pentax Camera fitted to the microscope. The scale was estimated with a standard graticule. These measurements were performed by Dr. R. Abeysekera at the University of York

3.2.2.5. Particle charge detector (Mutek)

Particle charge detectors are widely used in paper industry and in research on colloidal systems. This measuring system uses polyelectrolyte titration and /or acid/alkali titrations to determine total charge and isoelectric point respectively.

3.2.2.5.1. Basic principles of the technique

The main element of a particle charge detector is shown in Figure 3.4. A cylindrical vessel (1) with an oscillating displacement piston (2) forces the colloidal solution through the annular space between piston and bore. The movement of the piston creates a streaming potential between two electrodes (3) above and below the bore.

The absorption of particles, gelatin or other polymer molecules to the surface of the vessel and piston (made in PTFE) is due to Van der Waals forces. The flow induced by the oscillating piston causes the diffuse outer part of the electric double layer to be sheared off. The induced streaming potential is processed electronically and monitored on a display.

3.2.2.5.2. Experimental conditions

Solutions were prepared by dissolving 10g of each sample of caramel in 100ml of distilled water, and were titrated with HCl 0.1N until the point of zero charge (streaming current=0mV), the isoelectric point was reached. Mutek particle charge detector PCD 03 pH was used to monitor the steam current. Three replicates were done for each sample and the results were expressed as the average value ± standard deviation.

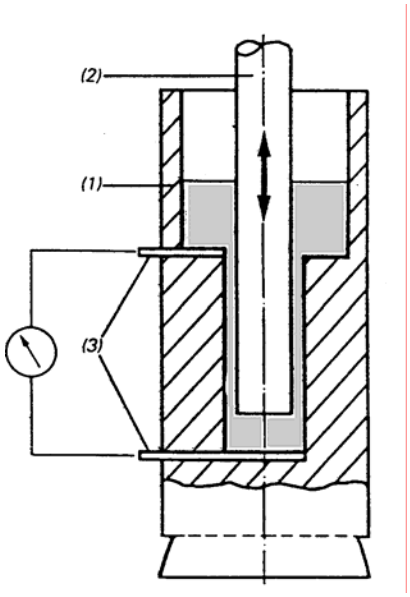

Figure. 3.4 Schematic representation of a particle charge detector

3.2.3. Rheological methods

Rheology has been properly defined by Prof. Bingham (Barnes et al., 1989), as the study of the flow and deformation of materials. In flow, elements of the liquids are deforming, and adjacent points in the liquids are moving relative to one another.

There are two basic kinds of flow with relative movement of adjacent particles of liquids; they are called shear and extensional flows. In shear flows liquid elements flow over or past each other, while in extensional flow, adjacent elements flow towards or away from each other (Figure 3.5).

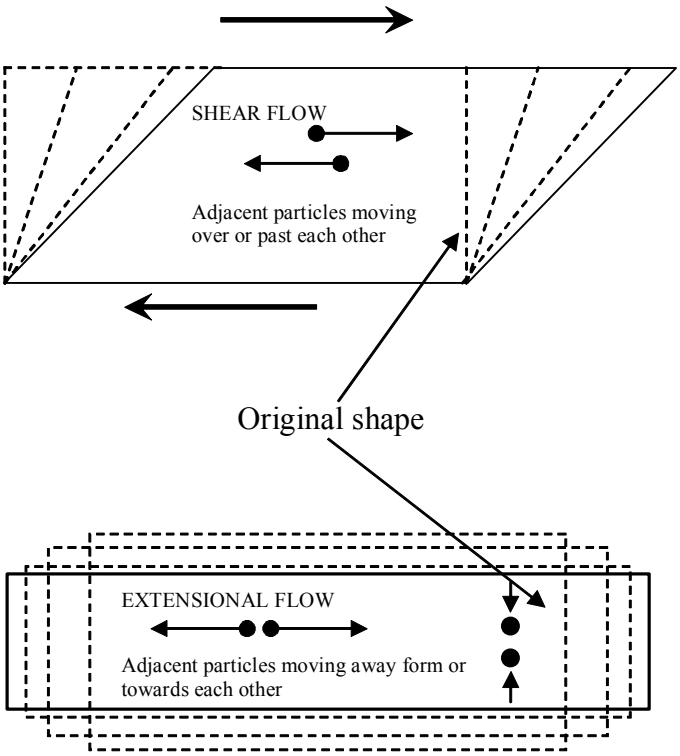

Figure 3.5 Particle motion in shear and extensional flows**.**

Two different rheological techniques have been used in this work, rotational rheometry, allowing the study of the shear flow, and high pressure capillary rheometry, allowing the study of both shear and extensional flow.

3.2.3.1 Rotational rheology

Viscosity is the internal friction of a fluid or its tendency to resist to flow. Liquids are made to flow by imparting a velocity by applying a force. For a given velocity the resulting force increases when the viscosity is increased, whereas for a given force, the velocity is reduced when the viscosity is increased. In Figure 3.6 the shear flow is visualized as the movement of hypothetical layers of fluid sliding over each other. In the simplistic case the velocity of each layer increases linearly with respect to its neighbour below, so that the layers twice the distance from any stationary edge

move at double the speed. The gradient of the velocity in the direction at right angles to the flow is called shear rate ($\dot{\gamma}$). In this simple example, the shear rate is the ratio between the velocity u and the distance h of the layer from the stationary edge. The force per unit area creating or produced by the flow is called the shear stress (σ = F/A). The apparent viscosity (η_a) is the ratio between the shear stress and the shear rate

$$\eta_a = \frac{\text{Shear Stress}}{\text{Shear rate}} = \frac{\sigma}{\dot{\gamma}}. \qquad \text{Eq 3.4}$$

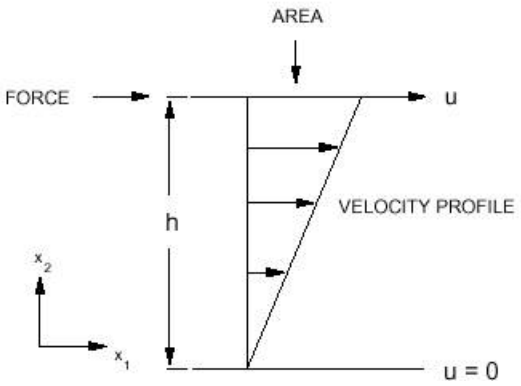

Figure 3.6 Shear flow

3.2.3.1.1 Principle of operation of rotational rheometers and viscometers.

The principal components of a controlled stress Rheometer are shown in Figure 3.7.

The rheometer has a constant torque motor which works through a drag cup system. An angular position sensor detects the movement of the measuring system attached to the shaft.

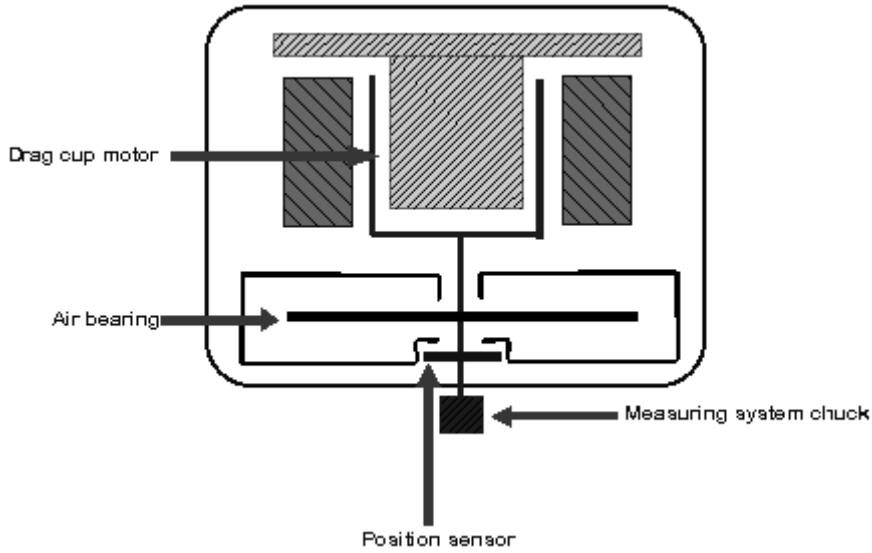

Figure 3.7 Components of a controlled stress rheometer

Modern rheometers have software that automatically converts the applied value of torque to a shear stress when displaying data. The reading from the position sensor is converted to a strain. The conversion factors used depend on the type of measuring system.

The principal components of a controlled rate rheometer are shown in Figure 3.8.

The rheometer is a constant speed motor with a torque detection system. The torsion bar is suspended on an air bearing to give a virtually frictionless bearing.

When the drive system turns, the sample resistance (viscosity) tries to twist the

torsion bar. By measuring the resultant twist and knowing the stiffness of the bar, the torque is obtained.

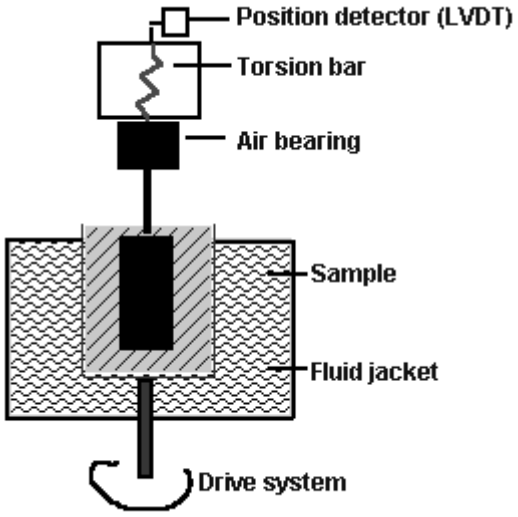

Figure 3.8 Components of a controlled rate rheometer

The measuring systems used in this work were:

(1) Cone and Plate
(2) Parallel Plates
(3) Cup and bob

The choice of the appropriate geometry depended on the kind of test need to perform and on the physical characteristic of the material analyzed.

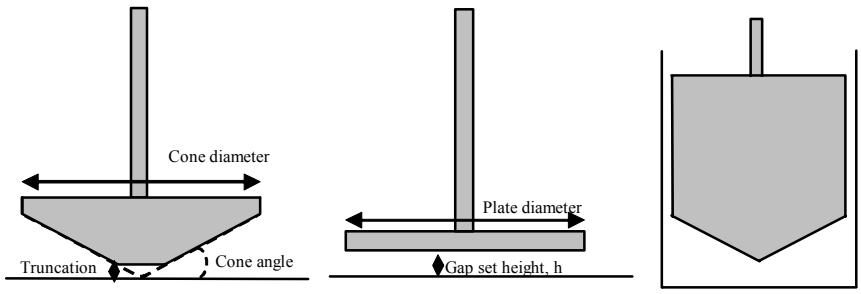

a b c

Figure 3.9 Cone plate (a), parallel plate (b) and cylindrical concentric geometries (c)

Figure 3.9 shows a schematic representation of the cone plate (a), parallel plate (b) geometries and cylindrical concentric geometry (c).

The torque and angular velocity is multiplied by the "form factors" C_1, and C_2 to give the shear stress, σ, and the shear rate, $\dot{\gamma}$, respectively.

Shear Stress $\sigma = C_1 \times M$ Eq. 3.5

Shear Rate $\dot{\gamma} = C_2 \times \omega$ Eq. 3.6

Viscosity $\eta = \sigma / \dot{\gamma}$ Eq. 3.7

Where M is the torque and ω is the angular velocity

For some measuring systems such as parallel plates, the gap between the measuring systems can be set by the user. In this case the equation used is :

$$\dot{\gamma} = \frac{C_2 \times \omega}{L} \quad \text{Eq. 3.8}$$

where L is the gap.

Form factors are associated with the measuring systems and the equation are shown in the following sections.

Cone plate $C_1 = \frac{1}{\frac{2}{3}\pi r^3}$ and $C_2 = \frac{1}{\theta}$ Eq. 3.9

Where r = radius of cone θ= cone angle in radians

Parallel plates $C_1 = \frac{1}{\frac{2}{3}\pi r^3}$ and $C_2 = \frac{3r}{4}$ Eq. 3.10

Where r = radius of plate

Because for a parallel plate the shear stress varies across the radius, the above formula refers to the 3/4 radius position if the test sample is Newtonian.

Coaxial cylinders $C_1 = \frac{1}{2\pi r_a^2 H}$ and $C_2 = \frac{2r_i^2 r_0^2}{r_a^2(r_0^2 - r_i^2)}$ Eq. 3.11

Where $r_a = (r_i + r_0) / 2$
r_i = inner radius
r_0 = outer radius
H = height of cylinder

3.2.3.1.2 Flow characterization

3.2.3.1.2.1 Flow curves

Rheometers of this type can monitor the apparent viscosity when the shear stress or the shear rate is varied. The measured viscosity of a fluid can often be seen to behave in one of four ways when sheared, namely:

1 Viscosity remains constant no matter what the shear rate (Newtonian behaviour)

2 Viscosity decreases as shear rate is increased (shear thinning behaviour)

3 Viscosity increases as shear rate is increased (shear thickening behaviour)

4 Viscosity appears to be infinite until a certain shear stress is achieved (plastic behaviour)

Fluid can also be time dependent where the viscosity will depend on how long the liquid has been shared.

Over a sufficiently wide range of stresses, it is often found that the material has a more complex characteristic made up more then one of the above flow patterns.

Since it is the relationship of shear stress to shear rate that are strictly related to flow the flow characteristics of a material can be directly shown by plotting shear stress or the apparent viscosity as function of the shear rate. A graph of this type is called a flow curve. Figure 3.10 shows the flow curves and viscosity curves for the four basic flow patterns. Plastic behaviour has been modelled using Bingham and Herschel-Bulkley relationship. These are discussed below

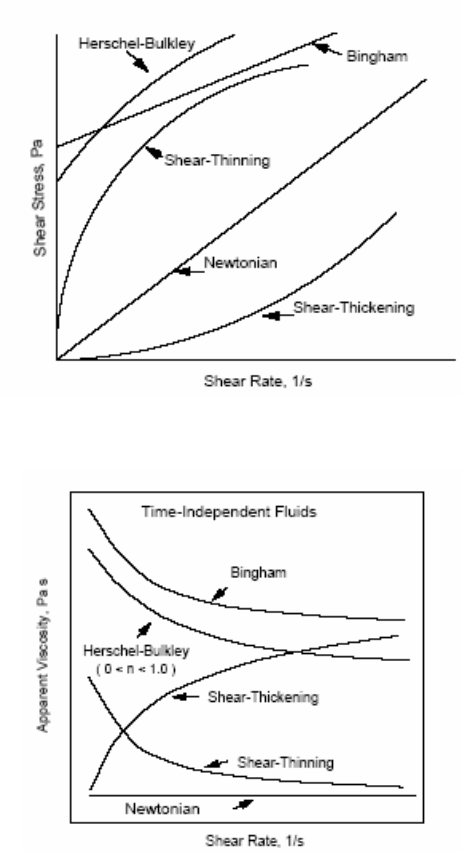

Figure 3.10 Types of flow behaviour. Newtonian, Shear Thinning, Shear Thickening, Bingham and Herschel-Bulkley (Steffe, 1992)

The exact behaviour of materials can often be described by some form of rheological model. Simple flow behaviour can be described by the models shown in Figure 3.10

Newtonian

In Newtonian fluid the shear stress is directly proportional to the shear rate. This is the simplest type of flow where the materials viscosity is constant and independent of the shear rate.

$$\sigma = \dot{\gamma} \times \eta \qquad \text{Eq. 3.12}$$

Water, Oils and dilute polymer solutions are some examples of Newtonian materials.

Power law - (or Ostwald model)

Many non-Newtonian materials undergo a simple increase or decrease in viscosity as the shear rate is increased. If the viscosity decreases as the shear rate is increased the material is said to be shear thinning or pseudo plastic.

The opposite effect is known as shear thickening. Often this thickening is associated with a change in sample volume. This is called dilatancy. This relationship is often reported by a power equation of the form

$$\sigma = K \times \dot{\gamma}^{n} \qquad \text{Eq. 3.13}$$

Where K, the consistency index, is the shear stress at a shear rate of 1.0 sec^{-1} and the exponent n is the flow behaviour index

If n <1 material is shear thinning, if n >1 material is shear thickening, if n is 1 the material is Newtonian.

Polymer solutions and melts as well as some solvent based coatings show power law behaviour over limited shear rates range.

Bingham

Some materials exhibit an 'infinite' viscosity until a sufficiently high stress as applied to initiate flow. Shear stress and shear rate are then linearly related. The Bingham model covers these materials; The equation is

$$\sigma = \sigma_0 + K \times \dot{\gamma} \qquad \text{Eq. 3.14}$$

The limiting stress value (σ_0) is often called Bingham yield stress or simply the yield stress of the material.

Many concentrated suspensions and colloidal systems show Bingham behaviour.

Herschel Bulkley

This model incorporates the elements of the three previous models

$$\sigma = \sigma_0 + K \times \dot{\gamma}^n \qquad \text{Eq. 3.15}$$

Special cases of the model:

A pure Newtonian material has limiting stress=0 and n=1

A power law fluid has limiting stress=0 and n=power law index

A Bingham fluid has limiting stress= σ_0 and n=1

There are models for more complex flow behaviour. These relationships have been developed as 'enhancements' to the fundamental models. They tend to give a

more realistic prediction of flow over a wider range of conditions. The most important and applied are the Ellis, Casson, and Moore, Cross, Sisko, and Carreau models. (Steffe 1992; Rao 1999)

Structured liquids such as polymer solutions, emulsion, dispersions etc show shear-thinning behaviour. The pattern of the viscosity, measured over a wide-enough range of shear rates is shown in Figure 3.11

At low-enough shear rate or shear stress, the viscosity is constant (with value η_0), but at some point it begins to decrease, and usually enters a straight-line region on a logarithmic plot, which indicates power-low behaviour. This decrease of viscosity with the shear rate (shear thinning) corresponds to a loss of structure or orientation of particles along the flow direction. At higher shear rate, when these processes of alignment or loss of structure are completed, there is a flattering out of the viscosities with shear rate and then a second constant viscosity region, (with value η_∞) is obtained. They are thereby two limiting Newtonian viscosities η_0 and η_∞ separated by a power-law region.

A frequently used equation describing this is the Cross equation (Steffe, 1992; Rao, 1999):

$$\eta = \eta_\infty + \frac{\eta_0 - \eta_\infty}{1 + (\alpha_c \dot{\gamma})^m} \qquad \text{Eq. 3.16}$$

Where α_c is a time constant related to the relaxation times of the material and m is the dimensionless exponent.

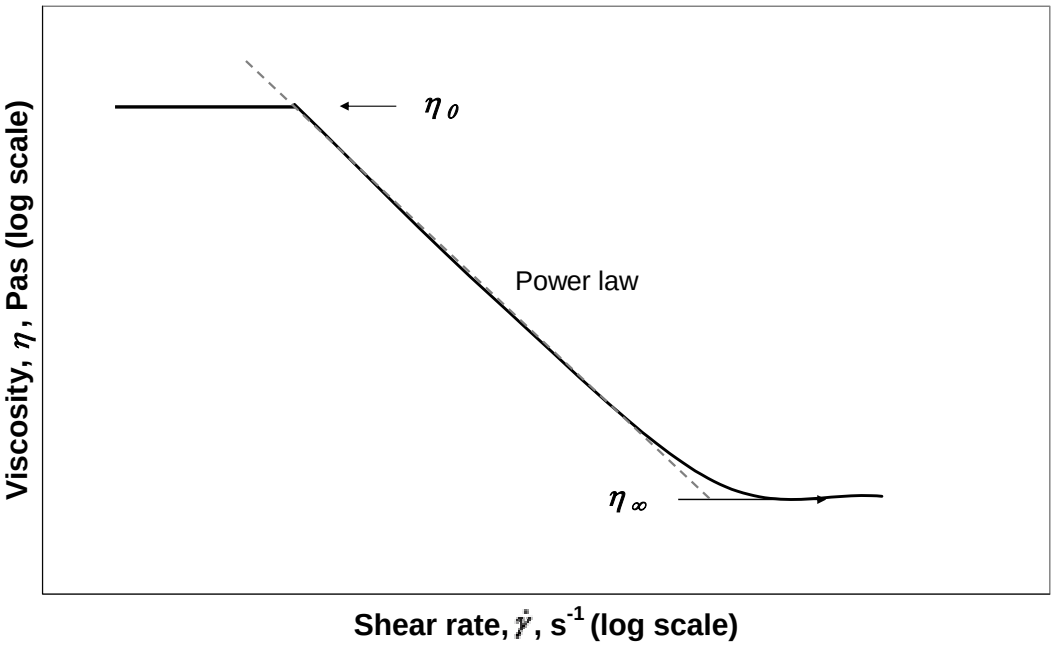

Figure 3.11 Viscosity, as a function of shear rate over a wide shear rate range.

3.2.3.1.2.2. Experimental conditions

Bohlin CVO (Creep, Viscosity, Oscillation) and CVOR (Creep, Viscosity, Oscillation, Relaxation) rheometers (controlled shear stress) were used to analyse the flow in rotational rheometry.

Cone and plate geometry (ϑ=4º, ϕ=40mm) was used. Measurements of viscosity were done in triplicate for each sample at a range of temperatures between 40 and 80°C. The flow curves were fitted with a power law model in order to obtain the flow behaviour and the consistency indices.

3.2.3.1.3. Viscoelasticity

A distinctive feature of the mechanical behaviour of viscoelastic materials is the way their response to an applied stress or strain depends upon the rate or time period of loading.

In process engineering applications or as end products, foods are often subject to stress for prolonged period of time, but it is not possible to know how they will respond to a particular load without a detailed knowledge of the materials viscoelastic properties.

A true fluid flows when it is subjected to a shear field and motion ceases as soon as the stress is removed. In contrast, an ideal elastic solid subjected to a stress recovers its original state as soon as the stress is removed. Some materials, such as structured liquids, exhibit viscoelastic characteristics and show both solid and liquid features.

In all structured liquids there is a natural rest condition of the microstructure that represents a minimum-energy state. When these liquids are deformed at small deformations, thermodynamic forces immediately begin to operate to restore this rest state. Like a spring the energy necessary for the movement from the rest is the storage energy and will be recovered as soon the rest state is restored. At small deformation there is a linear relationship between the force and the deformation just as in an ideal solid (Hooke's law).

Viscoelastic materials may either behave as viscoelastic solid where at long times after removal of the stress the original rest state is restored or as viscoelastic liquids where there is a permanent deformation. In both materials when the deformation becomes large the structures responsible for the elastic behaviour in a viscoelastic solid start to break and there is not longer full recovering of the deformation applied. A linear relationship between deformation and force will be not valid. At very high deformations the structure changes radically and the liquid became anisotropic. This system behaves as a pure liquid and it will be valid the linear relationship between the velocity of the deformation and the stress, (Newtonian law for ideal liquids).

In making measurements on viscoelastic materials it is important to work in the linear viscoelastic region below this point.

The most used techniques to measure the viscoelastic properties of a material are oscillatory techniques and creep-compliance testing.

3.2.3.1.4. Oscillatory shear flow

3.2.3.1.4.1 Basic principles of the technique

In small amplitude oscillatory shear (SAOS), experiments, a sinusoidal oscillating stress or strain with a frequency ω is applied to the material, and the phase difference between the oscillating stress and strain, as well as the amplitude ratio is measured.

If the applied stress varies as a function of time according to $\sigma = \sigma_0 \sin \omega t$ where ω is the angular frequency (2π times the frequency in Hz), the strain for an elastic material obeying the Hooke's law would vary in a similar manner as $\gamma = \gamma_0 \sin \omega t$. However, for a viscoelastic material the strain lags somewhat behind the stress and the result is that when a sinusoidal stress is applied to the sample the strain varies in a sinusoidal manner, but out of phase with the applied stress. The variation of the stress and strain with time, then, can be given by expression of the type:

$$\gamma = \gamma_0 \sin \omega t \qquad \text{and} \qquad \sigma = \sigma_0 \sin(\omega t + \delta) \qquad \text{Eq. 3.17}$$

where δ is the phase angle.

The equation for the stress can be expanded to give:

$$\sigma = \sigma_0 \sin \omega t \cos \delta + \sigma_0 \cos \omega t \sin \delta \qquad \text{Eq. 3.18}$$

the stress can therefore be considered as being resolved into two components; one of $\sigma_0 \cos \delta$ which is in phase with the strain and another $\sigma_0 \sin \delta$ which is $\pi/2$ out of phase with the strain. Hence it is possible to define two dynamic moduli G' which is

in phase with the strain and G", $\pi/2$ out of phase with the strain. Since $G' = (\sigma_0 / \gamma_0)\cos\delta$ and $G'' = (\sigma_0 / \gamma_0)\sin\delta$, the equation for the stress can be written as :

$$\sigma = G'\gamma_0 \sin\omega t + G''\gamma_0 \cos\omega t \qquad \text{Eq. 3.19}$$

G', called storage modulus, expresses the magnitude of the energy that is stored in the material and recoverable per cycle of deformation, G", named viscous or loss modulus, is a measure of the energy that is lost per cycle through viscous dissipation.

The phase angle δ is then given by:

$$\tan\delta = G''/G' \qquad \text{Eq. 3.20}$$

A complex notation is often favoured for the representation of the dynamic properties of viscoelastic materials. The stress and the strain are given as

$$\gamma = \gamma_0 \exp(i\omega t) \qquad \text{Eq. 3.21}$$

and

$$\sigma = \sigma_0 \exp(i\omega t + \delta) \qquad \text{Eq. 3.22}$$

where $i = \sqrt{-1}$

The overall complex modulus $G^* = \sigma/\gamma$ is given by

$$G^* = \frac{\sigma_0}{\gamma_0} \exp i\delta = \frac{\sigma_0}{\gamma_0}(\cos\delta + i\sin\delta) \qquad \text{Eq. 3.23}$$

it then follow that :

$$G^* = G' + iG'' \qquad \text{Eq. 3.24}$$

Additional frequency dependent material functions in addition to the complex modulus (G*) are the complex viscosity (η*), dynamic viscosity (η'), out of phase component of the complex viscosity (η").

$$|G^*| = \sqrt{G'^2 + G''^2} \qquad \text{Eq. 3.25}$$

$$\eta^* = \frac{G^*}{\omega} = \sqrt{\eta'^2 + \eta''^2} \qquad \text{Eq. 3.26}$$

$$\eta' = \frac{G''}{\omega} \quad \text{and} \quad \eta'' = \frac{G'}{\omega} \qquad \text{Eq. 3.27}$$

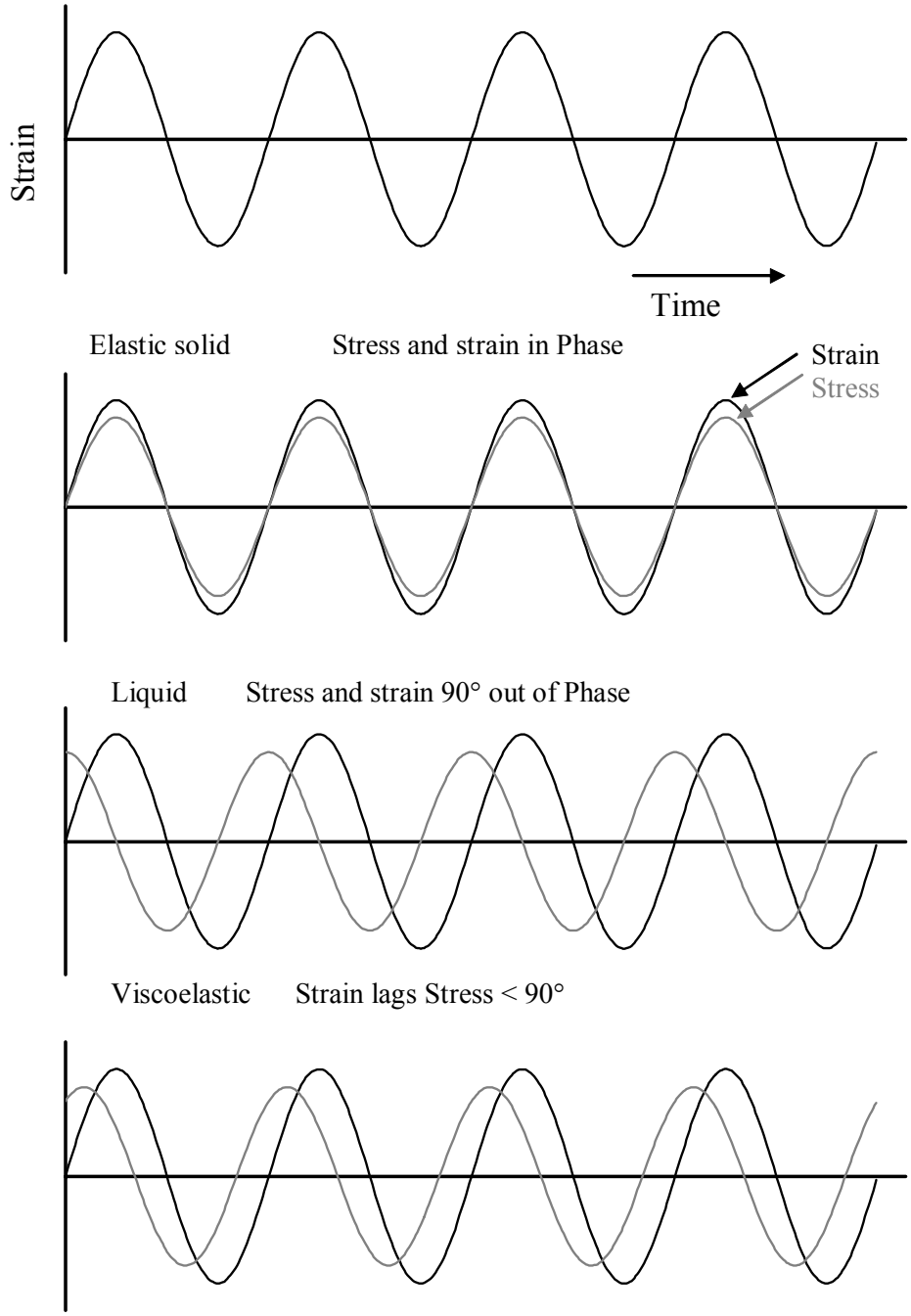

Figure 3.12 Stress or strain against time for solid, liquid and viscoelastic materials

3.2.3.1.4.2. Experimental conditions

Bohlin CVO and CVOR rheometers (controlled shear stress) were used to analyse the viscoelastic behaviour in oscillation tests.

Parallel plate, ϕ=40mm, was selected as the appropriate geometry and the gap was set at a value of 300μm.

Strain sweeps were carried out at a temperature range of 30-80C, at temperature intervals of 10ºC and a constant frequency of 1 Hz, in order to find the linear viscoelastic region. Frequency sweeps were performed (0.01-100Hz) at the same range of temperature and the viscoelastic parameters determined from the strain sweeps, within the linear viscoelastic region. The majority of the commercial rheometers have problems when they perform oscillation measurements in a frequency range between 20 and 30Hz. These problems are due to the natural resonant frequency of the rheometer. Bohlin has solved these problems in CVO and the CVOR rheometers, and claim that it is possible to perform accurate oscillation test in a range of frequency between 10^{-6} and 150 Hz.

3.2.3.1.5 Creep tests

3.2.3.1.5.1. Basic principles of the technique

In a creep test, an instantaneous stress is applied to the sample and the change in strain (called the creep) is observed over time. When the stress is released, some recovery may be observed as the material attempts to return to the original shape.

Idealized creep and recovery curves are illustrated in Figure 3.13

When subjected to a constant stress, ideal elastic material would give a constant strain, and the material would return to the original shape upon removal of stress. An

ideal viscous material would show steady flow, producing a linear response to stress with the inability to recover any of the imposed deformation. Viscoelastic materials (e.g.,bread dough) would exhibit a nonlinear response to strain and, due to their ability to recover some structure by storing energy, show a permanent deformation less than the total deformation applied to the sample, i.e. they behave as a viscoelastic liquid. This strain recovery, or creep recovery, is also called recoil and may be modelled by a recoil function.

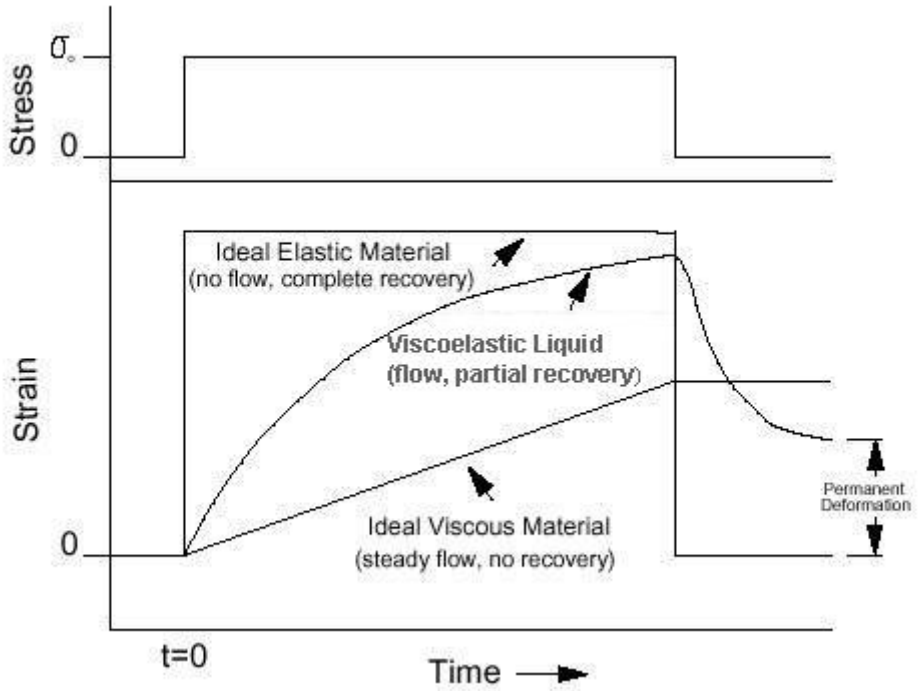

Figure 3.13 Idealized creep and recovery curves for liquid, solid and viscoelastic materials

Creep data is described using the creep compliance function:

$$J = f(t) = \frac{\gamma(t)}{\sigma} \qquad \text{Eq. 3.28}$$

where σ is the applied stress and γ the strain.

In the linear viscoelastic region the creep compliance response is independent of he magnitude of the applied stress. For a perfectly elastic solid, J =1/G ,the reciprocal of the shear modulus. To develop a mechanical analog describing creep behaviour, the starting point is the Kelvin model which contains a spring connected in parallel with a dashpot. When this system is subjected to shear strain, the spring and dashpot are strained equally:

$$\gamma = \gamma_{(spring)} = \gamma_{(dashpot)} \qquad \text{Eq. 3.29}$$

The total shear stress caused by the deformation is the sum of the individual shear stresses which can be written as $\sigma = G\gamma + \mu\dot{\gamma}$, where G is the modulus of the spring and μ the viscosity of the dashpot, and differentiating with respect to time yields,

$$\frac{1}{G}\frac{d\sigma}{dt} = \dot{\gamma} + (\lambda_{ret})\frac{d\dot{\gamma}}{dt} \qquad \text{Eq. 3.30}$$

Where the retardation time $(\lambda_{ret} = {}^{\mu}\!/_{G})$ is unique for any substance.

If a material was a Hookean solid, the retardation time would be zero and the maximum strain would be obtained immediately on application of stress. The time to achieve maximum strain in viscoelastic materials is delayed (or retarded).

In creep, where the material is allowed to flow after being subjected to a constant shear stress σ_0, the change in stress with time is zero, ${}^{d\sigma}\!/_{dt} = 0$ and the solution to the differential equation is:

$$\gamma = f(t) = \frac{\sigma_0}{G}\left(1 - \exp\left(\frac{-t}{\lambda_{ret}}\right)\right) \qquad \text{Eq. 3.31}$$

showing that the initial strain is zero, (γ=0 at t=0).

This equation predicts a strain that asymptotically approaches the maximum strain (σ_0/G) associated with the spring. λ_{ret} is the time taken for the delayed strain to reach 63.2% (1-1/e) of the final value. Materials with a large retardation time reach full deformation slowly.

The Kelvin model is not general enough to model creep in many biological materials. A better fit of data can be obtained using the Burgers model, which is a Kelvin, and a Maxwell model placed in series. Data following this mechanical analog show an initial elastic response due to the free spring, retarded elastic behavior related to the parallel spring-dashpot combination and Newtonian type flow after long periods of time due to the free dashpot:

$$\gamma = f(t) = \frac{\sigma_0}{G_0} + \frac{\sigma_0}{G_1}\left(1 - \exp\left(\frac{-t}{\lambda_{ret}}\right)\right) + \frac{\sigma_0 t}{\mu_0} \qquad \text{Eq. 3.32}$$

where $\lambda_{ret} = \mu_1/G_1$, the retardation time of the Kelvin portion of the model.

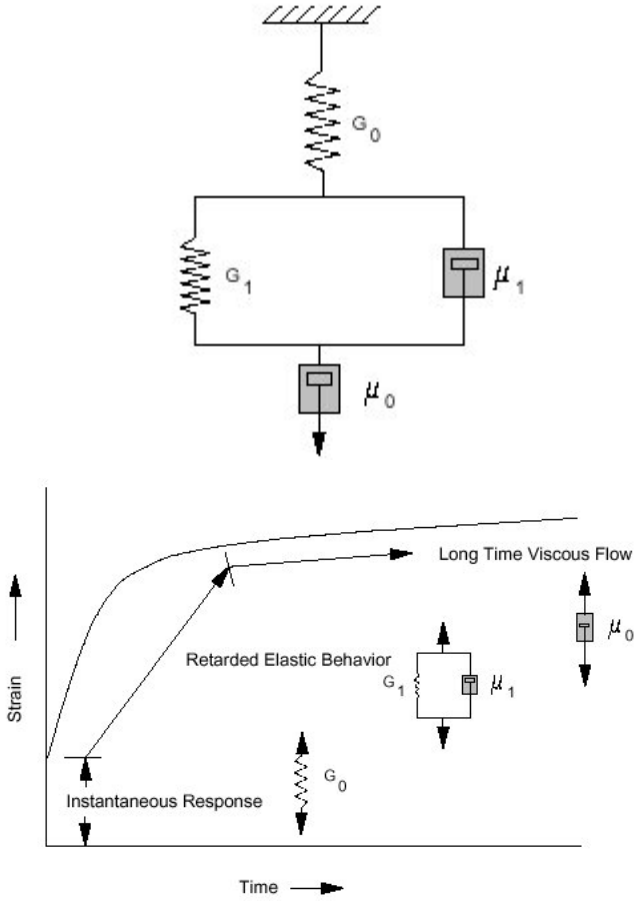

Figure. 3.14 Burger model: strain against the time

The Burger model can also be expressed in terms of creep compliance by dividing the last equation by the constant stress:

$$J = \frac{\gamma}{\sigma_0} == f(t) = J_0 + J_1\left(1 - \exp\left(\frac{-t}{\lambda_{ret}}\right)\right) + \frac{t}{\mu_0} \qquad \text{Eq. 3.33}$$

where J_0 is the instantaneous compliance, σ_0/G_0, J_1 is the retarded compliance, σ_1/G_1.

$\lambda_{ret} = \mu_1/G_1$, the retardation time of the Kelvin portion of the model, and μ_0 is the Newtonian viscosity of the free dashpot. The sum of J_0 and J_1 is called the steady state compliance.

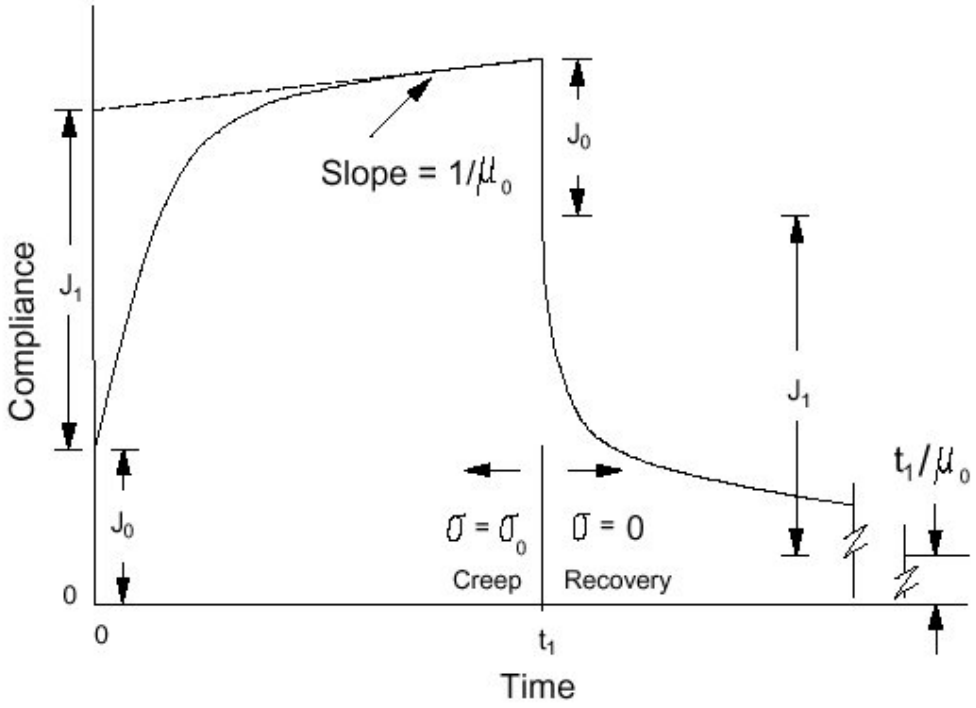

Figure 3.15 Burger model: compliance against the time

Figure 3.15 shows the complete creep and recovery curve expressed using the Burgers model; t_1 is the time when the constant stress is removed. At the beginning of creep, there is an instantaneous change in compliance (J_0) due to the spring in the Maxwell portion of the model. Then, the Kelvin component produces an exponential change in compliance related to the retardation time. After sufficient time has passed, the independent dashpot generates a purely viscous response. Data from the linear portion of the creep curve are related to two parameters: the slope is equal to $1/\mu_0$; and the intercept, sometimes called the steady state compliance, is equal to J_0+J_1. At $t=t_1$ the stress is removed and there is an instantaneous change in compliance equal to J_0. The free dashpot causes permanent deformation in the material related to a compliance of t_1/μ_0. This factor is directly related to the non-recoverable sample strain of $\sigma_0 t_1/\mu_0$.

If a substance obeying the Burger model is tested in the linear viscoelastic region, then the values of J_0 and J_1 determined from the creep curve will be equal to the values J_0 of and J_1 determined from the recovery curve.

If necessary, additional Kelvin elements can be added to the Burgers model to better represent experimental data. Mathematically, this idea can be described with the following equation:

$$J = \frac{\gamma}{\sigma_0} == f(t) = J_0 + \sum_{i=1}^{m}\left[J_i\left(1 - \exp\left(\frac{-t}{(\lambda_{ret})_i}\right)\right)\right] + \frac{t}{\mu_0} \qquad \text{Eq. 3.34}$$

Where m is the total number of Kelvin elements in the model, each having a unique retarded compliance and retardation time.

3.2.3.1.5.2. Experimental conditions

The Bohlin CVO rheometer (controlled shear stress) was used to analyse the creep response in rotation.

Roughened cylindrical concentric geometry (C25, ϕ=25mm) has been chosen to perform creep tests at a temperature of 20°C,

The deformation has been detected when a constant shear stress was applied for 100 sec, the response was followed for 100 sec after the stress had been released.

3.2.3.2. High-pressure capillaries rheology

3.2.3.2.1 Extensional flow
(Steffe 1992)

Pure extensional flows do not involve shearing. Many food processing operations involve extensional deformations. Extensional flows occur in sheet stretching, extruder dies, calendering and sagging.

The molecular orientation caused by extension, versus shear, can produce unique food products and behaviour. The differences in the behaviour of shear and extensional flow are partly due to the different way in which flow fields orient long molecules of high molecular weight. In shear flow, the preferred orientation corresponds to the direction of the flow; however, the presence of a differential velocity across the flow field encourages molecules to rotate thereby reducing the degree of stretching induced in molecular chains. The tendency of molecules to rotate, versus elongate, depends on the magnitude of the shear field: There is relatively more elongation and less rotation, at high shear rates. In extensional flow, the situation is very different. The preferred molecular orientation is in the direction of the flow field because there are no competing forces to cause rotation. Hence, extensional flow will induce the maximum stretching of the molecules producing a chain tension that may result in a large (compared to shear flow) resistance to deformation.

There are three basic types of extensional flow: uniaxial, planar, and biaxial (Figure 3.16). During uniaxial extension the material is stretched in one direction with a corresponding reduction in the other two directions. In planar extension, a flat sheet of material is stretched in one direction with a corresponding decrease in thickness (decreases) while the width (direction) remains unchanged. Biaxial extension looks like uniaxial compression, but it is usually thought of as a flow, which produces a radial tensile stress for a disc shaped object.

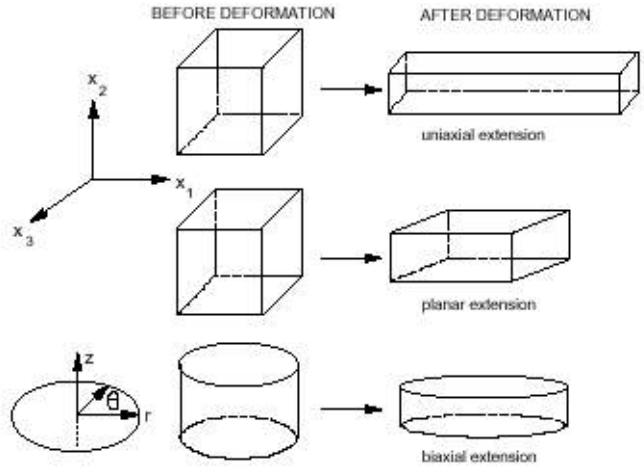

Figure. 3.16 Uniaxial, planar and biaxial extension.

These three kind of extensional flows results in three extensional viscosity: uniaxial (elongational) viscosity η_E, biaxial viscosity η_B and planar viscosity η_P.

The following limiting relationships between extensional and shear viscosities, η, can be expected for non-Newtonian fluids at small strains (Dealy, 1994; Walters, 1975; Petrie, 1979):

$$\lim_{\dot{\varepsilon}_h \to 0} \eta_E(\dot{\varepsilon}_h) = 3 \lim_{\dot{\gamma} \to 0} \eta(\dot{\gamma}) \qquad \text{Eq. 3.35}$$

$$\lim_{\dot{\varepsilon}_B \to 0} \eta_B(\dot{\varepsilon}_B) = 6 \lim_{\dot{\gamma} \to 0} \eta(\dot{\gamma}) \qquad \text{Eq. 3.36}$$

$$\lim_{\dot{\varepsilon}_h \to 0} \eta_P(\dot{\varepsilon}_h) = 4 \lim_{\dot{\gamma} \to 0} \eta(\dot{\gamma}) \qquad \text{Eq. 3.37}$$

Reliable relationships for non-Newtonian fluids in extension at large strains have not been developed. The above equations may only be precisely defined for the special case of Newtonian fluids:

$$\eta_E = 3\eta \qquad \text{Eq. 3.38}$$

$$\eta_B = 6\eta \qquad \text{Eq. 3.39}$$

$$\eta_P = 4\eta \qquad \text{Eq. 3.40}$$

These three equations can be used to verify the operation of extensional viscometers. Clearly, however, a Newtonian fluid must be extremely viscous to maintain its shape and give the solid-like appearance required in many extensional flow tests. Trouton established a mathematical relationship between tensile extensional viscosity and shear viscosity (Trouton, 1906) (he called it the coefficient of viscous traction). Presently, data for extensional and shear viscosities are often compared using a dimensionless ratio known as the Trouton number (N_{Tr}):

$$N_{Tr} = \frac{extensional \quad viscosity}{shear \quad viscosity} \qquad \text{Eq. 3.41}$$

Since extensional and shear viscosities are functions of different strain rates, a conventional method of comparison is needed to remove ambiguity. Based on a consideration of viscoelastic and inelastic fluid behavior, Jones et al. (1987) advocated the following conventions in computing the Trouton numbers for uniaxial and planar extensional flow:

$$(N_{Tr})_{uniaxial} = \frac{\eta_E(\dot{\varepsilon}_h)}{\eta(\sqrt{3}\dot{\varepsilon}_h)} \qquad \text{Eq. 3.42}$$

$$(N_{Tr})_{planar} = \frac{\eta_P(\dot{\varepsilon}_h)}{\eta(2\dot{\varepsilon}_h)} \qquad \text{Eq. 3.43}$$

The shear viscosities are calculated at shear rates equal to $\sqrt{3}\dot{\varepsilon}_h$ or $2\dot{\varepsilon}_h$ for uniaxial or planar extension, respectively. Using the similar considerations, Huang and Kokini (1993) showed that the Trouton number for case of biaxial extension should be calculated as

$$(N_{Tr})_{biiaxial} = \frac{\eta_B(\dot{\varepsilon}_h)}{\eta(\sqrt{12}\dot{\varepsilon}_h)} \qquad \text{Eq. 3.44}$$

The Trouton ratio for a Newtonian fluid may be determined from these equations. As shown also in the equation 3.38 to 3.40 in tensile extension it is equal to 3; it is 6 and 4, respectively, in biaxial and planar flow. Departures from these numbers are due to viscoelastic material behaviour. Experimental results may produce considerably higher values.

3.2.3.2.2. Flow in a tube viscometers

(Steffe, 1992)

Tube viscometers are very useful in collecting rheological data. These instruments may be placed into three basic categories: glass capillaries, high pressure capillaries and pipe viscometers. All establish a pressure difference to create flow.

The attention in this chapter is focused on high-pressure capillaries.

High-pressure capillaries, are typically piston driven or gas operated. A pump or gas system can be used to create a driven force in pipe viscosimeter. These units can be operated at elevated pressures such as those found in aseptic food processing equipment (Dail and Steffe, 1990a and 1990b).

Raw data for tube viscometers are pressure drop and volumetric flow rate. The pressure drop is determined from pressure transducers. In high-pressure capillaries, flow rates are calculated from the assumption that volumetric flow in the piston (or barrel) and the capillary are equivalent.

3.2.3.2.3.Rabinowitsch-Mooney Equation

Derivation of the Basic Equation. Numerous assumptions are required in developing the Rabinowitch-Mooney equation: flow is laminar and steady, end effects are negligible, fluid is incompressible, properties are not a function of pressure or time, temperature is constant, there is no slip at the wall of the tube meaning that the velocity of the fluid is zero at the wall-fluid interface, and radial and tangential velocity components are zero.

The starting point in the derivation of a tube viscometer equation is a force balance. Consider a fluid flowing through a horizontal tube of length (L) and inside radius (R).

A pressure drop (δP) over a fixed length (L) is causing flow.

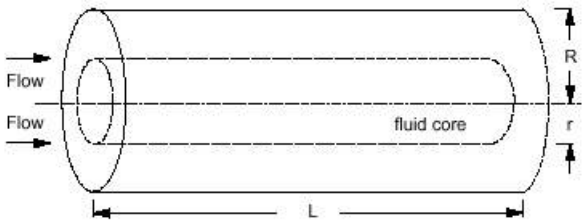

Figure 3.17 Core of fluid in tube flow geometry

The force balance, equating the shear stress causing flow to the shear stress resisting flow (i.e., the fluid), over a core of fluid (Figure 3.17) with radius r and length L yields

$$(\delta P)\pi r^2 = \sigma 2\pi rL \qquad \text{Eq. 3.45}$$

which can be solved for the shear stress:

$$\sigma = f(r) = \frac{(\delta P)\pi r^2}{2\pi rL} = \frac{(\delta P)r}{2L} \qquad \text{Eq. 3.46}$$

this equation depicts the shear stress varying over the pipe from zero at the centre (r=0) to a maximum at the wall (r=R) where the equation may be written as

$$\sigma_W = \frac{(\delta P)R}{2L} \qquad \text{Eq. 3.47}$$

To develop the shear rate equations, a differential flow element must be evaluated. This can be expressed by considering the steady, laminar flow of fluid moving through an annulus located between the core, with radius r , and the position $r + dr$:

$$dQ=u2\pi rdr \qquad \text{Eq. 3.48}$$

where u is the linear velocity at r. The total volumetric flow rate is found by integrating over the radius:

$$Q = \int_0^Q dQ = \pi\int_0^R u2rdr \qquad \text{Eq. 3.49}$$

by doing an integration by parts, it is possible to write:

$$Q = 2\pi\left[\left[\frac{r^2}{2}u\right]_0^R - \int_0^R \frac{r^2}{2}du\right] \qquad \text{Eq. 3.50}$$

Assuming the no slip condition which stipulates that the fluid velocity is zero at the wall of the pipe, mathematically u=0 at r=R, then the first term of this equation is zero.

$$Q = -\pi\int_0^R r^2 du = -\pi\int_0^R r^2 \frac{du}{dr}dr = -\pi\int_0^R r^2\dot{\gamma}dr \qquad \text{Eq. 3.51}$$

Substituting $r = \frac{\sigma}{\sigma_W}R$, $dr = \frac{R}{\sigma_W}d\sigma$ and the apparent shear rate $\Gamma = \frac{4Q}{\pi R^3}$ we obtain:

$$\Gamma = \frac{4}{\sigma^3{}_W}\int_0^{\sigma_W}\sigma^2\dot{\gamma}d\sigma \qquad \text{Eq. 3.52}$$

The solution of the latter integral gives the **Rabinowitsch-Mooney Equation:**

$$\dot{\gamma}_W = \frac{3}{4}\Gamma + \frac{1}{4}\sigma_W \frac{d\Gamma}{d\sigma_W} \qquad \text{Eq. 3.53}$$

that can be rewritten in the following simplified format:

$$\dot{\gamma}_W = \frac{3n'+1}{4n'}\Gamma \qquad \text{Eq. 3.54}$$

where $n' = \frac{d(\ln \sigma_W)}{d(\ln \Gamma)}$ is the slope of $\ln \sigma_W$ versus $\ln \Gamma$ at any particular point.

If the fluid behaves as a power law material, the slope of the derivative is a straight line and n'=n. This equation is a convenient form of the Rabinowitsch-Mooney equation because power law behavior is frequently observed with fluid foods.

3.2.3.2.4 Data correction

There are numerous measurement errors, which may occur in using tube viscometers. Some are generally applicable and others only apply to specific systems. In Table 3.3 the most important sources of error for high pressure capillary viscometers are summarised.

In the paragraph below the attention will be concentrated on end effects .

Energy losses due to fluid divergence at the end of a capillary are small and usually neglected but entrance losses can be very significant and must be evaluated. The entrance effect correction accounts for excess pressure loss occurring at the opening of the tube viscometer (entrance of the die). This is a result of a sudden convergence, and a losses in kinetic energy. This problem may be experimentally evaluated using a number of tubes having different length to diameter (L/D) ratios (Bagley, 1957). Data of total pressure drop versus flow rate are collected for each

tube. Pressure drop versus L/D are plotted at each flow rate (or apparent wall shear rate,) and the lines are extrapolated to zero L/D.

Table 3.3 *Sources of Error in Operating Tube Viscometers (from Van Wazer et al., 1963)*

Factor	Cause	Applicability
Kinetic energy losses	Loss of effective pressure because of the kinetic energy in the issuing stream.	General
End effects	Energy losses due to viscous or elastic behaviour when a fluid converges or diverges at the ends of a capillary	General
Elastic energy	Energy loss by elastic deformation of the fluid not recovered during flow in the capillary	Viscoelastic materials
Turbulence	Departure from laminar flow	General
Pressure losses prior to the capillary	Sticking of the piston or energy dissipated through flow of the material within the cylinder before entering the capillary.	Cylinder-piston viscosimeters
Heat effects	Conversion of pressure energy into heat energy through flow.	High-shear viscosimeters
Wall effects	Surface phenomena at the fluid-wall interface.	Polyphase fluids
Effect of time-dependent	Variations in the residence time properties in the capillary.	Thixotropic and rheopectic materials

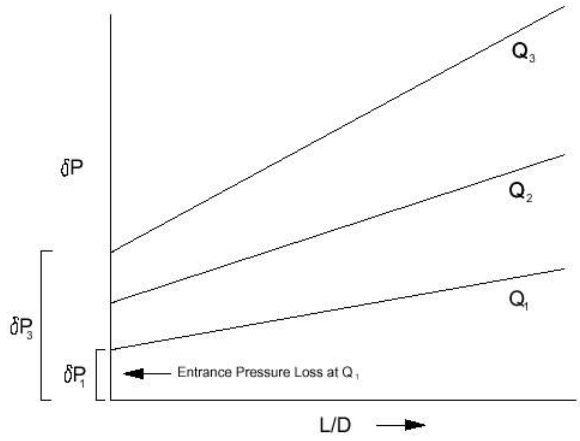

Figure 3.18: Bagley plot

These figures (Figure. 3.18) are sometimes called "Bagley plots." The resulting pressure drop is the entrance effect pressure loss at a particular flow rate and pipe diameter. To achieve the greatest level of accuracy, the same procedure must be followed for each diameter under consideration by using a number of tubes (at least three) having the same diameter but different lengths.

Pressure loss at the entrance has also been evaluated by subtracting data obtained with an orifice die (L=0 from capillary data. These calculations are made with an orifice and capillary of the same diameter using data taken at an equivalent volumetric flow rate.

Entrance pressure loss is used to correct the measured pressure drop values:

$$\delta P=\delta P_m-\delta P_{en} \qquad \text{Eq. 3.55}$$

where δP_m is the measured pressure drop, and δP_{en} is the entrance pressure loss. Corrected value of δP are used in calculating the shear stress at the wall.

3.2.3.2.5. Wall effects-slip correction

Slip occurs when a thin layer of fluid having a viscosity lower than that of the bulk fluid, forms at the wall of the tube (or the wall of any viscometer). This may be a problem in food suspensions like fruit and vegetable purees. Theoretically, the problem may be attacked by adding an additional term, representing added flow, to the overall flow rate term. The expression describing the volumetric flow rate may be written as:

$$Q_{whithoutslip} = Q_{Ws} = \frac{\pi R^3}{\sigma^3{}_W}\int_0^{\sigma_W}\sigma^2\dot{\gamma}d\sigma \qquad \text{Eq. 3.56}$$

where Q_{WS} is the volumetric flow rate without slip and σ_W is the shear stress at the wall. At constant values of σ_W, the above integral term is constant so a slip velocity may be introduced to account for variations in the measured values of flow rate:

$$Q_{measured}=Q_m=Q_{WS}+\pi R^2 u_s \qquad \text{Eq. 3.57}$$

Where u_s is the effective slip velocity which is assumed to be a function of the shear stress at the wall. In the absence of slip u_s =0.

3.2.3.2.6. Extensional Flow Through a Converging Die

Flow into a convergence involves an energy loss due to shear and an additional loss due to the extension (stretching) of fluid streamlines. Converging flow is sometimes called uncontrolled flow because fluid streamlines are a function of fluid properties. It is also not pure extensional flow because it involves a combination of both shear and extensional deformation. Analyses described here are based on separating the entrance pressure drop into two components: one due to shear and the other due to extension.

3.2.3.2.7 Cogswell's Equations

Cogswell (1972) assumed the entry pressure drop over an area of converging flow, from a circular barrel into a capillary die, was made up of two components, one related to shear flow and one related to extensional flow (Figure. 3.19):

$$\delta P_{en}= \delta P_{en,S}+\delta P_{en,E} \qquad \text{Eq. 3.58}$$

This flow situation could be referred to as unlubricated, constrained convergence (Cogswell, 1978). It is assumed that no slip occurs at the wall.

The pressure drop due to shear can be derived by considering the differential pressure drop, based on the power law form of the flow rate equation, over the length dl at radius r (Figure. 3.20):

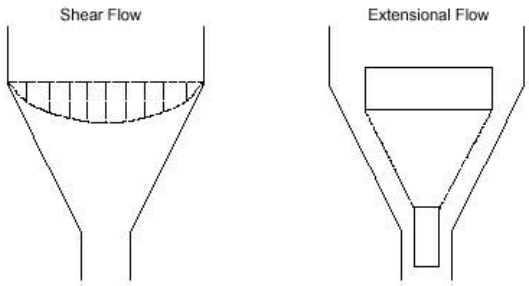

Figure 3.19 Shear (showing velocity profile) and extensional flow components causing pressure drop in a convergence

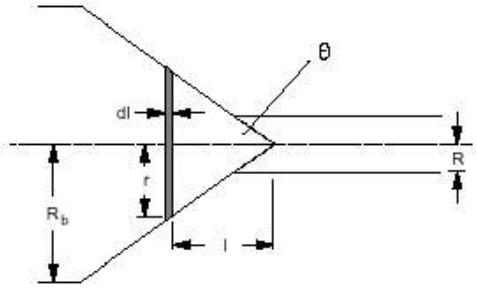

Figure. 3.20 Geometry for converging flow from a barrel of radius Rb into a capillary die of radius R

$$d(\delta P_{en,S}) = \frac{Q^n}{r^{3n+1}}\left(\frac{3n+1}{\pi n}\right)^n 2K dl \qquad \text{Eq. 3.59}$$

Substituing r/l=tanθ, dl=dr/tanθ in this equation yields

$$d(\delta P_{en,S}) = \frac{Q^n}{r^{3n+1}}\left(\frac{3n+1}{\pi n}\right)^n \frac{2K}{\tan\theta} dr \qquad \text{Eq. 3.60}$$

that integrated between the die and the barrel:

$$\int_0^{\delta P_{en,S}} d(\delta P_{en,S}) = \int_R^{R_b} \frac{Q^n}{r^{3n+1}}\left(\frac{3n+1}{\pi n}\right)^n \frac{2K}{\tan\theta} dr \qquad \text{Eq. 3.70}$$

gives:

$$\delta P_{en,S} = \Gamma^n \left(\frac{3n+1}{4n}\right)^n \frac{2K}{3n\tan\theta}\left(1-\frac{R}{R_b}\right)^{3n} \qquad \text{Eq. 3.62}$$

where $\Gamma=4Q/(\pi R^3)$, is the apparent wall shear rate in the die.

The volumetric average velocity at any particular cross section of the

die is:

$$\bar{u} = \frac{Q}{\pi r^2} = \frac{Q}{\pi l^2 \tan^2\theta} \qquad \text{Eq. 3.63}$$

this equation can be differentiated to give the average extensional strain rate at each cross section:

$$\dot{\varepsilon}_E = -\frac{d\bar{u}}{dl} = \frac{-(-2Q)}{\pi l^3 \tan^2\theta} = \frac{Q\tan\theta}{\pi r^3} \qquad \text{Eq. 3.64}$$

Unlike the shear rate, this expression does not depend on the form of the velocity profile. The differential pressure drop, due to the dissipation of extensional energy, may be written in terms of average extensional stress acting on an annulus:

$$(d\delta P_{en,E})\pi r^2 = \sigma_E(\pi(r+dr)^2 - \pi r^2 \qquad \text{Eq. 3.65}$$

because $(dr)^2$ is negligible this became:

$$(d\delta P_{en,E}) = 2\sigma_E \frac{dr}{r} \qquad \text{Eq. 3.66}$$

If the power law relationship between the average stress and the average strain rate, $\sigma_E = K_E(\dot{\varepsilon}_E)^m$ is valid, it is possible to write the pressure drop due to extensional flow as a function of the radius:

$$(d\delta P_{en,E}) = 2K_E\left(\frac{2Q\tan\theta}{\pi r^3}\right)^m \frac{dr}{r} \qquad \text{Eq. 3.67}$$

When this is integrated between the radius of the capillary(R) and the radius of the barrel (R_b) gives the component of the entrance pressure loss due to extensional flow:

$$(d\delta P_{en,E}) = \Gamma^m\left(\frac{2K_E}{3m}\right)\left(\frac{\tan\theta}{2}\right)^m\left(1-\left(\frac{R}{R_b}\right)^{3m}\right) \qquad \text{Eq. 3.68}$$

this equation can be written in logarithmic form:

$$\ln(d\delta P_{en,E}) = m\ln\Gamma + \ln\left[\left(\frac{2K_E}{3m}\right)\left(\frac{\tan\theta}{2}\right)^m\left(1-\left(\frac{R}{R_b}\right)^{3m}\right)\right] \qquad \text{Eq. 3.69}$$

which can be used in regression analysis to calculate m from the slope of the line, and K_E from the intercept. Values of K_E and m may be used to calculate the average extensional viscosity:

$$\eta_E = K_E(\dot{\varepsilon}_{E,R})^{m-1} \qquad \text{Eq. 3.70}$$

where $\dot{\varepsilon}_{E,R}$ is the average extensional strain rate at the die (where r=R)

$$\dot{\varepsilon}_{E,R} = \frac{\Gamma\tan\theta}{2} \qquad \text{Eq. 3.71}$$

Using the above equations, the following procedure can be utilized to calculate extensional viscosity from die entry pressure data:

1. Determine the total entrance pressure loss (δP_{en}) using the Bagley procedure discussed before. Also, determine the shear flow rheological parameters (K,

n) using standard methods in capillary viscometry. Although it may be convenient to find shear properties from capillary data, any standard rheological technique could be used to determine K and n.

2. Determine the pressure drop in the convergence due to shear flow, $\delta P_{en,S}$.
3. Subtract this from δP_{en} found in Step 1, to yield the component of the pressure drop in the entrance due to extensional flow, $\delta P_{en,E}$.
4. Use Eq. 3.69 in a regression analysis procedure to evaluate m and K_E. Calculate the strain rate and the extensional viscosity from the Eq. 3.70 and 3.71 respectively.

The preceding equations describe behaviour acceptably up to die angles of approximately 45 degrees (Gibson, 1988).

Cogswell (1972) formulated expressions for the net average extensional stress and net average extensional strain for flat entry dies as:

$$\sigma_E = \frac{3}{8}(n+1)\delta P_{en} \qquad \text{Eq. 3.72}$$

and

$$\varepsilon = \frac{4\eta\Gamma^2}{3(n+1)\delta P_{en}} \qquad \text{Eq. 3.73}$$

where η is the apparent shear viscosity based on a power law relationship: $\eta=K\Gamma^{(n-1)}$

The average extensional viscosity is easily calculated:

$$\eta_E = \frac{\sigma_E}{\dot{\varepsilon}_E} = \frac{9(n+1)^2(\delta P_{en})^2}{32\eta\Gamma^2} \qquad \text{Eq. 3.74}$$

this equation is very convenient for making a rapid comparison between

fluids.

3.2.3.2.8 Experimental conditions

A Rosand RH7 twin bore capillary rheometer was used (Figure 3.21). The sample was driven simultaneously through a capillary die (l=16mm, ϕ=0.5mm, ϑ= 180º) as well as an orifice die (l=260mm, ϕ=0.5mm, ϑ= 180º). The pressure was recorded as function of the piston speed.

The Bagley (1957) correction was applied to correct effects due to pressure loss occurring at the capillary end. Shear properties were determined at the wall, and the Rabinowitsch correction applied assuming a power law model.

Cogswell's (1972) equations for flat entry dies were used to determine extensional stress and strain.

The temperature was set at 70ºC.

Caramels samples were loaded by using a stainless steel funnel designed and built in our laboratory. (Figure 3.22). This funnel was provided with interchangeable edges that were allowing to equilibrate the sample in an oven at 70ºC before being loaded in the capillary rheometer.

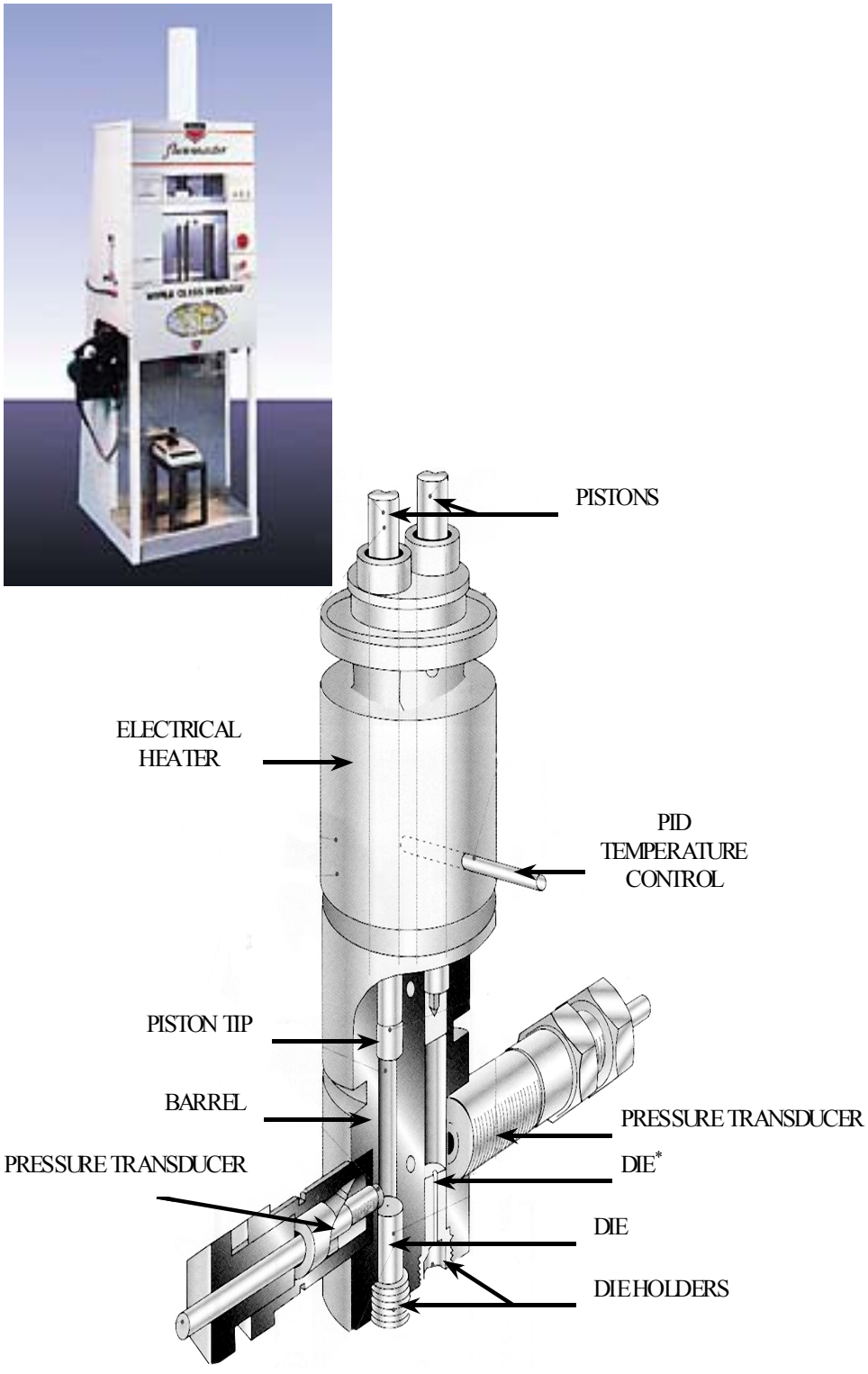

Figure 3.21 Capillary rheometer

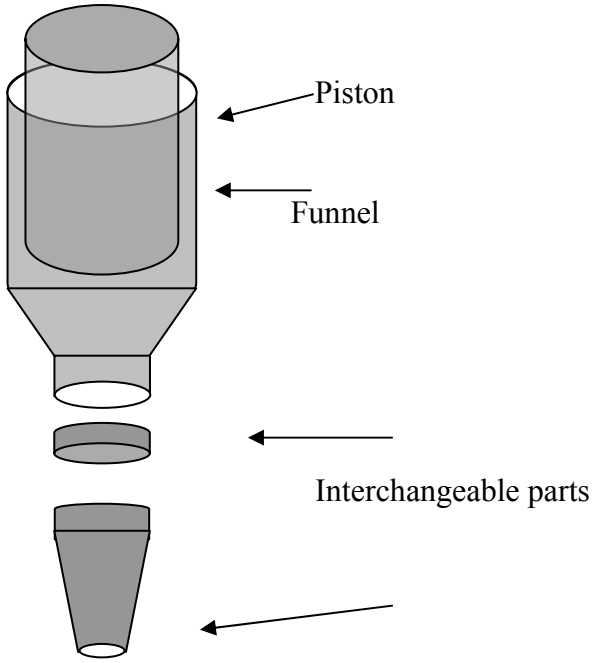

Figure 3.22 Stainless steel funnel for sample loading

CHAPTER 4. THE EFFECT OF THE PROCESSING TEMPERATURE

4.1 Introduction

The work described in this chapter is a structural and rheological characterization of caramels prepared from the same formulation but at different final cooking-temperatures.

The structural characterization has been performed by X-ray diffraction and differential scanning calorimetry (DSC). DSC will provide information both on crystallinity and the glass transition temperature (T_g). Information on the extent of the Maillard reaction has been obtained by determination of the protein isolectric point. For the rheological characterization viscosimetry tests with rotational and capillary rheometers and oscillation tests and creep tests using a rotational rheometer have been performed.

The shear viscosity has been interpreted using WLF and Arrhenius models and an empirical statistical model has been developed to allow viscosities to be predicted as a function of the water content and temperature.

The determination of the shift factor for the superimposition of the viscous modulus from the frequency sweep at different temperature has allowed the glass transition to be determined through an WLF analysis. This is compared to the value obtained from DSC.

4.2 Composition of Caramels

Caramel was prepared by heating to different temperatures as described in chapter 3. This resulted in products with a range of water content. The measured water contents were determined and from these the total ingredient composition was calculated.

Table 4.1 shows the composition of the final product obtained by assuming no chemical changes as a result of the Maillard reaction. It is possible, in addition to Maillard reaction, that some sucrose inversion to glucose and fructose occurs. However in view of the pH higher then 5.5 this is considered unlikely (Jackson, 1995). Some experiments, performed by the author and not shown in this thesis, have demonstrated that to vary the formulation with the introduction of the more Maillard reactive reducing sugar as xylose, did not affect the extent of the Maillard reaction in caramels. It was supposed that, for caramel systems, proteins were the limiting factor for Maillard reactivity, in view of the fact that their concentration was very low.

The composition of the non-fat phase is shown in Table 4.2.

4.3 Light microscopy

A micrograph obtained by light microscopy of the caramel cooked at 117ºC is shown in Figure 4.1.

It is evident the presence of a continuous matrix constituting a microemulsion of sugar water phase and fat. Some fat separation is also observable from the presence of two fat droplets which have diameter of about 70μm and 50μm.

Table 4.1 *Composition of the caramels (% w.w.b)*

Sample*	113	117	120	122
Water	13.2	10.5	8.9	7.9
Milk fat	0.1	0.1	0.1	0.1
Sucrose	4.9	5.1	5.2	5.2
Casein	0.9	0.9	0.9	1.0
Whey proteins	0.2	0.2	0.2	0.2
Lactose	1.5	1.6	1.6	1.6
Ash	0.2	0.2	0.2	0.3
Fructose	5.7	5.9	6.0	6.1
Dextrose	26.7	27.5	28.0	28.3
Maltose	17.2	17.7	18.0	18.2
Maltotriose	4.3	4.5	4.6	4.6
Higher sugars	12.3	12.7	12.9	13.0
Veg fat	12.2	12.5	12.8	12.9
Salt	0.4	0.4	0.4	0.4
Sodium carbonate	0.2	0.2	0.2	0.2

** The samples are designed in terms of the final cooking temperature in ºC*

Table 4.2 *Non-fat phase composition (% w.w.b.)*

Samples*	113	117	120	122
Water	15.3	12.2	10.4	9.2
Sucrose	5.7	5.9	6.0	6.1
Lactose	1.7	1.8	1.8	1.8
Ash	0.3	0.3	0.3	0.3
Fructose	6.6	6.8	7.0	7.1
Dextrose	30.8	31.9	32.5	33.0
Maltose	19.7	20.5	20.9	21.2
Maltotriose	5.0	5.2	5.3	5.4
Higher sugars	14.2	14.7	15.0	15.2
Salt	0.5	0.5	0.5	0.5
Sodium carbonate	0.2	0.2	0.3	0.2

** The samples are designed in terms of the final cooking temperature in ºC*

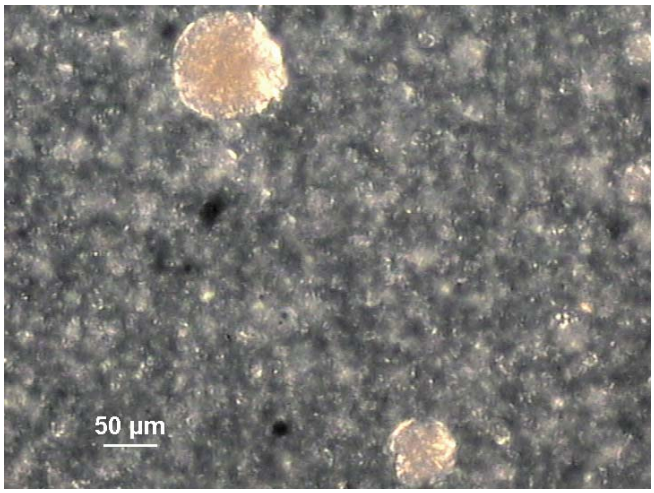

Figure 4.1 Micrograph of caramel sample 117 (bar marker=50µm)

4.4. Crystallinity

Information on crystallinity was obtained, as previously described, by DSC and X-ray diffraction.

4.4.1 X-Ray

Figure 4.2a shows the X-ray pattern for the different samples. Figure 4.2b shows the diffractogram for the vegetable fat and Figure 4.2c shows the X-ray pattern for crystalline sucrose, lactose and fructose. For caramels in the range between 18º and 35º 2θ, several peaks are present in each spectrum. The samples are semicrystalline. From a comparison between the diffractograms of the vegetable fat and the caramels it is evident that the crystallinity is mainly due to the fat, but in the sample cooked at higher temperature a small degree of fructose crystallinity is evident from the presence to the weak peaks at 2θ angles ~ 14º and 28º. The reason for fructose crystallinity is not clear but it is possible that some crystalline fructose was already

present in the HFCS (high fructose corn syrup) used for the preparation of caramels and this did not entirely melt out on heating. This ingredient is usually kept in an oven at 70ºC during storage to avoid fructose crystallization.

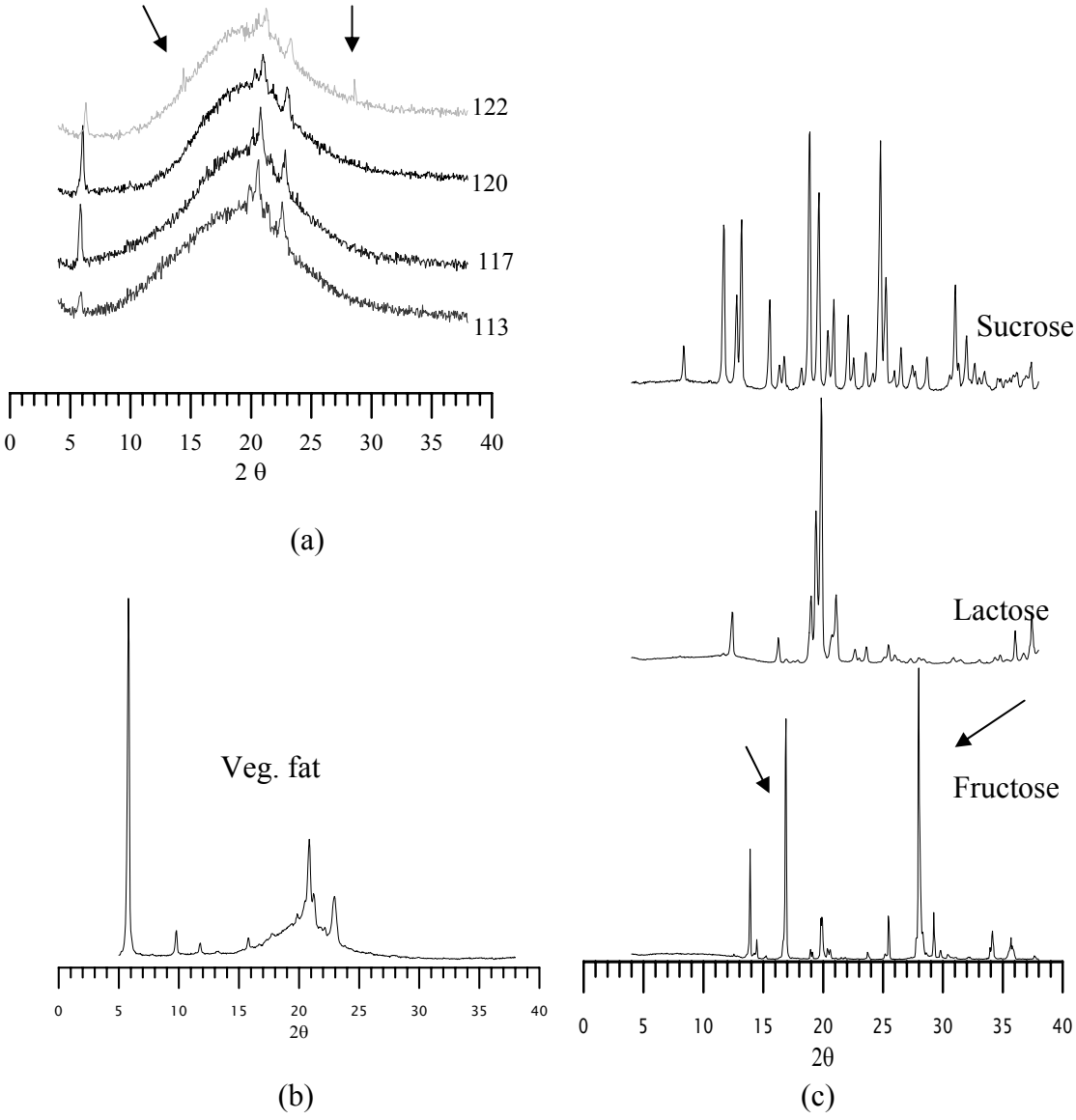

Figure 4.2 X-ray diffrattograms of sample 113, 117, 120, 122 (a); vegetable fat (b); and sucrose, lactose and fructose (c). The arrow indicates the peaks ascribed to crystalline fructose

4.4.2 DSC

Figures 4.3 a and b show the first scan and the reheating for all four samples. Two features can be elucidated from the curves: a glass transition of the amorphous syrup matrix and multiple endotherms at higher temperature due to the melting of the crystalline phases of the fat. On reheating the shape of the peak changes, suggesting the formation of different polymorphs on cooling following the reheat. As would be expected the T_g varies with the water content and the value of the midpoint are given in Table 4.3.

Table 4.3: *Glass transition temperatures from the calorimetric data*

Samples	Tg ºC	Water content of the non-fat matrix
113	-34	15.25
117	-24	12.2
120	-17	10.4
122	-13	9.2

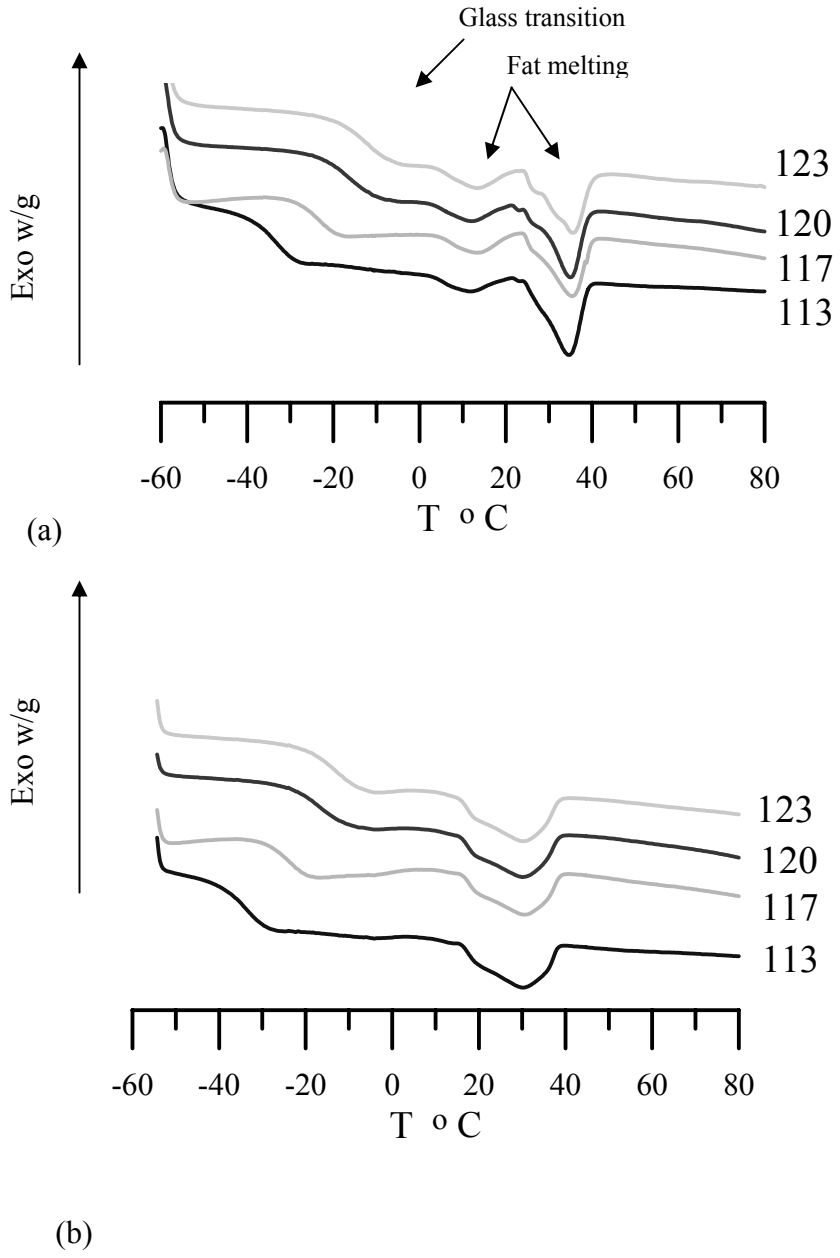

Figure 4.3 Thermograms for sample 113, 117, 120, 122 from first scan (a) and reheating (b).

4.5 ISOELECTRIC POINT

Figure 4.4 shows the pH at the isoelectric point as function of the water content, for the samples cooked at 113, 117, 120, 122ºC. A reduction of the pH at the isoelectric point is apparent when the water content decreases.

A decrease in the isoelectric point is probably a result of the loss of positively charged amide groups particularly on the lysine side chain as a result of participation in the Maillard reaction. Mohammed et al. (2000) found a decrease in the isoelectric point from ~4.5 to ~3.6, in heated milk powder and interpreted this as suggested above. It is possible that the measurement of the isoelectric pH could be a quick and easy method of measuring the extent of the Maillard reaction. In the case of caramels prepared at different boiling temperature, as the temperature of preparation increases, the Maillard reaction will be more developed and this results in a reduction in the number of positively charged groups in the protein and hence the isoelectric pH.

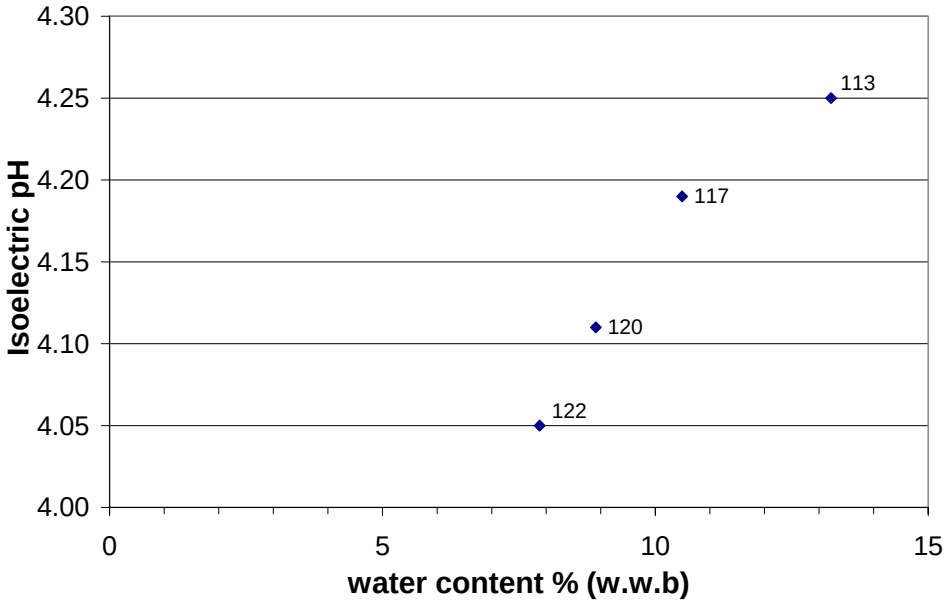

Figure 4.4 *Isoelectric pH of caramel samples as a function of the water content*

4.6 Rheology

4.6.1 SHEAR VISCOSITY

Figures 4.5 and 4.6 show the steady shear viscosity as function of the shear rate. The data for the three lower temperature samples shows predominantly Newtonian behaviour. The sample prepared at 122ºC, when measured at the lower temperature (40 and 50 °C), gave poor quality data. This may have been due to sample slip.

A power law model, $\sigma = K\dot{\gamma}^n$ where σ is the shear stress and $\dot{\gamma}$ the shear rate has been applied and the power law index, *n*, and the consistency index, *K*, have been determined. The values expressed as the average ± standard deviation are tabulated in Tables 4.5 and 4.6.

The flow behaviour index, *n*, reflects the closeness to Newtonian flow: if *n* is equal to 1, the fluid is Newtonian if *n* is lower than 1 the fluid is shear-thinning and if *n* is higher than 1 it is shear-thickening. For caramels n decreases with increasing temperature and decreasing water content.

The consistency index is the shear stress when the shear rate is 1.0 s^{-1}, and for Newtonian fluids *K* corresponds to the viscosity (η). Table 4.6 shows that, in the range of temperatures analyzed, the lower the water content the higher the consistency index. The consistency index K was one of the parameters used in subsequent data modelling.

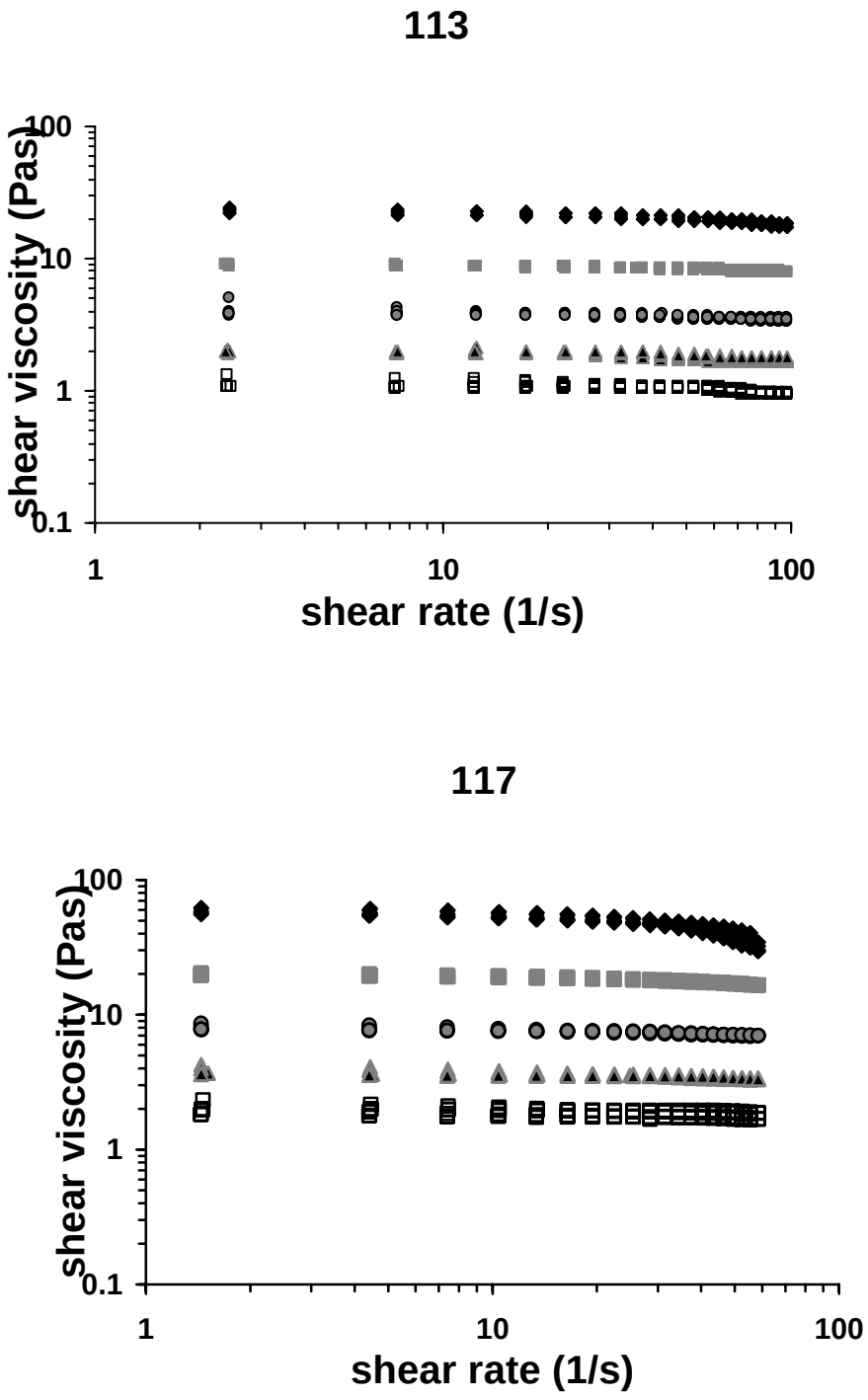

Figure 4.5 Viscosity curves for the caramel sample 113 and 117 at 40ºC(◆), 50ºC(■), 60ºC(●), 70ºC(▲), 80ºC (□).

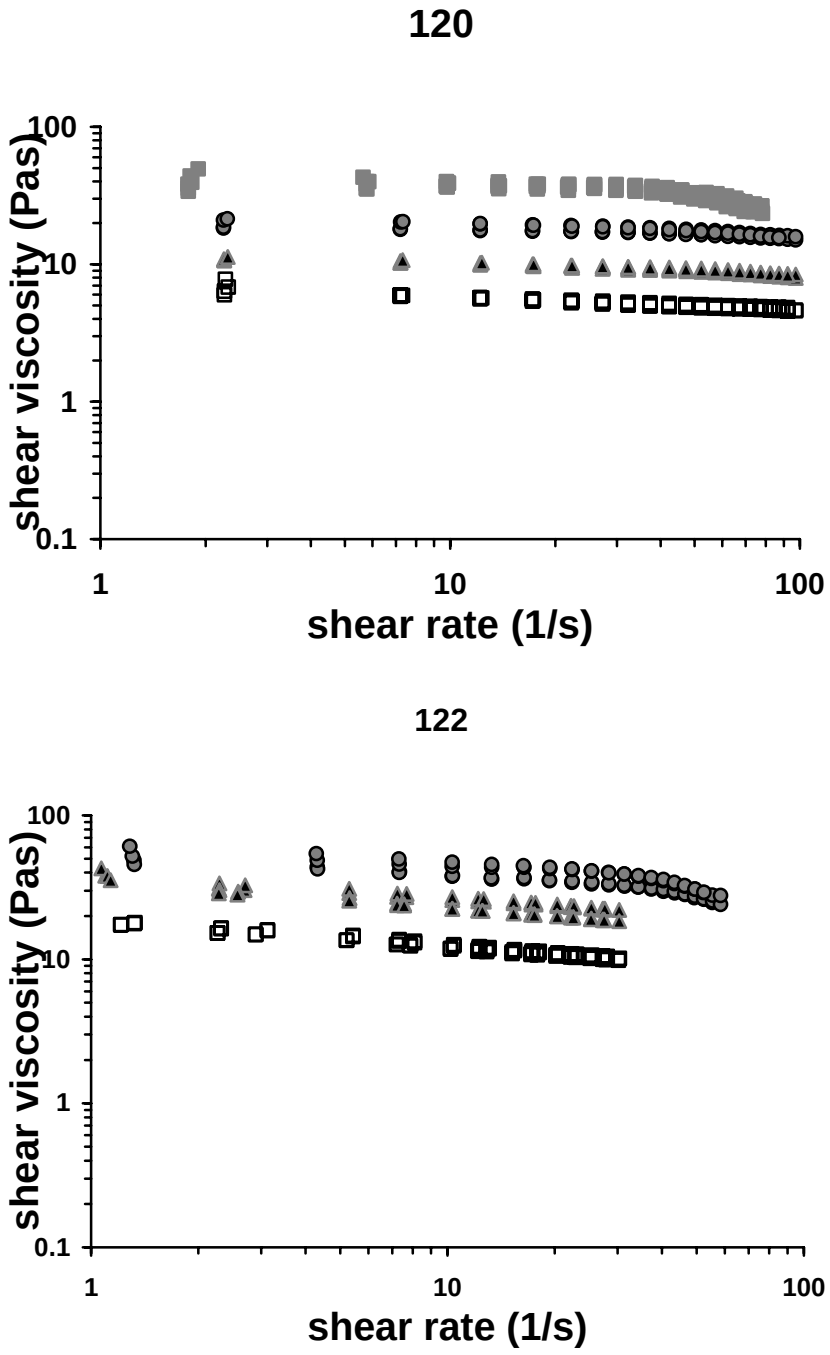

Figure 4.6 Viscosity curves for the caramel sample 120 and 122 at 50ºC(■), 60ºC(●), 70ºC(▲), 80ºC (□).

Table 4.5 *Power low indices (values are averages ± standard deviation obtained from triplicate measurements)*

Sample / T (ºC)	113	117	120	122
40	0.93 ± 0.008	0.860 ± 0.018		-
50	0.964 ± 0.006	0.949 ± 0.004	0.884 ± 0.036	
60	0.954 ± 0.027	0.961 ± 0.015	0. 923 ± 0.020	0.875 ± 0.023
70	0.961± 0.005	0.963 ± 0.025	0.922 ± 0.008	0.883 ± 0.016
80	0.963 ± 0.014	0.97 1± 0.023	0.904 ± 0.024	0.870 ± 0.007

Table 4.6 *Consistency indeces (K (Pa·s^n) values are averages ± standard deviation obtained from triplicate measurements)*

Sample / T (ºC)	113	117	120	122
40	26.0 ± 1.2	71.8 ± 1.8	-	-
50	9.4 ± 0.2	21.1 ± 0.4	48.1 ± 5.6	-
60	4.3 ± 0.5	8.3± 0.4	22.2 ± 2.4	55.7± 7.9
70	2.1 ± 0.1	3.9 ± 0.3	12.2 ± 0.4	31.9 ± 3.2
80	1.2± 0.1	2.0 ± 0.2	7.2 ± 0.5	16.3± 0.7

4.6.2.OSCILLATION

Strain sweeps were performed for every sample at all temperatures to determine the appropriate amplitude strain to carry out the frequency sweep in the linear viscoelastic region.

The frequency sweep was carried out by varying the frequency from 0.1 to 100Hz at temperatures in the range from 20ºC to 80ºC. Compared with steady shear measurements this approach allowed convincing viscosity data to be obtained for the more solid samples (lower temperature and lower water content) accept at higher frequencies. Figures 4.7-4.14 show the viscoelastic functions: complex viscosity, storage and loss moduli, and the phase angle for every caramel in the range of temperature analysed. At lower temperatures a plateau value of 10^5 Pa for G' and G" was obtained at the higher frequencies, which corresponded with an anomalous decrease in phase angle and viscosity. This phenomenon occurred at lower frequencies as the viscosity increases and is believed to be due to instrument compliance effects. This data although shown in the graphs was not used in the modelling of the viscoelastic behaviour.

Oscillation data confirms the viscous character of the caramels (phase angle close to 90^0 over most of the frequency range). As expected, the viscous and elastic modulus as well as the complex viscosity decreased with increasing temperature and at the same temperature the moduli and the viscosities are higher for the low water content samples.

The complex viscosity at 1 rad/sec is shown in Table 4.6. These values have been used, together with the viscosities from steady shear measurements and from creep in the modelling developed in the next section. This approach assume the validity of the Cox –Merz rule for the equivalence of the complex viscosity determined at 1 ω=rad/sec with the power law consistency index (K) from steady shear measurements.

Table 4.6 *Complex Viscosity(Pa·s) at ω=1rad/sec*

Sample / T (ºC)	113	117	120	122
20		1120		15900
30	57.3	240	669	2330
40	16.2	57.8	121	426
50	7.36		31.2	
60	4.30	6.87	10.7	36.1
70	3.2		4.54	
80	0.876	1.40	4.26	6.93

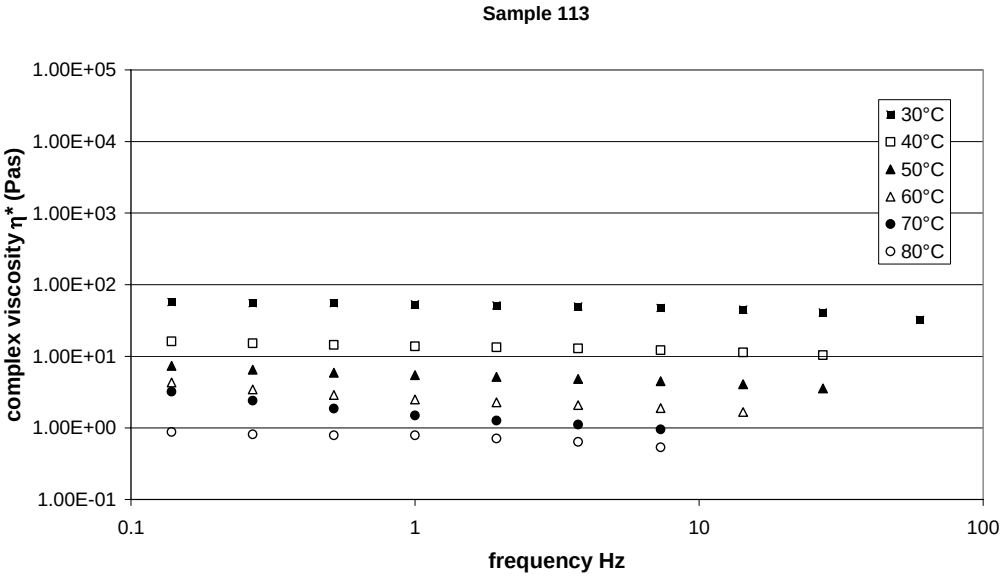

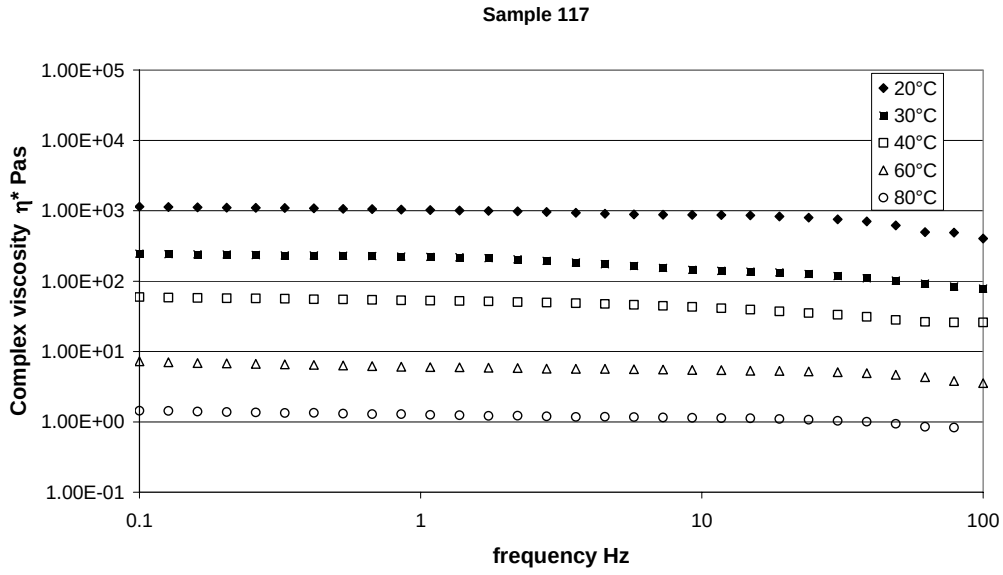

Figure 4.7 Complex viscosity for the sample 113 and 117, at different temperatures: 20(♦), 30 (■) ,40 (□) , 50(▲), 60 (Δ), 70(●), 80(○) °C.

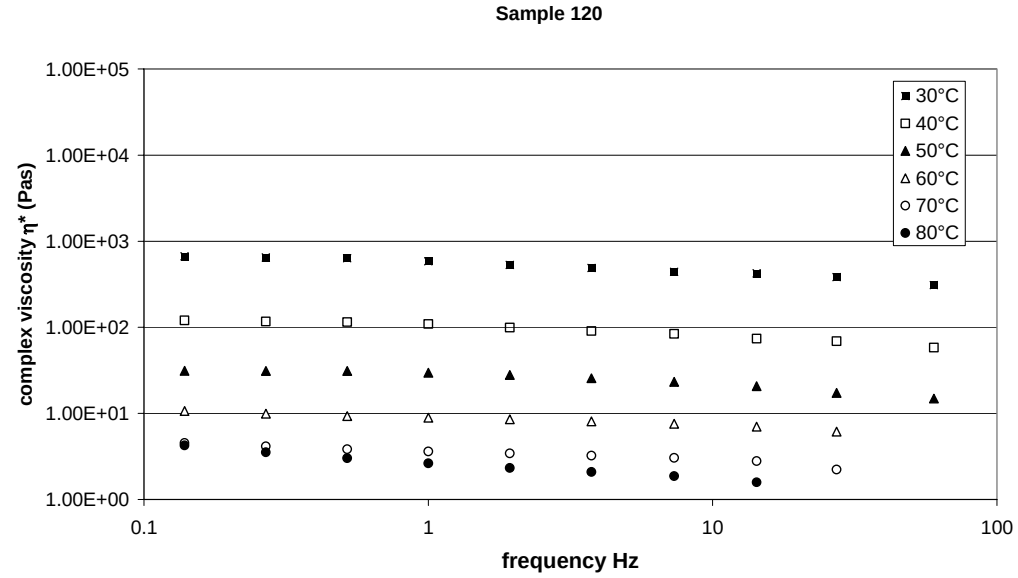

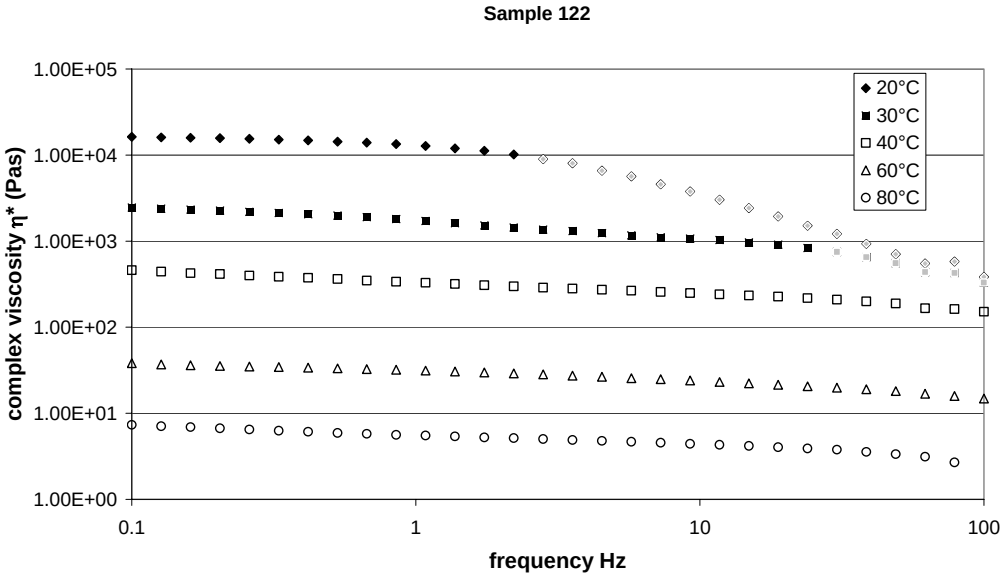

Figure 4.8 Complex viscosity for the sample 113 and 117, at different temperatures: 20(♦), 30 (■) ,40 (□) , 50(▲), 60 (Δ), 70(●), 80(○) °C. In this and subsequent Figures data for 20ºC and 30ºC data represented by the open symbols is believed to be affected by instrument compliance and removed in subsequent modelling.

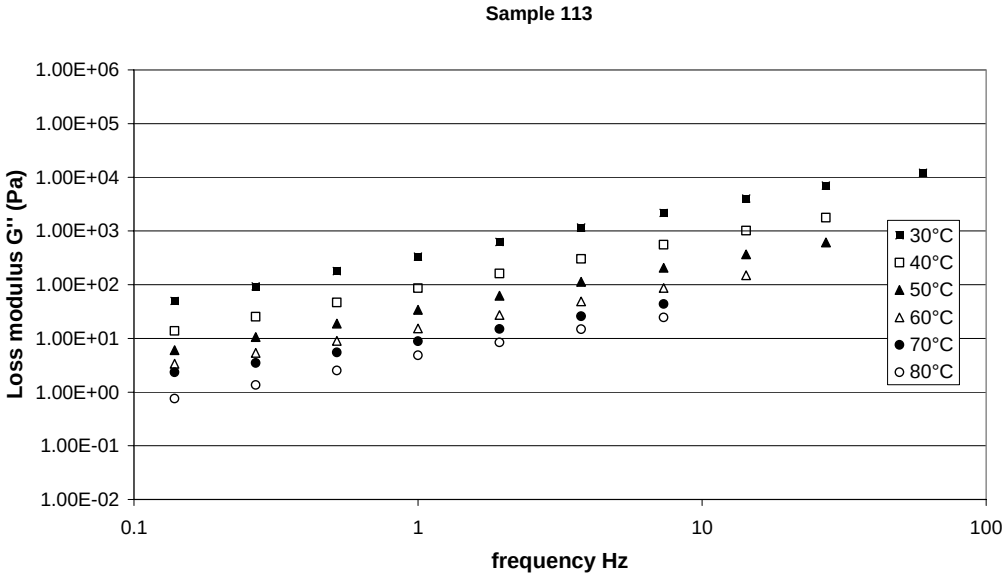

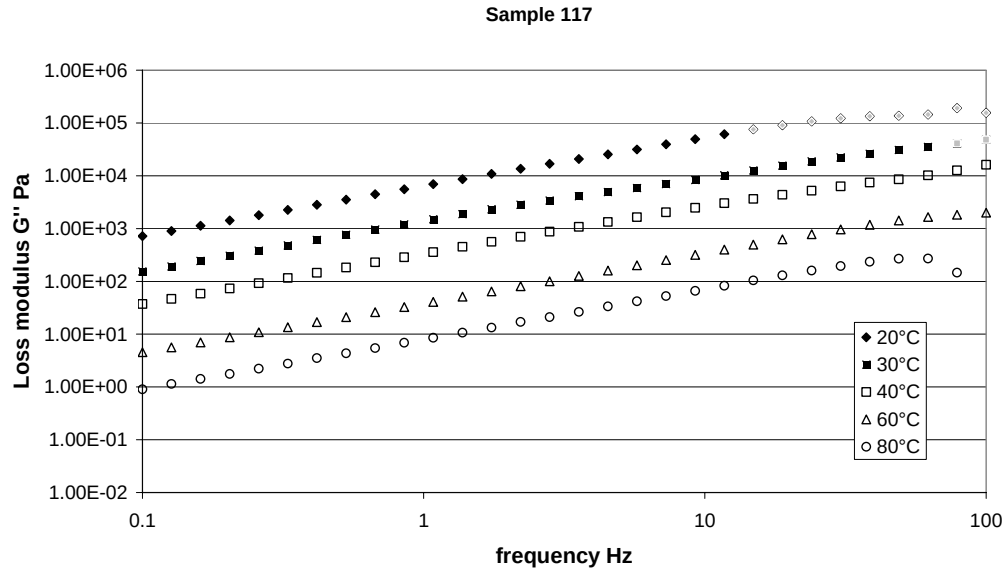

Figure 4.9 Loss modulus, for the sample 113 and 117, at different temperatures: 20(♦), 30 (■),40 (□), 50(▲), 60 (Δ), 70(●), 80(○) °C.

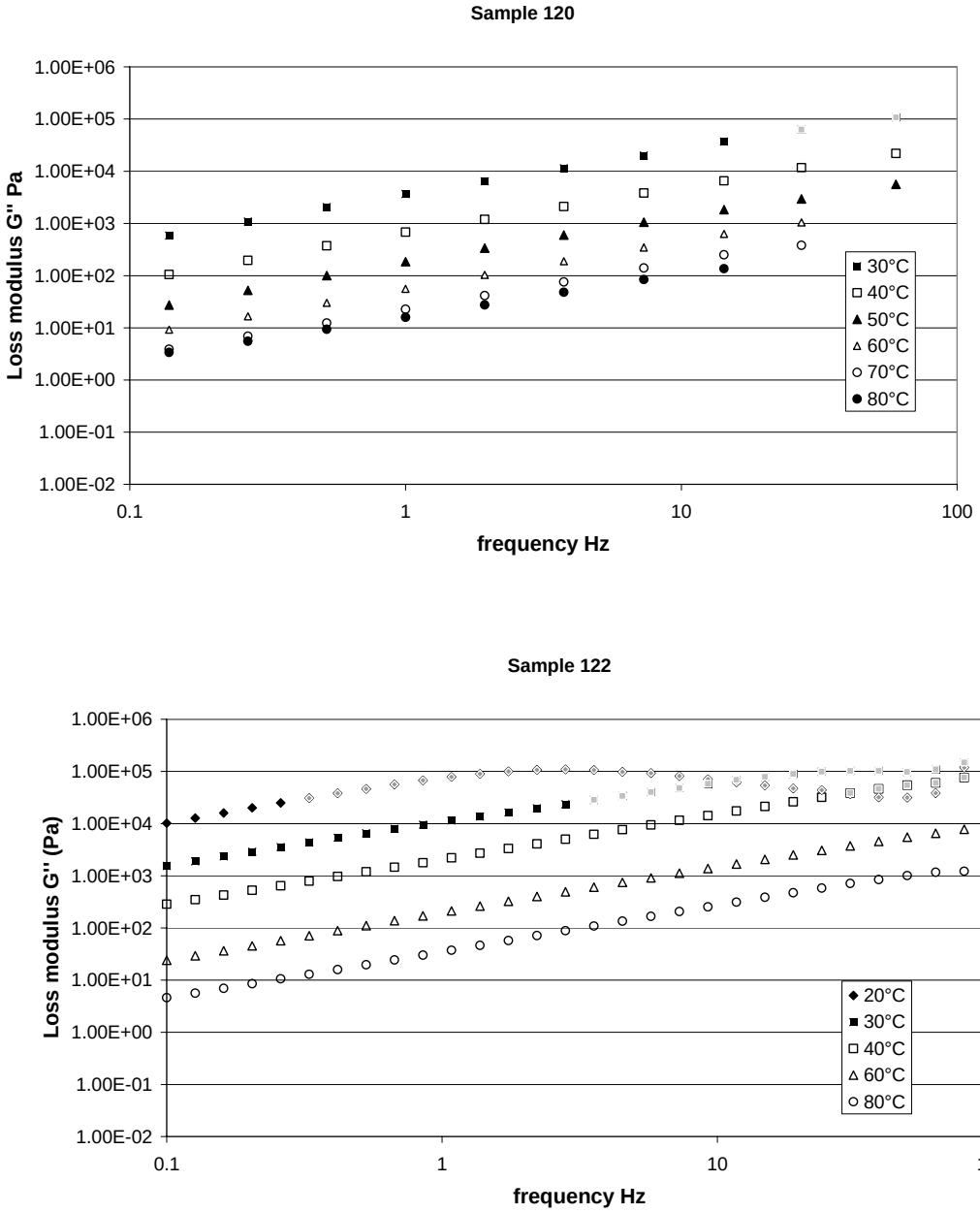

Figure 4.10 Loss modulus, for the sample 120 and 122, at different temperatures: 20(♦), 30 (■) ,40 (□) , 50(▲), 60 (Δ), 70(●), 80(○) °C

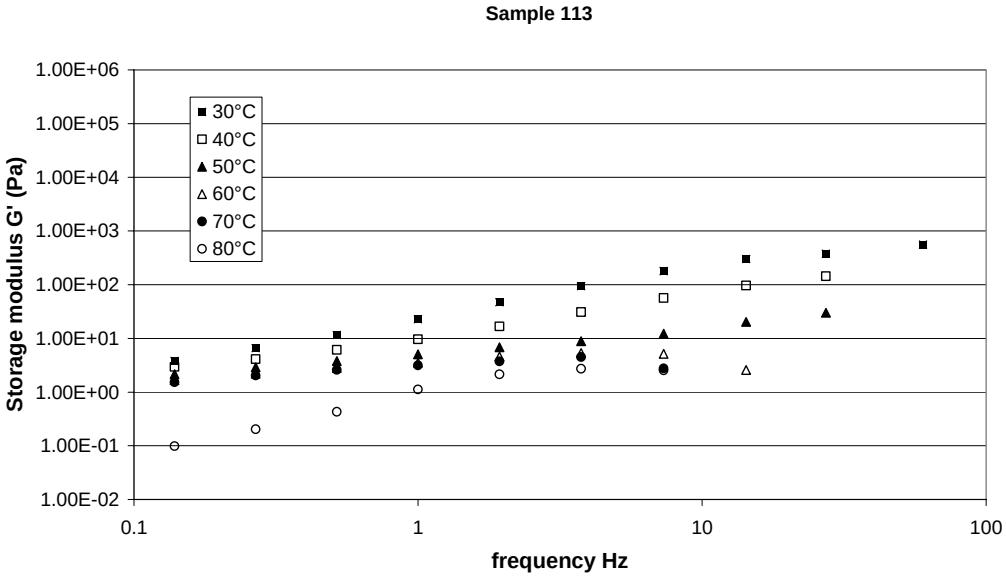

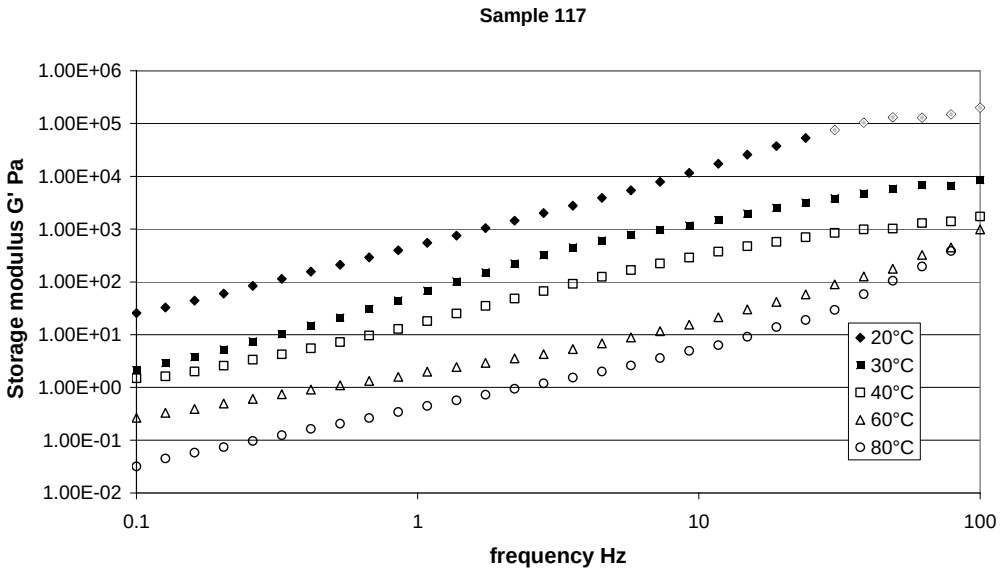

Figure 4.11 Storage modulus, for the sample 113 and 117, at different temperatures: 20(♦), 30 (■),40 (□) , 50(▲), 60 (Δ), 70(●), 80(○) °C

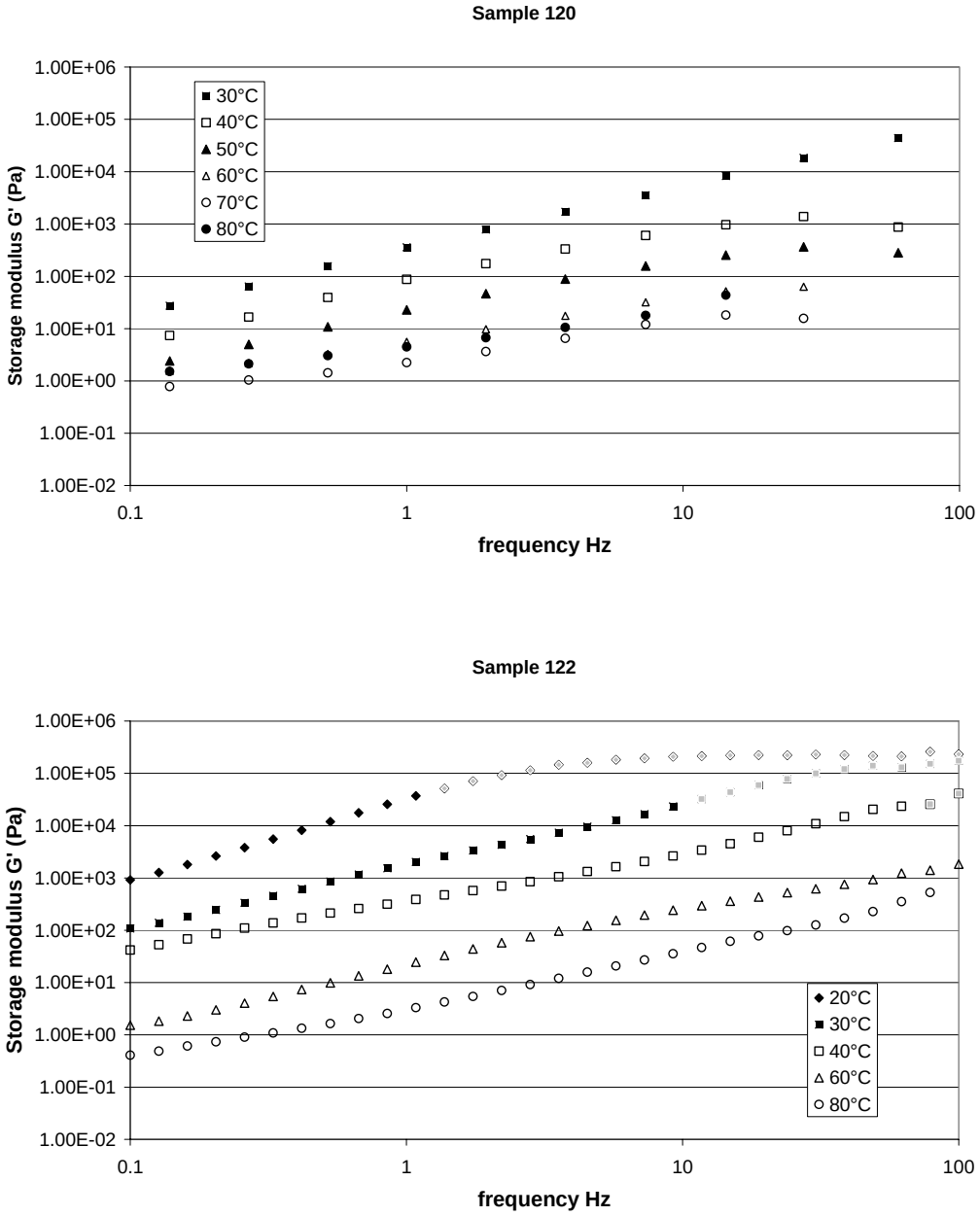

Figure 4.12 Storage modulus, for the sample 120 and 122, at different temperatures: 20(♦), 30 (■) ,40 (□) , 50(▲), 60 (Δ), 70(●), 80(○) °C

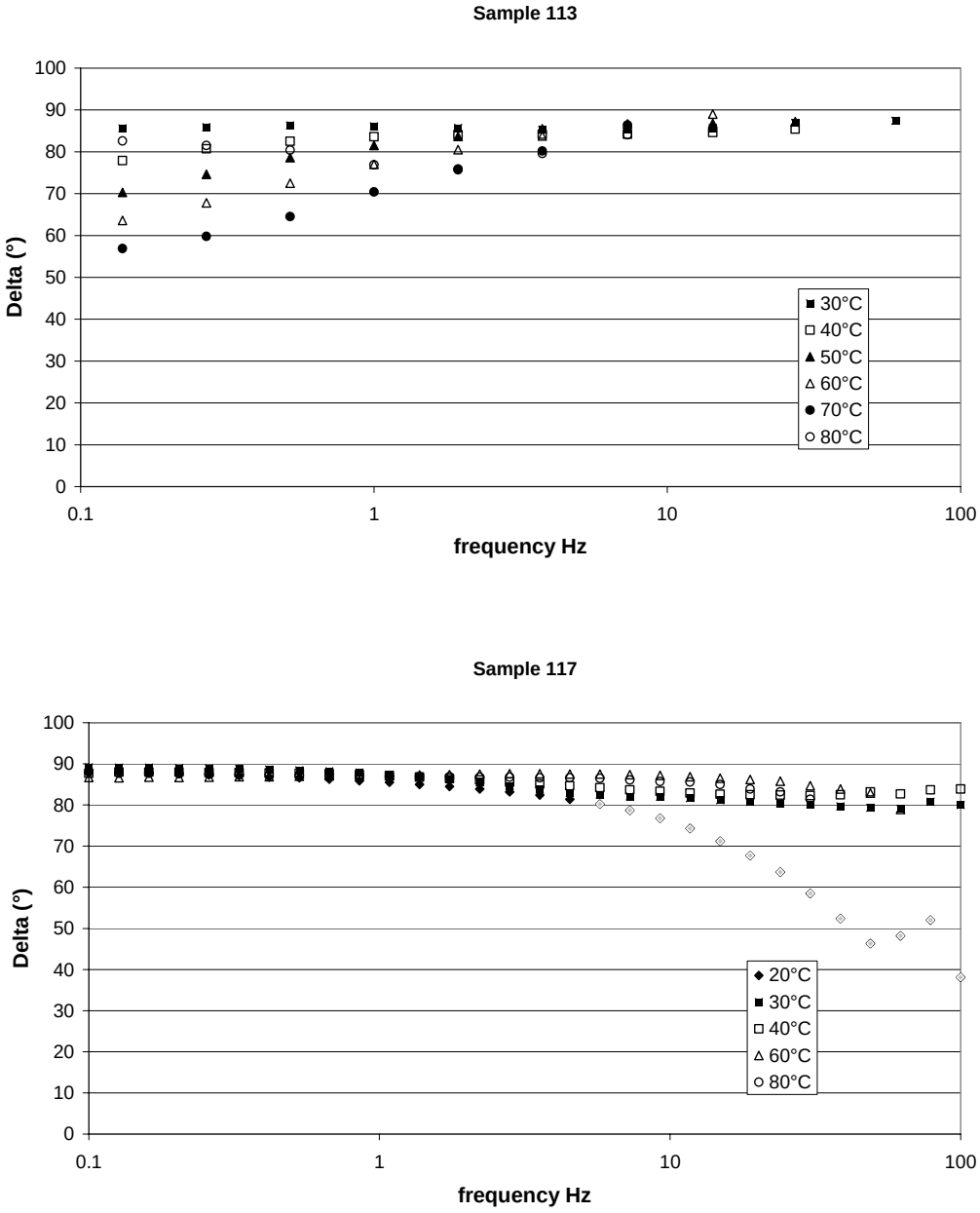

Figure 4.13 Phase angle, δ, for the sample 113 and 117, at different temperatures: 20(♦), 30 (■) ,40 (□) , 50(▲), 60 (Δ), 70(●), 80(○) °C

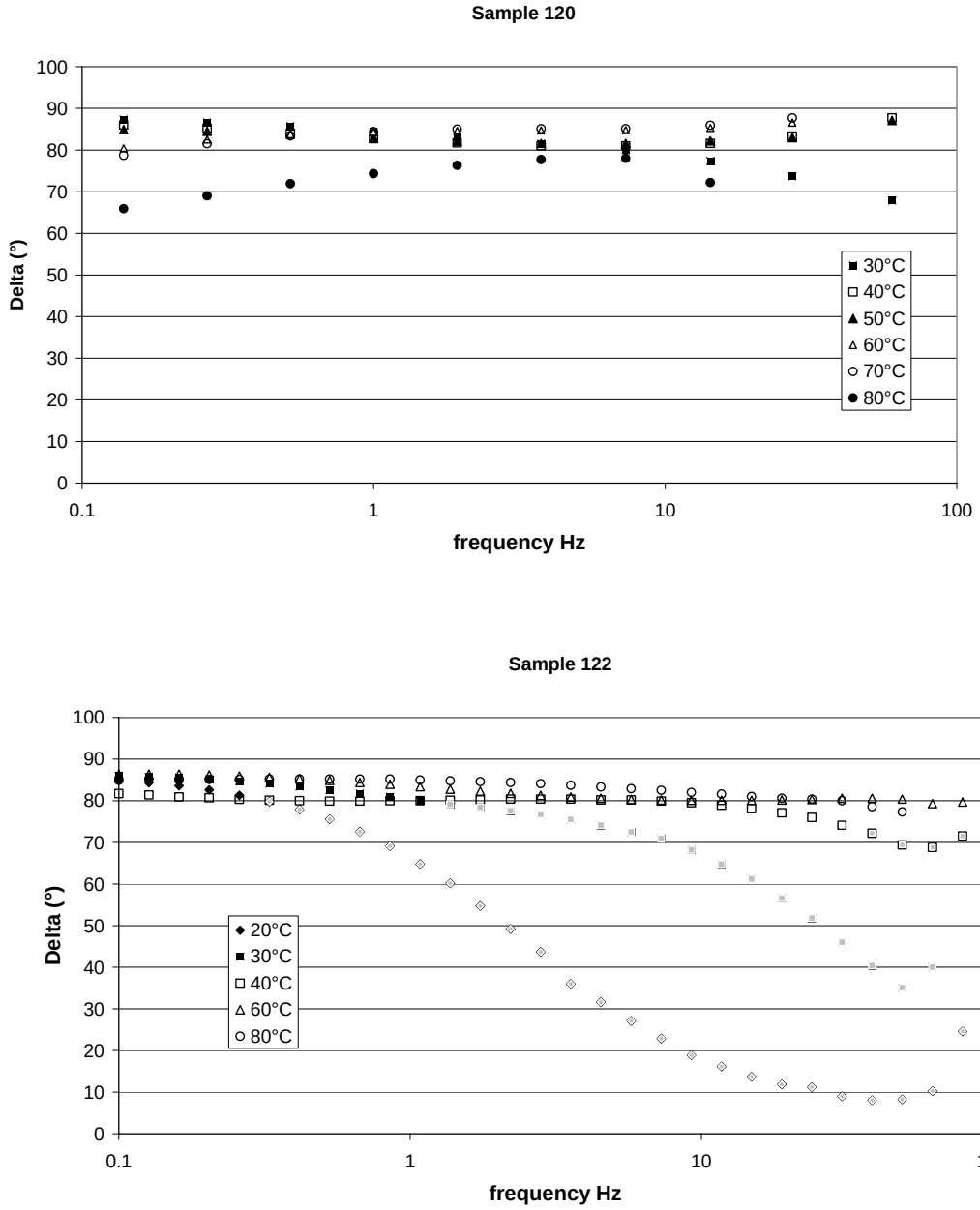

Figure 4.14 Phase angle, δ, for the sample 113 and 117, at different temperatures: 20(♦), 30 (■) ,40 (□) , 50(▲), 60 (Δ), 70(●), 80(○) °C.

Composite curves (Figures. 4.15 and 4.16) were constructed by defining an arbitrary reference temperature (T_0 = 40 °C) and shifting horizontally the loss modulus data along a logarithmic frequency axis. This procedure, known as the time-temperature superimposition (TTS), allowed a wider frequency window (7-8 orders of magnitude) to be obtained. The shape of these curves represented the frequency dependence of viscoelasticity at the reference temperature of 40°C. As it has been discussed in section 2.3.2 for a non-entangled liquid material the loss modulus G" and the storage modulus G' are proportional to ω and ω^2 respectively. A linear dependence of the loss modulus with the frequency is experimentally found for all the caramel samples. However a quadratic dependence of the storage modulus with the frequency was not found. For these samples showing close to Newtonian behaviour ($\tan\delta \approx 90^{o}$) the storage modulus is to low to measure with any confidence. These patterns, where a rubbery plateau is not observable, are characteristic for non polymeric glass-former materials (Plazek and Bero, 2003).

Scatter in the delta values, at low frequencies for sample 113 are believed to be due to experimental error because of the very low value of the measured storage modulus.

The shift factor determined from superimposition has been used in the WLF modelling and determination of the glass transition. This analysis is shown in the following section.

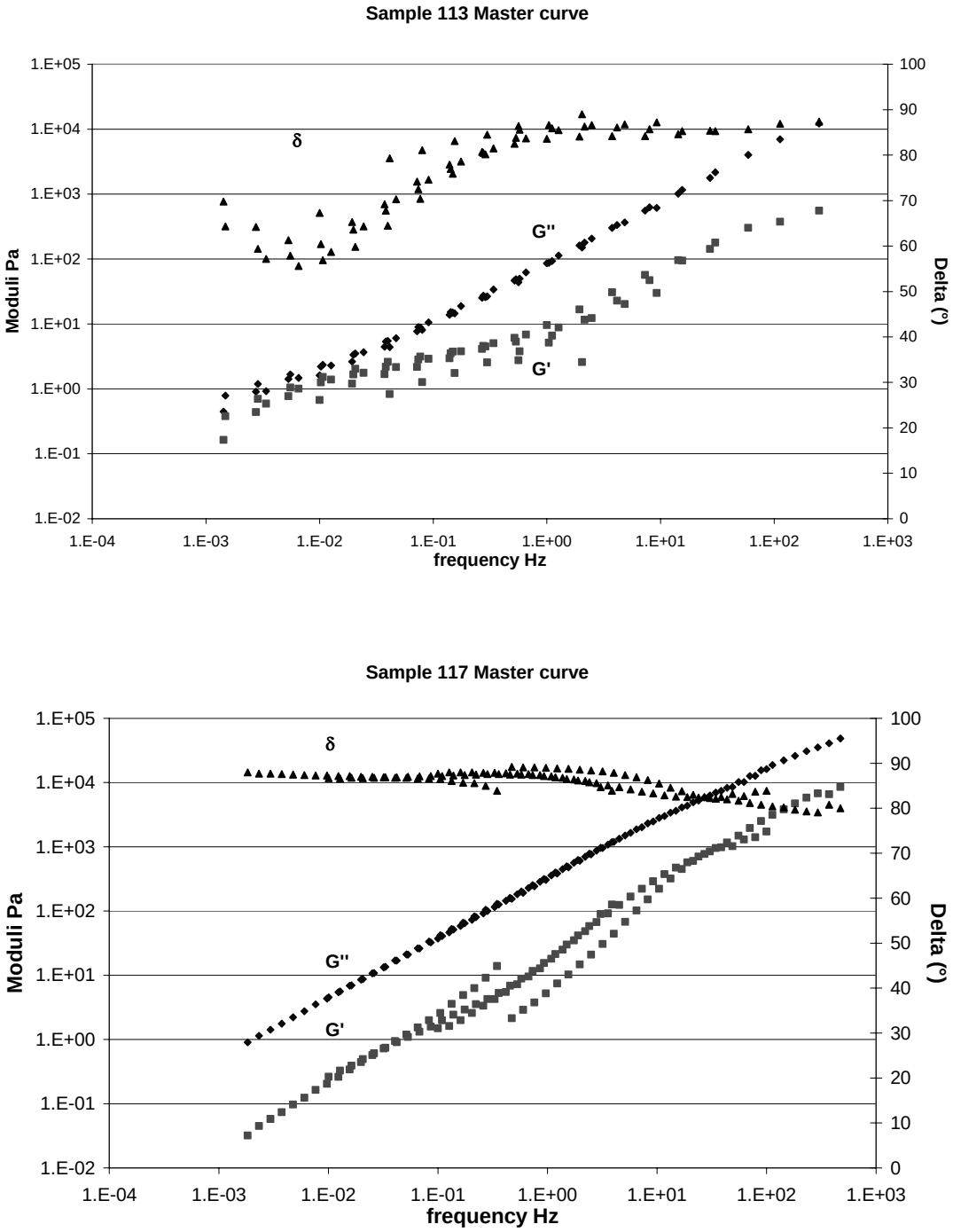

Figure 4.15 Master curves (T_0=40°C) for the caramels 113 and 117

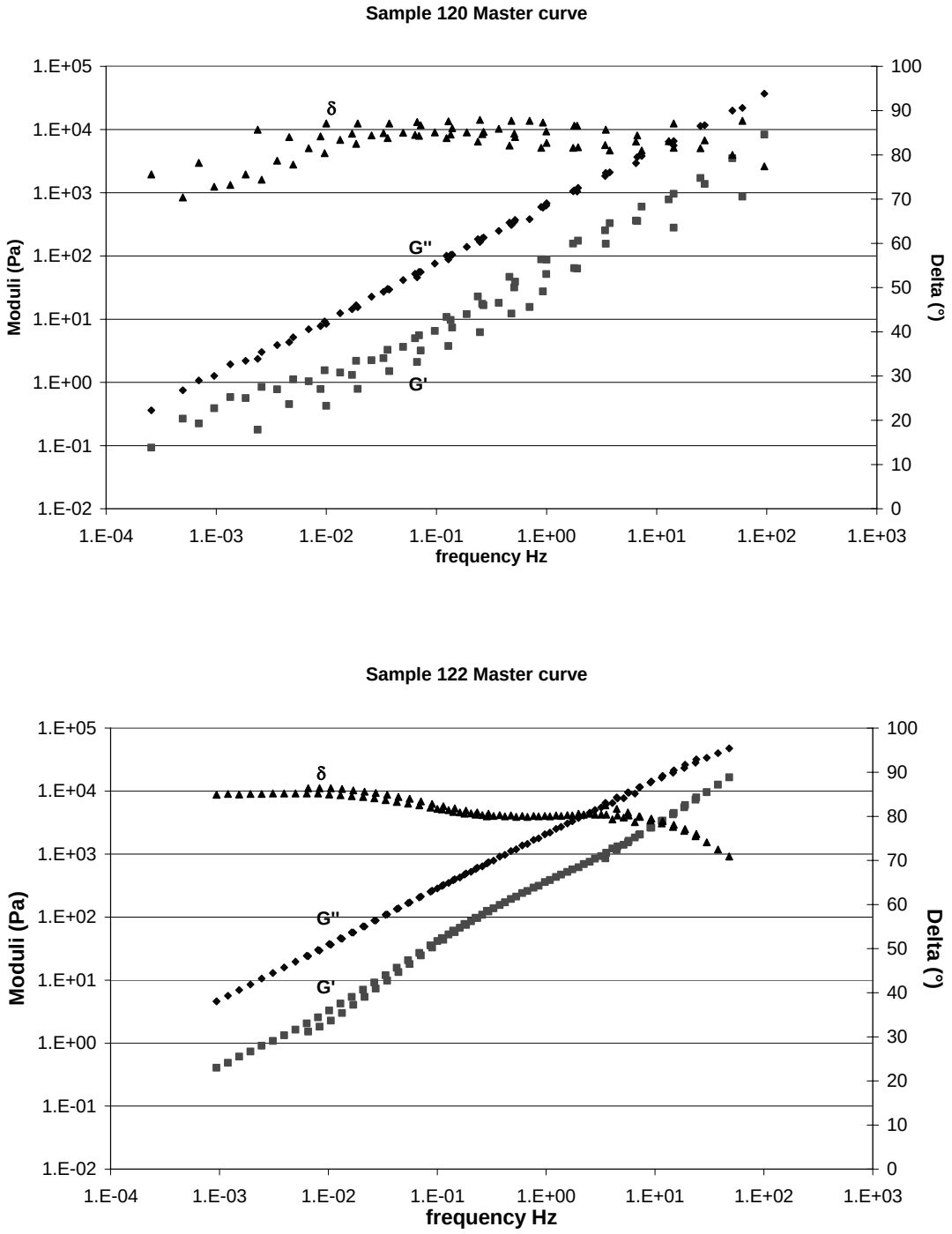

Figure 4.16 Master curves (T_0=40°C) for the caramels 120 and 122

4.6.3 CREEP

The creep compliance response is shown in Figures 4.17, 4.18 and 4.19.

The data obtained at different stresses collapsed onto the same line indicating they have been performed in the linear viscoelastic region.

The compliance, at the maximum time the stress was applied increased, with increasing water content, and all the samples showed no recovery when the stress applied was removed. These results were in agreement with the viscosity and oscillation data discussed previously in that caramel behaved as a predominant non-elastic material.

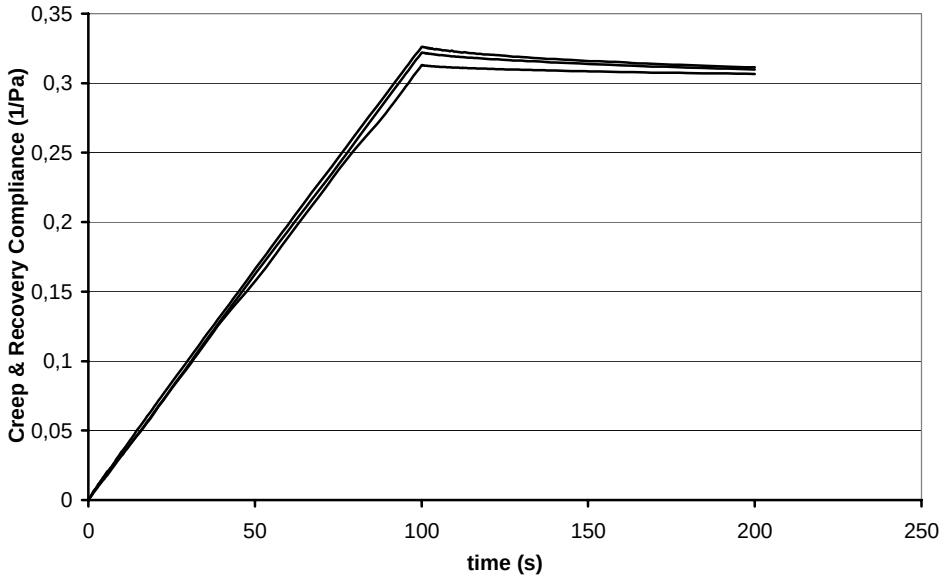

Figure 4.17 Creep and recovery compliance test performed at 20°C on the sample 113 for stresses of 0.25, 1 and 4 Pa. (Results obtained at the different stresses are coincident)

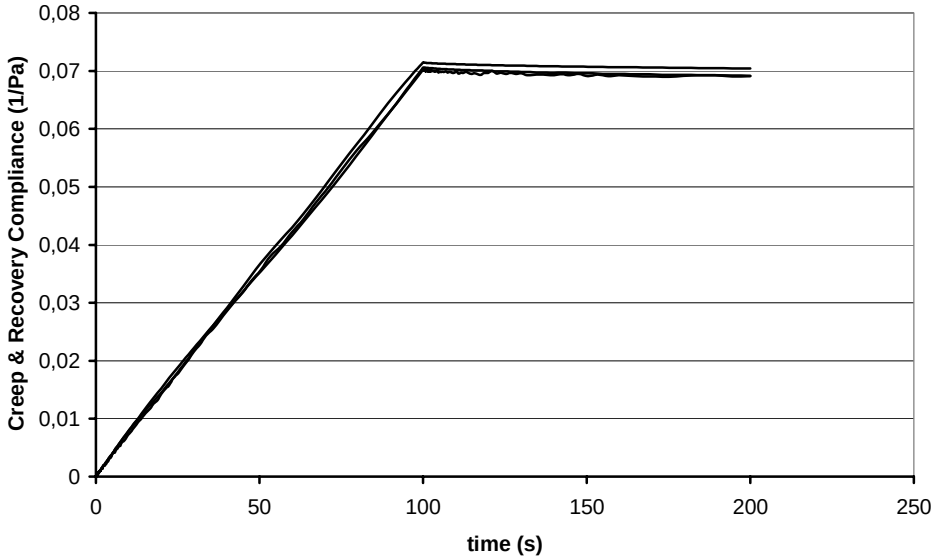

Figure 4.18 Creep and recovery compliance test performed at 20°C on the sample 117 for stresses of 0.25, 4 and 16 Pa. (Results obtained at the different stresses are coincident)

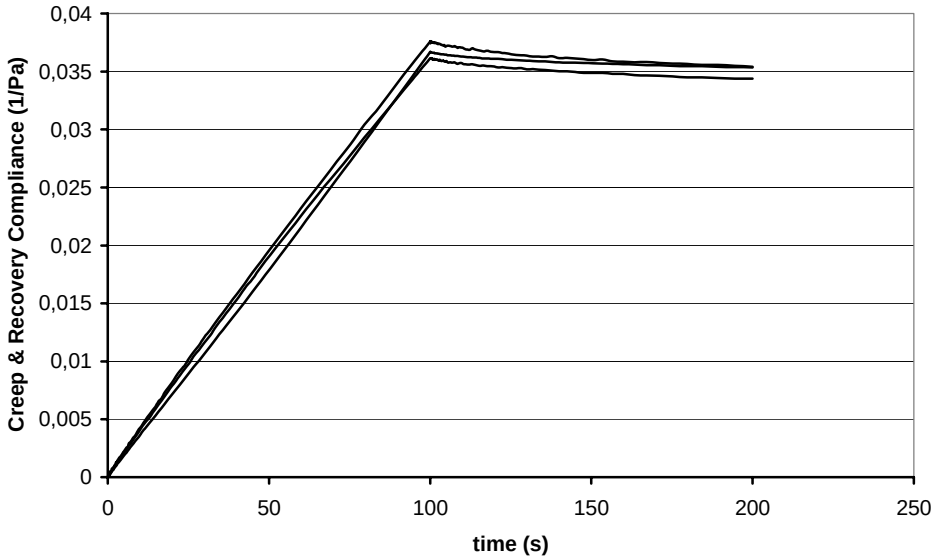

Figure. 4.19 Creep and recovery compliance test performed at 20°C on the sample 120 for stresses of 0.5, 1 and 4 Pa. (Results obtained at the different stresses are coincident)

The creep compliance behaviour of a viscoelastic material can be described by using a mechanical analogue model. Often a series of *m* Kelvin models combined with a Maxwell model as shown in Figure 4.20 is used.

This model has been widely described in the material and methods section.

The resultant equation of the compliance as function of the time is (Steffe, 1992):

$$J = \frac{\gamma}{\sigma_0} = f(t) = J_0 + \sum_{i=1}^{m}\left[J_i\left(1 - \exp\left(\frac{-t}{(\lambda_{ret})_i}\right)\right)\right] + \frac{t}{\mu_0} \qquad \text{eq 4.1}$$

where J_0 is the instant compliance arising from the spring in the Maxwell element , Ji is the compliance in Kelvin element i, the retardation time, $(\lambda_{ret})_i$, is the ratio between the Newtonian viscosity of the dash pot , μ_i, and the modulus of the spring, G_i, in the Kelvin element i. The free dashpot with viscosity η_0 at the end of the mechanical model with viscosity μ_0 causes permanent deformation in the material.

Bohlin software allows the analysis of creep and recovery. For the non-hydrocolloid containing samples the only parameter of importance is μ_0. Table 4.7 shows this parameter for the three caramels for which creep measurement were performed. These values were used in subsequent modelling.

Table 4.7 *Creep viscosities μ_0 (Pa·s) at 20ºC and correlation coefficient R*

	113	**117**	**120**
R	0.9999	0.9988	0.9992
μ_0	323.3	1334	2679

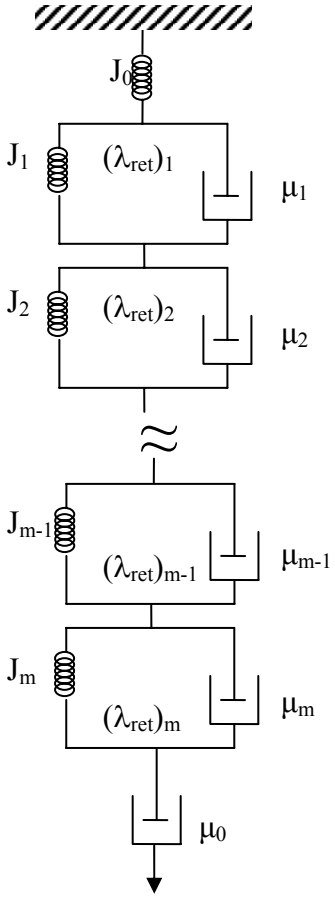

Figure 4.20 m Kelvin elements in series with a single Maxwell element.

4.6.4 CAPILLARY RHEOMETRY

In contrast to the samples containing hydrocolloids described in the next chapter, it was more difficult to obtain reproducible results with the standard samples. The Rosand capillary twin bore was designed to be used with synthetic polymer melts of high viscosities at high temperatures. Measurements on caramel have been performed at 70 ºC at the lower limit of the temperature that can be easily controlled by this rheometer. Poor temperature control could be one of the reasons for the difficulty in obtaining reproducible results. Shear induced heating effects could add to this problem. The samples containing hydrocolloids were easier to obtain good data. Thus may suggest that other factors such as fat separation inducing slip effect could contribute to the problems with the non-hydrocolloid containing samples. A further factor could be trapped air bubbles. Data improved when the barrel was filled using the funnel shown in Figure 3.22. The sample was preheated in the funnel which released trapped air prior to filling the rheometer barrel.

The graph of shear (empty symbols) and extensional (filled symbols) viscosity curves, shown in Figure 4.21, covers 4 decades in strain rate and 4 orders of magnitude in viscosity.

Figure 4.22 shows an ideal pattern for material having high concentration of alignable entities, such us liquid with a high concentration of suspended fibres or polymer solutions or melts, in both of the cases there are contacts between particles or entanglements whose concentration will dominate the viscosity. The upper curve is the extensional viscosity and the curve at the bottom is the shear viscosity.

There will be a critical deformation where the extensional viscosity starts to increase.

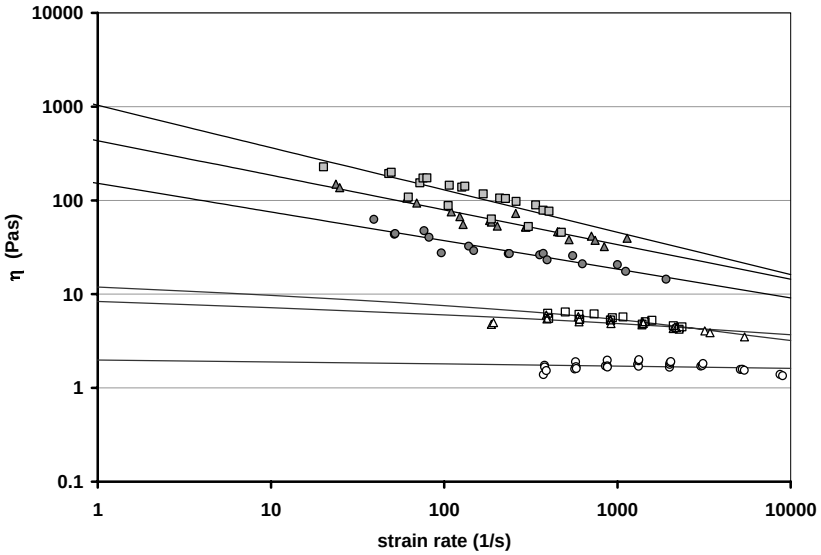

Figure 4.21 Viscosity as function of the strain rate for the sample 117 (●), 120 (▲) and 122 (■). Filled symbols are extensional capillary data and empty symbols are shear data

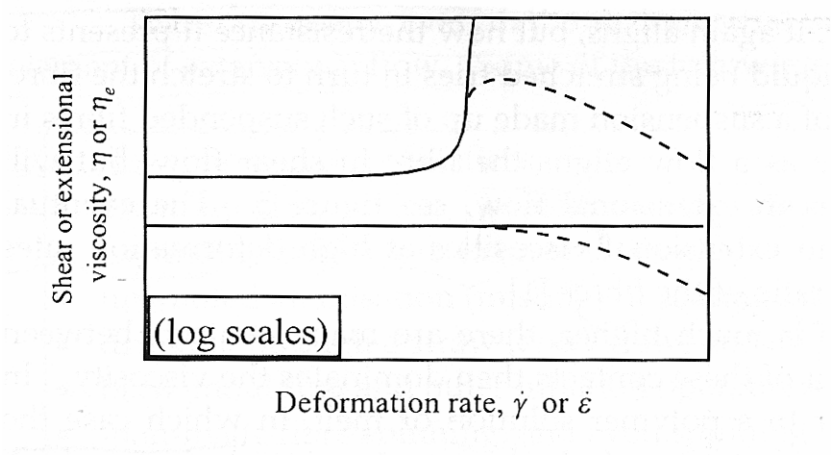

Fig 4.22 The shear and extensional viscosities of a polymer network, network dynamic effects shown as solid lines, and the effect of loss of junction as dotted lines (Barnes, 2000)

During both extensional and shear flow particles or polymeric chains align in the direction of the flow. In the extensional case the liquid being stretched tries in turn to stretch the aligned particles and the increasing of the extensional viscosity is related to the resistance of these particles to stretching. In contrast, in shear flow the liquid can move with less resistance when particles are aligned and in this situation the shear viscosity will decrease while the extensional viscosity will increase. The extensional viscosity will increase until the contacts or entanglements start breaking. At this point a decrease in the extensional viscosity is observable.

In the case of caramels, shown in Figure 4.21, only the last part of the ideal polymer curve is observable.

There is a marked thinning behaviour in extensional flow. The lower the water content the higher the extensional viscosity. The dependence on the water content is less marked in shear flow, and behaviour closer to Newtonian is observed.

The Trouton ratio is the ratio between extensional and shear viscosity at the same strain rate; it can be mathematically demonstrated that for a Newtonian fluid in uniaxial flow it is equal to 3 (eq. 3.35) (Steffe 1992). The higher this value the higher the elasticity and also the deviation from the ideal Newtonian behaviour. Figure 4.23 shows the Trouton ratio dependence on the strain rate, obtained as a result of dividing the best fit of the extensional flow curve by the best fit of the shear flow curve.

There are not many differences in the pattern of the Trouton ratio with the strain rate between the three samples, in the limit of the experimental error. The value of the Trouton ratio range between 40 (this is an extrapolation of the data) at lower shear rate and 7 at higher rates. These high values at low strain rates are surprising for a Newtonian material and probably affect anomalies in the capillary data.

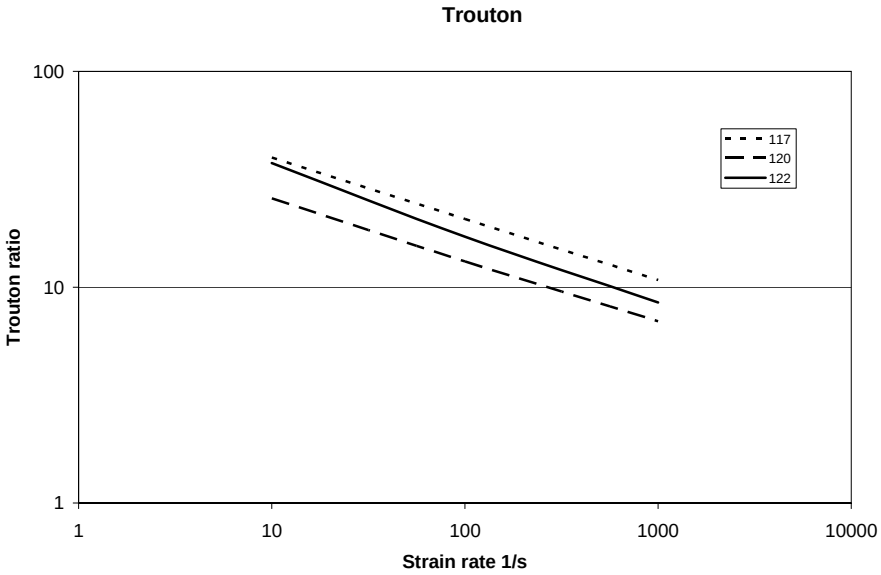

Figure 4.23 Trouton ratios as function of the strain rate for samples 117, 120 and 122.

4.7 Modelling

4.7.1 MODELLING OF CALORIMETRIC DATA

The plasticizing effect of water is usually described by the dependence of the glass transition temperature on either the weight or volume fraction of water. The function giving the dependence between the glass transition and the water content is called the plasticizing function and is of special interest for food formulation and a number of food manufacturing processes. This function also serves to estimate the T_g of a dry biopolymer or a food product. For the prediction of the water plasticization effect in food systems the Gordon-Taylor and Couchman-Karasz equations are most often used. The Gordon-Taylor equation is based on an assumed volume additivity of repeat monomer units and constant partial specific volumes in copolymers. It was derived for the prediction of the glass transition temperature of a binary miscible copolymers from the T_g values of pure polymers in their ideal mixture and their expansion coefficients in the glassy and rubbery states.

The Gordon-Taylor equation (eq 4.2) has often been used for the predicting the T_g values of mixtures of low-molecular weight sugars and food biopolymers (Roos, 1995)

$$T_g = \frac{T_{g_1} X_1 + k T_{g_2} (1 - X_1)}{X_1 + k(1 - X_1)} \qquad \text{eq. 4.2}$$

where:

T_{g1} is the glass transition temperature of the water =138K

T_{g2} is the glass transition temperature of the dry sugar matrix

$k=\Delta C_{p2}/\Delta C_{p1}$ the ratio between the change in the specific heat capacities at T_g of the sugar matrix and the water (ΔC_{p1} = 1.94 Joule$\cdot g^{-1}K^{-1}$)

The glass transition temperature and the water content for the caramel samples has been reported previously in Table 4.3. This data was fitted to the Gordon-Taylor equation (Figure 4.24), allowing an extrapolation of the glass transition temperature of the dried sugar matrix. The resulting fit leads to the equation:

$$T_g = \frac{138X_1 + 163(1 - X_1)}{X_1 + 0.535(1 - X_1)} \qquad \text{eq 4.3}$$

and give values for the constants: $T_{g(\text{dry sugars})} = 304.6\text{K} = 31.6^{\circ}\text{C}$ and $\Delta C_{p(\text{dry sugars})} = 0.535$ Joule$\cdot g^{-1}K^{-1}$

Two fundamental thermodynamic relations, based on entropy and volume continuity conditions and an assumed single glass transition of compatible polymer-polymer and polymer-plasticizer mixture underlie the Couchman-Karasz relationship.

The Couchman-Karasz equation, $T_g \sum_i x_i \Delta C_{p_i} = \sum_i T_{g_i} x_i \Delta C_{p_i}$, allows a theoretical calculation of the glass transition, when the composition of the food is known. The composition of the sugar phase in the caramels and literature data above the glass transition and the ΔC_p of different sugars are shown in Table 4.8. These data have been used for application of the Couchman-Karasz to the sugar phase of the caramels and leads to a value of glass transition of dry caramels of = 348.0K equivalent to 75.8°C. This is about 50K higher than the extrapolated value from the Gordon-Taylor equation.

The Couchman-Karasz equation has been also used to calculate the theoretical value of the glass transition temperature of the caramel at their water contents. Table 4.9 shows the percentage composition of the four samples of caramel normalised to the sugar and water content. Table 4.10 show a comparison between the experimental and calculated values of glass transition temperature. Again there is a difference of about 40K.

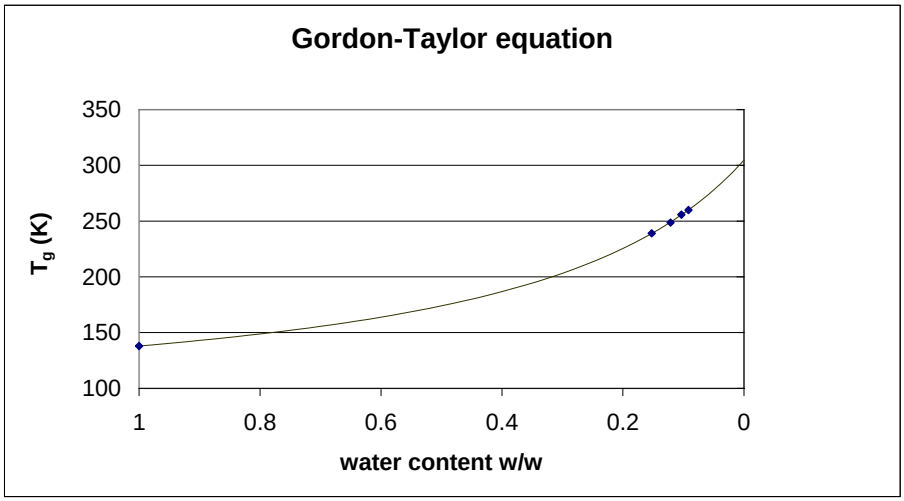

Figure 4.24. Gordon-Taylor fit of experimental data

Table 4.8: *Caramel sugar composition and glass transition temperatures and ΔCp from literature data (Orford et al. (1989)).*

	Caramels sugars composition	T_g K	ΔC_p J/gK
Sucrose	**0.068**	**343**	**0.73**
Lactose	**0.021**	**374**	**0.52**
Fructose	**0.079**	**280**	**0.83**
Dextrose	**0.367**	**311**	**0.88**
Maltose	**0.236**	**368**	**0.79**
Maltotriose	**0.06**	**408**	**0.53**
Higher sugars	**0.169**	**502**	**0.41 (pectin)**
tot	**1**		

Table 4.9 *Composition of caramels normalised to the only sugars ingredients and water. Glass transition temperature and ΔC_p are also shown for every component.*

	113	**117**	**120**	**122**	**T_g K**	**ΔC_p J/(gK)**
Water	0.154	0.123	0.105	0.093	138	1.94
Sucrose	0.057	0.060	0.061	0.062	343	0.73
Lactose	0.017	0.018	0.018	0.019	374	0.52
Fructose	0.067	0.069	0.071	0.071	280	0.83
Dextrose	0.311	0.322	0.329	0.333	311	0.88
Maltose	0.200	0.207	0.212	0.214	368	0.79
Maltotriose	0.051	0.052	0.054	0.054	408	0.53
Higher sugars	0.143	0.149	0.152	0.154	502	0.41
tot	1	1	1	1		

Table 4.10 *Comparison between experimental and calculated glass transition*

	113	**117**	**120**	**122**
Experimental T_g (ºC)	-34.2	-24.2	-17.4	-13.3
Calculated T_g (ºC)	6.7	18.2	25.4	30.2
ΔT (ºC)	40.9	42.4	42.8	43.5

The experimental glass transitions are lower compared with the theoretical value implying higher mobility in the caramel system compared with pure sugar solutions.

The disagreement between the experimental results and the predicted from the two models makes the author questioning the validity of the modelling approach for the three mixtures. If the non-fat phase was entirely sucrose and water, examination of the phase diagram for sucrose (Figure 2.5) would give values for T_g in the range of -5 ÷ -30ºC which is far closes to the DSC results.

The Couchman-Karasz equation prediction for sucrose-water mixtures is shown in Figure 4.25. Similar disagreement is also found for sucrose solution.

There are been considerable interest on the fragility of glasses. (Angell, 2002). A fragile glass is a glass with shows a large decrease in viscosity with temperature above Tg. It has been shown that sugars are fragile materials. it is possible that there is a link between the large decrease in T_g with water content compared with the Couchman-Karasz prediction and the large decrease in viscosity with temperature above the glass transition for these type of systems. The concept of fragility is discussed further in section 4.7.2.1.3.

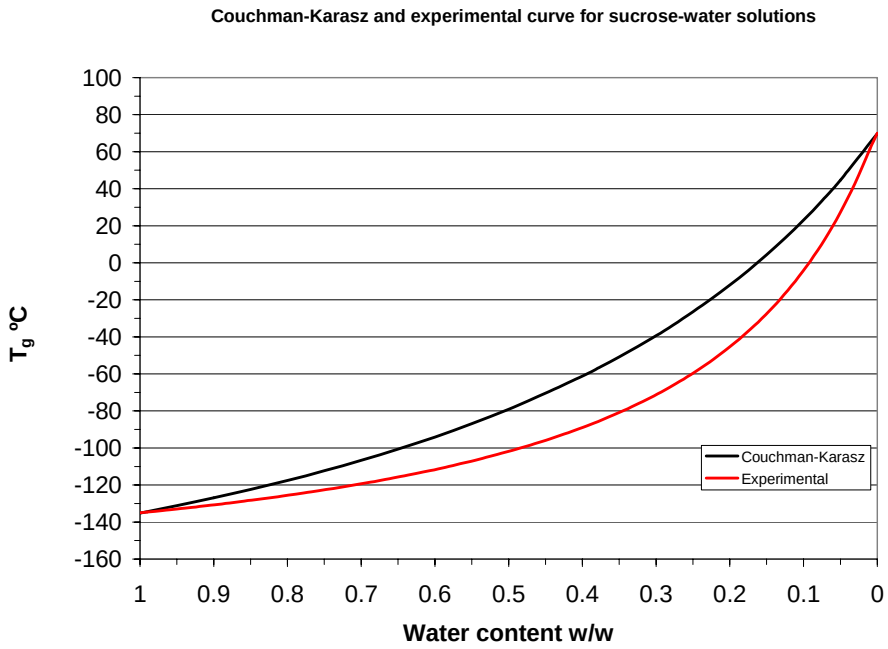

Figure 4.25. Couchman-Karasz prediction (black) and experimental pattern (red) (data from Figure 2.5) of glass transition temperatures for sucrose-water system.

4.7.2 Modelling of Rheological Data:

As stated in the introduction to this chapter three approaches were used to model the data. These were applied to the viscosities obtained from the rotational rheometer. The oscillation data was further modelled using time temperature superimposition.

4.7.2.1 Viscosity

K obtained from the power law equation, η* at 1 rad sec^{-1} and the creep viscosity were combined.

Table 4.11 displays these viscosity data

Table 4.11 *Consistency indices, η* at 1 rad sec^{-1} and the creep viscosity*

	Sample / T (C)	113	117	120	122
Shear	**40**	26.0 ± 1.2	71.82 ± 1.78	-	-
viscosity	**50**	9.45 ± 0.17	21.10 ± 0.42	48.07 ± 5.64	-
(Consistency	**60**	4.27 ± 0.46	8.33± 0.42	22.20 ± 2.44	55.70± 7.90
Index)	**70**	2.15 ± 0.04	3.95 ± 0.35	12.16 ± 0.37	31.91 ± 3.17
Pa·s^{n-1}	**80**	1.18± 0.09	2.02 ± 0.20	7.21 ± 0.54	16.33± 0.68
	20		1120		15900
η* (Pa·s)	**30**	57.3	240	669	2330
at	**40**	16.2	57.8	121	426
ω=1rad/sec	**50**	7.36		31.2	
	60	4.30	6.87	10.7	36.1
	70	3.2		4.54	
	80	0.876	1.40	4.26	6.93
Creep					
viscosity	**20**	320	1330	2680	
η_0 (Pa·s)					

A comparison of these values obtained from the different techniques shows reasonable but not perfect consistency. The creep viscosity at 20ºC for sample 117 of 1330 Pa·s compares with η* of 1120 Pa·s. η* with the exception of the sample 113 at 70ºC, is somewhat lower than the consistency index from the viscosity data.

4.7.2.1.1 Statistical model

An empirical model has been created in order to generalize the behaviour of the viscosity with the temperature and the water content. All the data have been represented in a 3-D plot in Figure 4.26

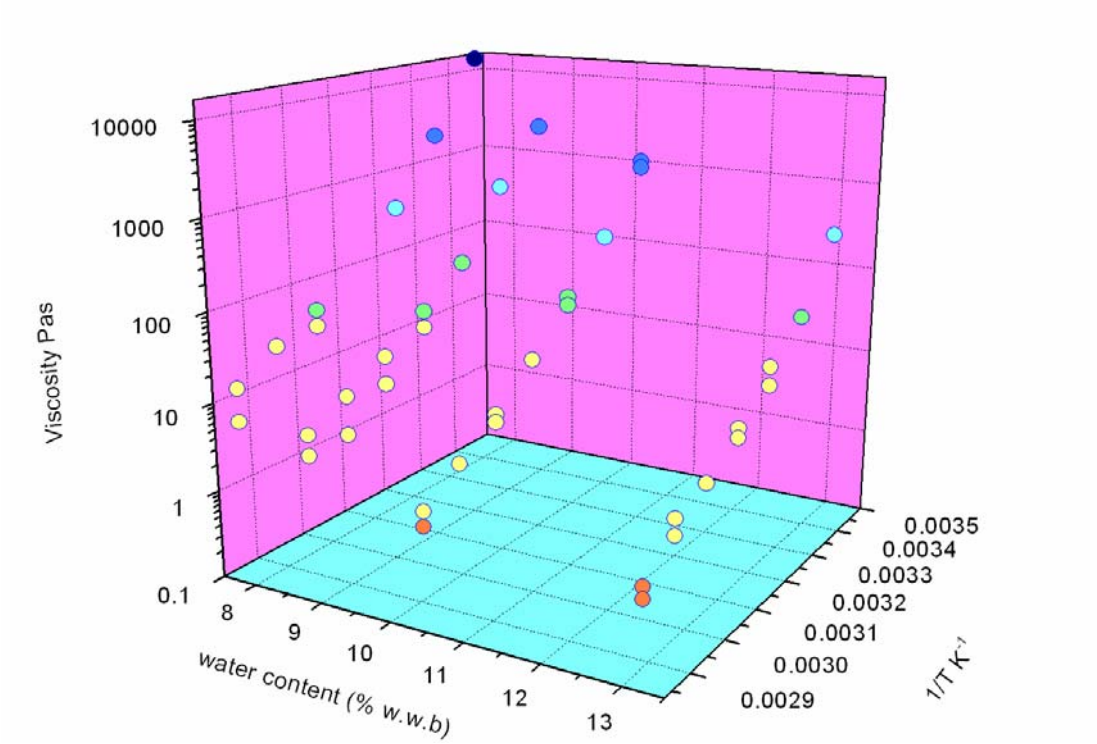

Figure 4.26 Experimental points

The design expert software was used to fit the model.

Attemps to find a linear model were not succesful resulting in a model with a significant lack of fit. The Anova analysis, whose results are reported in the appendix at the end on this chapter, showed that a quadratic fit was the best option.

The equation was of the form:

$$\log(\eta) = a_0 - \frac{a_1}{T} - a_2 X_w + \frac{a_3}{T^2} + a_4 X_w{}^2 - \frac{a_5 X_w}{T} \qquad \text{eq.4.4}$$

where X_W is the % water (w.w.b.) and T is the temperature in K; a_0 to a_5 are constants.

The coefficients and the standard error assigned to the coefficients are shown in Table 4.12

Table 4.12 *Coefficients and standard error for the statistical model*

Factor	Actual Coefficient Estimated	Standard Error
a_0	21.74	0.69
a_1	-15560	-360
a_2	-0.43	0.02
a_3	3602000	628000
a_4	0.041	0.007
a_4	-210	55

The resulting equation :

$$\log(\eta) = 21.75 - \frac{1.556 \cdot 10^4}{T} - 0.431 X_w + \frac{3.60 \cdot 10^6}{T^2} + 0.041 X_w{}^2 - \frac{209.5 X_w}{T} \quad \text{eq 4.5}$$

is represented in a 3-D surface view in Figure 4.27

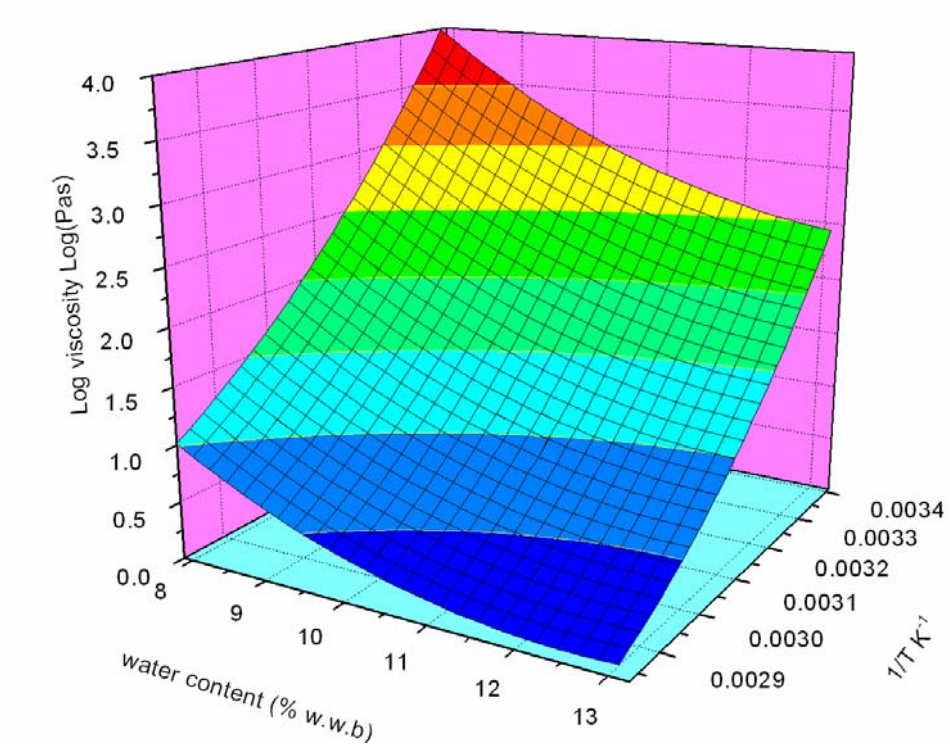

Figure 4.27 3-D surface view of the model.

4.7.2.1.2 Arrhenius kinetics

The viscosity of sugar solutions has been reported by an Arrhenius expression of the form(Barnes, 2000):

$$\eta = \eta_0 \exp\left(\frac{-E_0}{RT}\right) \qquad \text{eq. 4.6}$$

that can be rewritten as

$$\ln(\eta) = \ln(\eta_0) - \frac{E_0}{RT} \qquad \text{eq. 4.7}$$

Figure 4.28 shows a plot of Log η against the reciprocal of absolute the temperature.

From the slope of the line it is possible to obtain the activation energies. These are shown in Table 4.13. The values range from 75 K Joules mol^{-1} for the samples at higher water content to 100.9 K Joules mol^{-1} for the sample at low water content, for an average value of 90±11 K Joules mol^{-1}.

As already said in the literature review chapter Mathlouthi and Genotelle (1995) reported activation energy from 17 K Joules/mol for very dilute solutions to 105.17 K Joules/mol for the 85% sucrose solution. As it would be expected our values are close to those reported for the more concentrated sugar solutions. A curvature of the data in Figure 4.28 shows that for the low water content in particular the Arrhenius model does not fit the data well. This is not unexpected as at temperatures above but close to the glass transition WLF rather then Arrhenius behaviour would be expected (Slade and Levine 1991) The data was therefore also modeled using a WLF model.

Figure 4.29 shows the T_g scaled Arrhenius plot.

Value of viscosity at the temperature limit of T=Tg and T=∞ are from Angell, 1997. For simple liquids deviation from Arrhenius behaviour are well described by the Vogel-Tammann-Fulcher (VTF) equation:

$$\eta = \eta_0 \exp\left(D \frac{T_0}{T - T_o} \right) \qquad \text{eq. 4.8}$$

where D is a parameter that assumes value from 5 to 100, and changes the curvature of the plot between fragile and strong extremes. The fragility of a liquid in a range of temperature close to the glass transition can be related to the C_2 parameter of the WLF model and this will be subject to a discussion in the next section.

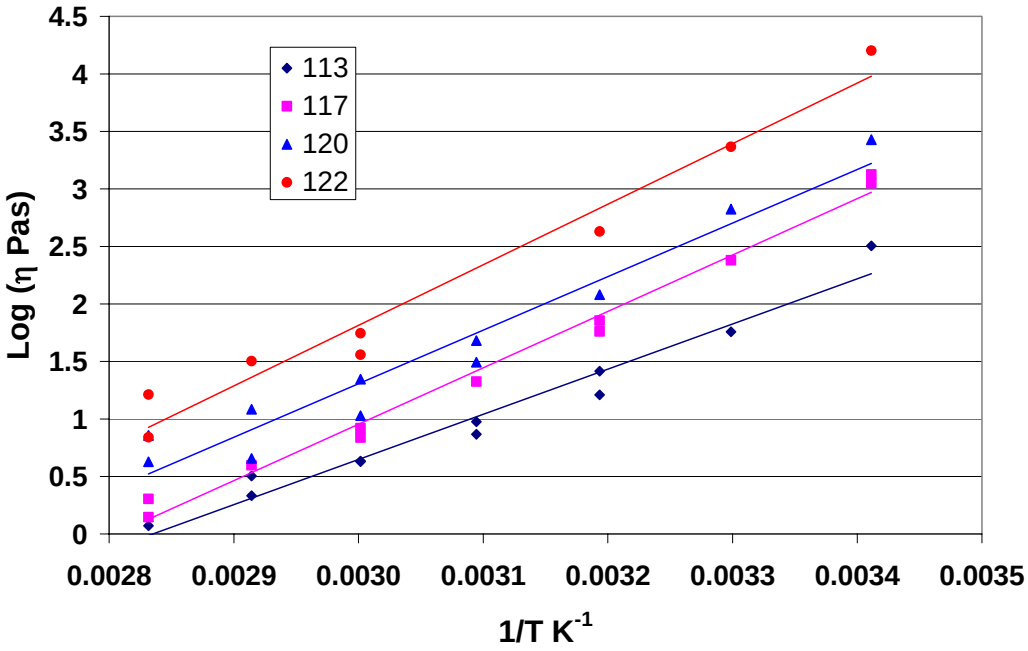

Figure 4.28 Arrhenius plot of the viscosities for the different caramel samples.

Table 4.13 *Linear fit parameters Y=A+Bx*

	113	117	120	122	Average	STD
R^2	0.9703	0.9805	0.9454	0.9708		
A	-11.1	-13.8	-12.7	-14.0		
B	3930	4900	4660	5270		
Ea ($KJmol^{-1}$)	75	94	89	101	90	11

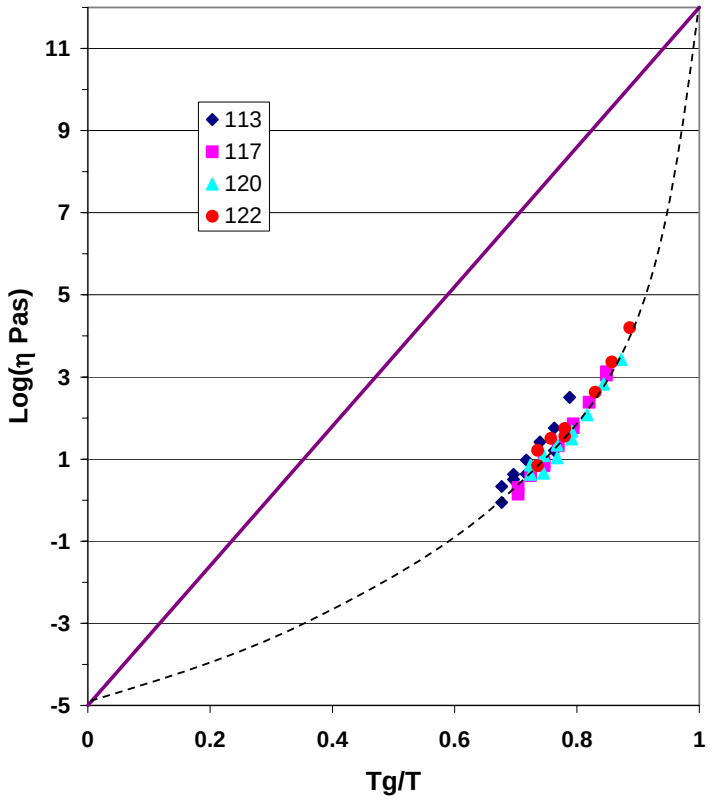

Figure 4.29 Tg-scaled Arrhenius plot of the viscosity for caramel samples at different water content. The value of the viscosity at T=Tg and T= ∞ are taken from ref. Angell, 1997. The solid line is the scaled Arrhenius plot to the Tg assuming a glass transition viscosity of 10^{12}Pa·s and a dotted line is a manual fit of the data. The greater is the distance between the two lines the higher is the fragility.

4.7.2.1.3 WLF Kinetics

WLF/free volume approach allows the dependence of the rheological properties on temperature and water content to be generalized. Central to this is the glass transition temperature.

According to the free volume theory Williams et al (1955), Angel (1997), Slade and Levine (1991), Kasapis and Sworn (2000) in amorphous systems above the glass transition temperature, in the range from T_g and T_g+100 ºC the viscosity varies with the temperature following the WLF equation (Williams et al, 1955).

$$\log a_T = \frac{\log(\eta)}{\log(\eta_0)} = \frac{-C_1^0(T-T_0)}{C_2^0+T-T_0} \qquad \text{eq 4.9}$$

where T_0 is an arbitrary reference temperature and η_0 is the viscosity at temperature T_0. The coefficients C_1^g and C_2^g are model parameters and as already said in the literature review chapter $C_1^g = \frac{B}{2.303 f_0}$ and $C_2^g = \frac{f_0}{\alpha_f}$ where f_0 is the dimensionless ratio of free volume to total volume, and α_f is the thermal expansion coefficient with the value of B being approximately unity.

WLF constants, obtained at any reference temperature (T_0), can be used to calculate the corresponding values at T_g, using the following relationships (Ferry 1988):

$$C_1^g C_2^g = C_1^0 C_2^0 \qquad \text{eq. 4.10}$$

$$C_2^g = C_2^0 + T_g - T_0 \qquad \text{eq. 4.11}$$

The viscosity is assumed to be 10^{12} Pa·s at the glass transition temperature Tg. (Soesanto and Williams, 1981; Angel, 1997).

Using the glass transition as reference temperature the WLF model takes the form:

$$Log(\eta) = 12 + \frac{C_1^g (T - T_0)}{C_2^g + T - T_0} \qquad \text{eq . 4.12}$$

Williams et al, 1955, by fitting the WLF for many polymeric materials proposed that the constants C_1^g and C_2^g would assume universal values of C_1^g =17.4 and C_2^g =51.6 K, however specific systems may show big variations (Peleg 1992; Champion, Hervet et al. 1997; Yildiz and Kokini 2001).

According to Angell (1997) C_1^g assumes universal value of 17 as it is the difference in order of magnitude between the viscosity when the material has vibration time comparable to the average atomic molecular vibration time, 10^{-14}s, and the viscosity in the glassy state where the vibration time is in the order of 10^2s, and C_2^g is a system dependent variable reflecting the non-Arrhenius character (fragility) of the system (Angell, 1997).

In food systems, where the complexity governs and affects the volumetric expansion coefficients it is necessary to treat both C_1^g and C_2^g as material specific coefficients rather than universal values.

Figure 4.30 shows the viscosities as a function of T-Tg, where the glass transition has been determined calorimetrically (Table 4.3), and the line correspond to a WLF fit with the universal values C_1^g =17.4 and C_2^g =51.6. It is evident that the WLF fit with the universal values is not suitable for the caramel samples.

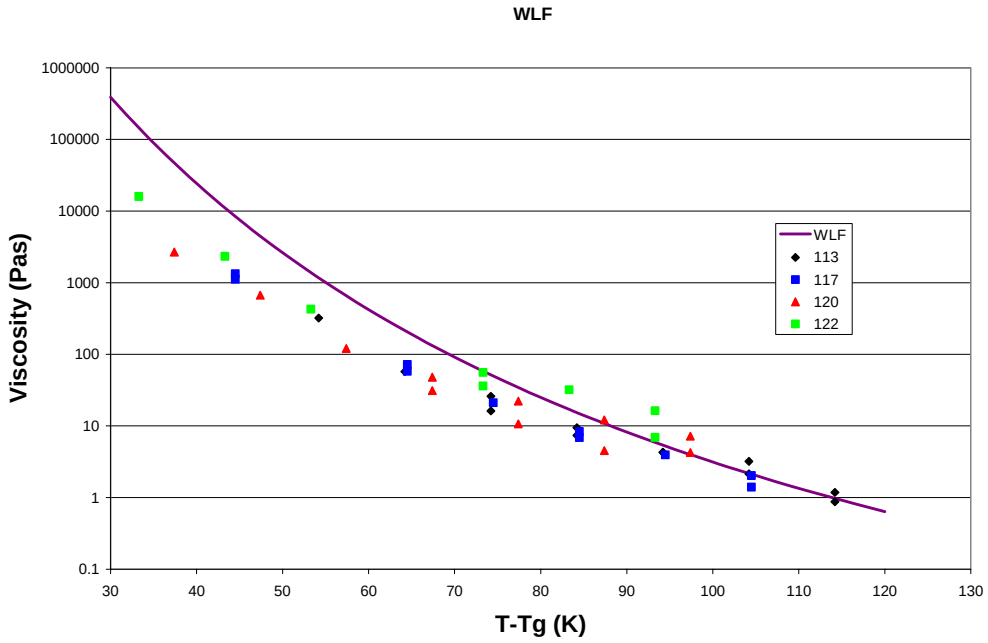

Figure 4.30 WLF fit with universal constants and measured viscosities as a function of T-Tg.

Figure 4.31 shows the best fit obtained for the viscosity of each sample. The values of C_1^g and C_2^g, the associated error, the correlation coefficient R and the χ^2 are shown in Table 4.14.

The fragility of a liquid can be defined as the steepness of the Arrhenius plot near the Tg. The more fragile a liquid the greater is the dependence of viscosity on the temperature in the Tg region. Angel on the basis of the equivalence of the Williams-Landel-Ferry (WLF) equation and the Vogel-Tamman-Fulcher (VTF) equation has quantified the fragility of a liquid in terms of WLF parameters C_2^g as (1- C_2^g/Tg), ranging between 0 and 1 with increasing fragility. Values of fragility are shown in Table 4.15. They increase with decreasing water content. This data agrees with the literature on sucrose solution, (Angell, 2002) where fragility has been reported to decrease slowly as the water content increases.

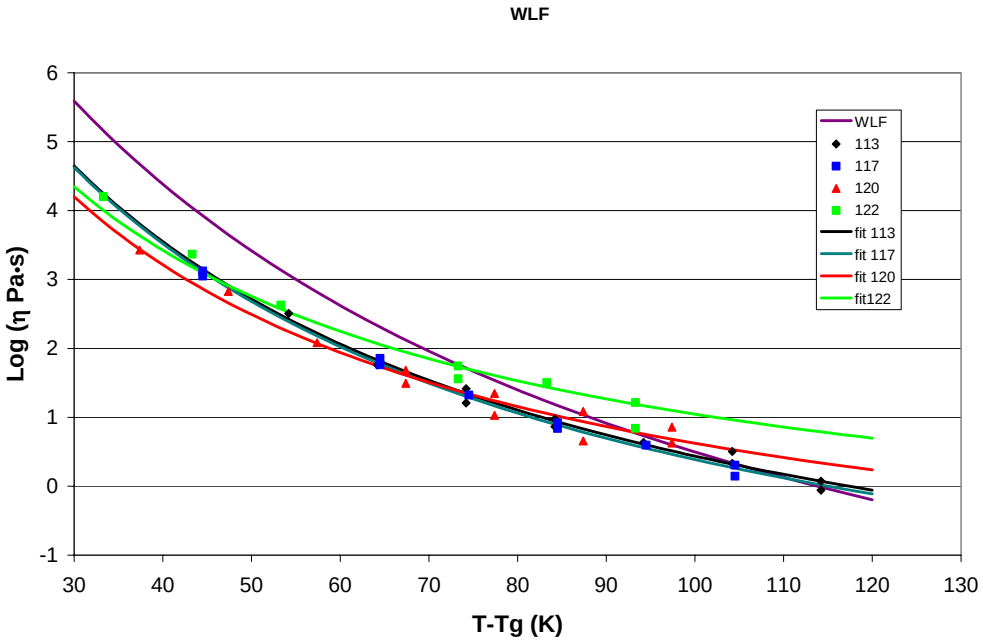

Figure 4.31 WLF fit for sample 113, 117 120 and 122

Table 4.14 *Values of C_1^g and C_2^g with the standard error, the correlation coefficient, R, and the chi squared (χ^2) for the four caramel samples.*

	113		**117**		**120**		**122**	
	Value	Error	Value	Error	Value	Error	Value	Error
C_1^g	-15.3	0.26	-15.4	0.15	-14.2	0.5	-13.4	1.1
C_2^g **(K)**	32.5	1.9	32.7	1.00	24.5	3.3	22.7	7.0
Chisq	0.094		0.034		0.578		1.92	
R	0.992		0.998		0.964		0.893	

Table 4.15 *Fragility for the four samples*

Sample	**Tg (K)**	**1-C_2^g/Tg**
113	239	0.86
117	249	0.87
120	256	0.90
122	260	0.91

Attempts to fit all the viscosities to a single WLF model are given in Figure 4.32. Table 4.16 shows the parameters with the associated error, the correlation coefficient R and the χ^2 .

The resulting equation is:

$$\log(\eta) = 12 + \frac{\text{-}14.956(T - T_g)}{30.28 + T - T_g}. \qquad \text{Eq 4.13}$$

This equation is not meant to be used in order to give structural information but it can be a useful tool to use together with the Gordon-Taylor fit to estimate the viscosity of caramels at a certain temperature and water content.

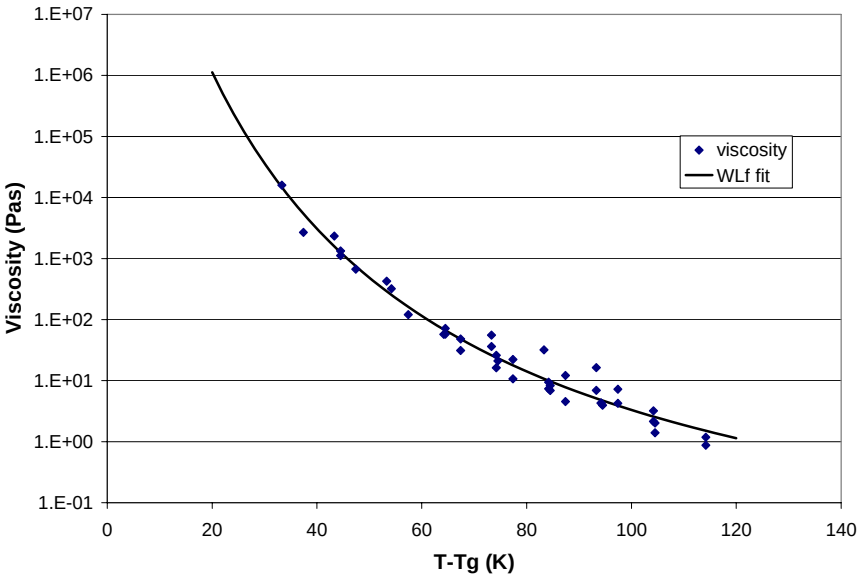

Figure 4.32 Generalized WLF kinetics

Table 4.16 *Coeffients C_1 and C_2 with the standard error, the correlation coefficient R and the chi squared (χ^2) for the generalized WLF kinetics.*

	Value	Error
C_1^g	-15.0	0.2
C_2^g **(K)**	30.28	1.4
Chisq	1.32	
R	0.98	

4.7.2.2 Oscillation and Time temperature superimposition

Rheologically a glass transition temperature can be measured directly by Dynamic-Mechanical methods. In our case it was not possible using rotational methods to access directly to the glass transitions, but the glass transition has been calculated using the WLF approach.

The steps involved are:

a) Determination of the shift factor a_T required to superimpose master curves at a reference temperature, As previously mentioned this has been taken as 40ºC. The master curves obtained have been shown in a previous section (4.5.2 Oscillation)

b) Fitting the shift factor as function of the temperature to determine C_1^0 and C_2^0 constants.

c) Calculating T_g from: $T_g = C_2^g - C_2^0 + T_0$. The value of C_2^g for each sample is taken from the previous fit of the WLF equation to the viscosity data.

Data in Table 4.17 are the decimal logarithm of the shift factor determined from TTS for reference temperature of 40ºC.

There are not enough data for every sample to give an appropriate determination of C_1 and C_2. Particularly for the sample 113 there are available only 5 points of which at least the last one at 70ºC is out of the range of validity of the WLF fit as the glass transition for this sample is -34.2C and for the sample 117 and 122 only 4 points are available.

Table 4.17 *Shift factors Log* a_T

Sample / T(°C)	113	117	120	122
30	1.4195	1.5534	1.8967	1.8876
40	0	0	0	0
50	-1.0831		-1.4347	
60	-1.9483	-2.2953	-2.6665	-2.7285
70	-2.5669		-3.6552	
80		-3.9984		-4.6667

The determination of the parameters with so very few available points for each sample data is arbitrary because there are many combinations of C_1 and C_2 which are equally probable.

Cruz et al, (2001) presented some DMTA test on sugar solutions. They applied the WLF kinetics and obtained the WLF parameter by fixing C_1 at 16 and relaxation times τ_g at 100 and 1000 s by asserting that while C_2 is a system dependant value C_1 could be considered a universal constant.

This hypothesis is quite contestable, particularly when the system analysed is a complex system such as caramel, but it does provide a way of simplifying the WLF model allowing one parameter, C_2, to be determined.

By observing the WLF parameters referred to the glass transition or rather the values obtained from viscosity measurements, it seems that C_1 is an almost constant value, it ranges from -13.4 for the sample 122 to -15.4 for the sample 117, but within the limits of the error these correspond to the average value of -15.0 obtained from the general WLF fit.

On the basis of these considerations, it is believed that it is possible to determine the C_2 WLF parameter at the reference temperature of 40ºC from the shift factors by fixing C_1 as an average value determined by a WLF fit and combining all the resulting shift factors from the oscillatory experiments.

Figure 4.33 shows the general WLF plot of the shift factors, the resultant line is the best fit.

The parameters so determined are shown in Table 4.18.

Table 4.18 *WLF parameters and standard errors*

	Value	Error
C_1	-14.10	3.1
C_2 (K)	96.3	25.7
Chisq	1.65	
R	0.99	

The WLF plots obtained by fixing the C_1 at -14.0 are shown in Figure 4.34.

The obtained parameters are shown in Table 4.19

The worst correlation is for the sample 113 where the C_2 parameter is 118±4.

From the relationship shown in the previous section it is possible determine the glass transition from rheological measurements by using equation 4.31 which in this case becomes:

$$T_g^{rheo} = C_2^g - C_2^0 + T_0 \qquad \text{eq. 4.14}$$

C_2^0 is the C_2 parameter determined from the application of the WLF to the shift factors obtained from oscillation experiments at the reference temperature T_0 of 40ºC

C_2^g is the the C_2 parameter determined by applying the WLF kinetic to the viscosities.

The T_g^{rheo} obtained with this analysis is shown in Table 4.20.

Apart from the sample 113, whose application of the WLF model was in the limit of the range of temperature where the model is valid, $T_g < T < T_g + 100$, the glass transitions determined rheologically is only 4-6ºC lower than the calorimetric glass transition. In view of the breadth of the glass transition it could appear that the DSC and rheological analysis are measuring the same properties.

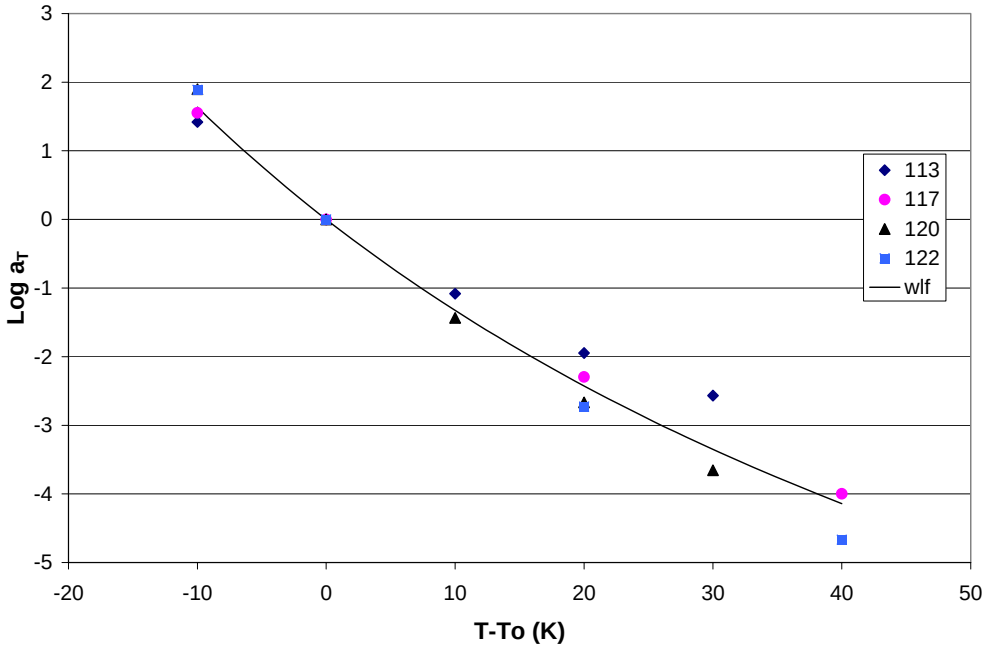

Figure 4.33 General WLF fit

Table 4.19 *WLF parameters*

	113		**117**		**120**		**122**	
	Value	Error	Value	Error	Value	Error	Value	Error
C_1^g	-14.0	-	-14.0	-	-14.0	-	-14.0	-
C_2^g (K)	118.4	4.1	101.4	0.5	85.6	0.5	82.4	0.5
Chisq	0.022299		0.0001		0.003		0.008	
R	0.998		1.00		1.00		1.00	

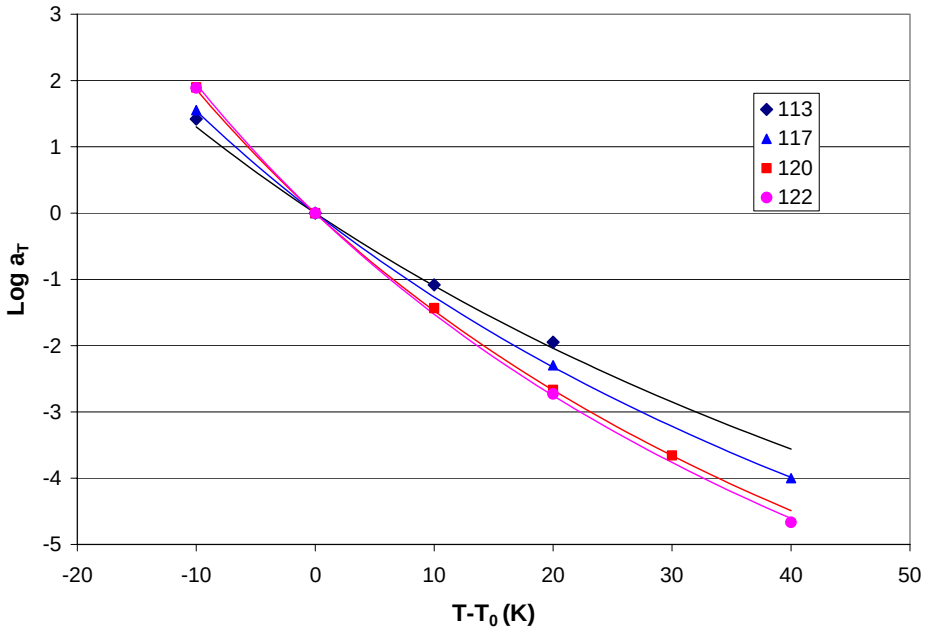

Figure 4.34 WLF fit for the single samples

Table 4.20 *Comparison between rheo-T_g and T_g from DSC.*

Sample	C_2^{40} (K)	C_2^g (K)	$T_g^{rheo}=(C_2^g - C_2^{40}+40)$ (°C)	T_g DSC (°C)
113	**118.4**	**32.5**	**-45.9**	**-34.2**
117	**101.4**	**32.7**	**-28.8**	**-24.5**
120	**85.6**	**24.5**	**-21.2**	**-17.4**
122	**82.4**	**22.7**	**-19.7**	**-13.3**

4.8 Conclusions

The results obtained from the various are summarized in Table 4.21.

Table 4.21 *Effect of the processing temperature on physical properties of caramels*

DSC	T_g decreases with the water content showing the plasticization effect of water on the sugar matrix. Experimental T_gs were lower than calculated using the Couchman-Karasz equation.	
Isoelectric point	The pH at the isoelectric point decreased with increasing processing temperature, due to protein modification through the Maillard reaction.	
Viscosity and modelling	Decreasing viscosity with increasing of the water content and increasing temperature.	Primarily Newtonian behaviour, some departure from Newtonian behaviour for caramel at lower water content.
	Empirical statistical model: T is in Kelvin and water content is %w.w.b.	$\log(\eta) = 21.75 - \frac{1.556 \cdot 10^4}{T} - 0.431 X_w + \frac{3.60 \cdot 10^6}{T^2} + 0.041 X_w^{\,2} - \frac{209.5 X_w}{T}$
	Arrhenius model was not applied successfully as curvature was present in the data	Activation energies decreased with increasing water content. The value obtained for caramels are very close to what is reported in the literature for highly concentrated sugar solutions.
	WLF model good fit of the data	Fragilities increased with decreasing of water content in agreement with literature for sugar solutions.
Creep recovery	No recovery was shown in the creep recovery compliance curves for samples 113 and 117. Sample 120 shows a small degree of recovery The creep compliance increased with the water content.	
Oscillation	Mechanical spectra typical of non polymeric materials. Time temperature superimposition and application of the WLF model allowed the rheo-T_g to be obtained which is in reasonable agreement with the DSC T_g.	
Extensional behaviour	No variation of the Trouton ratio at $100s^{-1}$ with water content, in the limit of the experimental error. Trouton ratio was 12 for sample 122 and 15 for sample 120 and 20 for the sample 117.	

Appendix to the chapter 4:

Anova response for the statistical model of the viscosities shown in section 4.7.2.1.

ANOVA for Response Surface Quadratic Model

Analysis of variance table

Source	Sum of Squares	DF	Mean Square	F Value	Prob > F
Model	41.15313	5	8.230626	469.096	< 0.0001 significant
A	32.13276	1	32.13276	1831.374	< 0.0001
B	7.702066	1	7.702066	438.9713	< 0.0001
A2	0.576712	1	0.576712	32.86912	< 0.0001
B2	0.601659	1	0.601659	34.29092	< 0.0001
AB	0.254068	1	0.254068	14.48032	0.0005
Residual	0.631646	36	0.017546		
Lack of Fit	0.285057	21	0.013574	0.587474	0.8715
Pure Error	0.346589	15	0.023106		
Cor Total	41.78478	41			

The F distribution is a probability distribution used to compare variances by examining their ratio. If they are equal then the F value would equal 1. The F value in the ANOVA Table is the ratio of model mean square (MS) to the appropriate error mean square. The larger the ratio, the larger the F value and the more likely that the variance contributed by the model is significantly larger than random error.

The Model F-value of 469.10 implies the model is significant. There is only a 0.01% chance that a "Model F-Value" this large could occur due to noise.

Values of "Prob > F" less than 0.0500 indicate model terms are significant.

Values greater than 0.1000 indicate the model terms are not significant.

In this case A, B, A^2, B^2, AB are significant model terms and a model reduction will worsen the model

The result of experimentation should be a model which will adequately predict the response within the design space. If all of the points in the design are needed to calculate the model coefficients, there will be no points left over to see how well the model fits. The model may fit the design points, but not be very good predictor at other points. This will be especially true if certain design points have a strong influence on the model. Beyond those needed for determining the model coefficients so it would need to added some extra point to check the model fit. The variation between the model prediction and the extra points is compared with the pure error to test the lack of fit. In the statistical output, the lack of fit should NOT be significant. A small F value and high p value (greater than 0.1) are good in this test. If a model has a significant lack of fit it is not a good predictor of the response and should not be used.

The "Lack of Fit F-value" of 0.59 implies the Lack of Fit is not significant relative to the pure error. There is a 87.15% chance that a "Lack of Fit F-value" this large could occur due to noise.

Std. Dev.	**0.13246**	**R-Squared**	**0.984883**
Mean	**1.460098**	**Adj R-Squared**	**0.982784**
C.V.	**9.072014**	**Pred R-Squared**	**0.979474**
PRESS	**0.857654**	**Adeq Precision**	**79.14758**

The Predicted Residual Sum of Squares (PRESS) is a measure of how well the model fits each point in the design. The model is used to estimate each point using all of the design points except that one. The difference between the predicted value and actual value at each point is squared and summed over all of the points. The smaller the PRESS statistic, the better the model fits the data points.

The correlation coefficient "Pred R-Squared" of 0.9795 is in reasonable agreement with the "Adj R-Squared" of 0.9828.

The "Adeq Precision" measures the signal to noise ratio. A ratio greater than 4 is desirable. This ratio for this model is 79.148 indicating an adequate signal.

As conclusion of this analysis this model can be used to navigate the design space.

Table 4.22 shows the equation in terms of coded factors with the errors and table 4.23 in terms of actual factors.

Finally a diagnostics case statistics is shown in Table 4.24.

Table 4.22 *Final equation in terms of coded factors with the errors*

	Coefficient		Standard	95% CI	95% CI	
Factor	Estimate	DF	Error	Low	High	VIF
Intercept	1.346335	1	0.042638	1.259862	1.432808	
A-1/T	1.367787	1	0.031962	1.302965	1.432608	1.055996
B-water content %	-0.61341	1	0.029277	-0.67279	-0.55403	1.169589
A2	0.302447	1	0.052754	0.195457	0.409437	1.027242
B2	0.289072	1	0.049365	0.188956	0.389189	1.065685
AB	-0.16207	1	0.042591	-0.24845	-0.07569	1.133891

Table 4.23 *Final equation in terms of actual factors with the errors*

Log10(visc)	=
21.74557	
-15555.8	* 1/T
-0.43148	* water content %
3601868	* 1/T2
0.040549	* (water content %)2
-209.474	* 1/T * water content %

Table 4.24 *Diagnostics Case Statistics (This table is the output of the software Design-Expert; a reduction of the decimal places has not been performed)*

Standard	Actual	Predicted			Student	Cook's	Outlier
Order	Value	Value	Residual	Leverage	Residual	Distance	t
1	0.305351	0.291305	0.014046	0.151845	0.11514	0.000396	0.113551
2	0.62893	0.667309	-0.03838	0.124646	-0.30968	0.002276	-0.30575
3	0.630428	0.575305	0.055123	0.102887	0.43936	0.00369	0.434381
4	0.071882	0.118745	-0.04686	0.244616	-0.40706	0.008943	-0.4023
5	0.596597	0.534124	0.062473	0.092513	0.495096	0.004165	0.489841
6	0.50515	0.314374	0.190776	0.133965	1.547646	0.061752	1.579446
7	-0.0575	0.118745	-0.17624	0.244616	-1.53087	0.126486	-1.56113
8	0.837178	0.845078	-0.0079	0.09193	-0.06259	6.61E-05	-0.06172
9	0.332438	0.314374	0.018065	0.133965	0.146549	0.000554	0.144543
10	0.857935	0.667309	0.190627	0.124646	1.538176	0.056151	1.5691
11	0.656855	0.937438	-0.28058	0.061098	-2.18608	0.051831	-2.3146
12	0.146066	0.291305	-0.14524	0.151845	-1.19059	0.042296	-1.19775
13	0.840714	1.021434	-0.18072	0.213078	-1.53799	0.106748	-1.56889

14	0.633468	0.575305	0.058163	0.102887	0.463595	0.004108	0.458482
15	0.866878	0.912729	-0.04585	0.109136	-0.36674	0.002746	-0.36229
16	0.920645	0.845078	0.075567	0.09193	0.598666	0.006047	0.593253
17	0.975432	0.912729	0.062703	0.109136	0.501527	0.005136	0.496249
18	1.028937	1.277344	-0.24841	0.060207	-1.93447	0.039956	-2.01502
19	1.084934	0.937438	0.147495	0.061098	1.149164	0.014323	1.154464
20	1.209515	1.339939	-0.13042	0.133686	-1.05787	0.028782	-1.05968
21	1.212986	1.021434	0.191553	0.213078	1.630184	0.11993	1.670211
22	1.324282	1.235621	0.088661	0.102486	0.706525	0.0095	0.701524
23	1.346353	1.277344	0.069009	0.060207	0.537407	0.003084	0.532029
24	1.414973	1.339939	0.075035	0.133686	0.60861	0.009527	0.603209
25	1.503927	1.309368	0.194559	0.132999	1.577453	0.063619	1.612102
26	1.558096	1.668146	-0.11005	0.1244	-0.88788	0.018667	-0.8852
27	1.681874	1.69863	-0.01676	0.07446	-0.13148	0.000232	-0.12968
28	1.745855	1.668146	0.077709	0.1244	0.626948	0.009307	0.621582
29	2.62944	2.647221	-0.01778	0.158906	-0.14637	0.000675	-0.14437
30	2.505557	2.530305	-0.02475	0.427	-0.24693	0.007588	-0.24368
31	2.380338	2.312437	0.0679	0.098582	0.539913	0.005313	0.53453
32	2.081815	2.215057	-0.13324	0.078165	-1.04768	0.015512	-1.04914
33	1.856245	1.719342	0.136903	0.098496	1.08854	0.021577	1.091428
34	1.762101	1.719342	0.042759	0.098496	0.33998	0.002105	0.335764
35	1.758155	1.872794	-0.11464	0.20345	-0.96971	0.04003	-0.96889
36	4.202161	4.08129	0.120871	0.358	1.139257	0.120862	1.144136
37	3.427973	3.602119	-0.17415	0.207496	-1.47682	0.095173	-1.50239
38	3.367114	3.297909	0.069205	0.197966	0.583384	0.014001	0.577963
39	3.125156	3.034298	0.090858	0.201419	0.767569	0.024767	0.763103
40	3.048636	3.034298	0.014338	0.201419	0.121128	0.000617	0.119458
41	2.825121	2.843016	-0.0179	0.08976	-0.1416	0.00033	-0.13966
42	1.494099	1.69863	-0.20453	0.07446	-1.605	0.034541	-1.64241

CHAPTER 5. THE EFFECT OF THE INCORPORATION OF HYDROCOLLOIDS

Recently there has been increased interest in the performance of hydrocolloids in low water content high sugar systems (Deszczynski et al., 2002, Kasapis et al., 2003, Kasapis et al., 2002; Kumagai et al., 2002; Mitchell, 2000; Tsoga et al., 1999). When small amounts of biopolymers are added to sugar solutions the flow assume a more solid-like behaviour, the temperature of the rheological glass transition increases, but the calorimetrically measured glass transtion temperature is the same as in the absence of the biopolymer.

Although caramel is an emulsion, its rheological behaviour is very close to a concentrated sugar solution and it constitutes a practical example of a high sugar system where hydrocolloids could be added in order to control rheology.

This chapter describes a rheological study of caramels obtained from standard preparation where the hydrocolloids κ-carrageenan and gellan gum are added. In addition to a qualitative analysis of shear and capillary flow, measurements obtained by small deformation dynamic oscillation are modelled according to the WLF model.

5.1 Composition of Caramels

Caramel containing hydrocolloids was prepared by heating at the same temperatures of 117°C with the formulations described in chapter 3. The measured water contents were determined and from these the total ingredient composition was calculated.

Table 5.1 shows the composition of the final product obtained by assuming no chemical changes as a result of the Maillard reaction. The composition of the non fat phase is shown in Table 5.2.

Table 5.1. *Composition of the caramels (%w.w.b.)*

	Gelgum0.1	Gelgum0.2	Gelgum0.4	Carrag005	Carrag01	Carrag02
water	13.3	11.3	9.5	10.4	10.4	10.1
milk fat	0.1	0.1	0.1	0.1	0.1	0.1
sucrose	5.0	5.1	5.2	5.1	5.1	5.1
casein	0.9	0.9	0.9	0.9	0.9	0.9
whey proteins	0.2	0.2	0.2	0.2	0.2	0.2
lactose	1.5	1.5	1.6	1.6	1.6	1.6
ash	0.2	0.2	0.2	0.2	0.2	0.2
fructose	6.4	6.5	6.6	5.9	5.9	5.9
dextrose	27.3	27.9	28.3	27.5	27.5	27.6
maltose	17.0	17.4	17.7	17.7	17.7	17.7
maltotriose	4.3	4.4	4.5	4.5	4.5	4.5
higher sugars	12.2	12.5	12.7	12.7	12.7	12.7
Vegetable Fat	10.7	11.0	11.2	12.5	12.5	12.6
Salt	0.4	0.4	0.5	0.4	0.4	0.4
Sodium carbonate	0.2	0.2	0.2	0.2	0.2	0.2
Sodium citrate	0.2	0.2	0.2			
Gellan gum	0.1	0.2	0.5			
κ-Carrageenan				0.05	0.1	0.2

Table 5.2. *Non-fat phase composition (% w.w.b.)*

	Gelgum0.1	Gelgum0.2	Gelgum0.4	Carrag005	Carrag01	Carrag02
water	15.1	12.8	10.8	11.0	12.1	11.7
sucrose	5.6	5.8	5.9	6.0	5.9	5.9
lactose	1.7	1.8	1.8	1.8	1.8	1.8
ash	0.3	0.3	0.3	0.3	0.3	0.3
fructose	7.2	7.4	7.5	6.9	6.8	6.9
dextrose	31.0	31.8	32.3	32.3	31.9	32.0
maltose	19.3	19.8	20.2	20.8	20.5	20.6
maltotriose	4.9	5.0	5.1	5.3	5.2	5.2
higher sugars	13.8	14.2	14.5	14.9	14.7	14.7
Salt	0.5	0.5	0.5	0.5	0.5	0.5
Sodium carbonate	0.2	0.2	0.3	0.2	0.2	0.2
Sodium citrate	0.2	0.2	0.3			
Gellan gum	0.1	0.3	0.5			
κ-Carrageenan				0.05	0.1	0.3

5.2 DSC

Figures 5.1 a and 5.1b show the first scan and the reheating for the all the samples containing hydrocolloids. As for the samples seen before, two features can be elucidated from the curves: a glass transition of the amorphous syrup matrix and a multiple endotherms at higher temperature due to the melting of the crystalline phases of the fat.

Table 5.3 shows the water content and the glass transition temperatures determined from calorimetric measurements for the sample analyzed. Figures 5.2 shows a comparison between samples with and without hydrocolloids of the glass transition from DSC. The small differences are attributed the experimental error and the difficulty in controlling the final temperature in caramel preparation. It is

concluded that the presence of hydrocolloids does not affect either the water content or the glass transition temperature.

Table 5.3. *Glass transition temperatures from calorimetric data*

Samples	T_g ºC	Water content of the non-fat matrix % w.w.b.
Gelgum0.1	-37	15.1
Gelgum0.2	-30	12.8
Gelgum0.4	-27	10.8
Carrag005	-29	11.0
Carrag01	-28	12.1
Carrag02	-27	11.7
117 Control	-24	12.2

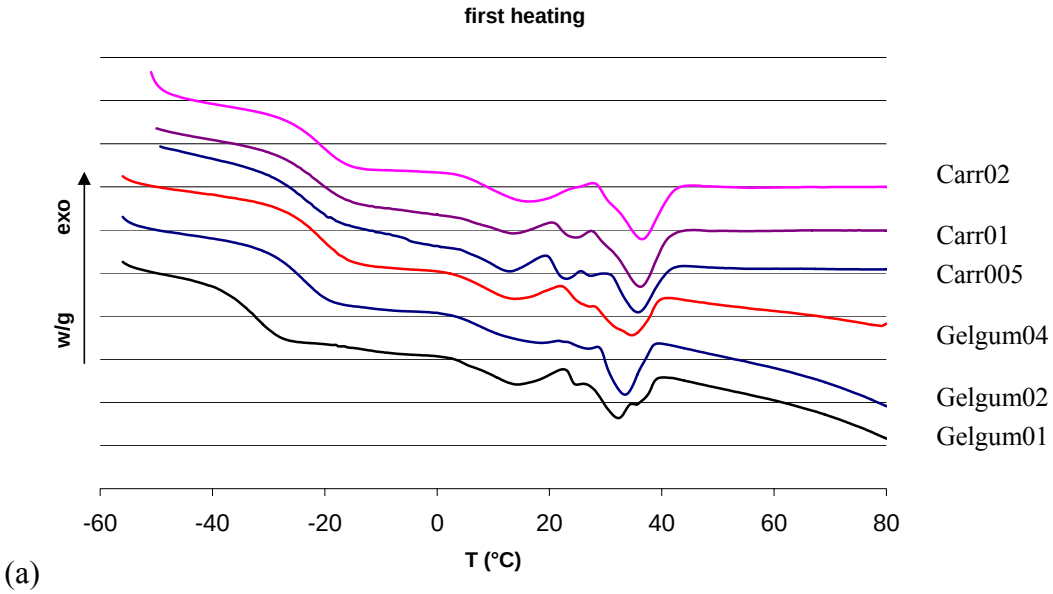

(a)

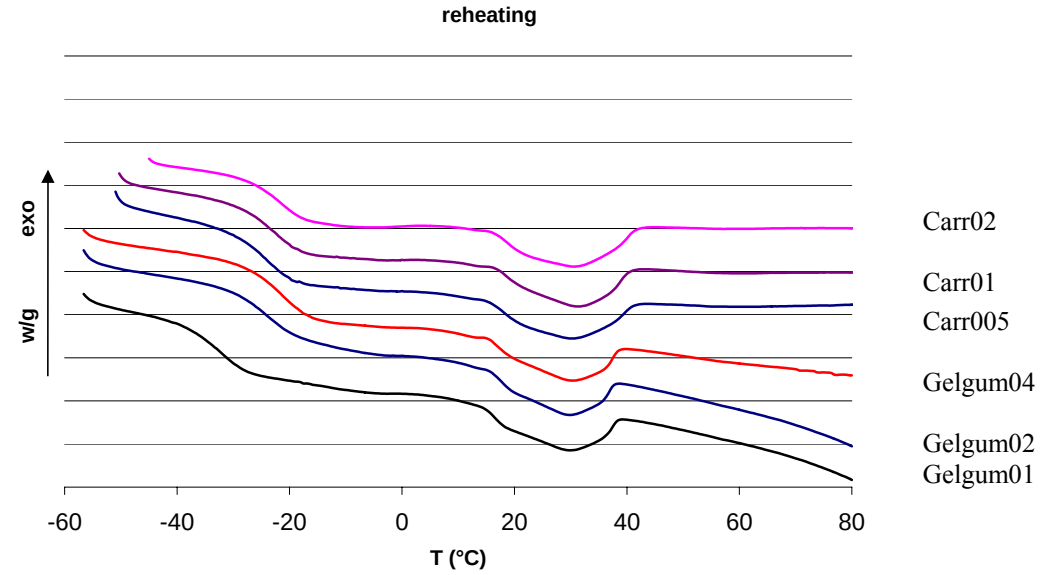

(b)

Figure 5.1. Thermograms for sample containing hydrocollids from first scan and reheating.

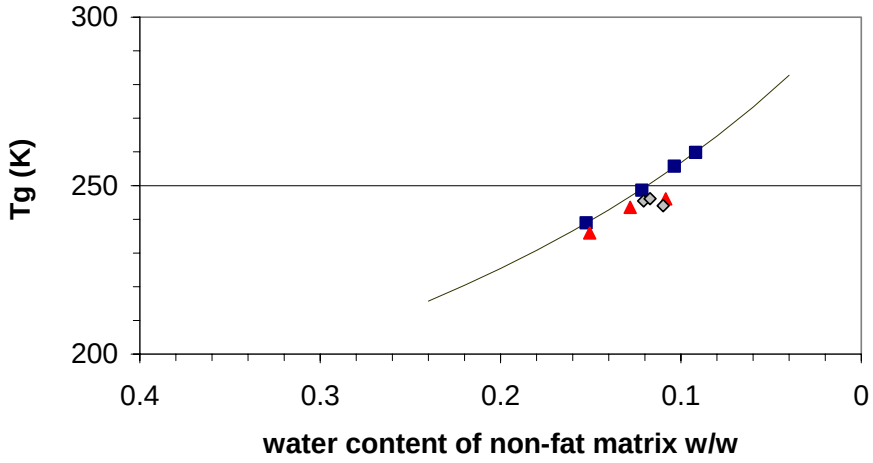

Figure 5.2. Calorimetric glass transition for samples containing Gellan Gum (▲), κ-carrageenan (♦) compared with samples without hydrocolloid incorporation (■). The line is the Gordon-Taylor applied for samples at different water content (chapter 4, eq 4.3).

5.3 Isoelectric point

Figure. 5.3 shows a comparison of isoelectric points of the sample cooked at different temperatures and the samples containing hydrocolloids. Small amounts of κ-carrageenan or gellan gum resulted in a large reduction in the pH at the isoelectric point.

In streaming potential measurements of these type colloidal particles, whose molecular weight is more than 300, are adsorbed on the surface of the wall of the cell and of the piston under the action of van der Wal forces and the counter-ions remain comparatively free. When the piston oscillates an intensive liquid flow is created, and the counter-ions separate from the adsorbed sample material, generating the streaming current.

κ-carrageenan and gellan gum are negatively charged polymers, the former contains sulphate groups and the latter contains carboxyl groups. They adsorb on the walls of the cell in the same way as the proteins contribute to the generation of free counter-ions together with the proteins. The measured value was not the pH at isoeletric point of the proteins but the pH where the sum of all the charges arising from both proteins and hydrocolloids was zero. The isoelectric point decrease depend on the amount of κ-carrageenan or gellan gum in the material, rather then the loss of amino groups in the protein as consequence of a Maillard reaction.

Table 5.4 *Isoelectric point for sample containing hydrocolloids*

Sample	iso pH ± std
Carr005	3.95 ± 0.01
Carr01	3.26 ± 0.04
Carr02	1.07 ± 0.06
Gelgum02	3.5 ± 0.2
117 control	4.19 ± 0.03

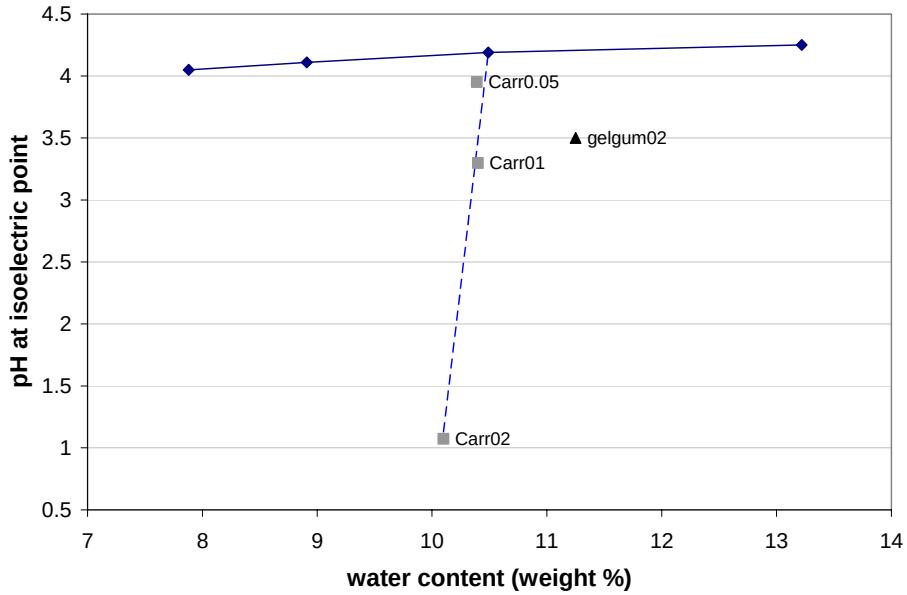

Figure 5.3 Isoelectric point as function of the water content for sample with and without hydrocolloid incorporation.

5.4 Rheology

5.4.1 Shear viscosity

Viscosity curves have been obtained for all the samples over a wide range of temperature, a power low model, $\sigma = K\dot{\gamma}^n$ where σ is the shear stress and $\dot{\gamma}$ the shear rate has been applied and the power low index, *n*, and the consistency index, *K*, have been determined.

Figures 5.4-5.7 show the flow curves obtained for the samples containing hydrocolloids. Several replications have been performed and all the data are shown. Some slipping effect is shown at high shear rates on measurements performed at low temperatures. These data were not fitted to the power law model.

As said in the previous chapter in the absence of hydrocolloids caramel behaviour is very close to a Newtonian liquid. The presence of the hydrocolloid results in shear thinning behaviour in shear flow and the curves show a greater degree of thinning behaviour (lower n) as the amount of hydrocolloids increased. Moreover the addition of hydrocolloids results in an increase in the viscosity indicated by the increase in K. This is also represented in Table 5.5 and 5.6 containing the consistency index and the power low index respectively. For instance at the same temperature of 50°C the consistency index is 12.3 $Pa{\cdot}s^n$ for the sample Gelgum01, through the value of 70.1 $Pa{\cdot}s^n$ for Gelgum02, and 199.7 $Pa{\cdot}s^n$ Gelgum04. The same pattern is followed by the samples containing carrageenan, where the consistency index at 50°C varies from 51.9 $Pa{\cdot}s^n$ for the sample Carr01 to 92.5 $Pa{\cdot}s^n$ for the sample Carr02.

The power law index generally decreased at constant temperature with increasing of hydroclooids content fro example at 50ºC varies from 0.94 for sample Gelgum 01 to 0.64 for the sample Gelgum04. It varies from 0.82 to 0.78 from the lower carrageenan content sample to the high amount of carrageenan.

The consistency indices determined for each sample containing hydrocolloids have been used for the modelling shown in the next section.

Table 5.5. *Consistency indeces (K (Pa·s^n) values are averages ± standard deviation obtained from triplicate measurements)*

Sample / T (C)	Gelgum01	Gelgum02	Gelgum04	Carr01	Carr02
35	62.3±0.9		-		
40	31.2±0.9				
45		135.4 ± 0. 7	248.7 ± 0.7	70 ± 0.8	
50	12.3±0.9	70.08 ± 0.9	199.7 ± 0.6	51.9 ± 0.8	92.5 ± 0.8
55		41.9 ± 0.8			101.5 ± 0.7
60	4.79±0.9	29.3 ± 0.8	92.3 ± 0.7	26.8 ± 0.9	61.3 ± 0.7
70	2.3±0.9	21.0 ± 0.8	42.2 ± 0.7	11.2 ± 0.9	43.6 ± 0.7
75		13.8 ± 0.8			26.1 ± 0.8
80		12.4 ± 0.8	20.5 ± 0.8	6.7 ± 0.9	21.0 ± 0.8

Table 5.6 *Power low indices (values are averages ± standard deviation obtained from triplicate measurements)*

Sample / T (C)	Gelgum01	Gelgum02	Gelgum04	Carr01	Carr02
35	0.87±0.03	-	-	-	-
40	0.95±0.01	-	-	-	-
45	-	0.70±0.03	0.74±0.03	0.78±0.01	-
50	0.94±0.02	0.81±0.01	0.64±0.06	0.84±0.03	0.78±0.01
55	-	0.83±0.01	-	-	0.72±0.02
60	0.96±0.01	0.82±0.03	0.69±0.02	0.91±0.05	0.74±0.01
70	0.96±0.02	0.82±0.03	0.71±0.02	0.87±0.01	0.75±0.01
75	-	0.83±0.01	-	-	0.78±0.01
80	-	0.80±0.02	0.83±0.15	0.89±0.02	0.79±0.01

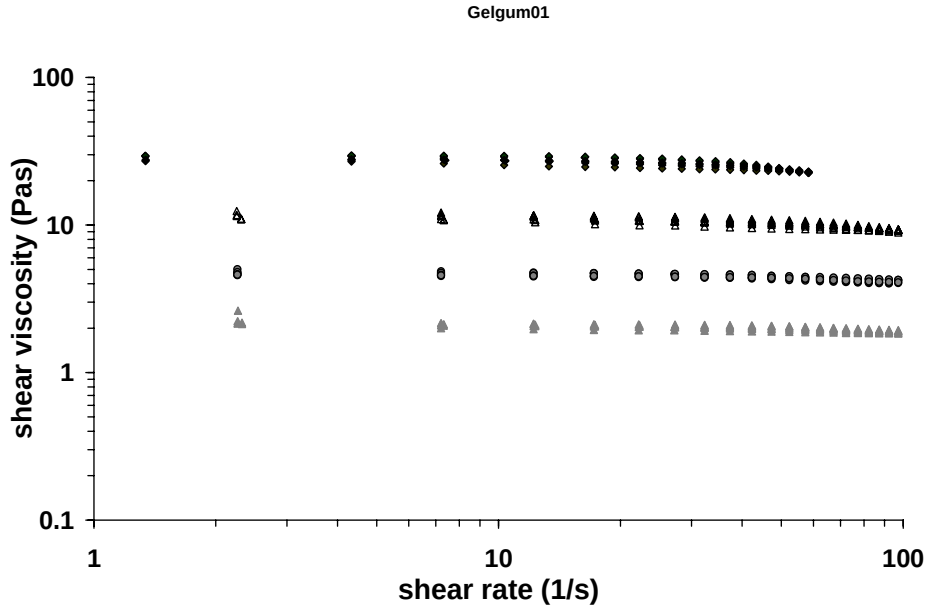

Figure 5.4 Viscosity curves for the caramel sample Gelgum01 at 40ºC(◆), 50ºC(△), 60ºC(●), 70ºC(▲), 80ºC

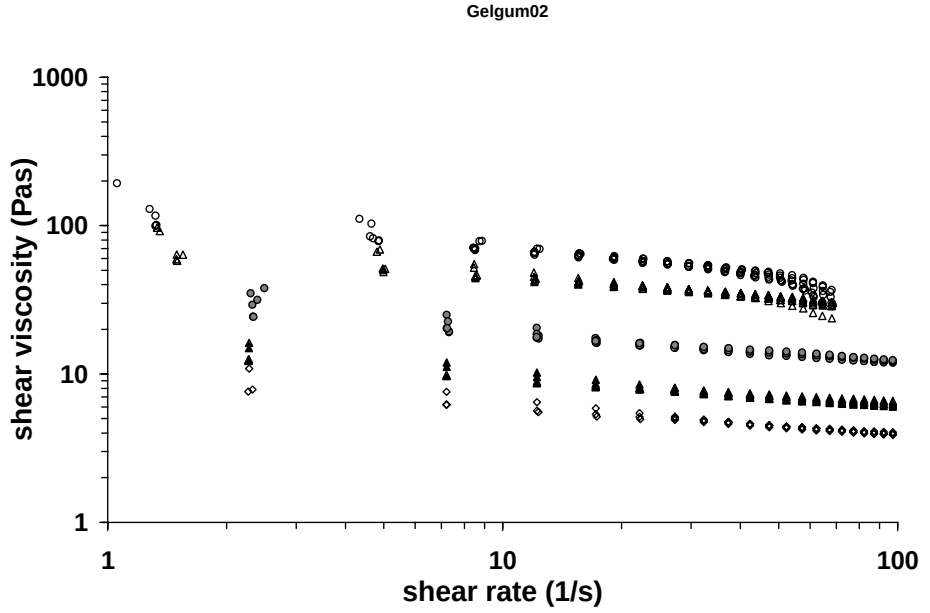

Figure 5.5 Viscosity curves for the caramel sample Gelgum02 at 45ºC(○), 50ºC(△), 60ºC(●), 70ºC(▲), 80ºC (◊).

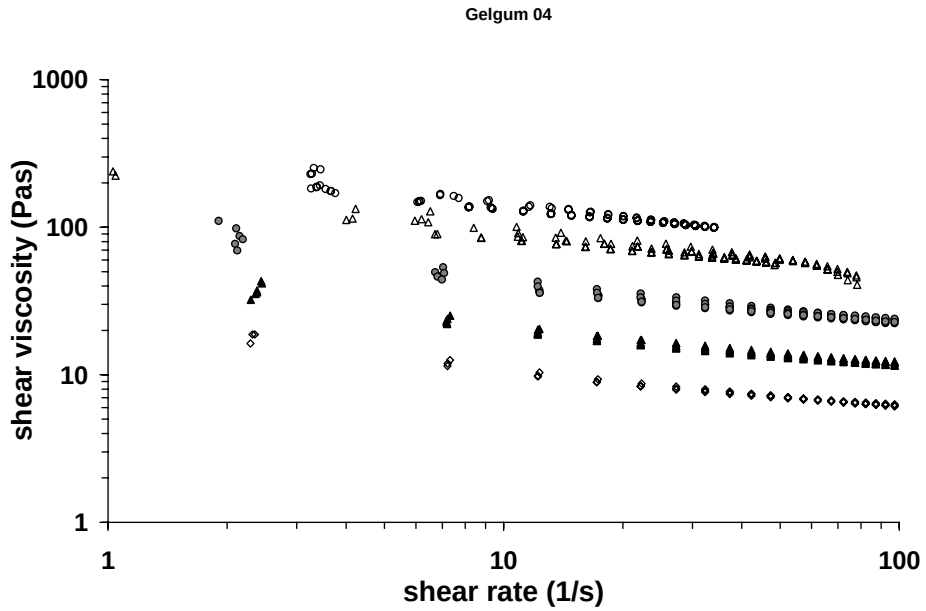

Figure 5.6 Viscosity curves for the caramel sample Gelgum04 at 45ºC(○),50ºC(△), 60ºC(●), 70ºC(▲), 80ºC (◊).

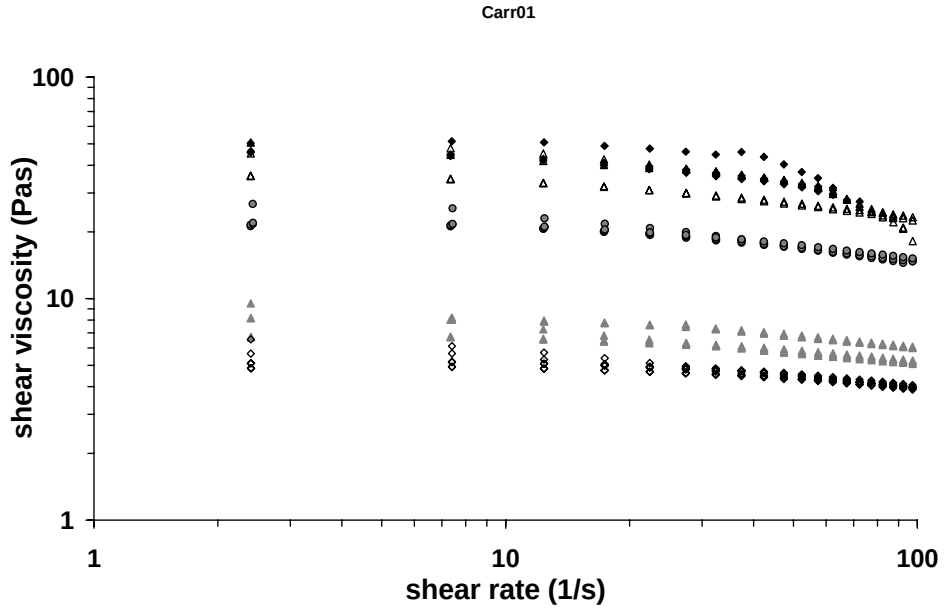

Figure 5.7 Viscosity curves for the caramel sample Carr01 at 45ºC(♦),50ºC(△), 60ºC(●), 70ºC(▲), 80ºC (◊).

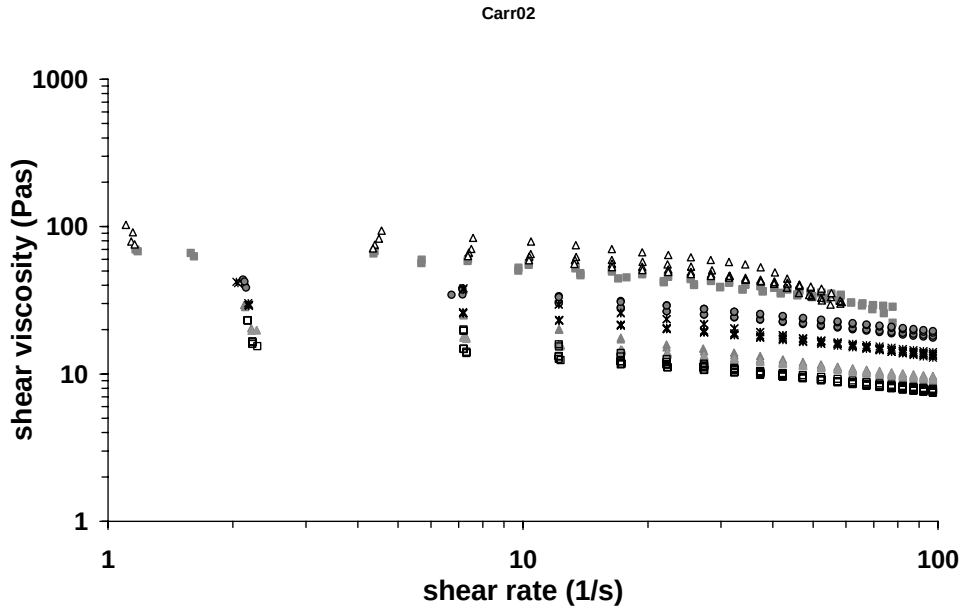

Figure 5.8 Viscosity curves for the caramel sample Carr02 at 50ºC(△), 55ºC(■), 60ºC(●), 65ºC(✳), 70ºC(▲), 75ºC (□).

5.4.2. Oscillation

As for the sample at different water contents, strain sweeps were performed on every sample for all temperatures in order to determine the appropriate amplitude strain to carry out the frequency sweep in the linear viscoelastic region. Frequency sweep was carried out by varying the frequency from 0.1 to 100Hz at temperature in the range from 20ºC to 80ºC.

Figures 5.9-5.20 show the viscoelastic functions: complex viscosity, storage and loss moduli, and the phase angle for every caramel in the range of temperature analysed. Unreliable data because of instrumental compliance are marked with symbols filled in grey colour. This data although shown in the graphs are not used in the interpretation of the viscoelastic behaviour of caramel.

Oscillation data confirms the presence of a greater elastic component (deviation of the phase angle at low frequencies from 90) in samples containing hydrocolloids in accord with the pervious viscosity curves. As expected, the viscous and elastic modulus decreased with increasing temperature as well the complex viscosity and at the same temperature both these viscoelastic parameters are higher for the samples with more added hydrocolloids.

Sample Gelgum02 gave very poor quality data particularly at high temperature (80ºC). The reason of this is not clear and it has been considered necessary to remove data obtained at high temperature in the analysis of the viscoelastic behaviour.

Estimation of the complex viscosity at 1 rad/sec are shown in Table 5.7. These values, with exception of the complex viscosity at 80ºC for the sample Gelgum02, have been used, together with the others obtained from viscosity shear measurements and from creep recovery test for the modelling developed in the next section, on the assumption of the validity of the Cox –Merz rule on the equivalence of the complex viscosity determined at 1 rad/sec with the power law consistency index (K) from shear viscosity measurements.

Table 5.7 *Complex Viscosity η* (Pa·s) at ω =1rad/sec*

Sample / T (C)	Gelgum01	Gelgum02	Gelgum04	Carr01	Carr02
20	449	3250	11700		
30	147	974	2120	860	1060
40	51.0	442	426	202	268
50				60.3	88.5
60	3.26	118	70.9	22.7	36.5
70				12.7	18.4
80	0.74	98.7	26.4	4.90	

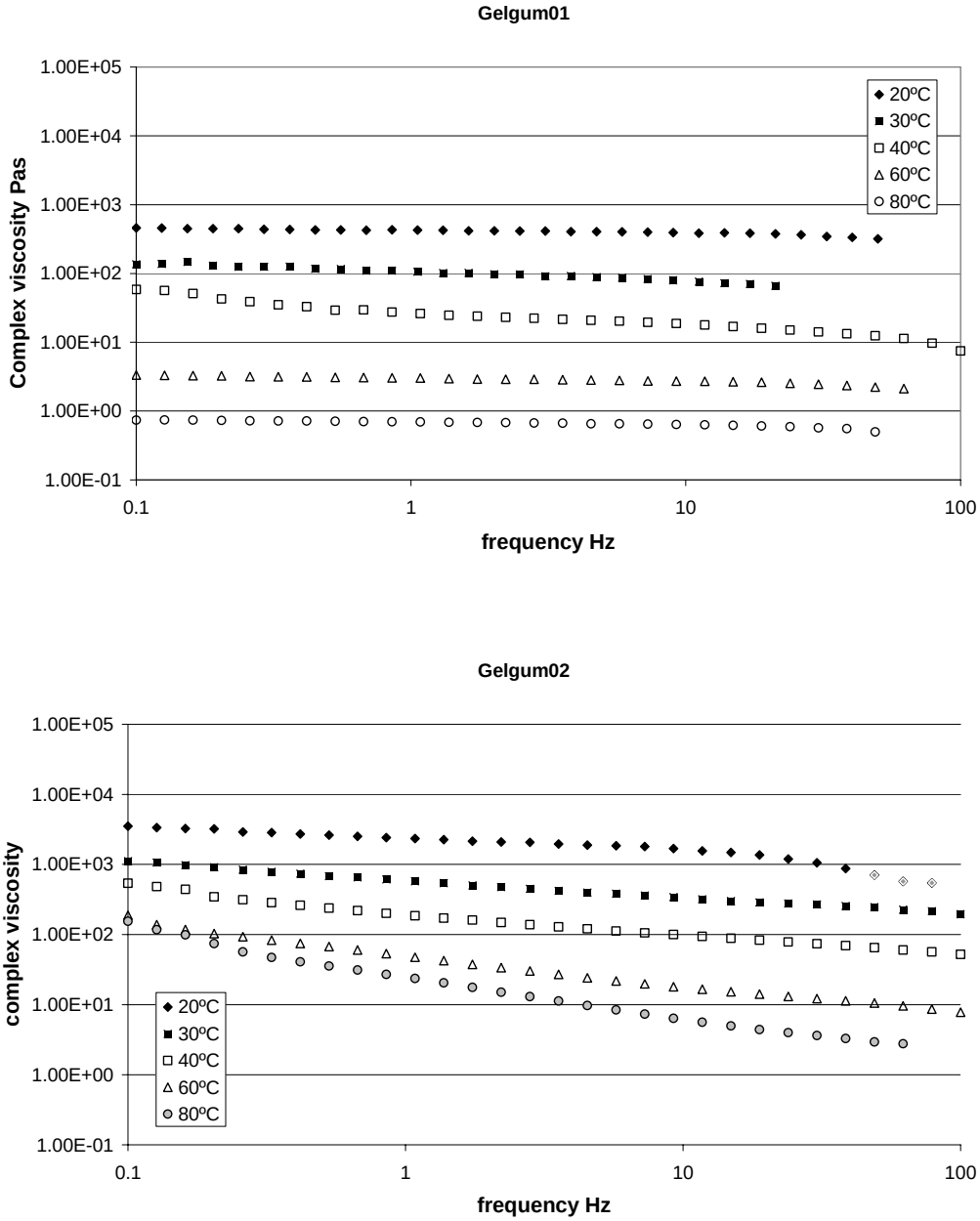

Figure 5.9 Complex viscosity for the sample Gelgum01 and Gelgum02, at different temperatures: 20(♦), 30 (■), 40 (□), 50(▲), 60 (Δ), 70(●), 80(○) °C. Data points filled in grey have not been used in subsequent modelling.

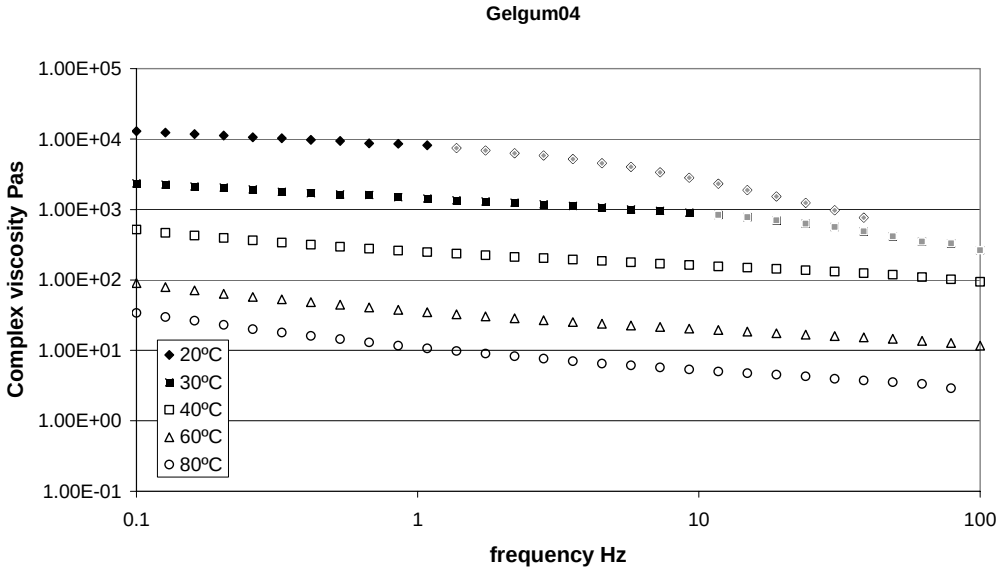

Figure 5.10 Complex viscosity for the sample Gelgum04 at different temperatures: 20(♦), 30 (■) ,40 (□) , 50(▲), 60 (Δ), 70(●), 80(○) °C. Data points filled in grey have not been used in subsequent modelling.

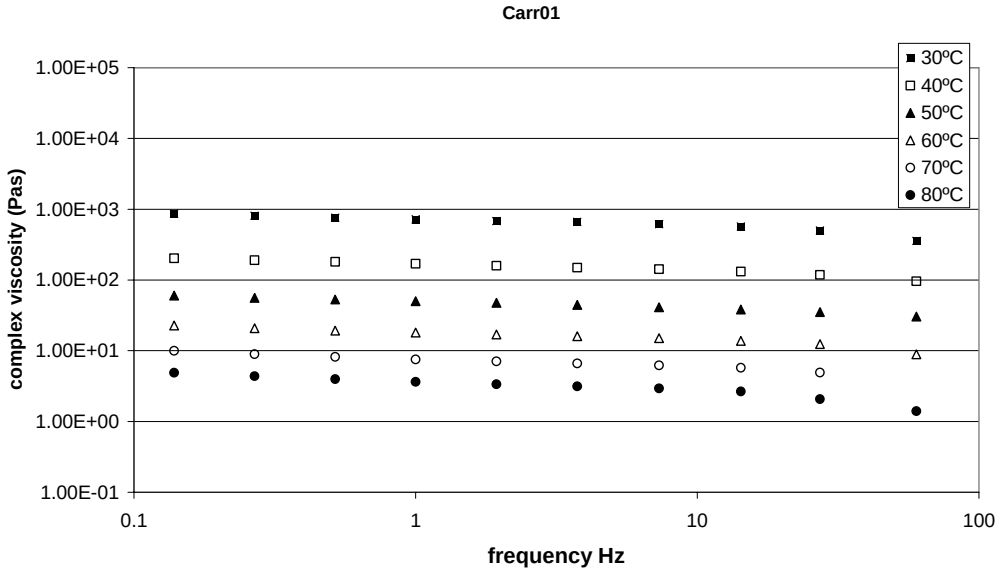

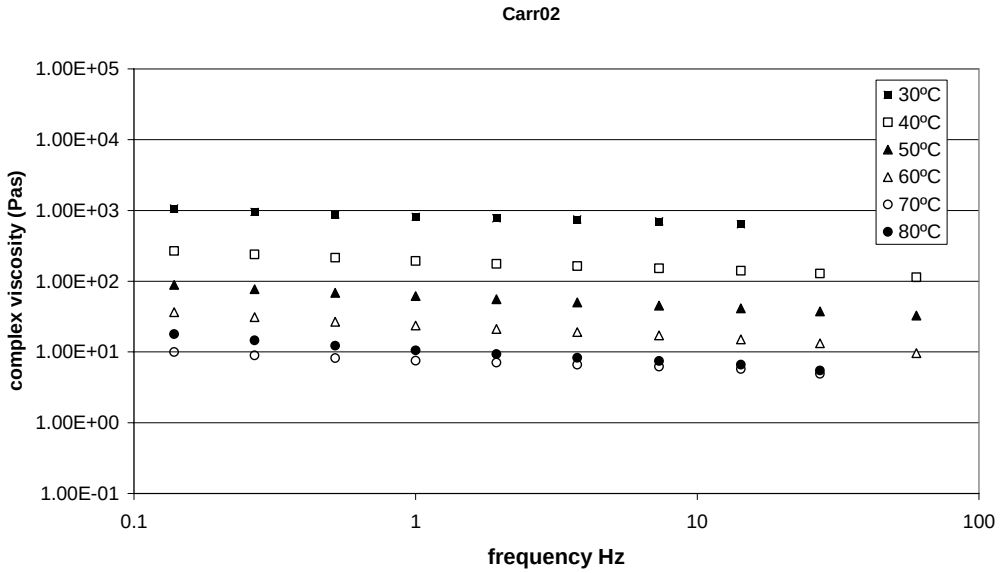

Figure 5.11. Complex viscosity for the sample Carr01 and Carr02, at different temperatures: 30 (■) ,40 (□) , 50(▲), 60 (Δ), 70(●), 80(○) °C.

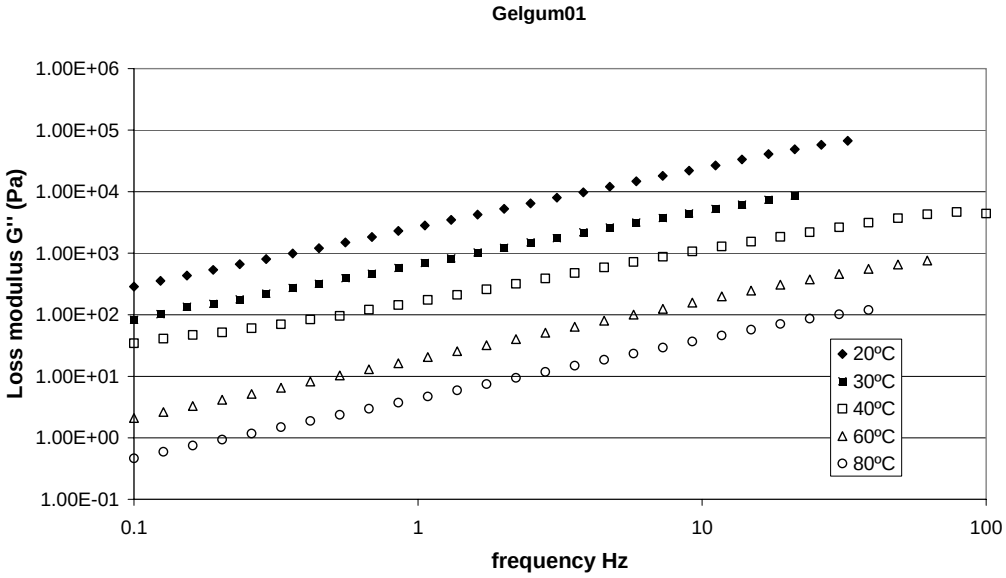

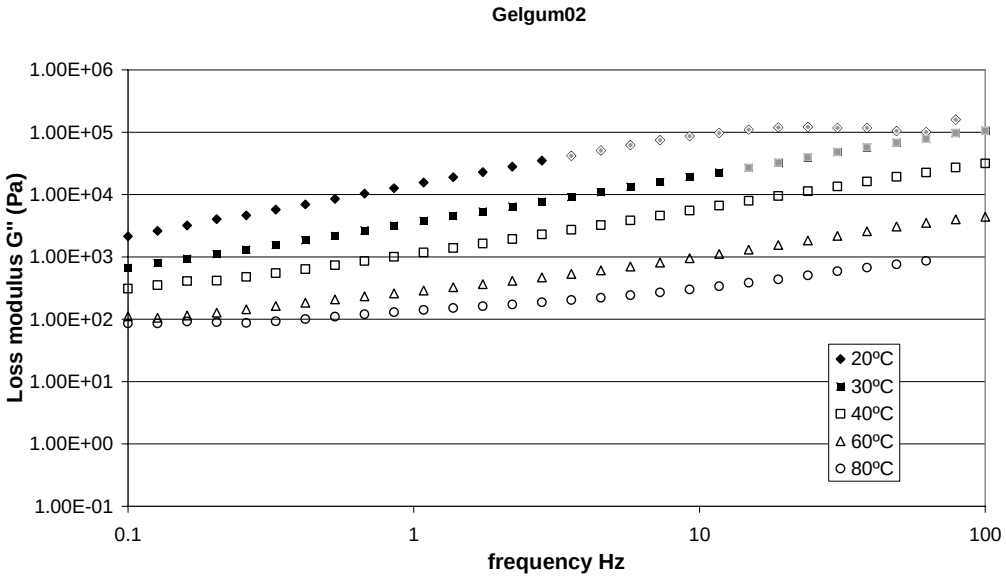

Figure 5.12 Loss modulus G'' for the sample Gelgum01 and Gelgum02, at different temperatures: 20(♦), 30 (■) ,40 (□) , 50(▲), 60 (Δ), 70(●), 80(○) °C. Data points filled in grey have not been used in subsequent modelling.

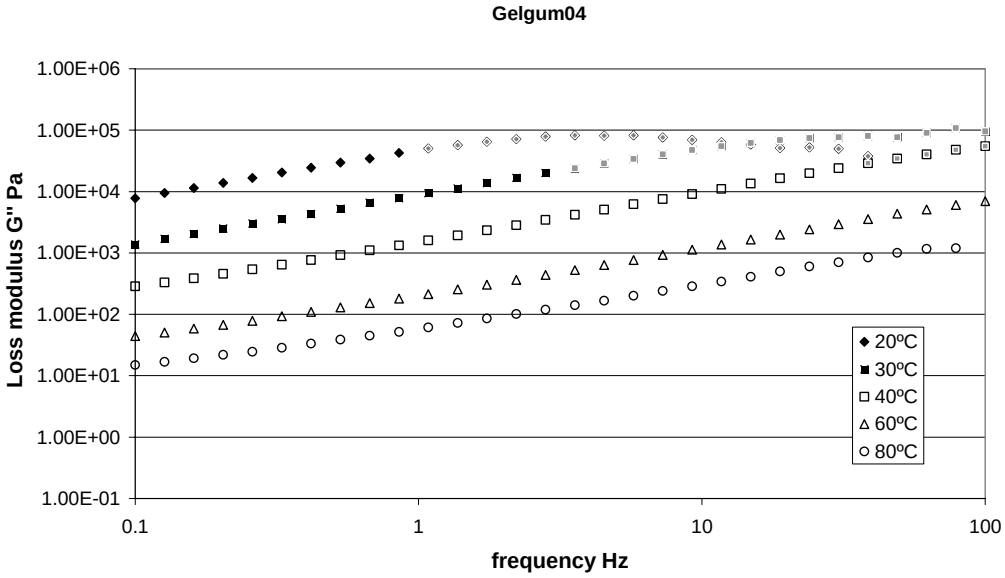

Figure 5.13. Loss modulus G'' for the sample Gelgum04 at different temperatures: 20(♦), 30 (■) ,40 (□) , 50(▲), 60 (Δ), 70(●), 80(○) °C. Data points filled in grey have not been used in subsequent modelling.

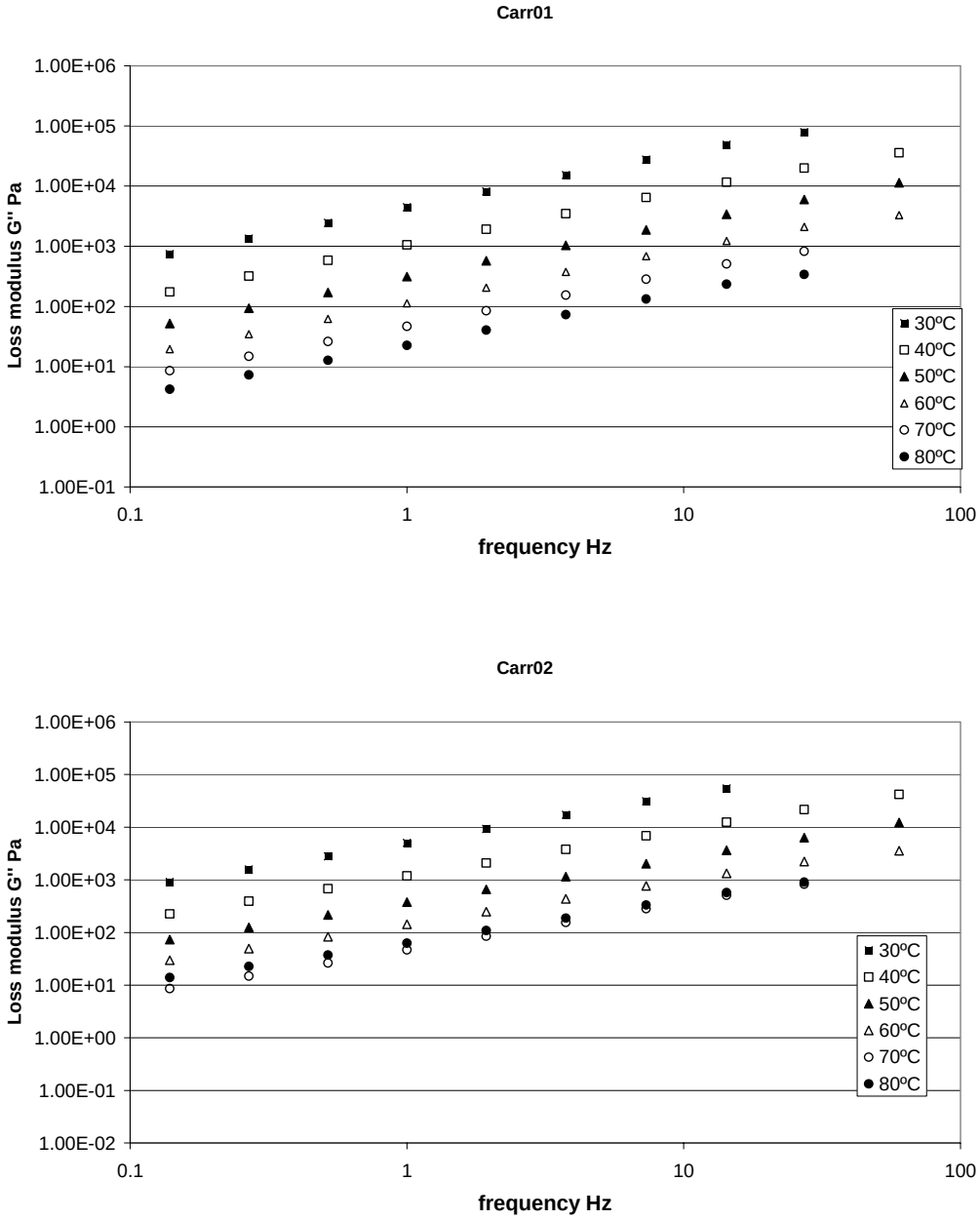

Figure 5.14 Loss modulus G'' for the sample Carr01 and Carr02, at different temperatures: 30 (■) ,40 (□) , 50(▲), 60 (Δ), 70(●), 80(○) °C. Data points filled in grey have not been used in subsequent modelling.

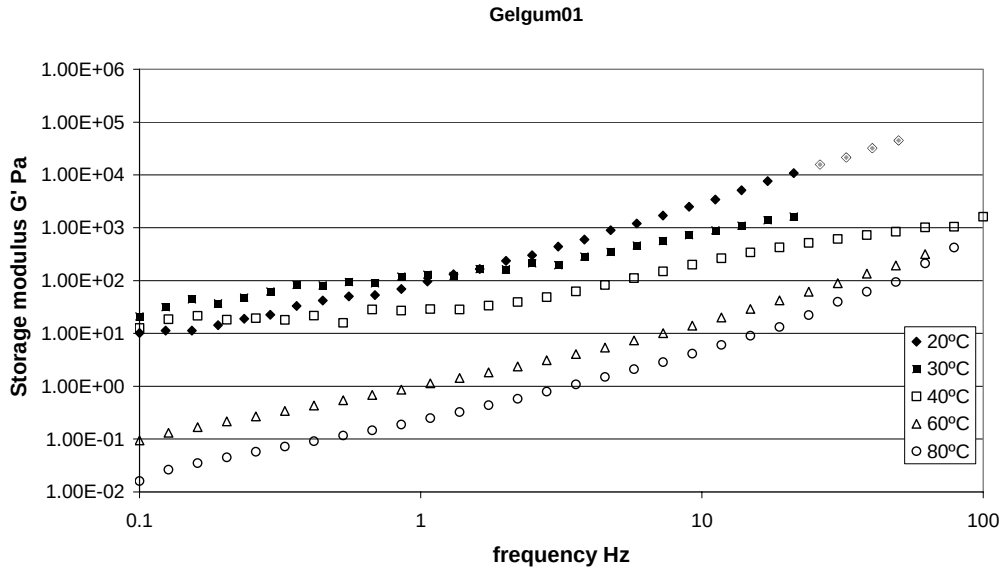

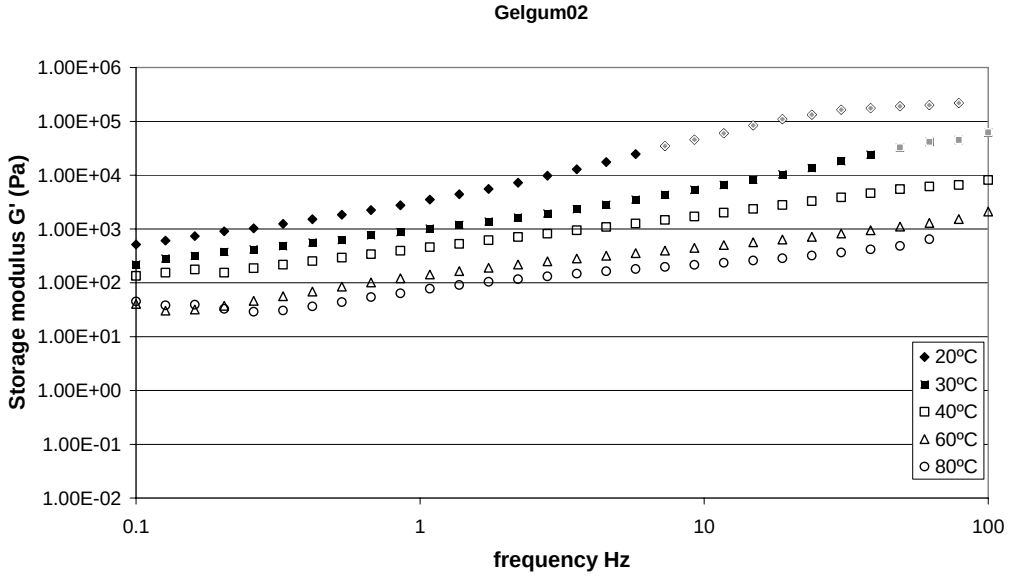

Figure 5.15 Storage modulus G' for the sample Gelgum01 and Gelgum01 at different temperatures: 20(♦), 30 (■) ,40 (□) , 50(▲), 60 (Δ), 70(●), 80(○) °C. Data points filled in grey have not been used in subsequent modelling.

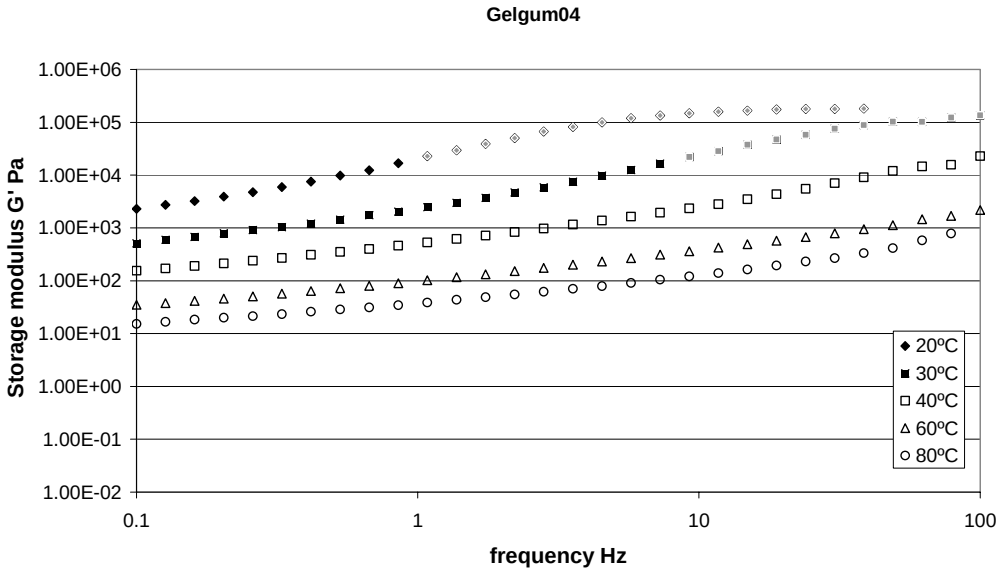

Figure 5.16 Storage modulus G' for the sample Gelgum04 at different temperatures: 20(♦), 30 (■) ,40 (□) , 50(▲), 60 (Δ), 70(●), 80(○) °C. Data points filled in grey have not been used in subsequent modelling.

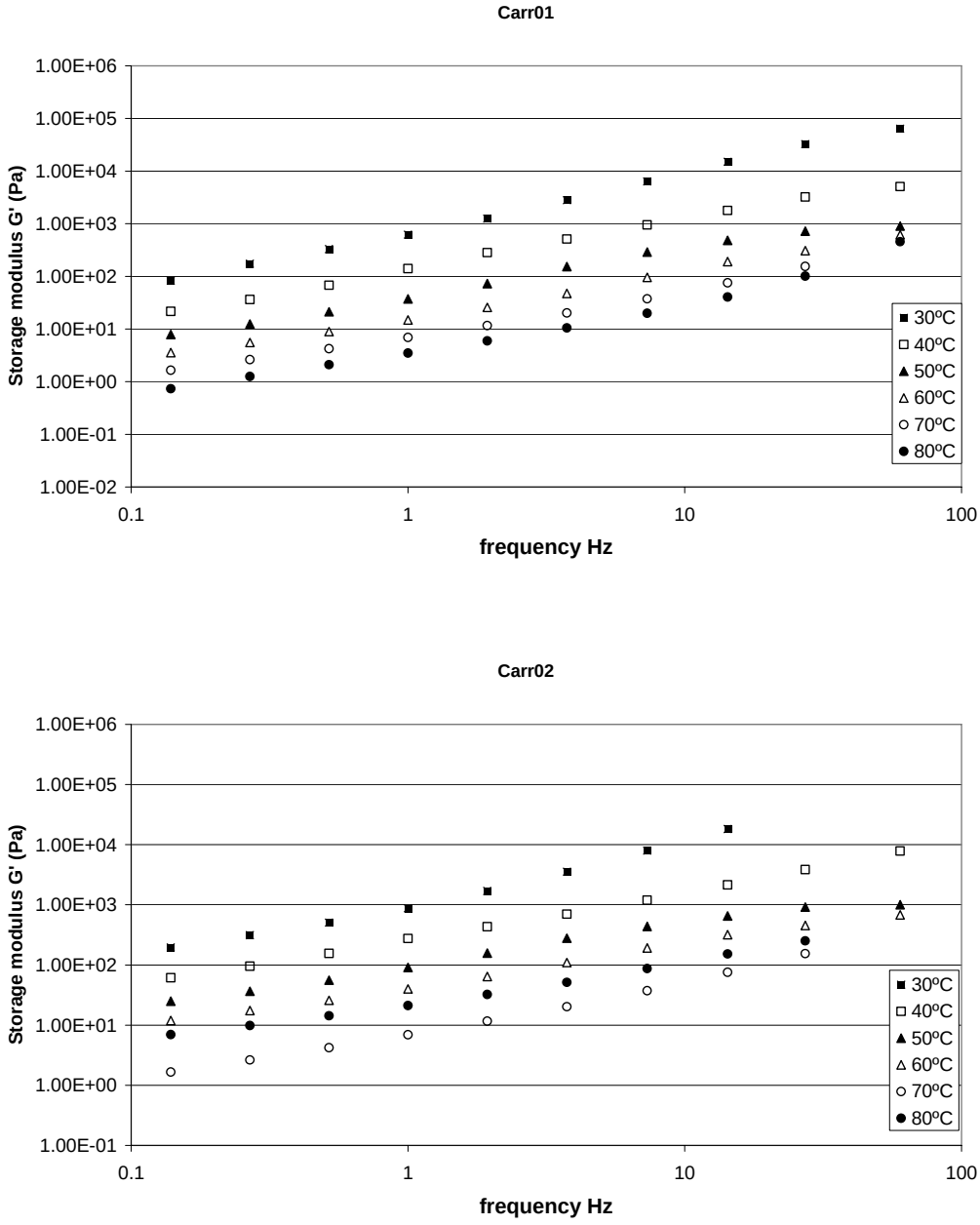

Figure 5.17 Storage modulus G' for the sample Carr01 and Carr02, at different temperatures: 30 (■) ,40 (□) , 50(▲), 60 (Δ), 70(●), 80(○) °C.

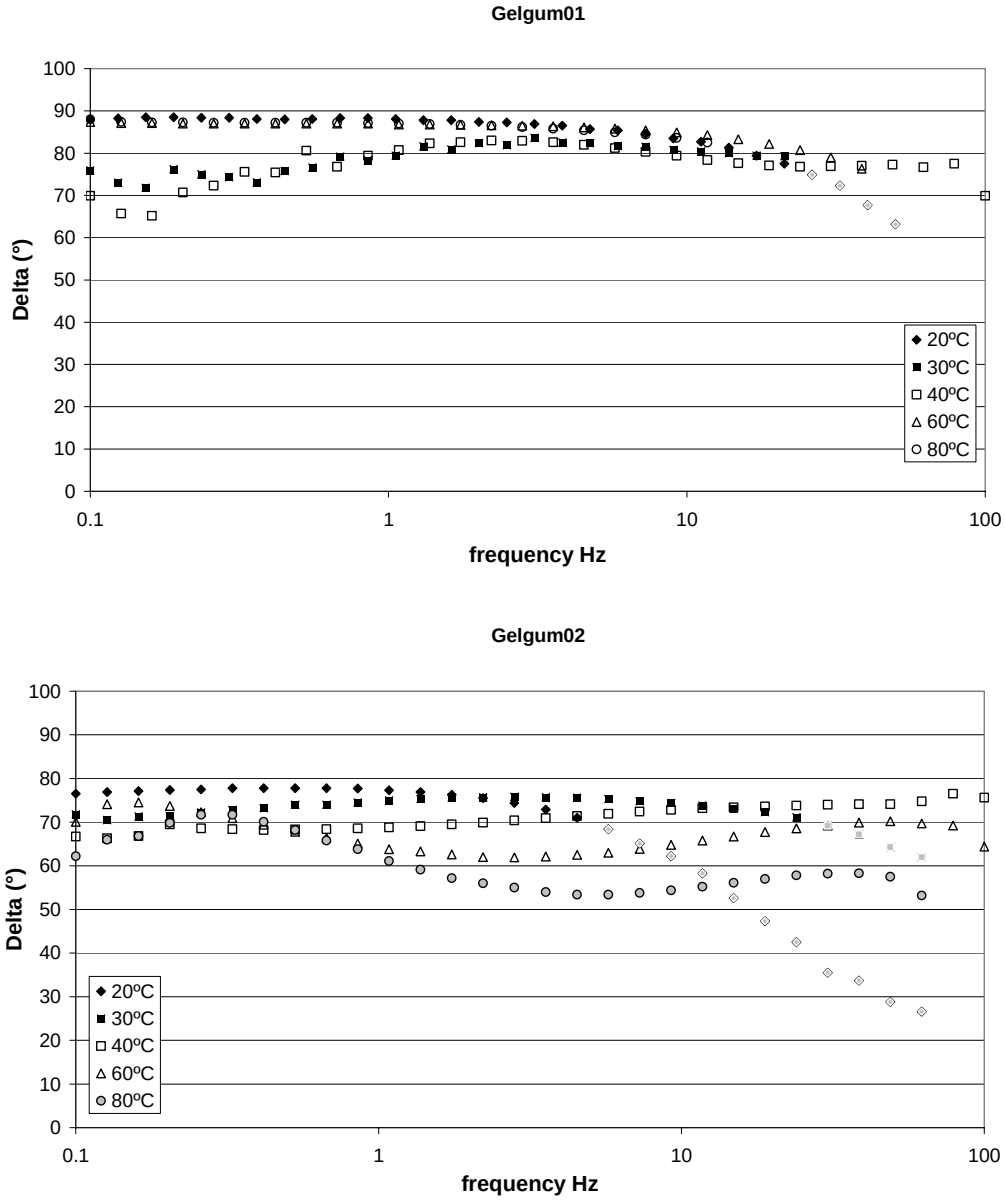

Figure 5.18 Phase angle, δ, for the sample Gelgum01 and Gelgum02, at different temperatures: 20(♦), 30 (■) ,40 (□) , 50(▲), 60 (Δ), 70(●), 80(○) °C. Data points filled in grey have not been used in subsequent modelling.

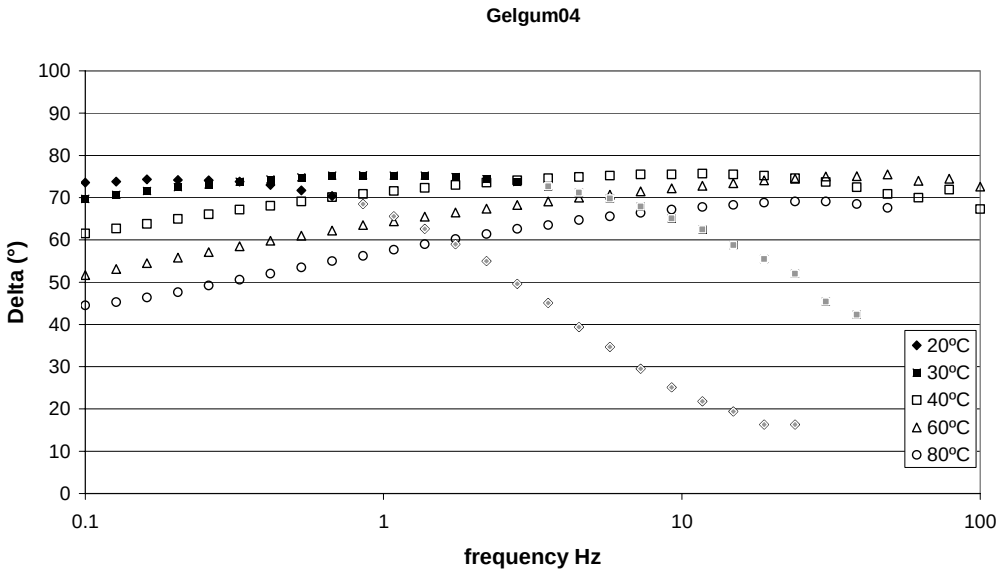

Figure 5.19 Phase angle, δ, for the sample Gelgum04 at different temperatures: 20(♦), 30 (■) ,40 (□) , 50(▲), 60 (Δ), 70(●), 80(○) °C. Data points filled in grey have not been used in subsequent modelling.

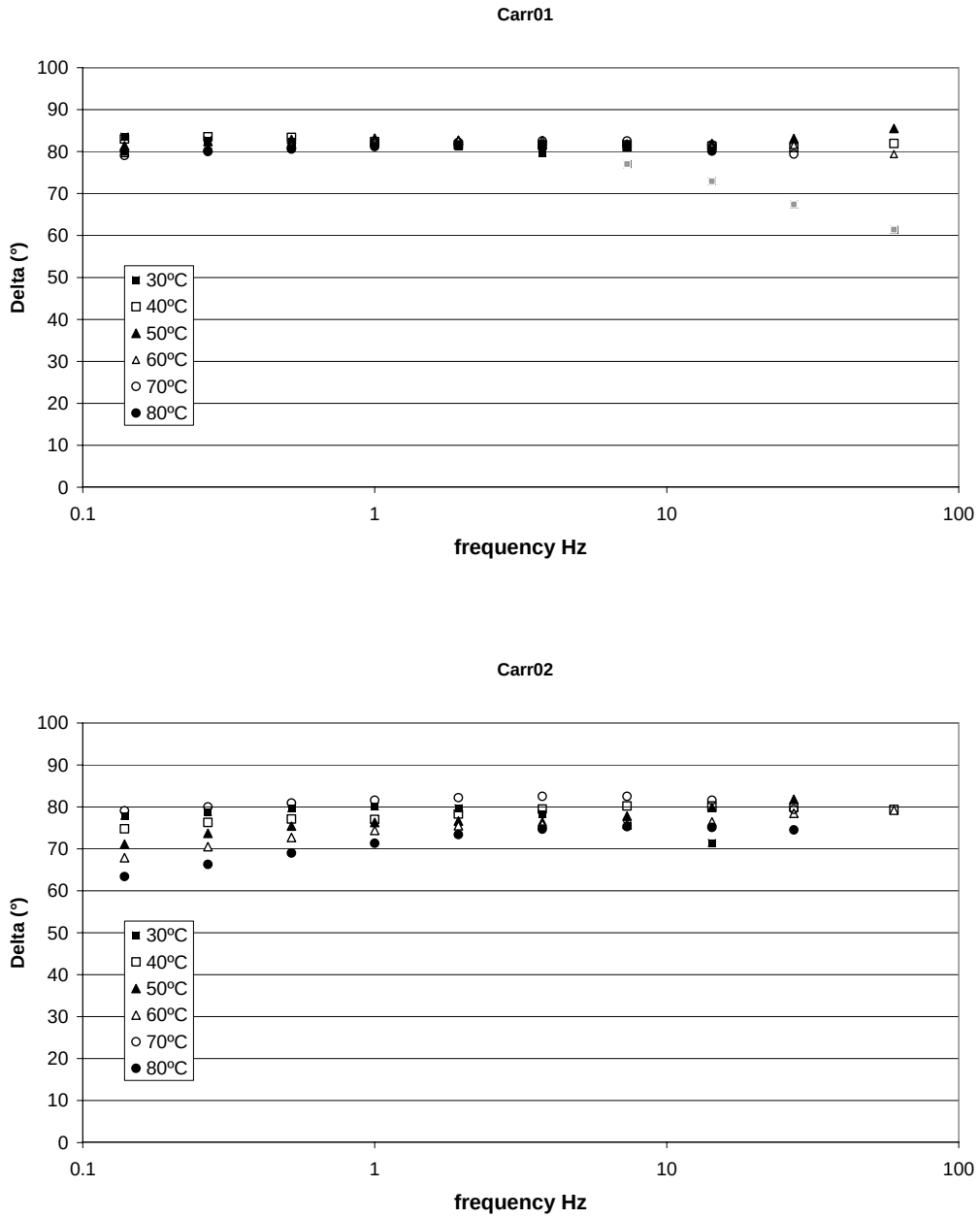

Figure 5.20 Phase angle, δ, for the sample Carr01 and Carr02 at different temperatures: 30 (■) ,40 (□) , 50(▲), 60 (Δ), 70(●), 80(○) °C. Data points filled in grey have not been used in subsequent modelling.

Time (frequency)-temperature superimposition (TTS) has been applied on oscillation data by choosing as reference temperature T_0 = 40 °C. The composite curves are shown in Figures. 5.21 - 5.23.

For the superimposition process the variable used was the loss modulus. At low frequencies and particularly for sample whose concentration of biopolymer was not very high a scattering in the delta value and storage modulus was detected. The scattering was more evident where the elastic component of the modulus was negligible. As we said before for the sample Gelgum02, some problems during the measurements occurred at higher temperature (maybe a incorrect estimation of the linear viscoelastic range at these temperatures), and this is reflected on the quality of the master curve, but overall in all the samples loss moduli superimpose quite well.

Master curves obtained for sample Gelgum01 are very similar to a typical mechanical spectrum of a very low molecular weight material. As the concentration of gellan gum increases a little maximum in G" that reflect the presence of a rubbery plateau is evident. The master curve obtained for the sample Gelgum04 is similar to a typical master curve for high molecular weight polymer, with the cross over of G' and G" at low frequencies. The same pattern if followed by sample containing κ-carrageenan

The shift factor determined with the superimposition has been used for the application of the WLF kinetics and determination of the glass transition. This analysis is shown in the following section.

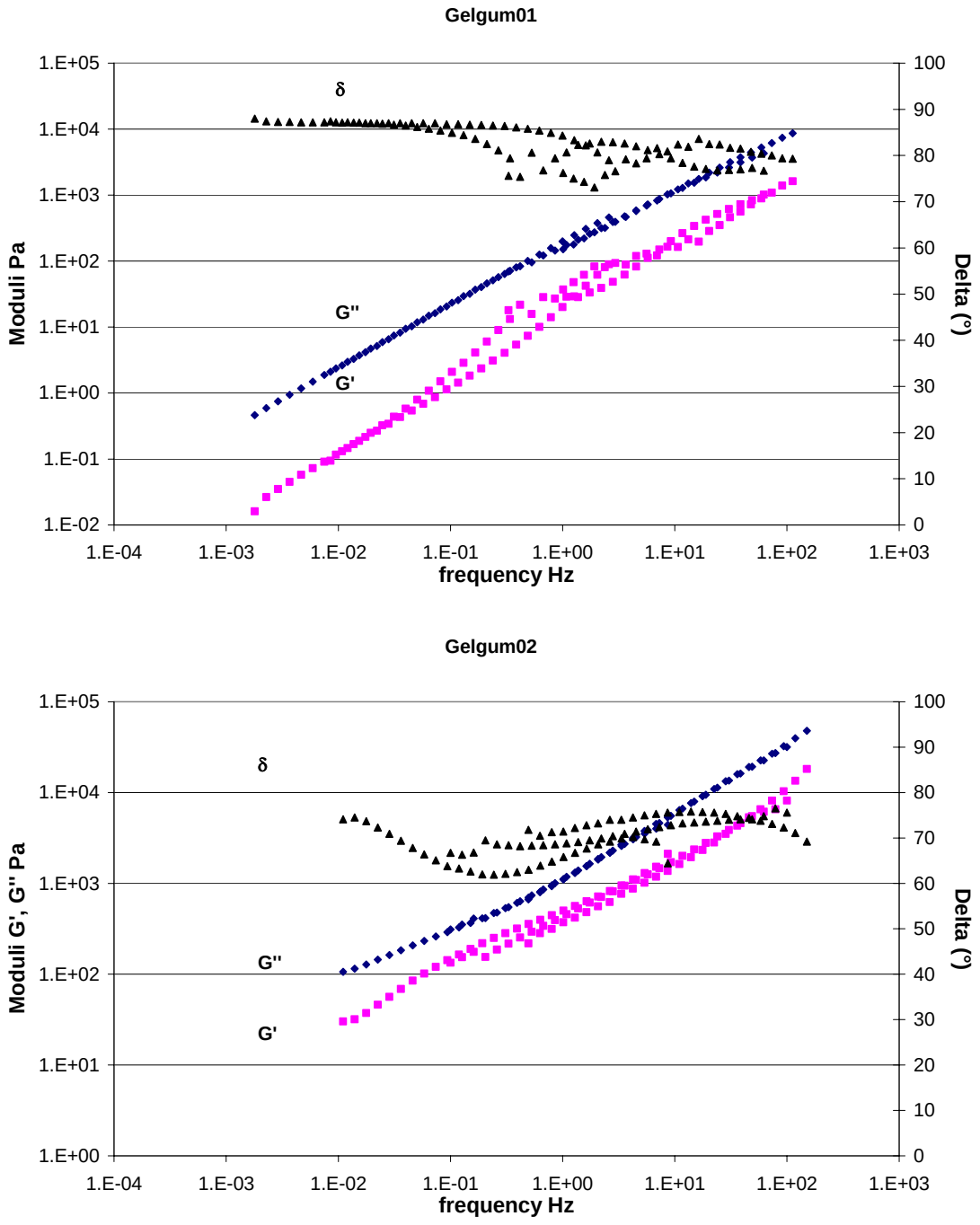

Figure 5.21 Master curves (T_0=40°C) for the caramels Gelgum01 and Gelgum02

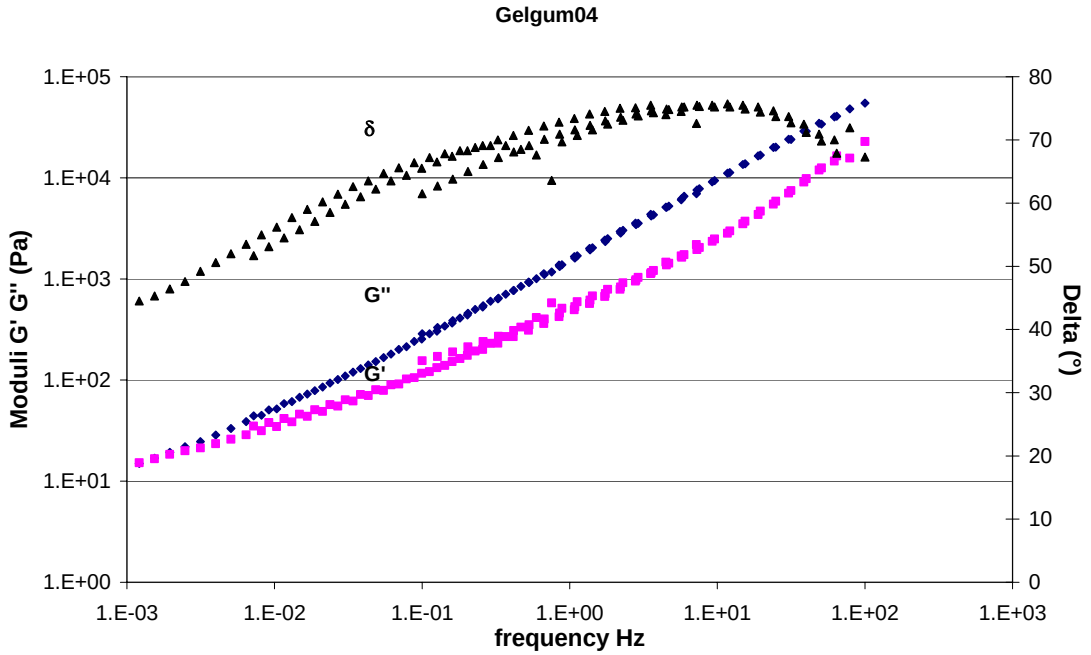

Figure 5.22 Master curves (T_0=40°C) for the caramels Gelgum04

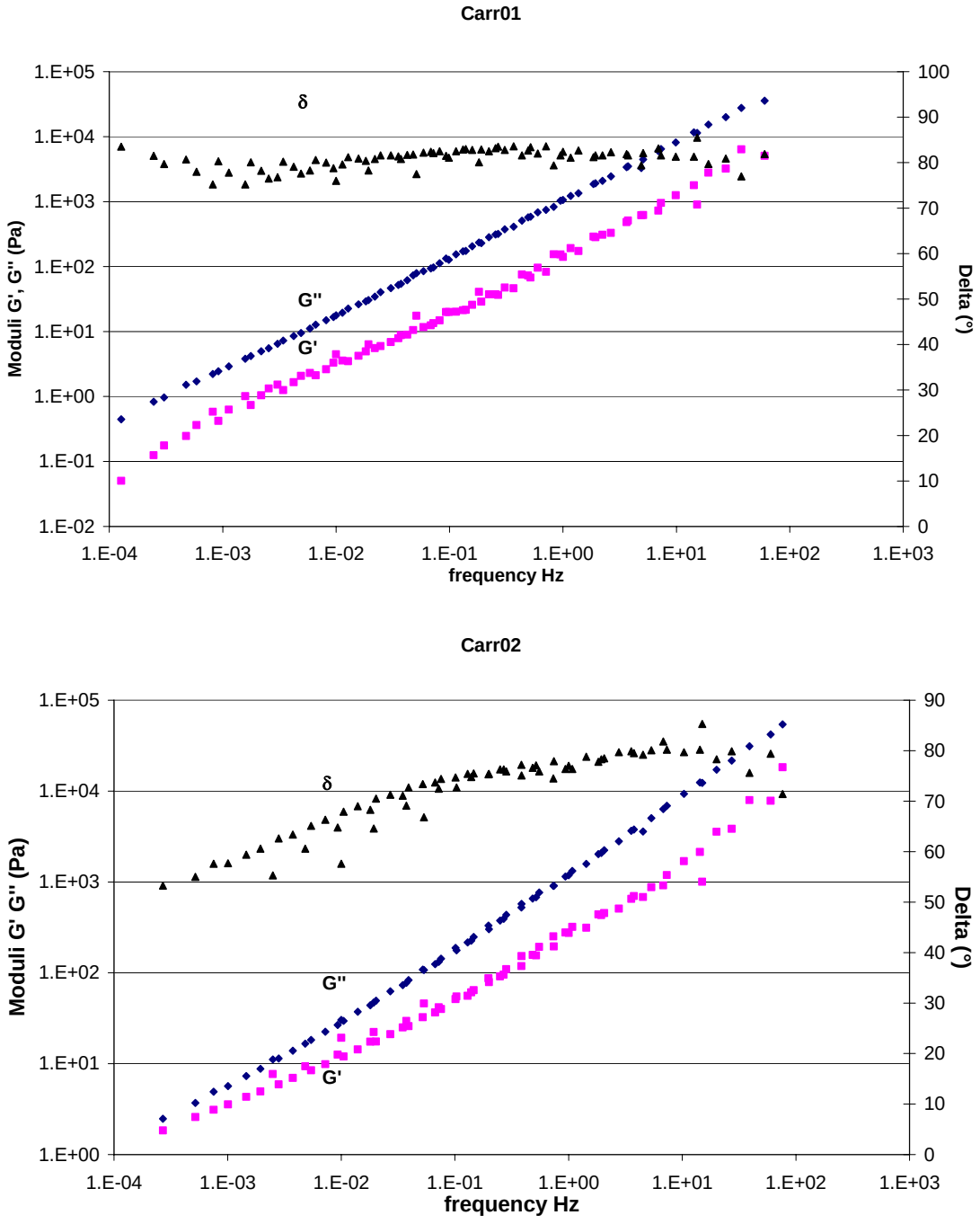

Figure 5.23 Master curves (T_0=40°C) for the caramels Carr01 and Carr02

5.4.3 Creep

The creep compliance response is shown in Figure 5.24-5.26.

The data obtained at different stresses collapsed onto the same line indicating that measurements were made in the linear viscoelastic region.

With the exception of the sample Gelgum01 the creep-recovery compliance pattern at 20°C is typical of a viscoelastic system showing a curvature in the compliance when a stress is applied and a recovery of more of the 50% of the deformation when the stress is released for the sample Gelgum2 and Gelgum04 and around 20-30% for the sample containing carrageenan.

The compliance, at the maximum time the stress was applied decreased, with increasing the amount of hydrocolloids incorporated; the lowest compliance was recorded for the sample Gelgum04.

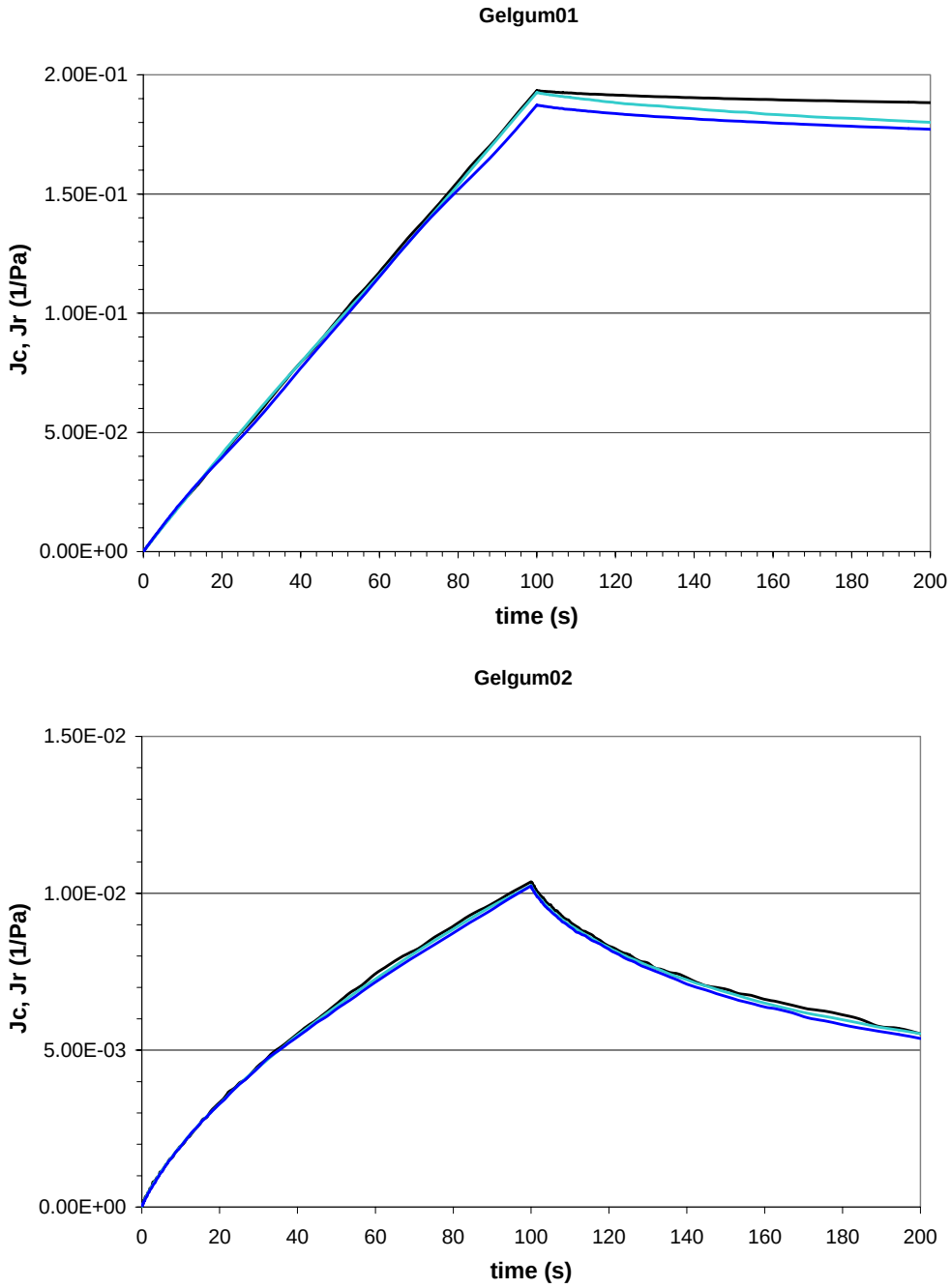

Figure 5.24 Creep and recovery compliance test performed at 20°C on the sample Gelgum01 for stresses of 1, 4 and16 Pa and on the sample and Gelgum02 for stresses of 1, 2 and 4 Pa (Results obtained at the different stresses are coincident)

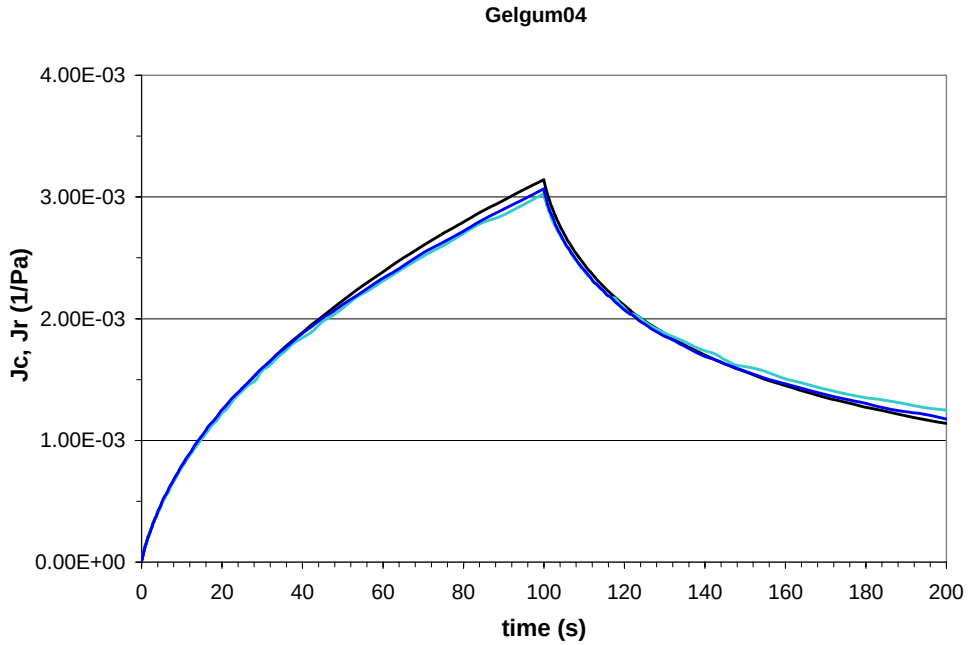

Figure. 5.25 Creep and recovery compliance test performed at 20°C on the sample Gelgum04 for stresses of 4, 8 and 16 Pa (Results obtained at the different stresses are coincident).

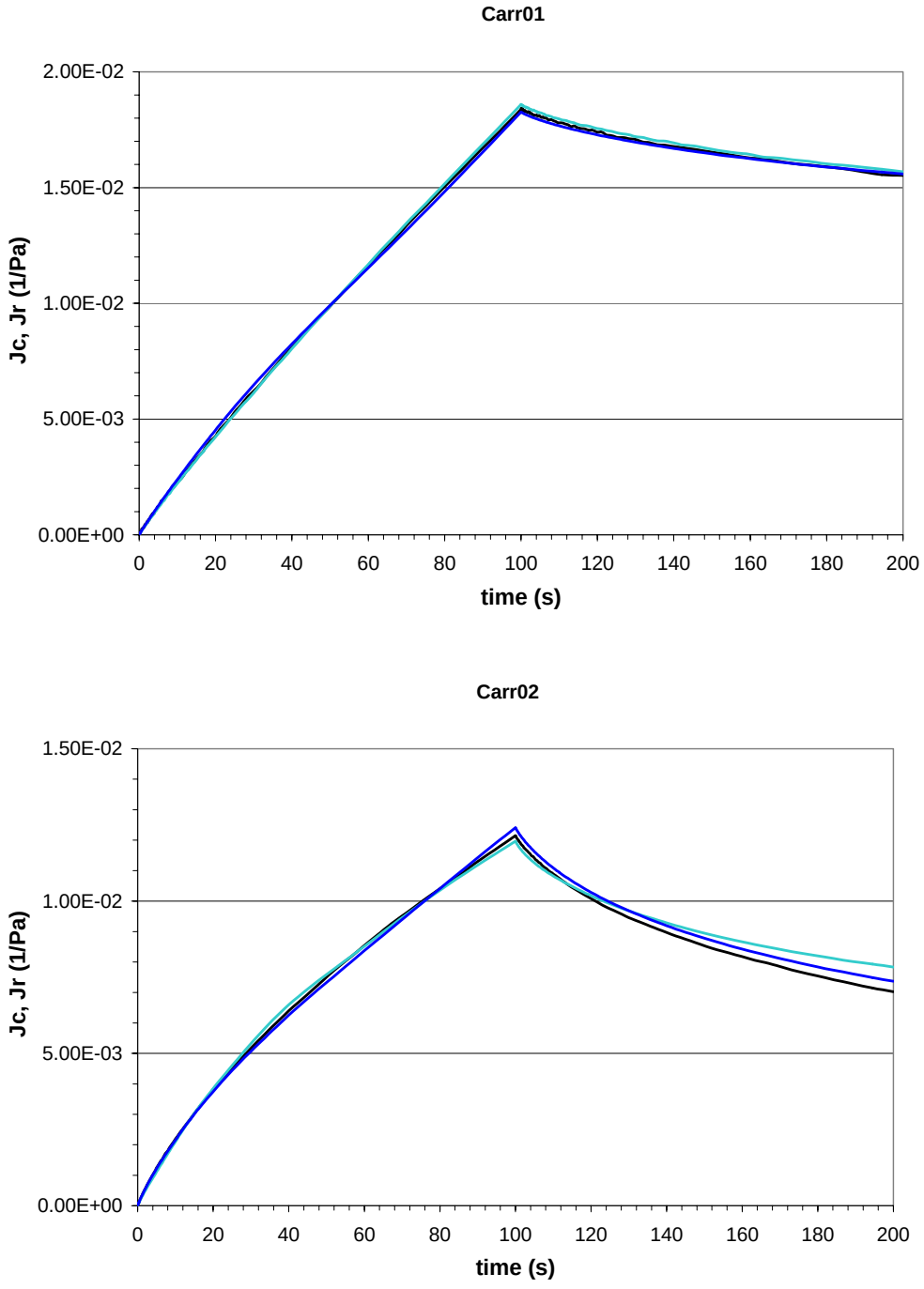

Figure. 5.26 Creep and recovery compliance test performed at 20°C on the sample Carr01 for stresses 1,2 and 16 Pa and Carr02 for stresses of 4, 16 and 64 Pa (Results obtained at the different stresses are coincident).

The model discussed in Chapter 4 has been applied to the creep curves of sample containing hydrocolloids.

The viscosity of the dashpot of the Maxwell element μ_0, will be used for the modelling in the next section (Table 5.8)

Table 5.8 *Creep viscosities μ_0 (Pa·s) at 20ºC and correlation coefficient R*

	Gelgum01	**Gelgum02**	**Gelgum04**	**Carr01**	**Carr02**
R	0.9992	0.9988	0.9998	0.996	0.9978
μ_0	528	27360	76180	6198	12500

5.4.4 CAPILLARY RHEOMETRY

Increase of solid-like behaviour on hydrocolloid addition is also confirmed by capillary measurements performed at 70°C on samples where the κ-carrageenan concentration ranged between 0 (as it has been used as standard the sample 117) and 0.2%. Figure 5.27 shows the extensional and the shear viscosity as function of the strain rate for sample containing carrageenan. As the carrageenan content increases the extensional viscosity increases more rapidly than the shear viscosity resulting in an increase in the Trouton ratio at 100 sec^{-1} from about 10 for the sample with no κ-carageenan to 500 for the sample containing 0.2% of carrageenan (Table 5.9).

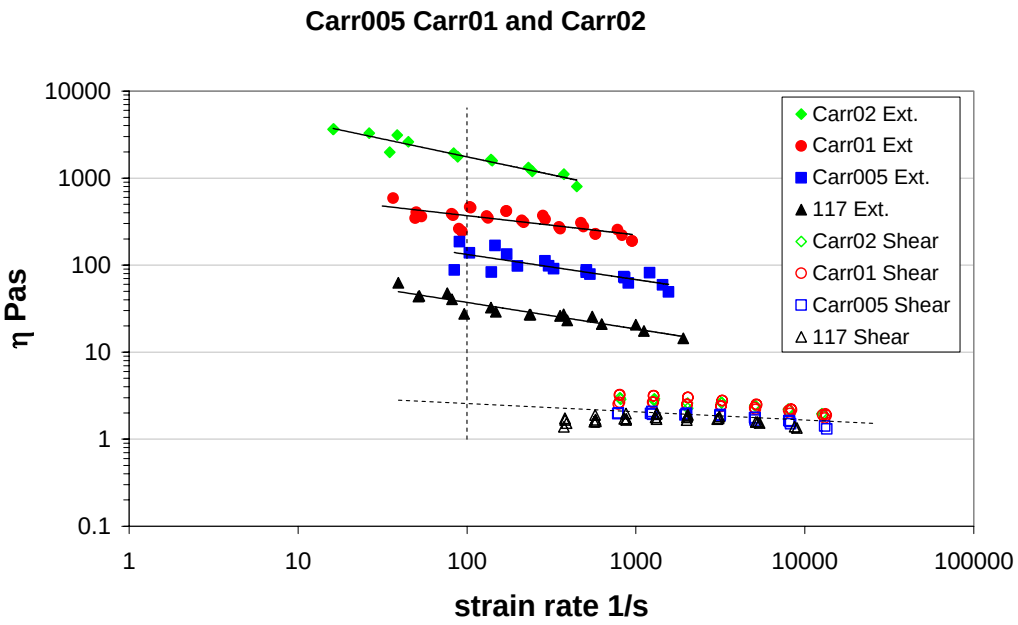

Figure 5.27 Viscosity as function of the strain rate for the sample cooked at 117ºC (▲), for the samples containing 0.05% (■), 0.1% (●) and 0.2% (◆) of carrageenan. Filled symbols are extensional capillary data and empty symbols are shear capillary data.

Different and surprising are the results for sample containing gellan gum. Figure 5.28 shows the curves of the extensional and shear viscosities obtained for the sample gelgum01 and gelgum04. For a better interpretation the extensional and shear viscosity for the samples 117 and 120 are also shown. The curves in extensional and shear flow for the sample gelgum01 lie at value lower then the curves for the sample 117. This is easily explainable in terms of water content that is 13.3% for the sample Gelgum01 and 10.5% for the sample 117.

The shear viscosity curve of the sample gelgum04 is a values in between the shear viscosity for sample 120 and the shear viscosity for sample 117. this is also explainable in terms of water content that for the sample gelgum04 is 9.5%, which is in between the water content of the sample 117 and the water content of the sample 120 (8.9%).

The extensional viscosity curves lie at value higher of the extensional curve of the sample 120. Again the extensional viscosity reflects the non-Newtonian character of the sample. However a comparison of the Trouton ratio at $100s^{-1}$ between the sample containing hydrocolloids (Table 5.9) shows that for the sample gelgum04 this effect is less marked than for the sample containing carrageenan although the samples containing carrageenan have a higher water content. It is suggested that some internal slippage of the gellan gum chains in the caramel bulk could contribute to a lower measured extensional viscosity.

Table 5.9 *Water content and Trouton ratio for sample containing hydrocolloids*

Sample	water content % w.w.b.	Trouton ratio at 100^{-1}
117	10.5	20
Carr005	10.4	37
Carr01	10.4	100
Carr02	10.1	500
Gelgum01	13.3	11
Gelgum04	9.5	43

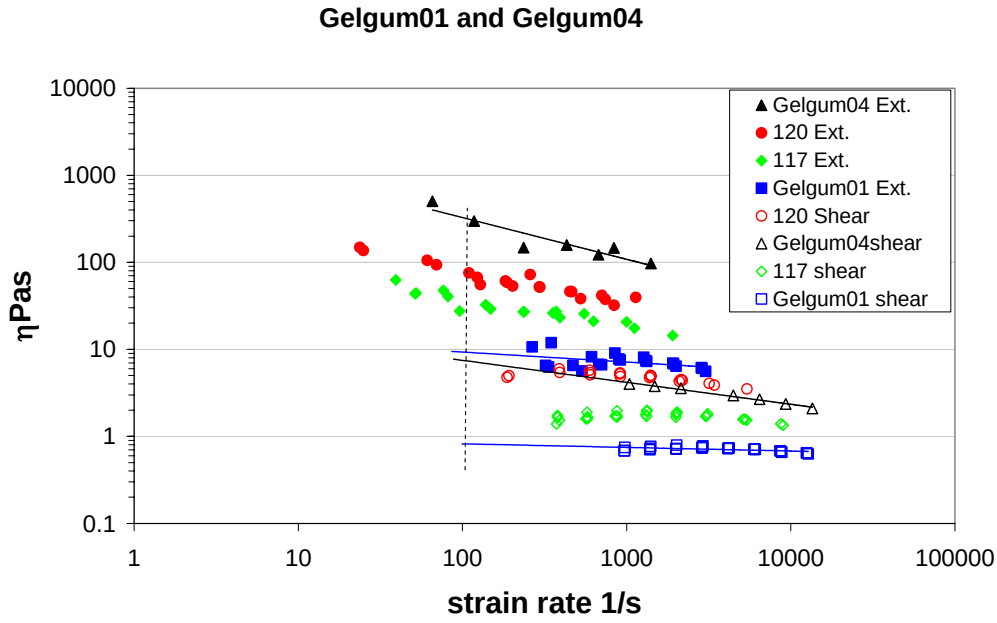

Figure 5.28 Viscosity as function of the strain rate for the sample Gelgum04 (▲) and for the sample Gelgum01 (■). For a better interpretation viscosity as function of strain rate are also shown for sample 117 (◆) and for sample 120 (●). Filled symbols are extensional capillary data and empty symbols are shear capillary data

5.5 Modelling of the rheological data

5.5.1 Viscosity

Table 5.10 shows a summary of all the viscosities value obtained for the samples containing gellan gum and Table 5.11 shows the viscosities for the samples containing κ-Carragenan over a range of temperature between 20 and 80°C from different rheological tests: shear viscosity, oscillation and creep-recovery.

A comparison between the techniques shows agreements for the sample Gelgum01. The value at 40ºC obtained from shear viscosity test is lower then the complex viscosity at the same temperature (31Pa·s against 51 Pa·s), but at 60ºC the value obtained with both the techniques are comparable. The creep viscosity is also comparable with the complex viscosity at 20ºC.

The response for the sample Gelgum02 in oscillation is very different from the measurements in shear viscosity. In fact at 60 and 80 ºC the complex viscosities are four times higher compared with the shear viscosity taken as the power law index k. Moreover the complex viscosities are even higher then the ones obtained at the same temperature for the sample Gelgum04. For this reason it has been decided to omit the oscillation data at 60 and 80ºC for Gelgum02 in the modelling. The test in oscillation and shear viscosity gave agreement for the sample Gelgum04.

For both Gelgum02 and Gelgum04 the complex viscosity is much lower than the creep viscosity. This may reflect the differences in the time scales of measurement. The time scale in creep is much longer which than the 1 rad sec^{-1} used to obtain the complex viscosities. The hydrocolloid containing materials show a decrease I complex viscosity with increasing frequency.

As we will see later with the modelling at 20ºC, a temperature not very far from the glass transition, the viscosity for samples at higher gellan gum content is in a range of the curve of the viscosity against the temperature where there is a steep slope:

little changes in temperature results in higher variation of the viscosity. This could be another reason for the disagreement between the value obtained by creep and oscillation for the samples Gelgum02 and Gelgum04.

Regarding the samples containing κ-carragenan the complex viscosities are somewhat lower then the power law consistency, k, for the measurements performed at the same temperature. As no oscillation test has been performed at 20ºC no comparison has been made with the creep viscosity.

Table 5.10 *Consistency indices, η* at 1 rad sec^{-1} and the creep viscosity for samples containing gellan gum.*

	Sample / T (ºC)	Gelgum01	Gelgum02	Gelgum04
Shear	**35**	62.3±0.9		-
viscosity	**40**	31.2±0.9		
	45		135.4 ± 0. 7	248.7 ± 0.7
(Consistency	**50**	12.3±0.9	70.1 ± 0.9	199.7 ± 0.6
	55		41.9 ± 0.8	
Index)	**60**	4.79±0.9	29.3 ± 0.8	92.3 ± 0.7
Pa·s^n	**70**	2.3±0.9	21.0 ± 0.8	42.2 ± 0.7
	75		13.8 ± 0.8	
	80		12.4 ± 0.8	20.5 ± 0.8
Oscillation	**20**	449	3250	11700
Viscosity	**30**	147	974	2120
at	**40**	51	442	426
ω=1 rad/sec	**60**	3.26	118	70.9
Pa·s	**80**	0.74	98.7	26.4
creep				
viscosity	**20**	528	27400	76200
Pa·s				

Table 5.11 *Consistency indices, η* at 1 rad sec^{-1} and the creep viscosity for samples containing carrageenan.*

	Sample / T (C)	Carr01	Carr02
Shear	**45**	70 ± 0.8	
viscosity	**50**	51.9 ± 0.8	92.5 ± 0.8
	55		101.5 ± 0.7
(Consistency	**60**	26.8 ± 0.9	61.3 ± 0.7
Index)	**70**	11.2 ± 0.9	43.6 ± 0.7
Pa·s^{-n}	**75**		26.1 ± 0.8
	80	6.7 ± 0.9	21.0 ± 0.8
Oscillation	**30**	860	1060
Viscosity	**40**	202	268
at	**50**	60.3	88.5
ω=1rad/sec	**60**	22.7	36.5
Pa·s	**70**	12.7	18.4
	80	4.90	10.9
creep			
viscosity	**20**	6200	12500
Pa·s			

5.5.1.1 Arrhenius kinetics

Arrhenius kinetics are represented by the following expression:

$$\ln(\eta) = \ln(\eta_0) - \frac{E_0}{RT} \qquad \text{eq 4.27}$$

Figure 5.29 and 5.30 show the plot of log η against the reciprocal of the temperature for the sample containing gellan gum and carrageenan respectively.

The activation energies determined from the slope of the line are shown in Table 5.12., the water content is also indicated.

Table 5.13 shows the water content and the activation energies of the sample cooked at different temperature to allow a comparison.

For samples containing gellan gum the activation energies are higher then the sample with no addition of hydrocolloids at the same water content. For example Gelgum01 has energy of activation 20KJ/mol higher then the sample 113 although their water content is the same. Gelgum has activation energy 30KJ/mol more then the sample 117 although his water content is higher by about 1%. Gelgum 04 has activation energy 99KJ/mol almost 12KJ/mol higher than the value obtained for the sample 120 although the water content is higher. These higher values in activation energies may reflect the destruction of the hydrocolloid induced structures with increasing temperature

Samples containing κ-carrageenan have the same water content of sample 117. For these no differences in the activation energy are observed.

Curvatures of the data in Figures 5.29 and 5.30 are shown for all the samples indicating that the Arrhenius model does not fit the data well. This is not unexpected

because as discussed previously WLF rather then Arrhenius would be expected as T_g is approached. The data was also modelled using a WLF model.

Figure 5.31 shows the T_g scaled Arrhenius plot for sample containing gellan gum (a) and κ-carrageenan (b). It is observable that with the increasing of the amount of hydrocolloid the viscosity curve moves in the direction of the straight line. This indicates that hydrocolloids contribute to a reduction on the fragility of the liquid in the range of the glass transition temperature.

Table 5.12 *Linear fit parameters Y=A+Bx and Activation energy*

	Gelgum01	**Gelgum02**	**Gelgum04**	**Carr01**	**Carr02**
water content % w.w.b.	13.27	11.25	9.5	10.4	10.1
R^2	0.99	0.94	0.92	0.96	0.94
A	- 13.9	-14.4	-12.7	-13.3	-12.8
B	4870	5330	5184	4909	4832
Ea ($KJmol^{-1}$)	93	102	99	94	92

Table 5.13 *Activation energy for sample cooked at different temperatures*

	113	117	120	122
water content % w.w.b	13.2	10.5	8.91	7.88
Ea ($KJmol^{-1}$)	75	93	89	101

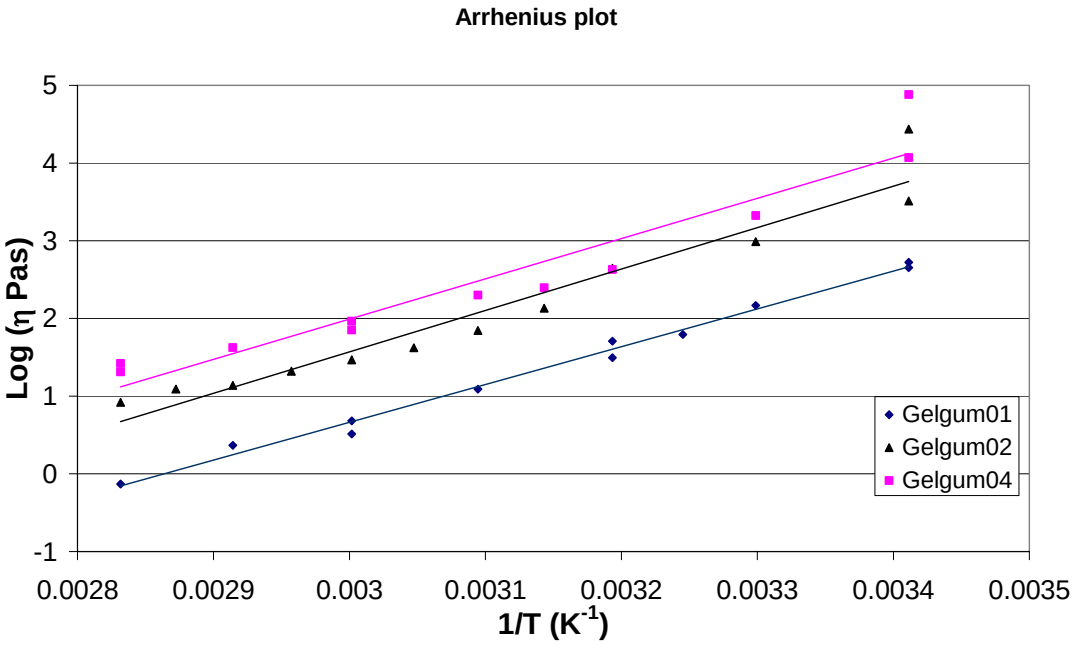

Figure 4.29 Arrhenius plot of the viscosities for sample containing gellan gum

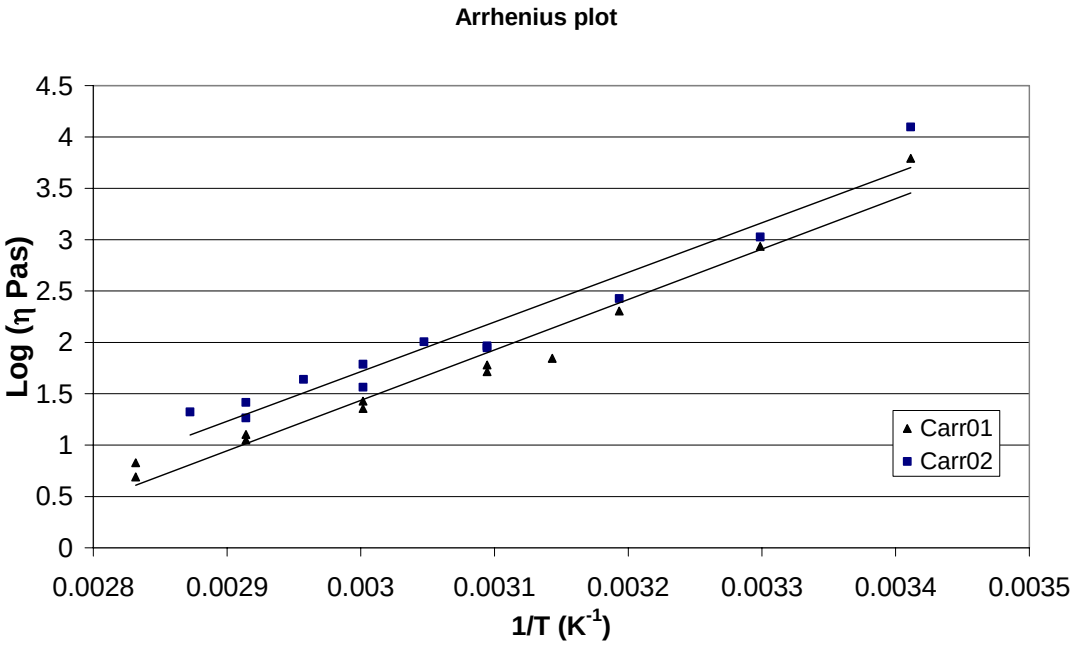

Figure 4.30 Arrhenius plot of the viscosities for samples containing κ-Carrageenan

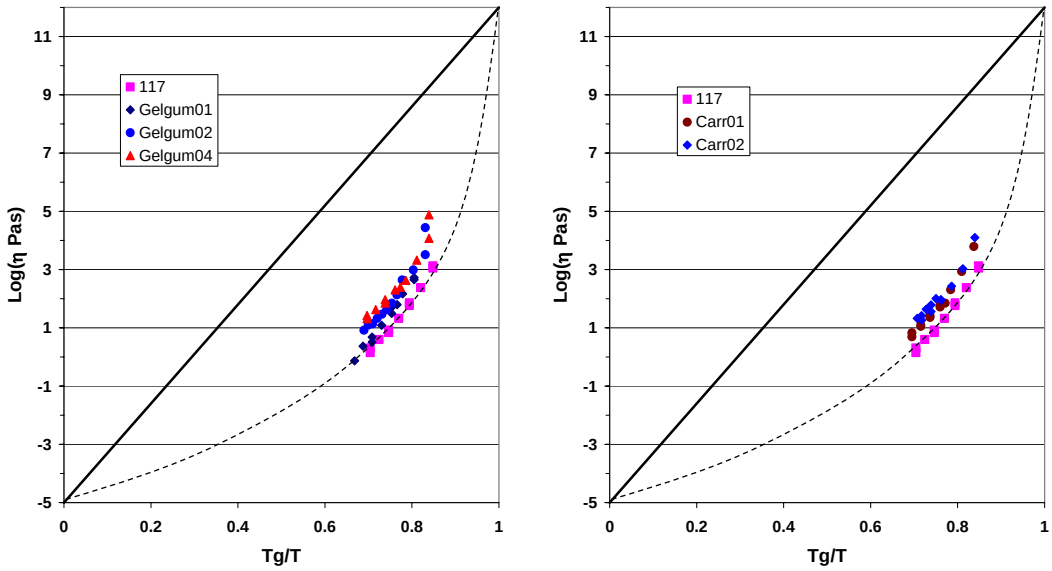

(a) (b)

Figure 5.31 T_g-scaled Arrhenius plot for sample containing gellan gum (a) and samples containing carrageenan (b).

5.5.1.2.WLF kinetics

Figure 5.32 shows the viscosities as function of T-T_g, where the glass transition arise from calorimetric measurements, and the line correspond to a WLF fit with the universal values C_1^g=17.4 and C_2^g=51.6 K. As for the sample of chapter 4, it is evident that the WLF fit with the universal values is not suitable for the caramel samples containing hydrocolloids.

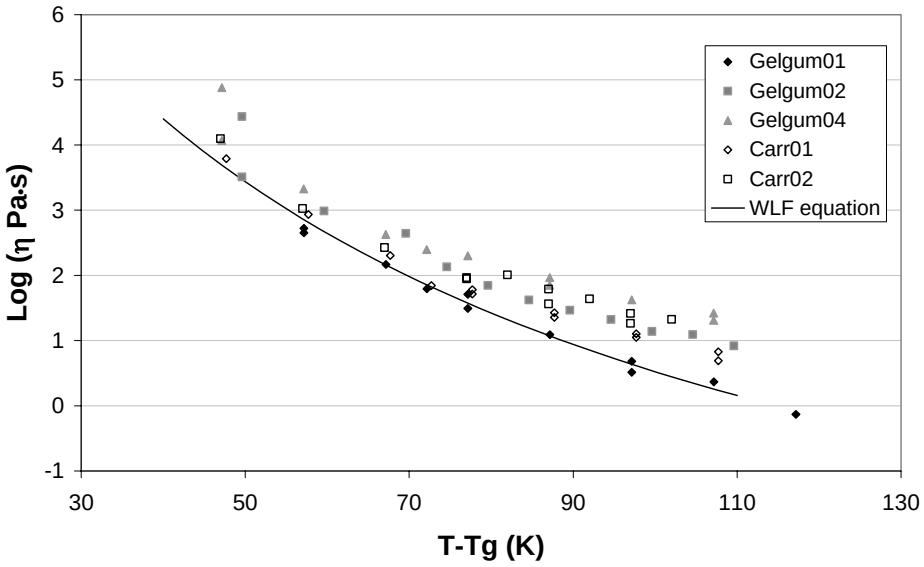

Figure 5.32 WLF fit with universal constant and viscosities of experimental viscosities as function of T-T_g

Figures 5.33 a and b shows the best fit obtained for the viscosity of each sample and the values of C_1^g and C_2^g, the correlation coefficient R and the chi squared χ^2 are shown in Table 5.14.

Table 5.15 shows the fragility as it has been defined in chapter 4. (1- C_2^g/T_g). For a better comparison value of fragility relative at the sample with no hydrocolloids and the water content is also shown. Values obtained for samples containing hydrocolloids are slightly lower compared with the fragility values obtained for

samples at the same water content with no incorporation of hydrocolloids. This is in accord with the previous consideration done on the T_g-scaled Arrhenius plot. ·

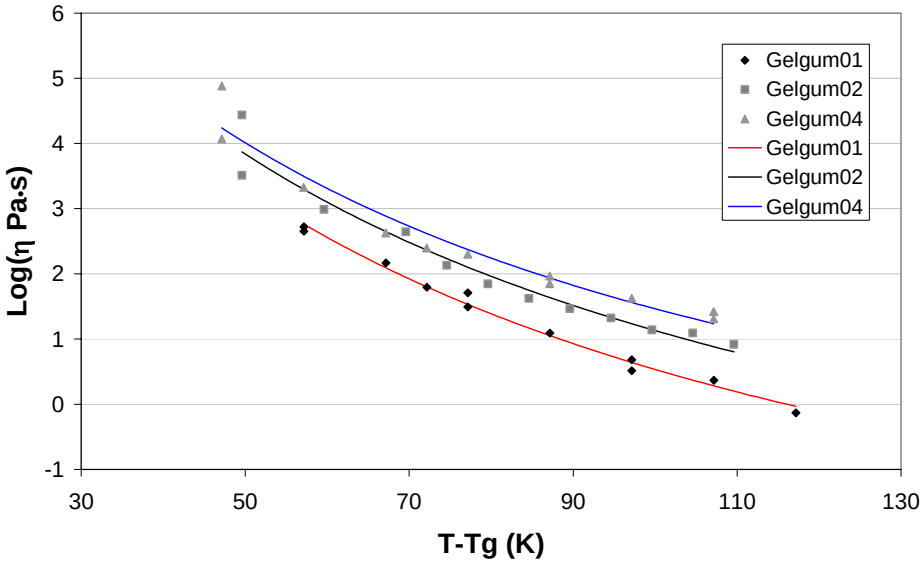

(a)

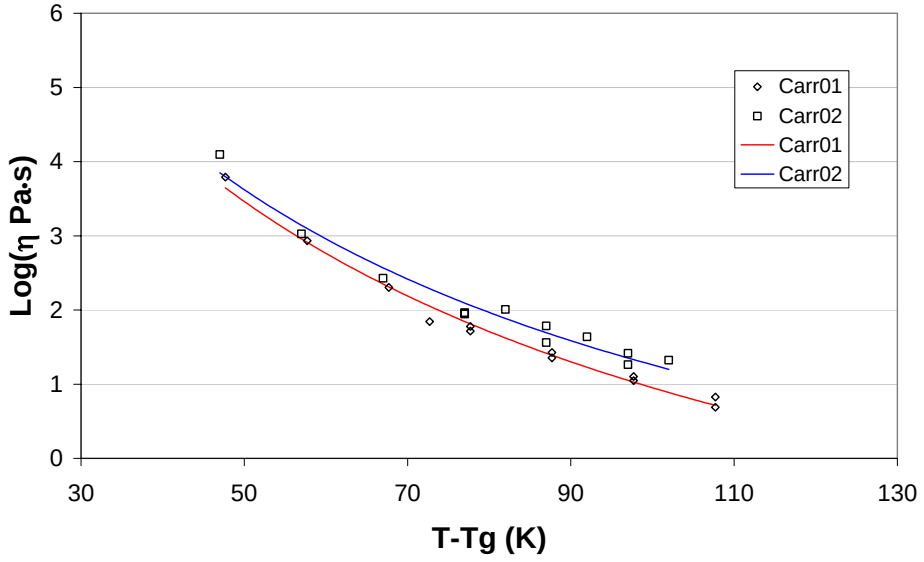

(b)

Figure 5. 33 WLF plot for samples containing gellan gum (a) and carrageenan (b)

Table 5.14 *WLF parameters*

	Gelgum01		**Gelgum02**		**Gelgum04**		**Carr01**		**Carr02**	
	Value	Error	Value	Error	Value	Error	Value	Error	Value	Error
C_1^g	-16.9	0.3	-16.3	0.7	-15.5	0.8	-15.6	0.3	-15.0	0.4
C_2^g (K)	47.4	2.5	49.7	5.9	46.8	6.3	41.7	2.3	39.2	3.6
Chisq	0.09		0.57		0.65		0.10		0.2	
R	0.99		0.98		0.97		0.99		0.98	

Table 5.15 *WLF fragilities*

Sample	**T_g (K)**	**Water content %w.w.b.**	**1- C_2^g /T_g**
Gelgum01	236	13.3	0.80
Gelgum02	243.5	11.25	0.80
Gelgum04	246	9.5	0.81
Carr01	245.4	10.4	0.83
Carr02	246.1	10.1	0.86
113	238.95	13.2	0.86
117	248.65	10.5	0.87
120	255.75	8.91	0.90
122	259.85	7.88	0.91

5.5.2 Oscillation and Time temperature superimposition

Table 5.16 shows the shift factors determined by time-temperature superimposition applied on oscillation data (loss modulus) at the reference temperature T_0 = 40 °C. They have been used for the application of the WLF kinetics and determination of the glass transition by using the same procedure as described in chapter 4.

Table 5.16 *Shift factors (Log a_T) obtained by TTS*

Sample / T(°C)	Gelgum01	Gelgum02	Gelgum04	Carr01	Carr02
20	3.29	-			
30	1.67	1.60	2.18	1.63	1.66
40	0	0	0	0	0
50				-1.37	-1.39
60	-2.46	-2.44	-2.63	-2.50	-2.58
70				-3.49	-3.61
80	-4.02	-4.19	-4.41	-4.36	

WLF model has been applied at reference temperature of 40ºC by fixing C_1 at an average value of -15.96 for samples containing Gellan gum and of -16.38 for samples containing carrageenan.

The C_1 values used are the ones obtained by applying the WLF model to the 3 samples containing gellan gum together (Figure 5.34 and Table 5.17) and to the two samples containing carrageenan (Figure 5.35 and Table 5.18).

Figure 5.36 and 5.37 show the WLF fit, with a C_1 fixed value for the sample containing gellan gum and carrageenan respectively.

The resulting parameter, C_2, the correlation coefficient R and the chi squared, χ^2 are shown in Table 5.19 and Table 5.20.

Rheo–T_g has been calculated from the expression (rheo-T_g= C_2^g - C_2^{40}+40) and the value obtained are shown in Table 5.21.

Table 5.21 shows also the calorimetric glass transition to allow a comparison between the two different techniques.

For samples containing gellan gum the glass transition temperature determined by rheological methods is higher by almost 10ºC compared with the glass transition determined calorimetrically. This is in accord with the works that Kasapis is performing on a very long series of high sugar systems containing small amount of hydrocolloids (Kasapis and Sworn 2000; Kasapis 2001; Kasapis and Mitchell 2001; Kasapis 2003; Sworn and Kasapis, 1998; Sworn and Kasapis, 1998[b]). He related the apparent increase in the T_g to the ability of the biopolymer to form a network in the presence of high level of sugars.

Samples containing carrageenan show the same glass transition for both the techniques.

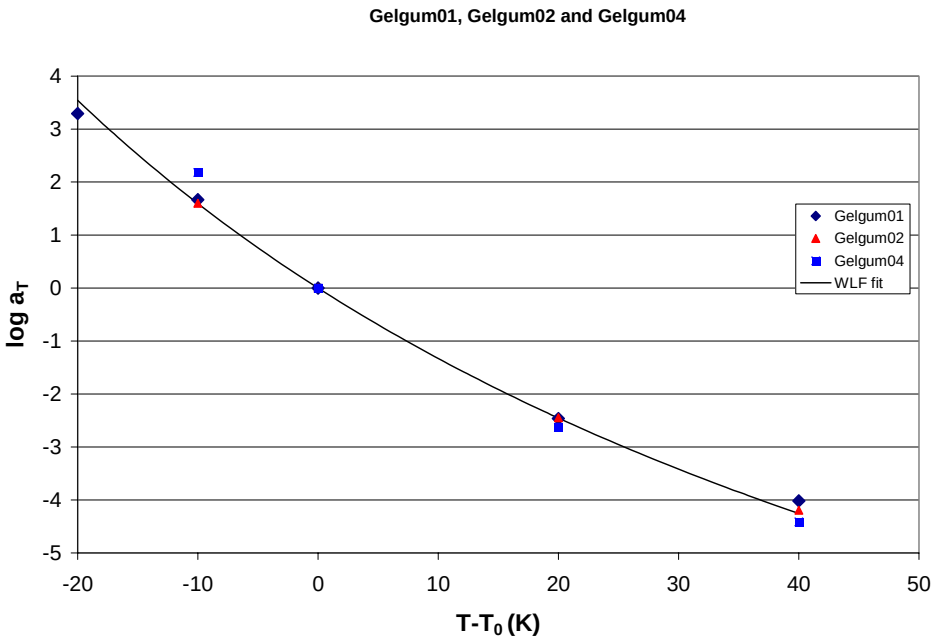

Figure 5.34 WLF plot for samples containing gellan gum analysed together

Table 5.17 *WLF parameters for samples containing gellan gum analysed together*

	Value	Error
C_1^{40}	-15.964	1.7683
C_2^{40} (K)	110.08	14.013
Chisq	0.52541	
R	0.99683	

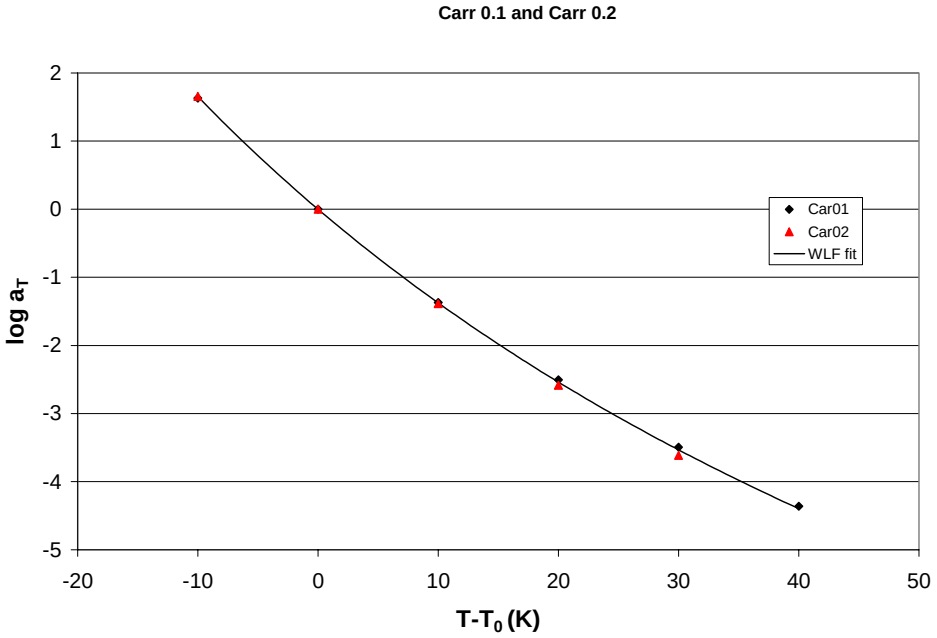

Figure 5.35 WLF plot for samples containing κ-carrageenan analysed together

Table 5.18 *WLF parameters for sample containing carrageenan analysed together*

	Value	**Error**
C_1^{40}	-16.381	0.63178
C_2^{40} **(K)**	109.06	5.1295
Chisq	0.013021	NA
R	0.99985	NA

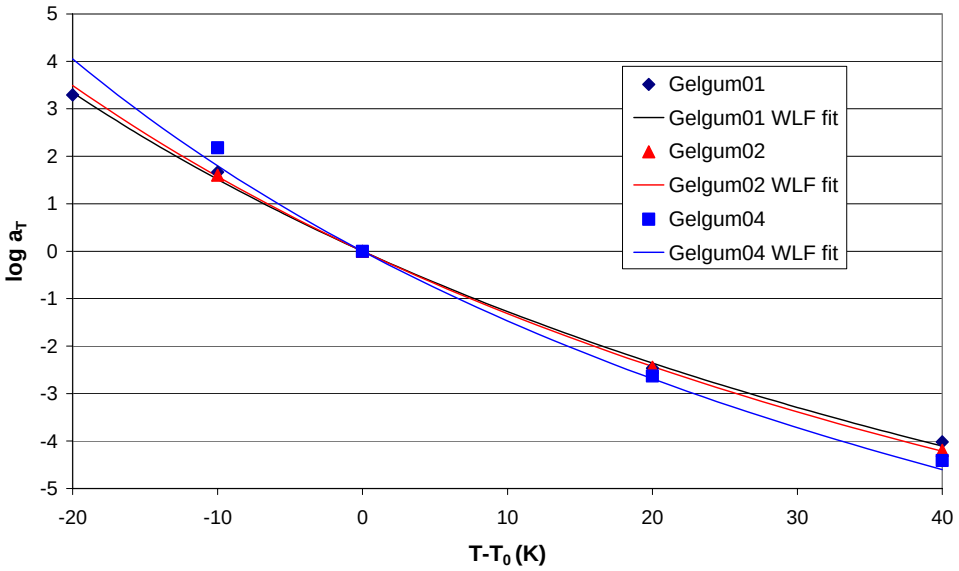

Figure 5.36 WLF plot for samples containing gellan gum

Table 5.19 *WLF parameters for samples containing gellan gum*

	Gelgum01		**Gelgum02**		**Gelgum04**	
	Value	Error	Value	Error	Value	Error
C_1^{40}	-15.96	-	-15.96	-	-15.96	-
C_2^{40} (K)	115.5	2.17	111.4	0.60	98.71	5.51
Chisq	0.04583		0.0014689		0.18476	
R	0.99935		0.99996		0.99633	

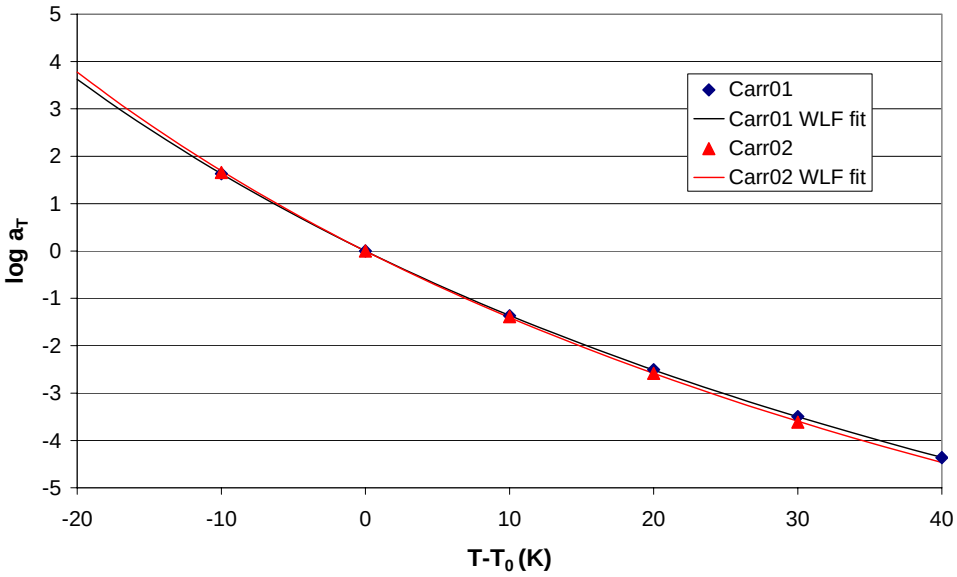

Figure 5.37 WLF plot for samples containing carrageenan

Table 5.20 *WLF parameters for sample containing carrageenan*

	Carr01		**Carr02**	
	Value	Error	Value	Error
C_1^{40}	-16.38	-	-16.38	-
C_2^{40} (K)	110.43	0.15	106.75	0.39
Chisq	0.00023801		0.00094704	
R	1		0.99997	

Table 5.21 *rheo-T_g and calorimetric T_g*

	Gelgum01	**Gelgum02**	**Gelgum04**	**Carr01**	**Carr02**
C_1^{40}	-15.96	-15.96	-15.96	-16.38	-16.38
C_2^{40} (K)	115.5	111.37	98.714	110.4	106.75
rheo-T_g= C_2^g - C_2^{40} +40 °C	-27.85	-21.66	-11.86	-28.33	-29.30
$T_{g\ DSC}$ °C	-37.16	-29.60	-27.14	-27.70	-27.00

5.6 Conclusions

Carrageenan and gellan gum addition increases caramel viscosity, however there are differences between the effect of the two hydrocolloids. The main results are summarised in Table 5.22.

Table 5.22 *Summary of rheological behaviour of sample containing gellan gum and carrageenan.*

DSC	No significant variation in the T_g between sample with and without hydrocollids	
Isoelectric point	Decrease of the pH at isolectric point with the increasing of hydrocolloid content	
Viscosity and modelling	Increase of viscosity with increasing hydrocolloid content.	Departure from Newtonian behaviour increasing with the concentration of hydrocolloid.
	Arrhenius model was not applied successfully as curvature was present in the plot	Apparent activation energies increased with increasing gellan gum concentration. No variation in the activation energies for samples with and without k-carrageenan
	WLF model good fit to the data	Fragilities decreased with increasing hydrocolloid concentration.
Creep recovery	Recovery of about 50% for sample containing gellan gum with exeption of the lowest concentration sampe (0.1%). Recovery of about 20% for samples containing k-carrageenan	
Oscillation	The mechanical spectra move from a typical spectra for non polymeric materials to a a typical spectra for high molecular weight polymeric materials as the concentration of hydrocolloid increase.	
WLF model	For samples containing gellan gum $_{rheo}\text{-}T_g = {}_{DSC}\text{-}T_g+10$ For samples containg k-carragennan $_{rheo}\text{-}Tg = {}_{DSC}\text{-}T_g$	
Capillary rheometry	Gellan gum contaning samples show little variation variation in the Trouton ratio at $100s^{-1}$ κ-carrageenan containing samples showed a marked increase in the Trouton ratio at $100s^{-1}$ with carrageenan concentration. Sample containing 0.2% carrageenan had a Trouton ratio at $100s^{-1}$ of 500.	

The reason could be found in the different nature of the eventual network that is formed as a result of interactions between the biopolymers and the sugars in the caramel systems.

Creep experiments and then extensional viscosity suggest those gellan gum containing samples are more elastic and easily extendable than those containing carrageenan. Furthermore the glass transition detected from small deformation oscillation experiments is higher than the glass transition determined via calorimetry. Gellan gum as we have already said in the literature review chapter is able to form gels at very low concentration. The presence of high level of sugar inhibits the formation of the gel, but a rubber type network is preserved. This imparts elasticity to the materials and has consequences on the glass transition detected via rheological techniques. In fact the rheological techniques are sensitive to the network structure, but not on the glass transition detected calorimetrically that reflects mainly the mobility of the sugar phase.

Carrageenan containing samples, at the concentration studied, shows just a little recovery during creep experiments but they show a marked increases in the extensional viscosity and hence in the Trouton ratio, they are not easily deformable in extension. Furthermore no differences between rheological and calorimetric glass transition temperature are detected. This last result is in agreement with the work done by Deszczynski et al (2002). They found no differences between the mechanical spectra obtained for a system of 0.7 % of carrageenan and 92.3% of sugar solids and for a 93% sugar solids solution. In the same paper the authors also said there was no differences between the rheological and the glass transition when non-gelling biopolymers such as locust bean gum were added in high sugar solutions. It seems that the ability of a biopolymer to form gels in aqueous environment is related to his ability to form network with the sugars.

κ-Carrageenan at concentration around 0.1% 0.2% 10mM KCl, have gel-sol transition at temperature around 25-30ºC (Mangione et al, 2003). They are not very

strong and hence at the same concentration in high sugars environment κ-carrageenan does not form a rheological detectable network in the high sugar environment until a particularly concentration is reached.

This has also consequences in the extensional properties of these materials. For samples containing κ-carrageenan the presence of entanglements results in higher extensional viscosities and Trouton ratios. For samples containing gellan gum it is suggested that some internal slippage of the macromolecular chains in the caramel bulk could have affected the obtained results.

It should be emphasized that in this work all the caramel samples are viscous materials and not solid. DMTA experiments could not be performed as they require the sample to be shaped as a solid bar or film. Rotational rheology test have instrument limitations, as we have already shown mainly due to compliance effects. For this reasons it has not possible to investigate directly the glass transition temperature region. Therefore WLF kinetics have been of primary importance in the determination of the rheo-T_g.

Kasapis in many publications has tried to rationalise the use of the WLF model for the understanding of the biopolymer vitrification in high sugar environment (Whittaker, Al-Ruqaie et al. 1997; Sworn and Kasapis 1998; Sworn and Kasapis 1998; Kasapis and Sworn 2000; Kasapis 2001). He asserts to have solved the compliance instrument problem by using a very wide gap and to be able to investigate the rheology in the glass transition region. Furthermore his theoretical approach is very different from the approach used in this work.

As this author does not believe in the universality of the C_1^g and C_2^g constants of the WLF model these constants have been determined for all the samples by fitting viscosity data on T-T_g, where the glass transition is determined calorimetrically, and considering the viscosity of the glassy materials be equal to 10^{12}Pa·s. The rheo-T_g

has been determined from oscillation experiments with the relationship: $T_g = C_2^g - C_2^0 + T_0$.

Kasapis instead consider C_2^g as universal value of 50K and determine C_1^g from the relation $C_1^g C_2^g = C_1^0 C_2^0$ after he determines C_1^0 and C_2^0 with oscillation experiments at an arbitrary temperature T_0 and assumes $T_g = 50 - C_2^0 + T_0$. And finally he calculates the free volume from the C_1^g according to the equations $C_1^g = \frac{B}{2.303 f_0}$

It was concluded that the effect of biopolymers can be generalized in terms of iso-free volume (Kasapis and Mitchell 2001; Kasapis, Al-Marhobi et al. 2003). Practically he compared the behaviour of several biopolymers and from small oscillation experiments and calculated the shift factors and the free volume at an arbitrary reference temperature. Then he arbitrarily chose the free volume obtained for samples containing k-carrageenan as iso-free volume (Figures 5.38 and 5.39). After he calculated the temperature where each biopolymer-high sugar systems would have the iso-free volume and plotted in graph the shift factor as function of T-T_{isofv}. The author stated: "*It is gratifying to find that in biological preparation with distinct chemical and conformational properties, molecular weight and ability to behave as gelling ot thickening agents, the temperature dependence of viscoelastic rate processes can be described by a single parameter T_{isofv} which is in turn relate to free volume."* (Kasapis and Mitchell 2001)

This affirmation seems to be very strong to the authors as very big differences in rheological behaviour are detected by using two different biopolymers in caramel systems.

This author believes that the temperature dependence on viscoelastic process is related to the free-volume but also that variation in free-volume with the temperature are strongly relate to the nature of the biopolymer and of the environment.

If the figures 5.38 and 5.39 are observed with more attention it is evident that the temperature dependence of viscoelastic rate processes is different for samples containing gellan gum (encircled by a red line) and samples containing carrageenan (encircled by a blue line) .

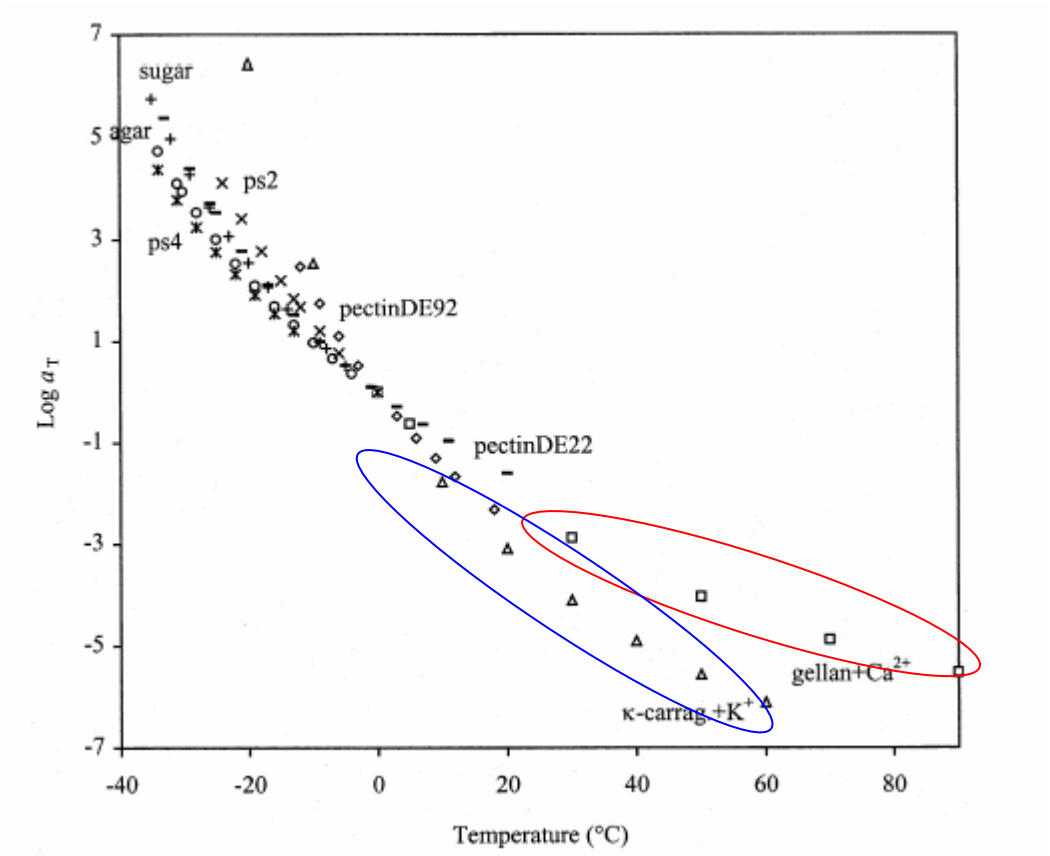

Figure 5.38 Temperature variation of shift factors normalised at 0 °C for polysaccharide/co-solute, gelatin/co-solute and single co-solute systems. (Kasapis and Mitchell, 2001)

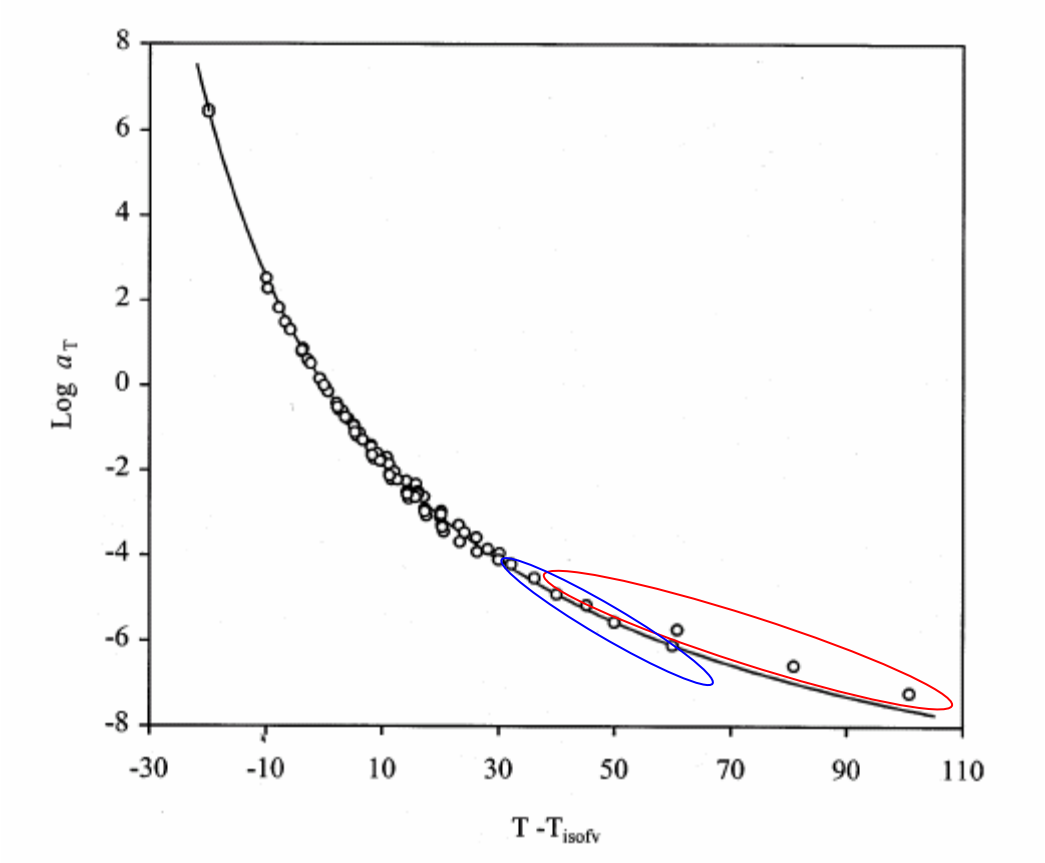

Figure 5.39 Shift factors of dynamic oscillatory mechanical spectra for the samples of Figure 5.38 reduced to their own T_{isofv}. (the line reflects the WLF fit). (Kasapis and Mitchell 2001)

CHAPTER 6. GENERAL DISCUSSION AND CONCLUSION

A structural and rheological characterization on samples prepared at the same formulation but varying the processing temperature has been carried out.

For these samples water content depended on the final cooking temperature and consequently the glass transition. Information about the crystallinity has been obtained using X-ray diffractometry and DSC. All the samples were semicrystalline. The crystallinity was due to the vegetable fat. Although for the lowest water content (highest cooking temperature) system there was a small amount of crystalline fructose.

The glass transition temperature was also measured from DSC and taken as the midpoint of the glass transition range. It decreased as the water content increased. This showed the plasticization effect of the water on the sugar matrix. This has been modelled by using the Gordon-Taylor equation and data extrapolated to the dry matrix have been compared to the calculated glass transition obtained by using the Couchman-Karasz equation.

The results were not consistent, the calculated glass transition of the dry sugar matrix was higher then the glass transition of the dry caramels obtained from the Gordon Taylor fit. Similar disagreements have been also found for sucrose solution,

therefore some the applicability of the Couchman-Karasz equation to model sugars-water systems has been questioned.

Information about the extent of Maillard reactivity was obtained by the determination of the isoelectric point. The pH at isoelectric point was different in each sample and was increasing as the cooking-temperature decreased. The isoelectric point depends on the nature of the protein and differences in its value in the samples analyzed (arising from the same formulation) have been attributed to transformations in the chemical structure of the proteins due to the Maillard reaction. The isoelectric point pH decreased as the Maillard reaction developed.

Rheological characterization was performed with rotational and capillary rheometers.

Oscillation tests and creep recovery have been performed on the samples at different water contents, viscosities obtained from oscillation when compared with the steady shear viscosity using the Cox Merz rule were generally some what lower.

Viscosity curves have been obtained for all the samples over a wide range of temperature, a power law model, $\sigma = K\dot{\gamma}^n$ where σ is the shear stress and $\dot{\gamma}$ the shear rate has been applied and the power law index, *n*, and the consistency index, *K*, have been determined. The flow behaviour index, *n*, reflects the closeness to Newtonian flow: if *n* is equal to 1, the fluid is Newtonian if *n* is lower than 1 the fluid is shear-thinning and if *n* is higher than 1 it is shear-thickening.

At the same temperature for samples at different water content the flow behaviour index slightly decreased when the water content decreased and for the same sample the flow behaviour index increased as the temperature decreased.

The values were ranged from 0.96 for measurements performed at 80ºC for the sample at higher water content to 0.87 for measured performed at 60ºC for the

sample at lower water content. This means that the samples were primarily Newtonian fluids.

Oscillation tests were performed on caramel samples. They confirmed the predominantly Newtonian characters of caramels. Time temperature superimposition was applied on loss moduli curves performed at different temperatures and master curves obtained.

Creep compliance test were performed at 20ºC. The compliance, at the maximum time the stress was applied, increased with increasing water content, and all the samples were viscous materials showing minimal recovery when the stress applied was removed. Those results were in agreement with the viscosity and oscillation data as discussed before. Despite the negligible elasticity Burgers model was applied to the creep data and the viscosity of the free dashpot of the Maxwell element was taken as the value for the creep viscosity at 20ºC. Viscosity data from all three tests was combined in subsequent modelling.

Capillary viscosity tests, performed on the caramels samples, allowed the determination of extensional and shear viscosity curves.

Extensional curves showed a marked thinning behaviour. The lower the water content the higher the extensional viscosity. The dependence on the water content appeared to be less marked in shear flow within the capillary, where behaviour closer to Newtonian was also observable.

In the limit of the experimental error, there were not many differences in the Trouton ratio, between the three samples. In the range of the analysed strain rate the Trouton ratio had an average value of 30. This high values compared with the expected Newtonian of 3 could reflect the contribution of polymeric material and fat to the extensional viscosity at the very high stress in the capillary, although it is possible that under the capillary condition there were artefacts perhaps due to fat separation and slip. Reproducible data was difficult to obtain with the capillary

rheometer, but results were improved when a purpose built funnel was used to fill the barrel.

Viscosity data, obtained from the three different techniques, were modelled in three ways.

An empirical statistic model was obtained by using Design expert software. The application of the ANOVA analysis on viscosities as function of the water content and temperature gave a second order polynomial model of the form:

$$\log(\eta) = a_0 - \frac{a_1}{T} - a_2 X_w + \frac{a_3}{T^2} + a_4 X_w{}^2 - \frac{a_5 X_w}{T}$$

and the resulting equation was:

$$\log(\eta) = 21.75 - \frac{1.556 \cdot 10^4}{T} - 0.431 X_w + \frac{3.60 \cdot 10^6}{T^2} + 0.041 X_w{}^2 - \frac{209.5 X_w}{T}$$

This equation will not give information about the physical state of the caramel, but is can be useful in practical issues as it give an estimate of the viscosity of simple caramel sistems at a certain temperature once the water content is known.

An Arrhenius equation was also used to model the viscosities. From the Arrhenius model the activation energies were determined. They, ranged between 75 and 101 KJoule/mole, and were consistent with the activation energy reported in literature for concentrated sugar solutions. However a curvature in the experimental data was observed in the Arrhenius plot, particularly at low water content. This curvature, indicating a deviation from the Arrhenius behaviour was more pronounced in the T_g-scaled Arrhenius plot. This was not surprising as the caramel at the experimental temperature, except for the higher water content sample, was in the region where the data would be better described by a WLF model. Since the latter is expected to be better that than Arrhenius model in the temperature range $T_g+100 > T > T_g$. However

the WLF equation with the universal values C_1^g=17.4 and C_2^g=51.6 did not fit the viscosity data well.

WLF parameters where the reference temperature is the glass transition, C^g_1 and C^g_2 were then determined. The fragility of a liquid can be defined as the steepness of the Arrhenius plot near the Tg. The more a liquid is more fragile the greater is the temperature dependence above the Tg. According to Angell the fragility of a liquid can be described in terms of WLF parameters C_2^g as (1- C_2^g /T_g), ranging between 0 and 1 with the increasing fragility. The value of fragilities obtained in this way increased with decreasing of the water content. This data was in agreement with what found in the literature on sucrose solutions, (Angell, 2002) whose fragility decreased slowly as the water content increases.

Attempts to fit all the viscosities obtained for the four samples in a unique general WLF model have been made. The resulting equation was:

$$\log(\eta) = 12 + \frac{\text{-}14.956(T - T_g)}{30.28 + T - T_g}$$

As with the equation obtained by the statistical model this equation could be considered as a useful tool to use together with the Gordon-Taylor fit to provide information on the water content dependance of the viscosity, for a quick estimation of the viscosity of caramels at a particular temperature and water content.

From the oscillation test, shift factors were determined by applying Time (frequency) temperature superimposition.

These were modelled to a WLF model at the reference temperature of 40ºC, and WLF parameters C^{40}_1 and C^{40}_2 were determined.

The rheo-T_g was determined by the relationship:

$$\text{rheo-}T_g = C_2^g - C_2^{40} + 40\ ^\circ C$$

The glass transition temperature obtained were, in the limit of the experimental error, consitant with the calorimetric glass transition temperature except for the high water content sample where the WLF model would be expected to be less apropriate.

Another set of samples, obtained at the same processing temperature but with incorporation of the hydrocolloids (gellan gum and κ-carrageenan) was characterized with both structural and rheological techniques.

The presence of hydrocolloids did not affect either the fat crystallinity or the glass transition temperature.

The glass transition temperature values, detrmined by calorimetry, superimposed, in the limit of the experimental error, to the Gordon-Taylor fit curve determined for samples at different water content.

The addition of small amount of κ-carrageenan or gellan gum resulted in a large reduction in the isoelectric pH. It is suggested that this technique could be used to detect the presence of low levels of polyelectrolyte additives in complex food system.

The presence of the hydrocolloid affected strongly the rheology of caramels. Marked shear thinning behaviour was observed in shear flow and the curves showed more thinning behaviour as the amount of hydrocolloids increased. Moreover the addition of hydrocolloids resulted in an increase in the viscosity.

In contrast to the caramels prepared in the absence of hydrocolloids the creep compliance response at 20°C was typical of a viscoelastic system showed a curvature in the compliance when a stress was applied and a recovery of the deformation, depending on the amount of added hydrocolloid added when the stress was released.

The Burgers model was applied to creep data and the viscosity of the free dashpot of the Maxwell element was taken as the value of the creep viscosity.

Oscillation tests confirmed the presence of an elastic component in sample containing hydrocolloids. The loss and storage modulus decreased with increasing temperature as well the complex viscosity and at the same temperature all these viscoelastic variables were higher for sample with more added hydrocolloids. As for the samples at different water content, the value of the complex viscosity at ω=1rad/sec, the consistency index and the creep viscosity were used together for the modelling of Arrhenius and WLF kinetics.

Increased elasticity on hydrocolloid addition was also confirmed by capillary measurements performed at 70°C on samples where the κ-carrageenan concentration ranged between 0 (the standard 117 sample) and 0.2%. The Trouton ratio is the ratio between extensional and shear viscosity at the same strain rate; it can be demonstrated that for purely Newtonian fluid it is equal to 3 (Steffe 1996), and the higher this value the higher the elasticity and the greater the deviation from ideal Newtonian behaviour. As the carrageenan content increased the extensional viscosity increased more rapidly than the shear viscosity. This resulted in an increase in the Trouton ratio from about 30 for the sample with no κ-carageenan to 500 for the sample containing 0.2% of κ-carrageenan.

The activation energies were determined from the slope of the Arrhenius plot.

While for sample containing gellan gum the activation energies were higher then the sample with no addition of hydrocolloids at the same water content, no differences were observed in the activation energies obtained for samples containing κ-carrageenan and samples at the same water content with no incorporation of hydrocolloids. Also in this case a curvature, indicating a deviation from the Arrhenius behaviour was observed.

WLF kinetics were applied on all the samples containing hydrocolloids and the WLF parameters were determined and also the fragility.

Values obtained for samples containing hydrocolloids are slightly lower compared with the value of fragility obtained for samples at the same water content with no incorporation of hydrocolloids.

Shift factors obtained by TTS on loss moduli from oscillation tests have been modelled by WLF kinetics at the reference temperature of 40ºC. This allowed the WLF parameters C^{40}_1 and C^{40}_2 and the rheo-T_g to be obtained. A comparison between the glass transitions temperatures determined rheologically showed surprising results. In fact for samples containing gellan gum the rheo-T_g was about 10ºC higher then the glass transition temperature determined calorimetrically, and for sample containing carrageenan no differences in these two values were observable.

Practical implication of the study

From a practical point of view an empirical model with allow η to be obtained for any temperature and water content has been developed. By obtaining process information on the viscosity that will result in tailing on deposition it will then be possible to use the model to design the process variables (final heating temperature, depositing temperature) so this high viscosity region is avoided.

The effect of hydrocolloids is interesting.

Cold flow will be governed by the creep viscosity η_0 at ambient temperature.

The value of η_0 for the sample containing 0.2% carrageenan is approximately 10 times higher then the control at the same water content. This would therefore predict that including carrageenan would reduce cold flow. This was indeed found to be the case when product was manufactured (Figure 6.1). It may therefore be possible to make caramel at higher water content than normally used which would reduce tailing

as the high temperature viscosity is lower, but produce a product which is acceptable on cooling. In this respect the difference between carrageenan and gellan merits further study.

(a) (b)

F**igure 6.1** Caramel filled chocolates manufactured during a depositing trial. a) 0.2% k-carrageenan containing caramel b) control (117) processed at the same conditions. No cold flow on storage is observable in (a), but very marked cold flow is seen in (b).

BIBLIOGRAPHY

Adam, G.; Gibbs, G. H. On the temperature dependence of cooperative relaxation properties in glass-forming liquids. *J. Chem. Phys*. **1965**, 43, 139-146.

Alexander, L. E. *X-Ray diffraction methods in polymer science*; John Wiley and Sons Inc: USA, 1969.

Al-Malah, K. I. M.; Abu-Jdayil, B.; Zaitoun, S.; Ghzawi, A. A. M. Application of WLF and Arrhenius kinetics to rheology of selected dark-colored honey. *Journal of Food Process Engineering* **2001**, 24, 341-357.

Angell, C. A. Liquid fragility and the glass transition in water and aqueous solution. *Chemical Reviews* **2002**, 102, 2627-2650.

Angell, C. A. Why C1=16 -17 in the WLF equation is physical - and the fragility of polymers. *Polymer* **1997**, 38, 6261-6266.

Angell, C. A.; Bressel, R. D.; Green, J. L.; Kanno, H.; Oguni, M.; Sarre, E. J. In *Water in Food*; P. Fito; B. Mulet and B. Mc Kenna, Eds.; Elselvier Appl. Sci.: New York, 1994; pp 115.

Anonimous (2003). toutsurlecaramel. http://toutsurlecaramel.free.fr, web reference.

Bagley, E. B. End corrections in the capillary flow of polyethylene. *J. Appl. Phys* **1957**, 28, 624-627.

Bainbridge, R. Production option for caramel/nut and chocolate clusters. *Manufactoring Confectioner* **1997**, 55, 85-89.

Barnes, H. A. *A handbook of elementary rheology*; University of Wales Institute of Non-Newtonian Fluid Mechanics: Aberystwyth, UK, 2000.

Barnes, H.A.; Hutton, J.F. and Walters, K. *An Introduction to rheology*. Elselvier, Amsterdam, 1989.

Bent, J.; Hutchings, L. R.; Richards, R. W.; Gough, T.; Spares, R.; Coates, P. D.; Grillo, I.; Harlen, O. G.; Read, D. J.; Graham, R. S.; Likhtman, A. E.; Groves, D. J.; Nicholson, T. M.; and McLeish T. C. B. Neutron-Mapping Polymer Flow: Scattering, Flow Visualization, and Molecular Theory *Science* **2003**; 301: 1691-1695

Blanshard, J.; Lillford, P. *The glassy state in food*; Nottingham University press: Loughborough UK, 1993.

Bondi, M.; Marcone, M.; Kakuda, Y. Effect of heat treatment on the properties of sweetened and condensed milk and its relationship to the manufacturing of caramel. *47th Annual Production Conference of the Pennsylvania Manufacturing Confectioners Association* **1993**, 98-103.

Carroll V,.; Miles M.J.; Morris V.J.; Fiber-diffraction studies of the extracellular polysaccharide from pseudomonas-elodea *Int. J. Biol. Macromol*. **1982**, 4 (7): 432-433

Carroll, V.; Chilvers, G.R.; Franklin, D.; Miles, M.J.; Morris, V.J.; Ring, S.G. Rheology and microstructure of solutions of the microbial polysaccharide from pseudomonas-elodea, *Carbohyd Res* **1983**, 114 (2): 181-191

Castro, E.; Silva, C.; Osorio, F.; Miranda, M. Characterization of caramel jam using back extrusion technique. *Latin American Applied Research* **2000**, 30, 227-232.

Champion, D.; Hervet, H.; Blond, G.; Le Meste, M.; Simatos, D. Traslational diffusion in sucrose solution in the vicinity of their glass transition temperature. *J. Phys. Chem. B* **1997**, 101, 10674-10679.

Champion, D.; Maglione, M.; Niquet, G.; Simatos, D.; Le Meste, M. Study of alpha- and beta-relaxation processes in supercooled sucrose liquids. *Journal of Thermal Analysis and Calorimetry* **2003**, 71, 249-261.

Chan, R. K.; PAthmanthan, K.; Johari, G. P. Dielectric relaxation in the liquid and glassy state of glucose and its water mixtures. *J. Phys. Chem.* **1986**, 90, 6358-6362.

Chung, M. S.; Ruan, R. R.; Chen, P. L.; Wang, X. Physical and chemical properties of caramel systems. *Food Science and Technology-Lebensmittel-Wissenschaft & Technologie* **1999,** 32, 162-166.

Cocero, A. M.; Kokini, J. L. Prediction of temperature dependence of the apparent shear viscosity of 40% moisture glutenin using Arrheniusn and WLF equations. *Inst. Food Technology Annu. Meet* **1992**, Abstract 60.

Cogswell, F. N. Converging flow and stretching flow: a compilation. *J. Non-Newtonian Fluid Mech* **1978**, 4, 23-38.

Cogswell, F. N. Converging flow of polymer melts in extrusion dies. *Poly. Engn. and Sci* **1972**, 12, 64-73.

Cohen, M. H.; Turnbull, D. Molecular transport in liquids and glasses. *J. Chem. Phys.* **1959**, 31, 1164-1169.

Couchmann, P. R. A classical thermodynamic discussion of the effect of composition on class-transition temperatures. *Macromolecules* **1978**, 11, 117-119.

Dail, R. V.; Steffe, J. F. Dilatancy in starch solutions under low acid aseptic processing conditions. *J. Food Sci* **1990**, 53, 1764-1765.

Dail, R. V.; Steffe, J. F. Rheological characterization of crosslinked waxy maize starch solutions under low acid aseptic processing conditions using tube viscometry techniques. *J. Food Sci* **1990**, 53, 1660-1665.

de Gennes, P. G. Reptation of a Polymer Chain in the Presence of Fixed Obstacles**,** *J. Chem. Phys.* **1971,** 55, 572.

De Mallie, R.B; Birnboim, M.H.; Frederick, J. E.; Tschoegl, N. W.; and Ferry. J.D. Viscoelastic properties of dilute polystyrene solutions and verification of the Zimm theory *J. Phys. Chem.*, **1962**, 66, pp 536 – 539

Deszczynski, M.; Kasapis, S.; MacNaughton, W.; Mitchell, J. R. High sugar/polysaccharide glasses: resolving the role of water molecules in structure formation. *Int. J. Biol. Macromol*. **2002**, 30, 279-282.

Doi M.; Edwards S.F., Dynamics of concentrated polymer systems .4. Rheological properties *Journal of the chemical society-faraday transactions II* **1979**, 75: 38-54 part 1

Doi M.; Edwards S.F., Dynamics of rod-like macromolecules in concentrated-solution .1. *Journal of the chemical society-faraday transactions II* **1978**, 74: 560-570 part 3

Edwards S.F Statistical mechanics with topological constraints: I , *Proc. Phys. Soc*., **1967** 91, pp513-519.

Edwards S.F. The statistical mechanics of polymerized material, *Proc. Phys. Soc*. **1967**, 92, pp9-16

Evageliou, V.; Kasapis, S.; Hember, M. W. N. Vitrification of k-carrageenan in the presence of high levels of glucose syrups. *Polymer* **1998**, 39, 3909-3917.

Ewing, G. W. *Instrumental methods of chemical analysis*.; McGraw-Hill Book company Inc.: London, 1960.

Gerdes, W. F. Streaming current detector measures colloid stability. *ISA Journal* **1966**, 13, 39-43.

Gibson, A. G. *Converging dies. In Rheological Measurements*; A. A. a. D. W. C. Collyer, Ed.; Elsevier Applied Science: New York, 1988; pp 49-92.

Gibson, W.; Sanderson, G. R. *Gellan Gum. In Thickening and Gelling Agents for Food*; A. Ineson, Ed.; Anspen: Gaithersburg, 1999; pp 119-143.

Gordon, M.; Taylor, J. S. Ideal copolymers and the second-order transition of synthetic rubbers. *Journal of Applied Chemistry* **1952**, 2, 493-499.

Graessle,W.W. Linear viscoelasticity in entangling polymer systems, *J Chem Phys*, **1971**, 54 (12): 5143

Guelfi, R. Critical factors in caramel quality. *42nd Annual Production Conference of the Pennsylvania Manufacturing Confectioners Association* **1988**, 132-135.

Gunning, A. P.; Morris, V. J. Light scattering studies of tetraethyl ammonium gellan. *Int. J. Biol. Macromol.* **1990**, 12, 338-341.

Gunter, J. "Electrokinetic characterization of gelatin and its reaction with polyelectrolytes by a streaming current detector," Mutek Analytic GmbH,

Huang, H.; J.L., K. Measurement of biaxial extensional viscosity of wheat flour doughs. *J. Rheol* **1993**, 37, 879-891.

Jeffery, M. The technology of caramel and fudge. *Food Technology International. Issued Europ. Fed. Food. Sci. and Technol*. **2001**, 110-113.

Johari, G. P. Glass transition and secondary relaxation in molecular liquids and crystals. *Ann. N.Y. Acad. Sci.* **1976**, 2, 117-140.

John, A.; Shastri, P. N. Studies on food macromolecules by Differential Scanning Calorimetry: A critical appraisal. *Journal of food science and technology Mysore* **1998**, 35, 1-14.

Jones, D. M.; Walters, K.; Williams, P. R. On the extensional viscosity of mobile polymer systems. *Rheol. Acta* **1987**, 26, 20-30.

Kasapis, S. The use of WLF kinetics to rationalise the rubber-to-glass transition in high sugar/k-carrageenan systems. *Food Hydrocolloids* **2001**, 15, 239-245.

Kasapis, S.; Al-Marhobi, I.; Mitchell, J. R. Testing the validity of comparison between the rheological and the calorimetric glass transition temperatures. *Carbohydrate Research* **2003**, 338, 787-794.

Kasapis, S.; Mitchell, J. R. Definition of the rheological glass transition temperature in association with the concept of iso-free-volume. *International Journal of Biological Macromolecules* **2001**, 29, 315-321.

Kasapis, S.; Sworn, G. Separation of the variables of time and temperature in the mechanical properties of high sugar/polysaccharide mixtures. *Biopolymer* **2000**, 53, 40-45.

Kumagai, H.; MacNaughton, W.; Farhat, I. A.; Mitchell, J. R. The influence of carrageenan on molecular mobility in low moisture amourphous sugars. *Carbohydrate Polymers* **2002**, 48, 341-349.

Le Meste, M.; Champion, D.; Roudaut, G.; Blond, G.; Simatos, D. Glass transition and food technology: A critical appraisal. *Journal of Food Science* **2002**, 67, 2444-2458.

Lodge A. S., *Elastic liquids- an introductory vector treatment of finite-strain polymer rheology*, Academic Press 1964.

Lodge, A.S. A network theory of flow birefringence and stress in concentrated polymer solutions *Transactions of The Faraday Society* **1956**, 52(1), 120-130.

Mac Naughton, J. L.; Mortimer, L. T. *Differential scanning calorimetry. In IRS physical chemistry*; Butterworths, 1975.

Maltini, E.; Anese, M. Evaluation of viscosities of amorphous phases in partially frozen systems by WLF kinetics and glass transition temperatures. *Food Research International* **1995**, 28, 367-372.

Mangione MR, Giacomazza D, Bulone D, Martorana V, San Biagio PL, Thermoreversible gelation of kappa-Carrageenan: relation between conformational transition and aggregation *Biophysical Chemistry* **2003**, 104 (1): 95-105

Marrucci G. Polymers go with the flow *Science* **2003**; 301: 1681-1682

Marrucci, G. Reologia (Modelli) In *Macromolecole Scienza e Tecnologia, Vol. II* ; F. Ciardelli, V. Crescenzi, G. Pezzin, E. Peggion Eds. Pacini editore, Pisa, **1986;** pp503-510

Mathlouthi, M.; Génotelle, J. *Rheological properties of sucrose solutions and suspensions. In Sucrose Properties and Applications*; M. Mathlouthi and P. Reiser, Eds.; M.Mathlouthi and P. Reiser, 1995; pp 126-154.

Matsuoka, S.; Hale, A. Cooperative relaxation processes in polymers. *J. Appl. Polym. Sci.* **1997**, 64, 77-93.

McMaster, T.; Smith, A. C.; Richmond, P. Physical and rheological characterization of a confectionery product. *Journal of Texture Studies* **1987**, 18, 319-334.

Mitchell, J. R. *Hydrocolloids in low water and high sugar environments. In Gums and stabilisers for the food industry*; P. A. Williams and G. O. Phillips, Eds.; The Royal Society of Chemistry: Cambridge, 2000 243-254.

Moirano, A. I. *Sulfated seaweed polysaccharides. In Food Colloids*; H. D. Graham, Ed.; The AVI Publishing company, inc: Westport, **1977**; pp 347-381.

Morris, E. R., Rees, D. A. and Robinson, GCation-specific aggregation of carrageenan helices: Domain model of polymer gel structure. *J. Mol. Biol.* **1980,**138, 349-362.

Morris, E.R.; Gothard, M.G.E.; Hember, M.W.N.; Manning, C.E.; Robinson, G. Conformational and rheological transitions of welan, rhamsan and acylated gellan *Carbohyd Polym.* **1996**, 30 (2-3): 165-175

Morris, V. J. *Gelation of polysaccharides. In Functional Properties of Food Macromolecules*; S. E. Hill; D. A. Ledward and J. R. Mitchell, Eds.; Aspen Publication: Gaithersburg, 1998; pp 143-226.

Morton, D. N.; Roberts, C. J.; Hey, M. J.; Mitchell, J. R.; Hipkiss, J.; Vercauteren, J. Surface characterization of caramel at the micrometer scale. *Journal of Food Science* **2003**, 68, 1411-1415.

Mueller, G.P., and Rees, D. A. *in Drugs from the sea*. Univ. of Rhode Island, Kingston, 1967.

Okuno, M.; Kishihara, S.; Otsuka, M.; Fujii, S.; Kawasaki, K. Variability of melting behaviour of commercial granulated sugar measured by differential scanning calorimetry. *International Sugar Journal* **2003**, 105, 29-35.

Oxford, P. D.; Parker, R.; Ring, S. G.; Smith, A. C. Effect of water as diluent on the glass transition behaviour of malto-olisaccharides, amylose and amylopectin. *International Journal of Biological Macromolecules* **1989**, 11, 91-96.

Patton, P. A.; Lee, D. T. Charge analyses: powerful tools in wet-end optimization. *Tappi Journal* **1993**, 76, 107.

Peleg, M. On the Use of the WLF model in polymers and foods. *Critical Review in Food Science and Nutrition* **1992**, 32, 59-66.

Perez, J. *Theories of liquid-glass transition. In Water in Foods*; P. Fito; A. Mulet and B. Mc Kenna, Eds.; Eselvier Appli. Science: New York, 1994; pp 89-114.

Plazek, D. J.; Bero, C. A. Precise glass temperature. *Journal of Physics: Condensed Matter* **2003**, 15, S789-S802.

Rao, M. A. *Rheology of fluid and semisolid foods Principles and applications*; Aspen Publisher, Inc: Gaithersburg, Mariland, 1999.

Rees, D. A. and Welsh, E. JSecondary and tertiary structure of polysaccharides in solutions and gels. *Angew. Chem. Int. Ed. Engl.* **1977,** 16, 214-224.

Rees, D. A. *Structure, conformation, and mechanism in the formation of polysaccharide gel and networks. In Advances in Carbohydrate Chemistry*; M. L. Wolform; R. S. Tipson and D. Horton, Eds.; Academic Press: New York, 1969.

Rees, D.A.; Steele, I.W.; Williamson, F.B. 1969 J. Polymer Sci. C, 28 261 Conformational analysis of polysaccharides .3. Relation between stereochemistry and properties of some natural polysaccharide sulfates (1), *J. Polym Sci Pol Sym* **1969**, (28PC): 261

Robinson, G.R.; Morris, E.R.; Rees, D.A. Role of double helices in carrageenan gelation - domain model *J Chem Soc Chem Comm* **1980**, (4): 152-153

Roos, Y. H. *Phase transitions in foods*; Academic Press, Inc: San Diego, CA, 1995.

Rouse, P.E. A Theory Of The Linear Viscoelastic Properties Of Dilute Solutions Of Coiling Polymers, *J Chem Phys*, **1953**, 21 (7): 1272-1280

Schausberger, A; Schindlauer, G; Janeschitzkriegl, H. Linear elastico-viscous properties of molten standard polystyrenes .1. presentation of complex moduli - role of short-range structural parameters**,** *Rheol. Acta*, **1985**, 24 (3): 220-227

Sjogren, L. *Mode coupling theory on the glassy transition. In Basic features of the glassy state*; J. Colmenero and A. Alegria, Eds.; World Sci.: Singapore, 1989; pp 136-151.

Sjogren, L.; Gotze, W. α-Relaxation spectra in supercooled Liquids. *J. Non-Cryst. Solids* **1994**, 172-174, 7-15.

Slade, L.; Levine, H. Beyond water activity Recent advances based on an alternative approach to the assessment of food quality and safety. *CRC Critical Reviews in Food Science and Nutrition* **1991**, 30, 115.

Slade, L.; Levine, H. Glass transition and water-food structure interactions. *Adv. Food. Nutr. Res.* **1995**, 103-269.

Slade, L.; Levine, H. *Polymer science approach to water relationship in foods. In Food preservation by moisture control. Fundamentals and applications*; G. Barbosa-Canovas and J. Welti-Chanes, Eds.; Technomic: Lancaster USA, 1995.

Soesanto, T.; Williams, M. C. Volumetric Interpretation of viscosity for concentrate and diluite sugar solutions. *J. Phys. Chem*. **1981**, 85, 3338-3341.

Steffe, F. J. *Rheological methods in food process engineering*; Freeman Press: East Lansing, USA, 1992.

Steiner, A. E.; Foegeding, E. A.; Drake, M. Descriptive analysis of caramel texture. *Journal of Sensory Studies* **2003**, 18, 277-289.

Sworn, G.; Kasapis, S. Effect of conformational and molecular weight of co-solute on the mecchanical properties of gellan gum gels. *Food Hydrocolloids* **1998**, 12, 283-290.

Sworn, G.; Kasapis, S. The use of Arrhenius and WLF kinetics to rationalize the mechanical spectrum in high sugar gellan systems. *Carbohydrate research* **1998**, 309, 353-361.

Thomas, W. R. *Carrageenan. In Thickening and Gelling Agents for Food*; A. Ineson, Ed.; Anspen: Gaithersburg, 1999; pp 45-59.

Trouton, F. T. On the coefficient of viscous traction and its relation to that of viscosity.; *Proceedings of the Royal Society of London*, **1906**; pp 426-440.

Tsoga, A.; Kasapis, S.; Richardson, R. K. The rubber-to-glass transition in high sugar agarose systems. *Biopolymers* **1999**, 49, 267-275.

Upstill, C.; Atkins, E.D.T.; Attwool, P.T. Helical conformations of gellan gum *Int J Biol Macromol* **1986**, 8 (5): 275-288

Van Wazer, J. R. *Viscosity and flow measurement*; Interscience Publishers: New York, 1963.

Vanhal, I.; Blond, G. Impact of melting conditions of sucrose on its glass transition temperature. *Journal of Agricultural and Food Chemistry* **1999**, 47, 4285-4290.

Watanabe, H. Viscoelasticity and dynamics of entangled polymers, *Prog. Polym. Sci*., **1999**, 24, pp 1253-1403

Weckel, K. G.; Steinke, J. Factors affecting consistency of caramel at depositing temperatures. *Manufacturing Confectioner* **1973**, 53, 24-30.

Whittaker, L. E.; Al-Ruqaie, I. M.; Kasapis, S.; Richardson, R. K. Development of composite structures in the gellan polysaccharide/sugar system. *Carbohydrate Polymers* **1997**, 33, 39-46.

Williams, M. C.; Landel, R. F.; Ferry, J. D. The temperature dependence of relaxation mechanism in amourphous polymers and other glass forming liquids. *J. Am. Chem. Soc*. **1955**, 3701-3706.

Yildiz, M. E.; Kokini, J. L. Determination of Williams-Landel-Ferry constants for a food polymer system: Effect of water activity and moisture content. *J. Rheol* **2001**, 45, 903-912.

Zimm, B.H. Dynamics Of Polymer Molecules In Dilute Solution - Viscoelasticity, Flow Birefringence And Dielectric Loss, *J Chem Phys*, **1956**, 24 (2): 269-278